TRANSIENT PROCESSES WITH HYDROGELS

Vom Fachbereich für Maschinenbau und Verfahrenstechnik
der Technischen Universität Kaiserslautern
zur Erlangung des akademischen Grades

Doktor – Ingenieur (Dr.-Ing.)

genehmigte Dissertation

vorgelegt von

Frau MSc.-Eng. Aisha Ahmad Naddaf

aus Nablus –Palästina

Eingereicht am: 29 Juni 2011
Mündliche Prüfung am: 30 April 2012

Promotionskommission:
Vorsitzender: Prof. Dr.-Ing. Alois K. Schlarb
Referenten: Prof. Dipl.-Ing. Dr. techn. Hans-Jörg Bart
Prof. Dr.-Ing. Matthias Kind

Dekan: Prof. Dr.-Ing. Bernd Sauer

D 386

Kaiserslautern, 2012

DEDICATION

The research work of this thesis was carried out at the TU Kaiserslautern, in the Chair of Separation Science and Technology, during the years 2006-2010. Part of the research was performed in close cooperation with the University of Chemical Technology and Metallurgy, in Sofia, Bulgaria. I would like to thank Prof. Hans-Jörg Bart for the opportunity of studying this interesting and challenging research work and for supervising this dissertation. I would also like to thank Prof. Tsibranska for her ideas and cooperation. Furthermore, I wish to thank my colleagues and the staff of the department of Separation Science and Technology for the pleasant working atmosphere. I would also like to thank the friends who made the years of my study so special and the teachers who taught me along more than twenty five year of my life. From my heart, I wish to give the warmest thanks to my parents Fatima Naser and Ahmad Naddaf, my brothers, my sisters, and my husband Dipl.-Ing. Soufiene Krimi for their patience, trust, and support. And to Allah is praise, at the first and at the last.

Kaiserslautern, 2012

Aisha Ahmad Naddaf

This dissertation is dedicated

to

my parents

ACKNOWLEDGMENTS

The Deutsche Forschungsgemeinschaft (DFG) is acknowledged for supporting this work financially.

ABSTRACT

Hydrogels are known to be covalently or ionic cross-linked, hydrophilic three-dimensional polymer networks, which exist in our bodies in a biological gel form such as the vitreous humour that fills the interior of the eyes. Poly(*N*-isopropylacrylamide) (poly(NIPAAm)) hydrogels are attracting more interest in biomedical applications because, besides others, they exhibit a well-defined lower critical solution temperature (LCST) in water, around 31–34°C, which is close to the body temperature. This is considered to be of great interest in drug delivery, cell encapsulation, and tissue engineering applications. In this work, the poly(NIPAAm) hydrogel is synthesized by free radical polymerization. Hydrogel properties and the dimensional changes accompanied with the volume phase transition of the thermosensitive poly(NIPAAm) hydrogel were investigated in terms of Raman spectra, swelling ratio, and hydration. The thermal swelling/deswelling changes that occur at different equilibrium temperatures and different solutions (phenol, ethanol, propanol, and sodium chloride) based on Raman spectrum were investigated. In addition, Raman spectroscopy has been employed to evaluate the diffusion aspects of bovine serum albumin (BSA) and phenol through the poly(NIPAAm) network. The determination of the mutual diffusion coefficient, D_{mut} for hydrogels/solvent system was achieved successfully using Raman spectroscopy at different solute concentrations. Moreover, the mechanical properties of the hydrogel, which were investigated by uniaxial compression tests, were used to characterize the hydrogel and to determine the collective diffusion coefficient through the hydrogel. The solute release coupled with shrinking of the hydrogel particles was modelled with a bi-dimensional diffusion model with moving boundary conditions. The influence of the variable diffusion coefficient is observed and leads to a better description of the kinetic curve in the case of important deformation around the LCST. A good accordance between experimental and calculated data was obtained.

KURZFASSUNG

Hydrogele sind kovalente oder ionisch vernetzte, hydrophile, dreidimensionale Polymer netze, die auch in unseren Körpern in einer biologischen Gelform zu finden sind. Ein Beispiel hierfür ist der Glaskörper, der das Innere unseres Auges füllt. Hydrogele aus Poly(N-isopropylacrylamid) (poly(NIPAAm)) finden große Beachtung in biomedizinischen Anwendungen, wegen ihrer klar definierten unteren kritischeren Lösungstemperatur (LCST) um 31-34°C in Wasser, was nahezu der Körpertemperatur entspricht. Folglich sind Hydrogele sehr interessant, zum Beispiel bei der Arzneimitteverabreichung, der Zellenverkapselung und beim „Tissue Engineering“. Das Ziel dieser Arbeit ist es verfahrenstechnischer Eigenschaften selbst synthetisierter Hydrogele unter transienten Bedingungen experimentell und theoretisch zu erforschen. Mithilfe der konfokalen Raman Spektroskopie wurde der Effekt von Temperatur und pH-Wert auf das Verhalten von selbst synthetisierten Poly(NIPAAm) Hydrogelen experimentell untersucht. Basierend auf Raman-Spektren wurde die Abhängigkeit des thermischen Quellens/Schrumpfens bei verschiedenen Temperaturen und Lösungen gemessen (wie z.B. Phenol, Ethanol, Propanol und Natriumchlorid). Mit den Lösungsmittelkonzentrationsprofilen wird das Ad- und Desorptionsverhalten eines Lösungsmittels in einem thermosensitiven Hydrogel charakterisiert. Die Abhängigkeit zwischen der Lösungsmittelkonzentration und der Raman intensität für Poly(NIPAAm) wurde verwendet, um den binären Diffusionskoeffizienten zu berechnen. Außerdem, wurde ein Versuchsaufbau entwickelt um die Diffusions- und die mechanischen Eigenschaften unter realitätsnahen Bedingungen näher zu untersuchen. Für die wärmeempfindlichen Poly(NIPAAm) Hydrogele wurde der gemeinsame Diffusionskoeffizient basierend auf den viskoelastischen Parametern des Hydrogels bestimmt. Die erhaltenen Daten wurden mit einem zweidimensionalen Diffusionsmodell mit variablen Randbedingungen, das auf dem Fick‘schen Gesetz basiert, verglichen. Die erhaltenen Diffusionskoeffizienten erlauben eine gute Beschreibung der Diffusionskinetik.

Table of Contents

1. Introduction 1

1.1. Scope of this work 3

2. Hydrogels: Overview 5

2.1. Classification 5

2.2. Temperature-sensitive hydrogels 5

2.3. Negatively temperature-sensitive hydrogels 6

2.4. Motivation 7

3. Experimental preparation 8

3.1. Materials 8

3.2. Synthesis 8

3.3. Characterization 10

3.3.1. Thermal analysis 11

3.3.2. Variation of the pH value 11

3.3.3. Volume phase transition 11

3.4. Protein loading 19

3.5. Protein release 19

3.6. Time- dependent volume change of the phenol/hydrogel system 20

3.7. Results and discussion 23

3.7.1. Release of phenol at different temperatures 23

3.7.2. Release of phenol at different initial concentrations 25

3.8. Summary 28

4. Raman spectroscopy: hydrogel characterization and experimental set-up.....30

4.1. Principle 30

4.2. Experimental setup 32

4.3. Swelling characterization experiments.....35

4.4. Thermal equilibrium swelling.....37

4.5. Hydrogel thermo reversibility.....39

4.6. Volume phase transition 40

4.7. Results and discussion.....43

4.7.1. Characterization and image analysis.....43

4.7.2. Diffusion coefficient: experimental determination.....44

4.8. Summary 49

5. Mechanical properties: hydrogel characterization and experimental setup 51

5.1. Introduction 51

5.2. Experimental setup 52

5.3. Viscoelastic characterization 54

5.3.1. Mechanical behaviour.....54

5.3.2. Young's modulus 60

5.4. Results and discussion.....64

5.4.1. Collective diffusion coefficient 64

5.5. Summary 69

6. Bi-dimensional moving boundary diffusion model: theory and implementation 71

6.1. Introduction 71

6.2. Protein loading and protein release 74

6.3. Kinetics of shrinking 74

6.4. Release kinetics 77

6.5. Modelling 79

6.5.1. Simulation with constant diffusion coefficient 82

6.5.2. Simulation with variable diffusion coefficient 84

6.6. Summary 86

7. Results in brief 87

7.1. Synthesis and equilibrium swelling 87

7.2. Raman investigations 89

7.2.1. Mutual diffusion coefficient 90

7.3. Mechanical properties 91

7.3.1. Collective diffusion coefficient 93

7.4. Collective versus mutual diffusion coefficient 94

7.5. Transport properties and the mathematical modelling 95

8. Summary 99

9. Symbols 102

10. References 106

APPENDIX A: Materials and Chemicals 120

APPENDIXB: Hydrogel Synthesis 122

APPENDIX C: Experimental Data 124

APPENDIX D: Hydrogel Characterization 128

APPENDIX E: Drug Release Data 132

APPENDIX F: Mechanical Properties Data 139

APPENDIX G: Collective Diffusion Coefficient Program 148

APPENDIX H: Bi-Dimensional Diffusion Model.....149

List of own Publications.....151

International Contributions 153

Supervised Undergraduate Projects.....155

Curriculum Vita 156

Transient Processes with Hydrogels

1. Introduction

Solving health disorder and problems of diseases are not anymore professional without combining the traditional treatment procedure with material and molecular science. The biomedical materials, which provide the clinical fields with wide applications for dressing wounds, drug release, blood oxygenators, heart valves, vascular grafts, kidney dialyzers, etc., are found in 8,000 different medical devices and 40,000 different pharmaceutical preparations [Roorda et al., 1986, Langer and Pappas, 2003, Zhang et al., 2004,Son et al. 2006]. Such materials usually contain therapeutic or diagnostic systems in contact with biological fluids. Chemical engineering has played a remarkable role in developing polymers as biomedical carriers, which could be encapsulated, or immobilized, with drugs, allowing the drug to reach a required site safely. These hydrophilic three-dimensional polymeric matrices are called *hydrogels*. They are known for integrity, biocompatibility, network structure, molecular stability, and flexibility. Hydrogels are also known as water containing but water insoluble homopolymers (or copolymer), which are covalently or ionic cross-linked. These three-dimensional networks interact with aqueous media by swelling to some equilibrium value by the retention of the aqueous media in their structures. Hydrogels are also known to be intelligent compatible polymeric networks that have a high absorption capacity during swelling, by which they increase their initial volume several times without losing their original form. In the last two decades, hydrogels have attracted much attention because of their significant properties. In addition, controlling the cross-linking determines the structural nature of the hydrogels and classifies the hydrogel's chemical and physical structure. The physical crosslinkage can be found as polymer chain entanglements, crystallites, or physical weak associations, such as van der Waals forces, ionic interactions, hydrophobic interactions, or hydrogen bonds [Jen et al., 1996, Peppas et al., 2000]. Therefore, the physical networks have transient junctions, whereas the chemically crosslinked networks have permanent junctions. Besides, they are also considered as stimulus responsive materials, which interact with the external stimuli by swelling and deswelling. These stimuli sensitive materials (SSM) undergo

reversible and discontinuous volume changes in response to changes in environmental conditions, such as temperature [Tanaka, 1978, Hong and Bae, 2002, Bignotti et al., 2004], pH value [Sudipto et al., 2002], ionic strength [Engish et al., 1996], light irradiation [Mamada et al., 1990, Bhardwaj, 2003], composition of the gel network [Dagani, 1997], solvent composition [Quinn and Grodzinsky, 1993], and the applied electric field [Doi et al., 1992, Whiting et al., 2001, Osada and Hasebe, 1985, Kishi and Osada, 1989, Nge et al., 2002]. Based on the application, one may orientate the behaviour of the hydrogels by adding some additives to control the pendent group and end up with a neutral or ionic structure; in other words, their composition can be tuned to exhibit large volumetric swelling in response to a variety of environmental stimuli [Hudson and Zhang, 2001]. In this case, they switch their physicochemical properties in response to external stimuli, i.e. 'environmental switchable materials' [Kim et al., 2003]. Due to such properties of the 'intelligent' polymers, their phase transitions accompany volume changes [Hirotsu et al., 1987]. Due to their integrity, biocompatibility, and degradability, hydrogels have been given a vast potential of applications in food additives, pharmaceutical polymers technology, biotechnology industry, environmental problems, engineering material science, and clinical applications fields. In the medicine technique, hydrogels are not only confined to drug delivery but they also can be used to produce soft contact lenses [Hiratani and Alvarez-Lorenzo, 2002, Beek et al., 2008, Ali et al., 2007, Santos et al., 2007], medical dressings [Quarfoot et al., 1990], biosensors [Iveković et al., 2004], artificial skin [Takahara et al., 1997], artificial heart valves [Jiang et al., 2004], and artificial muscles [Moa et al., 2005]. Furthermore, hydrogels are also found in numerous applications such as solid-phase extraction [Ansell et al., 1996] or chromatographic separation [Yoshida et al., 2000].

Temperature-sensitive hydrogels are probably the most commonly studied class of stimuli responsive polymer systems. N-isopropylacrylamide (NIPAAm) based hydrogels (poly(NIPAAm)) respond to temperature change by undergoing reversible phase transition [Bignotti et al., 2004, Tanaka, 1978]. Due to their well-defined lower critical solution temperature (LCST) in water (around 31-34°C), which is close to the body temperature, [Hirotsu et al., 1987, Sayil and Okay, 2000, Ratner et al., 2004, Peppas, 2004, Ding et al., 2006,

Naddaf and Bart, 2008], poly(NIPAAM) hydrogels are attracting more interest in biomedical applications. In addition, under the low critical solution temperature (LCST), they undergo a reversible phase transition from a swollen (hydrated) state to a shrunken (dehydrated) state, by which they lose about 90% of their mass [Naddaf and Bart, 2008]. In this case, at least one component of the polymer system should possess a temperature dependent solubility in a solvent [Amiya et al., 1987]. Also, poly(NIPAAm) hydrogels have been attracting more and more interest for their use in processing agricultural products [El Sayed et al., 1991], sensors [Galino et al., 2005], actuators [Linden et al., 2004], and for their use in separation processes of polymer molecules from aqueous solutions [Freitaz, 1987]. Moreover, they are excellent bioadhesives; they can adhere to mucosal linings within the gastrointestinal tract for extended periods, releasing their encapsulated medications slowly over time. Therefore, they are considered to be of great interest and have been intensively studied with respect to biomedical application and medical techniques, like drug delivery [Gutowska et al., 1992, Chung et al., 1999], cell encapsulation and tissue engineering applications [Stile and Healy, 2002], production of soft contact lenses [Ali et al., 2007], medical dressings [Quarfoo et al., 1990], biosensors [Iveković et al., 2004], artificial skin [Takahara et al., 1997], artificial heart valves [Jiang et al., 2004], and artificial muscles [Mao et al., 2005].

1.1.Scope of this work

The aim of this dissertation is to investigate, experimentally and theoretically, the transient processes in hydrogel. The thermosensitive poly(N-isopropylacrylamide) (poly(NIPAAm)) hydrogel was synthesized by free radical polymerization with different cross-linking ratios. It was used to study the release kinetics of BSA and phenol by thermal deswelling at different temperatures around the LCST. The solvent released through the hydrogel was modelled using a two-dimensional diffusion model with moving boundaries.

At early stages of the project, poly(NIPAAm) hydrogel was investigated experimentally to find out the effect of temperature, pH, solvent concentration, and solvent composition on the

hydrogel behaviour, i.e., the swelling reversibility. The dimensional changes accompanied with the volume phase transition of the thermosensitive poly(NIPAAm) hydrogel based on changing the diffusion and equilibrium parameters were investigated closely. Moreover, characterization of the presented hydrogel using Raman spectroscopy was performed. The effect of the hydrogel shrinking process on the drug release also has been discussed.

To achieve the goal of the research, two experimental setups were designed. The first (uniaxial compression apparatus) was designed to measure the viscoelastic properties of the cylindrical hydrogels as a function of their dimensions, swelling ratio, equilibrium temperature, and diffused solvent. In addition, this uniaxial compression apparatus was used to successfully determine the collective diffusion coefficient (D_{col}) for the moving boundary thermosensitive poly(NIPAAm) hydrogels swelled to equilibrium in a solvent. From the uniaxial compression apparatus, the collective diffusion coefficient was calculated using the correlation developed by Tanaka [Tanaka et al., 1973]. In addition, Raman spectroscopy was used as a modern non-destructive method to investigate the hydrogel und to determine the mutual diffusion coefficient (D_{mut}) in thermo-sensitive poly(NIPAAm) hydrogels.

Part of this doctoral thesis project was done in close cooperation with the University of Chemical Technology and Metallurgy, in Sofia, Bulgaria to develop a bi-dimensional diffusion model with moving boundary conditions describing the solvent release through the hydrogel.

In the first main chapter of this dissertation, a short introduction identifies the related topic and the required details of theory, experiment, and results. In the next Chapter, an overview about hydrogels is summarized. The synthesis and characterization of poly(NIPAAm) is given in Chapter 3. The characterization of hydrogel using Raman spectroscopy is introduced in Chapter 4. The mechanical properties of hydrogel and the corresponding experimental setup and data analysis are given in Chapter 5. Chapter 6 deals with the bi-dimensional diffusion model, and finally, Chapter 7 shows results of these simulations. Conclusions are given in Chapter 8.

2. Hydrogels: Overview

2.1. Classification

Gels that swell (or shrink) gradually over time were discovered in the latter half of the last century. Hydrogels, which have a definitive phase transition as a response to an external stimulus, were first discovered in 1975 by Toyoichi Tanaka. Even today, after decades of research, the intelligent gels (hydrogels) continue to attract many investigators, including chemists, biologists, and chemical engineers.

Hydrogels can be classified according to many categories. For example, based on the method of preparation, hydrogels are classified as homopolymer hydrogels, co-polymer hydrogels, and multi polymer hydrogels. Based on the nature of the pendent groups, hydrogels can be classified as neutral, anionic, cationic, and ampholytic hydrogels [Peppas et al., 2000]. Hydrogels are also classified based on the physical structure of the network as amorphous hydrogels, semi-crystalline hydrogels, super molecular structures, hydrocolloidal aggregates, and hydrogen-bonded hydrogels [Peppas et al., 2000]. And based on the mechanism controlling the drug release, they are classified as diffusion controlled release systems, swelling controlled release systems, chemically controlled release systems, and environment responsive systems [Peppas et al., 2000]. Finally, and according to external stimuli, hydrogels are classified into several categories, such as pH-sensitive hydrogels, temperature-sensitive hydrogels, and hydrogels reacting according to the electrical field, magnetic field, light irradiation, and solvent concentration [Dolbow et al., 2005].

2.2. Temperature-sensitive hydrogels

Temperature-sensitive hydrogels have the ability to swell or shrink because of temperature change. Therefore, they have received attention for use in drug delivery [Peppas, et al., 2000]. Based on the transition mechanism; these hydrogels can be classified into three categories: negatively temperature-sensitive, positively temperature-sensitive, and thermo-reversible gels [Qiu and Park, 2001].

If the hydrogel shrinks and releases solvent from its matrix at temperatures below the upper critical solution temperature (UCST), then the hydrogel is known as positively temperature-

sensitive hydrogel. Interpenetrating polymer network hydrogels (IPNs) are mostly known to have positive temperature dependency. The thermo-reversible gels, such as poly (vinyl chloride) and polyacrylates with discotic side-chains, undergo sol-gel phase transitions instead of swelling-shrinking transitions. In contrast to the positively temperature-sensitive hydrogels, the swelling behaviour of negative hydrogels is attributed to the lower critical solution temperature (LCST). In their case, a temperature above LCST results in a shrinking of the hydrogel structure.

2.3. Negatively temperature-sensitive hydrogels

Negatively temperature-sensitive gels shrink as the temperature of the surrounding solution increases above LCST and swell at lower temperatures. Poly(N-isopropylacrylamide) (Poly(NIPAAm)) is the most well-known example of a negatively temperature-sensitive hydrogel; it is composed of polymer chains that have both hydrophobic and hydrophilic domains below and above the LCST. Below the LCST, the isopropyl groups are surrounded with water, which interacts with the side chains through hydrogen bonds between water molecules and the hydrophilic parts, causing swelling [Robert, 2010, Zhang and Peppas, 2000]. However, above the LCST, the hydrophobic groups are in contact with both water and polymer segments [Robert, 2010], by which the hydrophobic interactions among hydrophobic segments become stronger compared to the hydrogen bonds. These interactions cause an inter-polymer chain association that results in the shrinking of the hydrogels [Qiu and Park, 2001]. The LCST could be controlled by increasing hydrophobic constituents in the polymeric chains, e.g., by adding small amounts of ionic copolymers in the gels [Yu and Grainger, 1993] or by changing the solvent composition [Suzuki et al., 1996]. On the other side, increasing the hydrophilic content in the copolymer network can reduce the poly(NIPAAm) temperature sensitivity [Beltran et al., 1991, Feil et al., 1993].

Negatively temperature-sensitive hydrogels, especially poly(NIPAAm), have LCST ranges between 32^{o}C and 34^{o}C, which is close to the human body temperature. Moreover, the poly(NIPAAm) has properties in common with soft biological materials such as muscles and tendons [Johnson et al., 2002]. Therefore, these hydrogels have been investigated intensively for various possible biomedical and pharmaceutical applications, such as contact lenses,

membranes for biosensors, linings for artificial hearts, materials for artificial skin, and drug delivery devices [Peppas and Langer, 1994, Walther et al., 1995, Chung et al., 1999, Peppas et al., 2000, Melekaslan et al., 2003]. For such load bearing applications, the mechanical properties of hydrogels are of great importance, i.e., the optimal hydrogel should be relatively strong yet elastic.

2.4. Motivation

The objectives of this research are to:

(1) characterize the self-synthesis thermosensitive poly(NIPAAm) hydrogels,

(2) determine the diffusion coefficient for the poly(NIPAAm) hydrogels, and

(3) investigate the relationship between the hydrogel properties and the release performance and compare it to model simulations.

3. Experimental preparation

3.1. Materials

As a monomer, N-isopropylacrylamide [NIPAAm, H_2C $CHCONHCH(CH_3)_2$] (Aldrich >97%) was used without any further modifications. N,N-methylenbisacrylamide [MBA, $(CH_2CHCONH)_2CH_2$] (Aldrich >99.5%) was functioned as a crosslinking monomer. The initiators, sodium metabissulfite [NaDS, $Na_2O_5S_2$] (Aldrich >98%) and ammoniumperoxodisulfat [APS, $(NH_4)_2S_2O_8$] (VWR >98%), were used as received. As a drug example, the slightly yellow leafs type of bovine serum albumin [BSA] protein (Merck, >98%) was used to prepare the required BSA solutions. In addition, aqueous phenolic solutions [C_6H_5OH] (MERCK, >98%) were used as a drug example (Appendix A).

3.2. Synthesis

The polymerization and the cross-linking of the non-ionic hydrogel were achieved by free radical polymerization at 25°C under oxygen-free conditions. Solutions of NIPAAm and MBA (about 70g) were prepared using deionized water and mixed together. In addition, 20mg of APS and 20mg of NaDS were dissolved separately into 25ml of deionized water. The two solutions were purged for approximately five minutes with nitrogen to expel the dissolved oxygen. Then, they were mixed together in a 100ml mixer for three minutes with stirring at 40 rpm. After mixing, the polymerized solution was filled to the neck into small glass vessels (20ml), which were immediately closed after filling to avoid any contact to the ambient air. After that, the glass vessels were stored in a water bath at 25°C for 24 hours to achieve complete polymerization. After the predefined time, the gel was removed smoothly from the glass vessel and cut into small cylinders. The small cylindrical hydrogels were each set in a separated stead in a six-well dish. Each of the hydrogel samples was washed with deionized water for about seven days to remove the non-reacted materials [Naddaf and Bart, 2008].

1. Thermostat

2. Mixer

3. Dropping funnel

4. Electric motor

5. Washing flask

6. N_2 supply

7. Vacuum pump

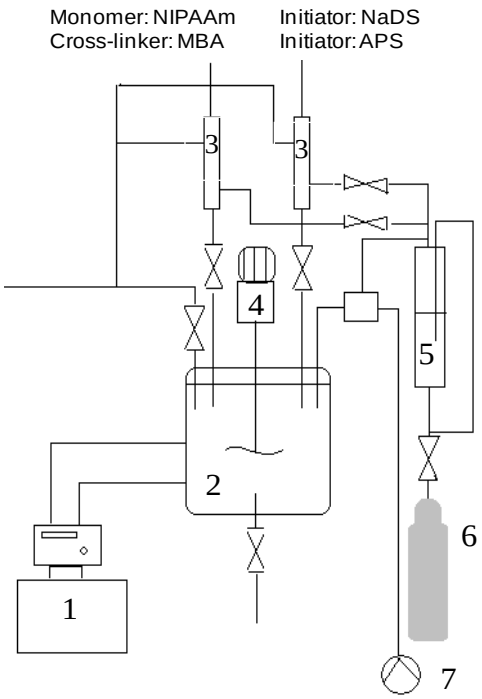

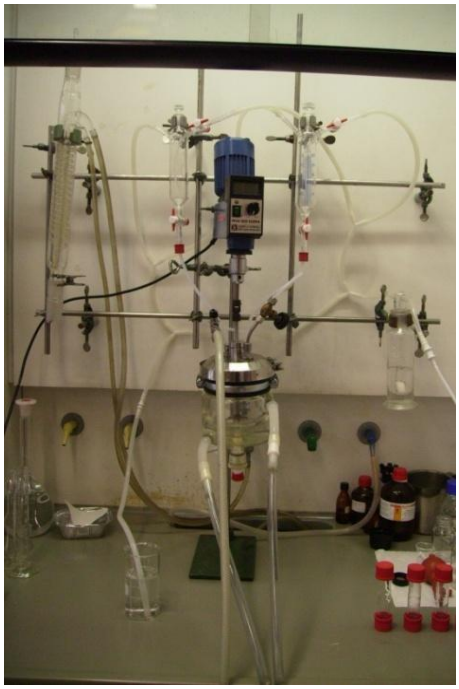

Fig. 3.1: The system used to synthesis poly(NIPAAm)

The synthesized hydrogel was characterized by calculating the hydrogel matrix ratio [Hüther et al., 2006], HMR, which is given by:

$$HNR = \frac{m_{NIPAAm} + m_{MBA}}{\sum m_{tot}}, \text{ where } m_{tot} = m_{NIPAAm} + m_{MBA} + m_{H_2O} \tag{3.1}$$

Here m is the mass in [g], the subscripts NIPAAm, MBA, tot., and H_2O refers to N-isopropylacrylamide, N,N-methylenbisacrylamide, total mass and water respectively. The acceptable matrix ratio should be within the range of 0.08 to 0.12 [Hüther et al., 2006]. In this work, poly(NIPAAm) hydrogels of different molar cross-linking ratio, y_{MBA} of 0.0115, 0.0136, 0.0168, and 0.025 with a matrix ratio of 0.11 were synthesised using the system shown in Fig. 3.1. Based on the cross linking ratio, four kinds of hydrogels were produced, as given in Table 3.1 (Tables B.1-B.4 appear in Appendix B).

Table 3.1: The four kinds of tested hydrogels based on the cross linking ratio

	m_{NIPAAm}/m_{MBA}	y_{MBA}
Hydrogel_1	63	0.0115
Hydrogel_2	53	0.0136
Hydrogel_3	43	0.0168
Hydrogel_4	33	0.025

After the synthesis, the hydrogel underwent several steps of cutting and washing before drying, as mentioned in Section 3.2 and Appendix C.

3.3. Characterization

The mass, diameter, and thickness of each hydrogel sample were measured directly after the synthesis. The weight was measured using a digital balance having an accuracy of ± 0.5 mg. Both diameter and thickness were measured using a microscope equipped with a CCD video camera and connected to a computer provided with Grab&View® program to shoot a photo of the sample and Image C® program to measure the sample dimensions accurately. Before rinsing the samples for about seven days, they were separated into different groups, i.e., six samples are included in each individual group. Every group was subjected to different equilibrium conditions by changing one of the swelling control parameters. To check the thermal reversibility of the poly(NIPAAm), each sample was set to the equilibrium twice and the changes in the hydrogel's behaviour were indicated after each one. Detailed experimental results are given in Appendix D.

As a next step to characterize the hydrogel, hydrogels were equilibrated at different temperatures using several concentrations of different solutions, including NaCl, NaOH, H_2SO_4, propanol, phenol, and bovine serum albumin (BSA). The hydrogel was then characterized based on several criteria, such as swelling ratio, water uptake, hydration value, and Raman intensity, as will be shown in the next sections.

3.3.1. Thermal analysis

One set of the experiments was performed to investigate the thermal behaviour of poly(NIPAAm). By which, each of the six samples of the poly(NIPAAm) hydrogel was immersed in a large volume of deionized water and sealed in a glass container. The glass containers, which contain the hydrogel, were set to different temperature in a thermostat having temperature control accuracy of ±0.03 K. The thermal swelling was conducted at equilibrium temperatures of 25°C, 30°C, 32°C, 34°C, 40°C, and 50°C. Measurements of the dimensions (diameter and thickness) and the weight of the cylindrical poly(NIPAAm) hydrogel were taken [Naddaf and Bart, 2008].

3.3.2. Variation of the pH value

Another set of experiments was performed to investigate the effect of the solution pH surrounding the poly(NIPAAm). Five samples of the hydrogel were sealed in glass containers filled with basic solution of NaOH, and another five samples were immersed in an acidic solution of H_2SO_4; all were surrounded by a temperature-controlled bath held at 25°C. The buffered solutions from both NaOH and H_2SO_4 were diluted to the required concentrations using deionized water and varied in pH values between 0.45 and 12 [Naddaf and Bart, 2008].

3.3.3. Volume phase transition

For studying the equilibrium swelling ratio, poly(NIPAAm) hydrogels were weighed in their dried state and again after equilibrium at different temperatures between 25ºC and 40ºC, which covers the expected range of their LCST. The samples were subjected to the equilibrium conditions for seven days. Then, the swelling ratio, q, was determined according to the following equation:

$$Swelling\ Ratio = \frac{W_s}{W_d} \tag{3.2}$$

where W_s is the weight of hydrogel after equilibrium and W_d is the weight of dried hydrogel. Fig. 3.2a and Fig. 3.2b show the variation of the swelling ratio with temperature for different concentrations of phenol and BSA, respectively. In addition, they show that swelling curves measured for hydrogels at different temperatures follow similar profiles, i.e., the swelling ratio decreases by increasing the temperature [Naddaf and Bart, 2011-b].

All of the poly(NIPAAm) hydrogels' cylinders, which were allowed to swell to equilibrium in different solutions, underwent a sharp volume change by temperature elevation to reach their minimum size below the LCST (Fig. 3.2). Regardless of the initial concentration of the phenol in hydrogel, all tested hydrogel cylinders collapsed into a similar network structure at a temperature above the LCST [Zhang et al., 2004].

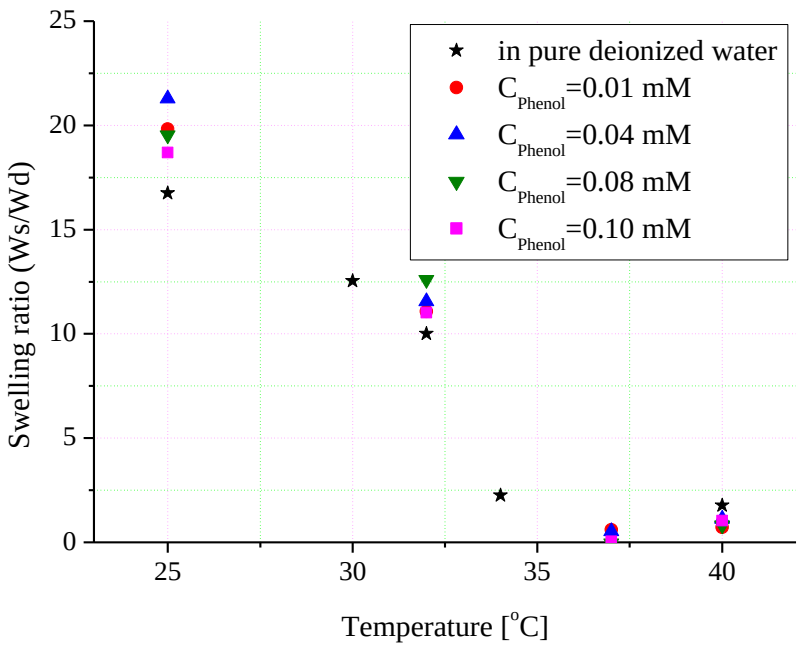

Fig. 3.2a: The swelling ratio of poly(NIPAAm) hydrogel_2 equilibrated at varied temperatures in phenol solutions of different initial concentrations [Naddaf and Bart, 2011-b]

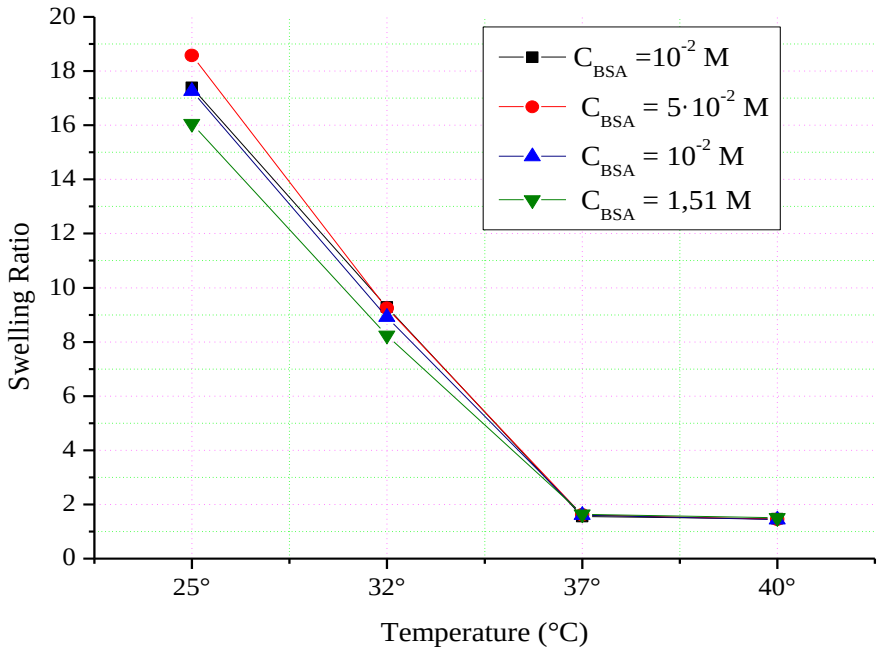

Fig. 3.2b: Variation of the swelling ratio with temperature for poly(NIPAAm)/BSA system

In case of swelling in pure deionized water, the hydrogel follows a continuous thermo-shrinking volume transition (Fig. 3.3) due to the effect of the entropy contribution; the reduction in the chemical potential of water molecules occurs by increasing the temperature [Kawasaki et al., 1996]. This continuous volume change is expected to vanish when increasing the concentration of phenol solution [Hirotsu et al., 1987]. The effect of the phenol molecules on the volume phase transition of the hydrogel was drastic due to the benzene ring, which plays a significant role in modifying the order structure of the bulk water. In addition, the phenol molecules enhance the formation of a hydrogen-bonded structure. The network basic structure in the layer, which surrounds the individual phenol molecules, differs from the tetrahedral structure of bulk water [Naddaf and Bart, 2011-b].

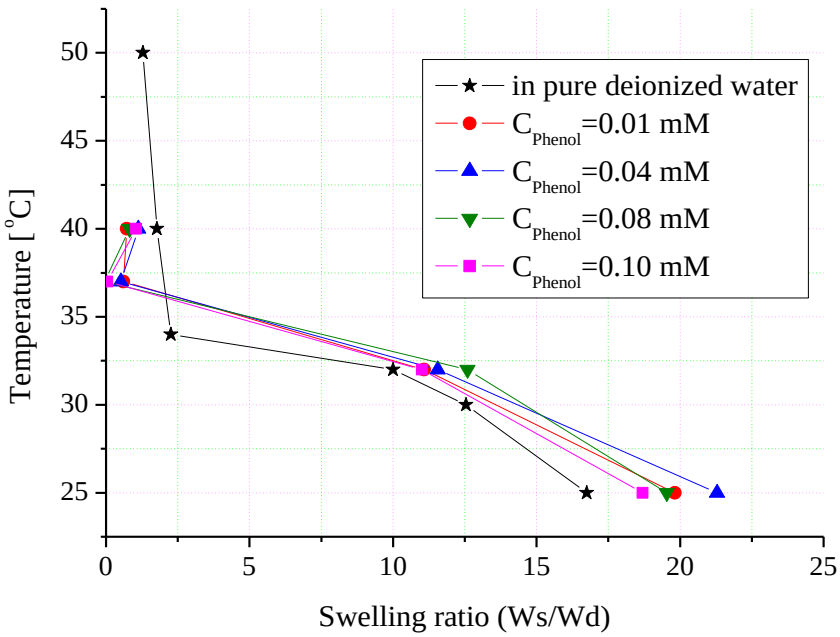

Fig. 3.3: The swelling ratio of poly(NIPAAm) hydrogel_2 equilibrated at varied temperatures in phenol solutions of different concentrations (Continuous lines are trend lines) [Naddaf and Bart, 2011-b]

The swelling equilibrium curves measured for hydrogels of different cross-linking ratios are shown in Fig. 3.4 [Naddaf and Bart, 2011-b]. Exceeding a certain threshold of the phenol concentration in the water eliminates the effect of the cross-linking ratio on phase transition. The appearance of the hydrogen bond influences the network structure [László et al., 2003]. The phenol concentration plays a role in altering the OH group, which can act as a proton donor or acceptor [László et al., 2003]. More about the effect of phenol on the thermosensitive hydrogel is available elsewhere [Kosik et al., 2007].

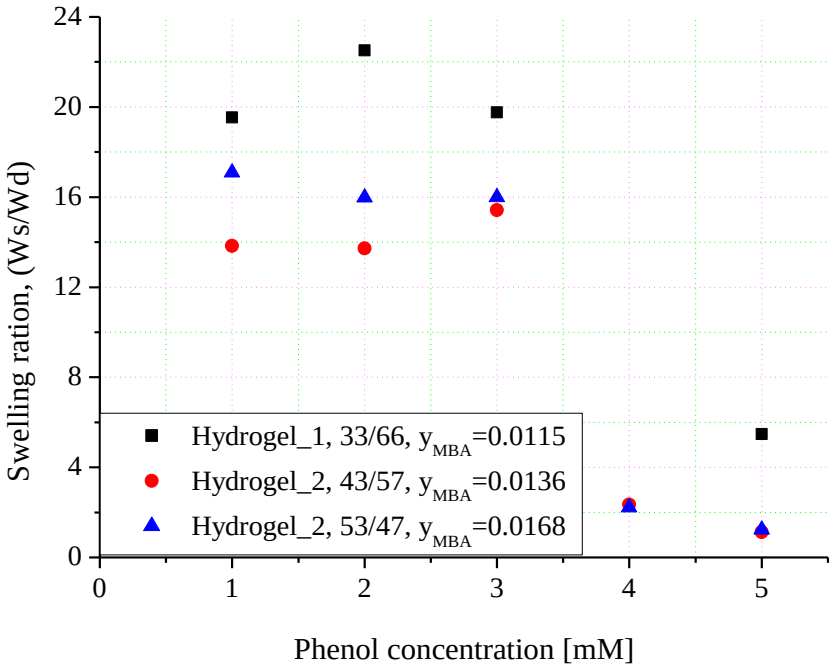

Fig. 3.4: The swelling ratio of poly(NIPAAm) hydrogel of different monomer concentration at 25°C as a function of phenol concentration [Naddaf and Bart, 2011-b]

According to our present work, at 25°C the phase transition is accompanied by a reversible volume and mass change for all tested phenol concentrations (see Fig. 3.5). This indicates that the high concentration of the phenol could have a temporary effect on the lattice by modifying the water-hydrogel interaction during the swelling at 25°C [Naddaf and Bart, 2011]. This effect, which is directly related to the hydrogen-bonded contribution, is supposed to disappear, by drying, without damaging the internal structure of the hydrogel or changing its swelling properties in the short term. This change in the local environment of the polymer is not expected at higher temperatures because the concentrated phenol solution lowers the LCST for the NIPAAm [László et al., 2003, Otake et al., 1990], which is accompanied by enthalpy reduction [Kosik et al., 2007]. This assumption is validated in this work using Raman spectroscopy (Chapter 4). Nevertheless, it is interesting here to mention that significant changes inside the hydrogel lattice are happening by increasing the concentration of phenol. Such changes were not observed when using other solutes, such as NaCl, NaOH, H_2SO_4, propanol,

and BSA for the tested concentrations, available in Appendixes C and D. Therefore, phenol was used in this work, preferably as a drug example.

The water uptake, which was calculated according to equation (3.2), follows the same trend as the swelling ratio (see Figures 3.5a and 3.5b) as a function of temperature change.

$$Water\ uptake = \frac{W_s - W_d}{W_d} \times 100 \qquad (3.2)$$

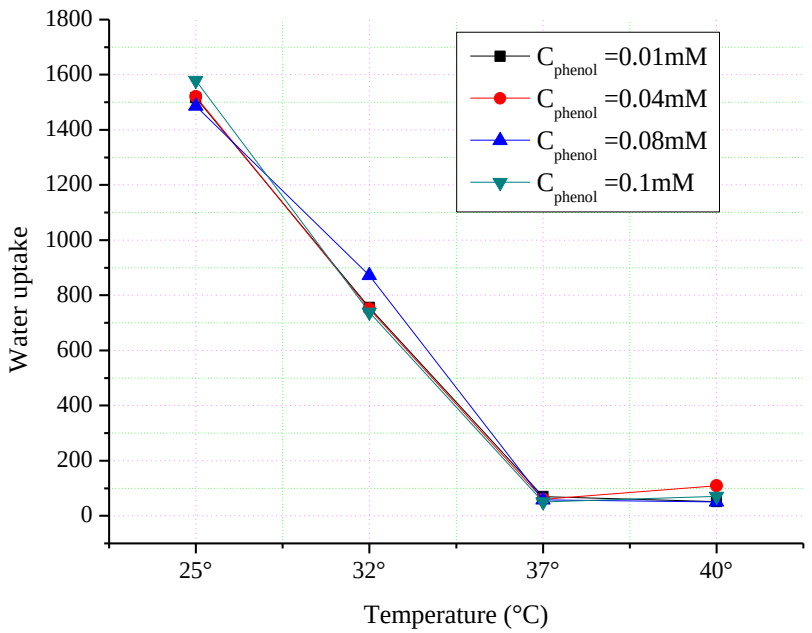

Fig. 3.5a: Water uptake changes with temperature for different concentrations for poly(NIPAAm)/phenol system

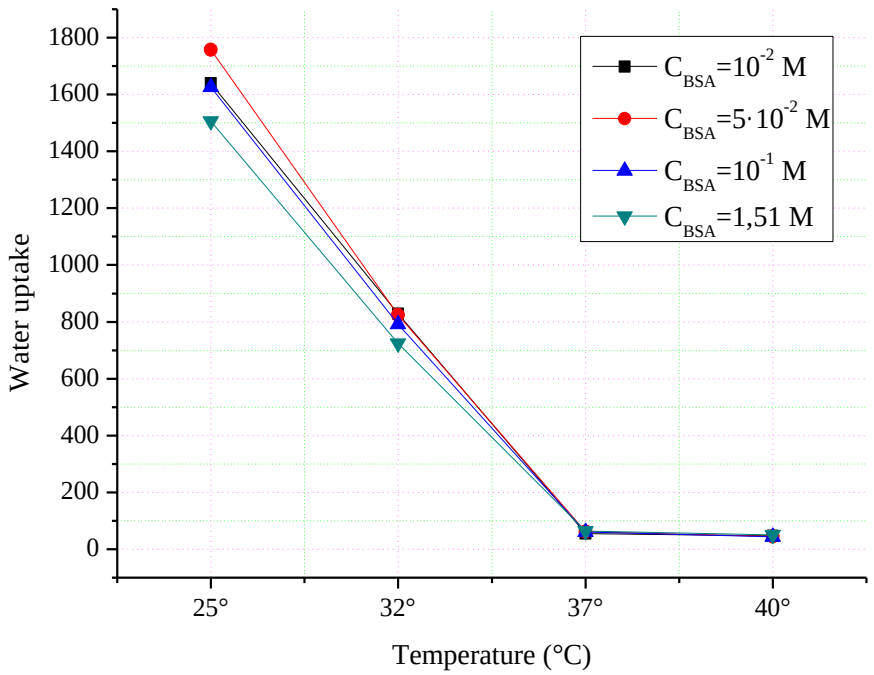

Fig. 3.5b: Water uptake changes with temperature for different concentrations for poly(NIPAAm)/BSA system

Increasing the external temperature from 25ºC to 40ºC will release the solution from the hydrogel, and this release is controlled by the diffusion coefficient. The swelling ratio (and water uptake) decreased sharply with temperature elevation from 25ºC to 32ºC and decreased slowly from 37ºC to 40ºC (Figures 3.5a-b). Changing the hydrogel dimensions with temperature elevation can be presented in terms of hydration:

$$Hydration\ value = \frac{t_s d_s^2 - t_d d_d^2}{t_d d_d^2} \qquad (3.3)$$

where t_s and d_s are the heights and the diameter of the swollen hydrogel cylinder at equilibrium, respectively; t_d and d_d are the thickness and the diameter of dried hydrogel. The variation of the hydration with temperature change for poly(NIPAAm)/drug example is given in Figures 3.6a and 3.6b.

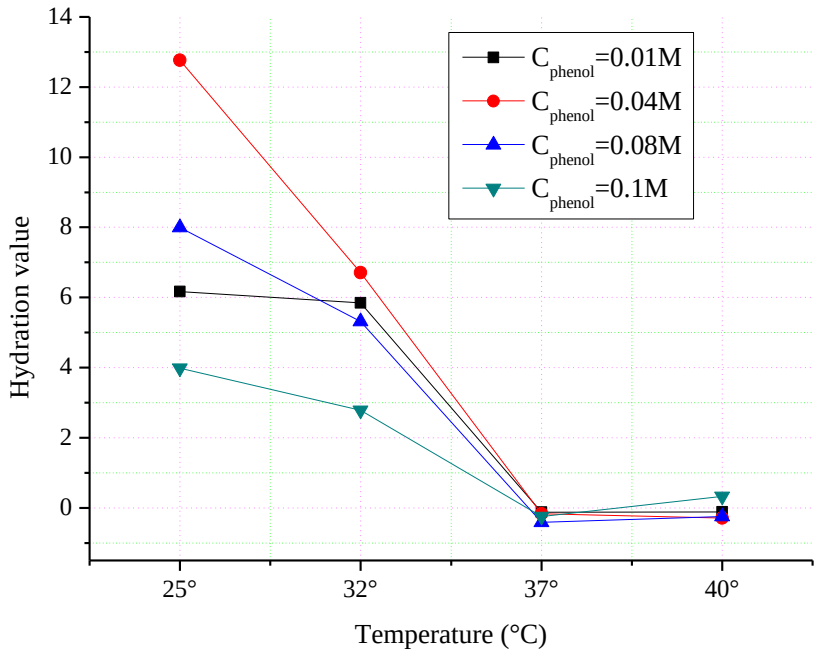

Fig. 3.6a: Variation of the hydration with temperature for poly(NIPAAm)/phenol system

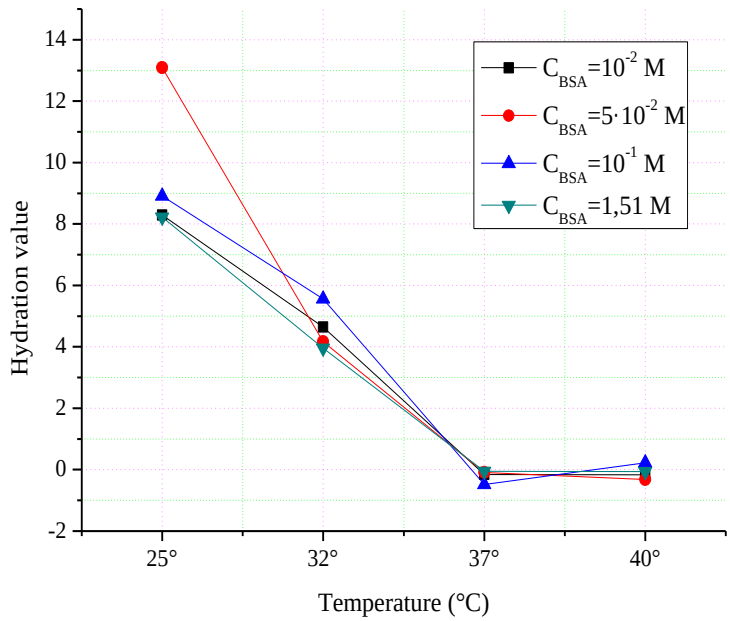

Fig. 3.6b: Variation of the hydration with temperature for poly(NIPAAm)/BSA system

3.4. Protein loading

After the synthesis and sample preparation (section 3.2), the hydrogels were weighted and their dimensions were measured. Swelling equilibrium method was used to load drug examples (BSA and phenol; separately) into poly(NIPAAm). Four different dried cylindrical samples of poly(NIPAAm) hydrogel were immersed in an excess volume of BSA solution (15 ml) and sealed in separate glass containers. They were allowed to swell in the drug solution (i.e., the drug was absorbed into the network of the self-fabricated dried non-swollen hydrogel) of known concentration for 72 h at 25°C. Thus, BSA was loaded into each hydrogel particle up to equilibrium by swelling in the BSA-containing solution and the BSA-loaded hydrogel samples were dried at room temperature and at atmospheric pressure for about 48 hours until constant weights were reached. Then, they were used for release kinetics study. The same loading procedure was followed to load hydrogel samples with phenol.

For the release experiments, the used phenol solutions were prepared with the concentrations 0.01mM, 0.04mM, 0.08mM, and 0.1mM, from a solution of 1g phenol/100ml H_2O (0.1M). Similarly, the used BSA solutions were prepared with the concentrations 0.01M, 0.05M, 0.10M, and 1.51M, from a BSA mother solution of 0.9998mg BSA/100ml H_2O (1.51M).

3.5. Protein release

The loaded hydrogel samples were then used for in vitro release studies. After reaching the equilibrium state, the loaded hydrogels were weighed and their dimensions were measured. Then, the samples were dried again at room temperature for 1-2 days to ensure complete dryness. After that, the samples were weighed and the dimensions were measured again. A calibration curve was determined by measuring the absorbance of BSA prepared solutions using UV spectrophotometer (Shimadzu UV-160A, UV-visible recording spectrophotometer) at wavelength, λ of 277 nm [Naddaf and Bart, 2011-b]. The data of the calibration curve are given in Appendix E. Using equation (3.4) the concentration of the drug example can be obtained by substituting the value of absorbance, A, measured by UV-VIS.

$$\text{Conc.} = \frac{A}{4.289} \tag{3.4}$$

To investigate the effect of the temperature-sensitive property of the poly(NIPAAm) hydrogel on protein release profiles, the in vitro release experiments were carried out at different release temperatures of 25°C, 32°C, 37°C, and 40°C. BSA (or phenol) release experiments were conducted by immersing the BSA-loaded (or phenol-loaded) hydrogel samples in glass beakers filled with 15ml of deionized water (pH 5) at 25°C (below LCST), 32°C (around the LCST), and 37°C and 40°C (above the LCST). The temperature was controlled with an accuracy of 0.03 K, and the containers were covered with PARAFILM® paper, thereby avoiding exposure of the solution to the ambient air that can eliminate the evaporation of the solution. At a fixed period of time, 2 ml of the aliquot release medium were taken out from the beaker and the concentration of the BSA (or phenol in case of phenol-loaded hydrogel) release at that time in the aliquot was measured by UV–VIS spectrophotometer (Shimadzu UV-160A) at 277 nm. At the same time, the hydrogels were removed from the glass beaker and were photographed to measure their dimensions. This procedure was repeated for 48 hours until reaching a constant release concentration of the drug sample and constant dimensions of the hydrogels, i.e., equilibrium state (Appendix E, Tables E.1-E.8). The samples used were returned to the original medium solution to maintain a constant volume of the surrounding release medium and to keep the overall drug loaded-sample concentration as constant as possible. In this work, the results are presented in terms of molar amount release as a function of time.

3.6. Time- dependent volume change of the phenol/hydrogel system

The dimensional response of the poly(NIPAAm) cylinders to changes in temperatures is governed by diffusion-limited transport of the solution in and out of the polymeric networks [Chu et al., 2007]. Fig. 3.7 shows a comparison of sizes of the evolution of four cylindrical phenol-loaded (loaded phenolic solution has a concentration of 10^{-5} M) hydrogel samples during the diffusion of deionized water at the test of four temperatures. The time t=0 refers to the time at which the diffusion process is initiated through the dried phenol-loaded sample. The t=2880min refers to the time at which the hydrogel cylinder was completely swelled and loaded with phenol at 25°C [Naddaf and Bart, 2011-b]. Around and above the LCST, a hard

shrunken thick layer, which is denser than the bulk matrix, formed on the hydrogel's outer surface. During the initial period of diffusion, this hard layer eliminates the release of phenol from the internal matrix of the hydrogel. In response, the internal pressure inside the hydrogels increases and causes an increase in the shrinking rate. Due to the accumulating of the internal pressure, the hydrogel shrinks at 40ºC faster than it shrinks at 32ºC, and the interior solute is rapidly expelled, causing the lowest cumulative release among the other tested temperatures, consistent with other findings [Kaneko et al., 1995, Naddaf and Bart 2010-b].We found that increasing the internal pressure with time caused swelling in the upper surface of the hydrogel, which formed a hunch at a crack position of the rigid layer. The hunch, which is clear in Fig. 3.6 at T=32°C and t=10 min, serves as a phenol vent zone by swelling and changing its form and volume dynamically over time. Despite these dramatic changes of the upper half of the hydrogel cylinder during the diffusion of water, the lower half retained almost the same dimensions at all tested temperatures during the first 60 minutes of diffusion. Moreover, the shrinking process and kinetics of the gel have been investigated in detail elsewhere [Kaneko et al., 1995, Matsumoto et al., 2004]. The continuous release with time causes a reduction in the internal pressure until the hunch completely disappears. Because this is not the case below the LCST (at 25°C), the swelling and the release rate of gels is relatively slow. At t=2880min equilibrium state is reached, through which the release process is accomplished by reaching a constant concentration of phenol accompanied by a constant volume of systematic cylindrical hydrogel. The hydrogel requires less time to reach its systematic shape at a higher release temperature, e.g., 65 minutes at 40°C compared to 1,380 minutes at 25°C (Fig. 3.7). Moreover, the effect of a higher temperature on shrinking rate and size is remarkable; at the end of the release time (t=2880 min), the volume of the hydrogel subjected to release at 40°C is about 16 times smaller than that at 25°C [Naddaf and Bart, 2011-b].

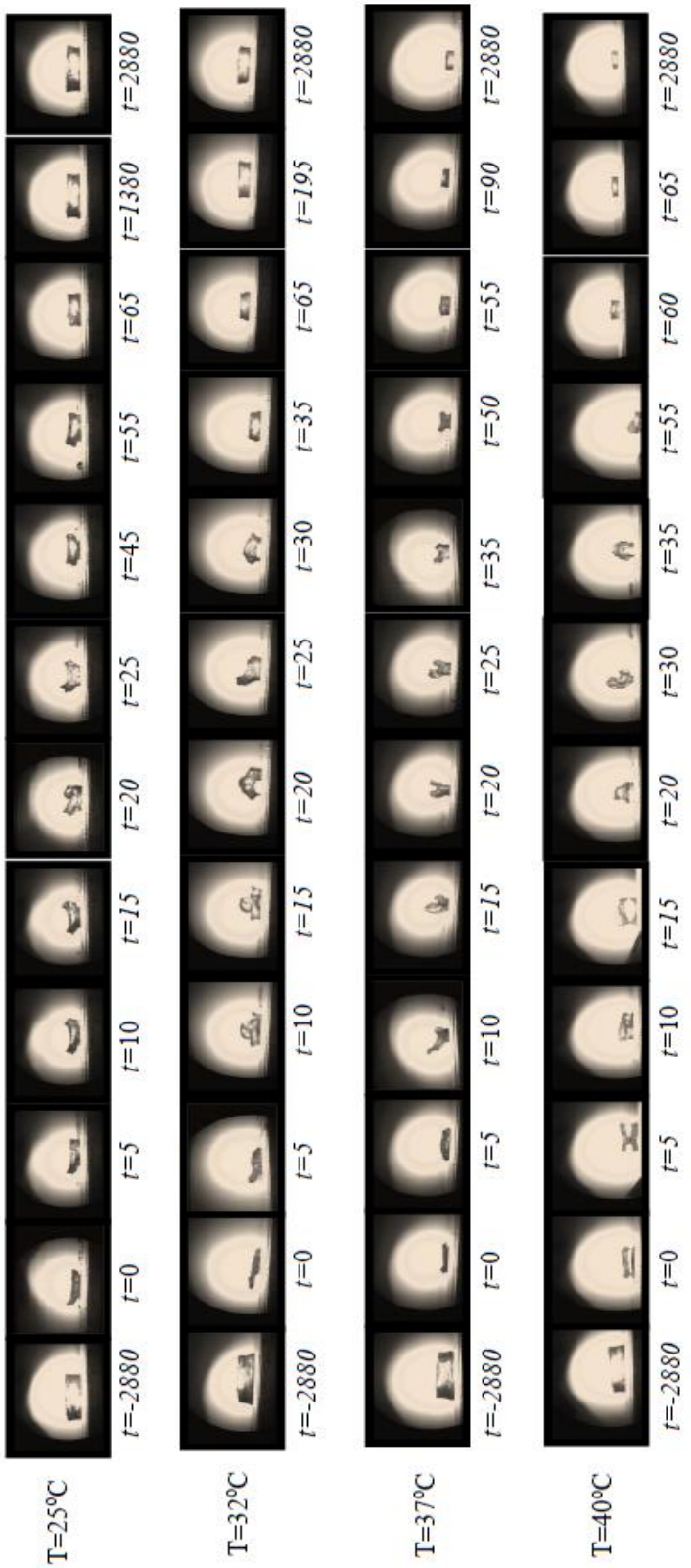

Fig. 3.7: Effect of diffusion on the dynamic volume-shrinking and swelling [Naddaf and Bart, 2011-b]

3.7. Results and discussion

In the case of swelling in pure deionized water, the hydrogels follow a continuous thermo-shrinking volume transition due to the effect of the entropy contribution [Kawasaki et al., 1996]; the reduction in the chemical potential of water molecules by increasing the temperature is shown in Fig. 3.2a and Fig. 3.3. The continuous volume changes are expected to vanish by increasing the concentration of phenol solution due to the presence of the benzene ring, which plays a significant role in modifying the order structure of the bulk water, modifying the hydrogel-water interaction and enhancing the formation of hydrogen bonded structure. At 25°C, the phase transition was accompanied with reversible volume and mass changes for all tested phenol concentrations. This effect was supposed to disappear, by drying, without damaging the internal structure of the hydrogel or changing its swelling properties in the short term. This change in the local environment of the polymer progress is not expected at higher temperatures because the concentrated phenolic solution lowers the LCST for the poly(NIPAAm), which is accompanied by enthalpy reduction and was accurately proven based on Raman spectra, as explained in detail in Chapter 4. The swelling equilibrium curves measured for hydrogels of different cross-linking ratios are shown above in Fig. 3.4. Exceeding a certain threshold of the phenol concentration in the equilibrium water eliminates the effect of the cross-linking ratio on phase transition.

3.7.1. Release of phenol at different temperatures

Fig. 3.8 represents the cumulative amount of released phenol from the poly(NIPAAm) at different temperatures of 25°C, 32°C, 37°C, and 40°C for different initial concentrations of phenol (0.01, 0.04, 0.08, and 0.10 mM) [Naddaf and Bart, 2011-b]. By increasing the initial concentration of phenol, the effect of the temperature (being around the LCST) is eliminated due to the contribution of the phenol ring causing the matrix to collapse. The gel-water interaction modifies due to the reduction in the LCST associated with increasing the phenol concentration [Otake et al., 1990].

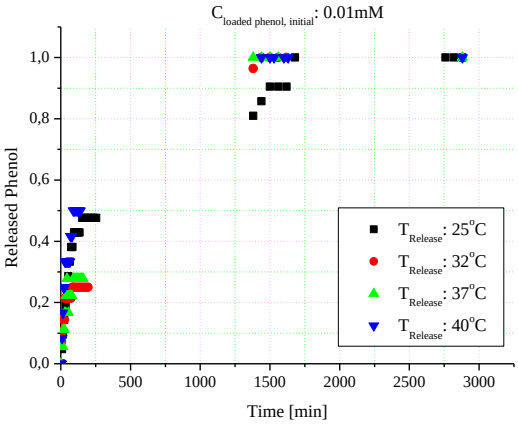
C loaded phenol, initial: 0.01mM
Released Phenol
Time [min]
T Release: 25°C
T Release: 32°C
T Release: 37°C
T Release: 40°C

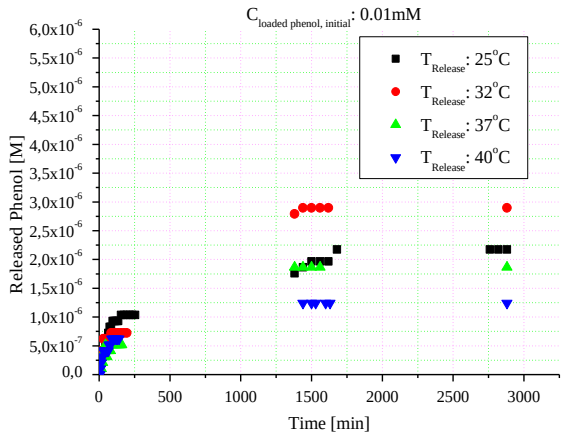
C loaded phenol, initial: 0.01mM
Released Phenol [M]
Time [min]
T Release: 25°C
T Release: 32°C
T Release: 37°C
T Release: 40°C

a

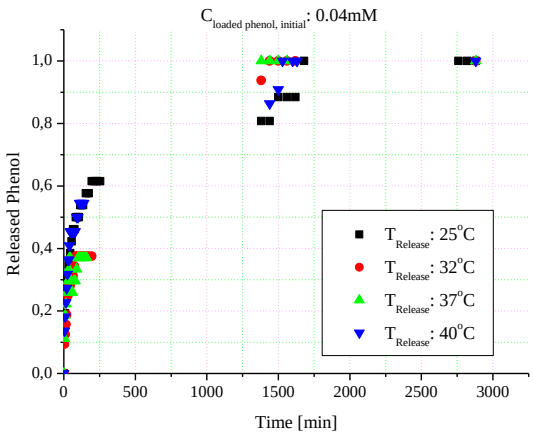
C loaded phenol, initial: 0.04mM
Released Phenol
Time [min]
T Release: 25°C
T Release: 32°C
T Release: 37°C
T Release: 40°C

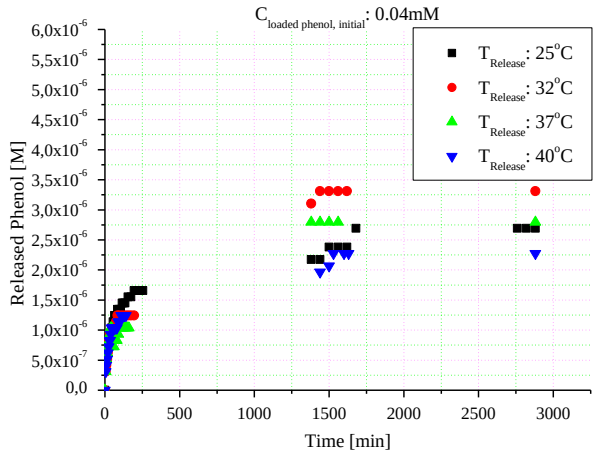
C loaded phenol, initial: 0.04mM
Released Phenol [M]
Time [min]
T Release: 25°C
T Release: 32°C
T Release: 37°C
T Release: 40°C

b

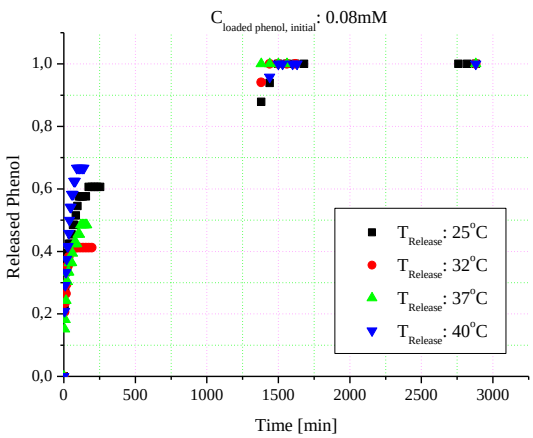
C loaded phenol, initial: 0.08mM
Released Phenol
Time [min]
T Release: 25°C
T Release: 32°C
T Release: 37°C
T Release: 40°C

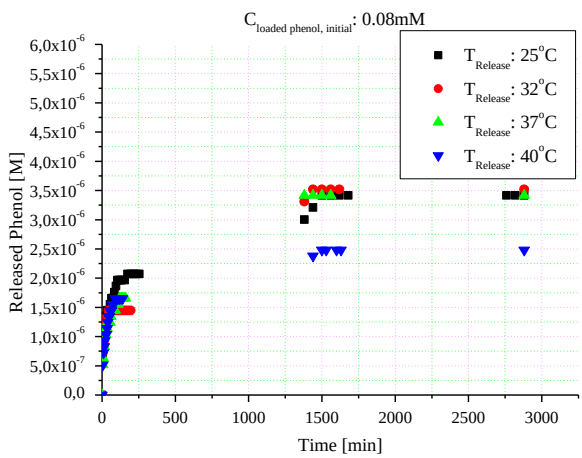
C loaded phenol, initial: 0.08mM
Released Phenol [M]
Time [min]
T Release: 25°C
T Release: 32°C
T Release: 37°C
T Release: 40°C

c

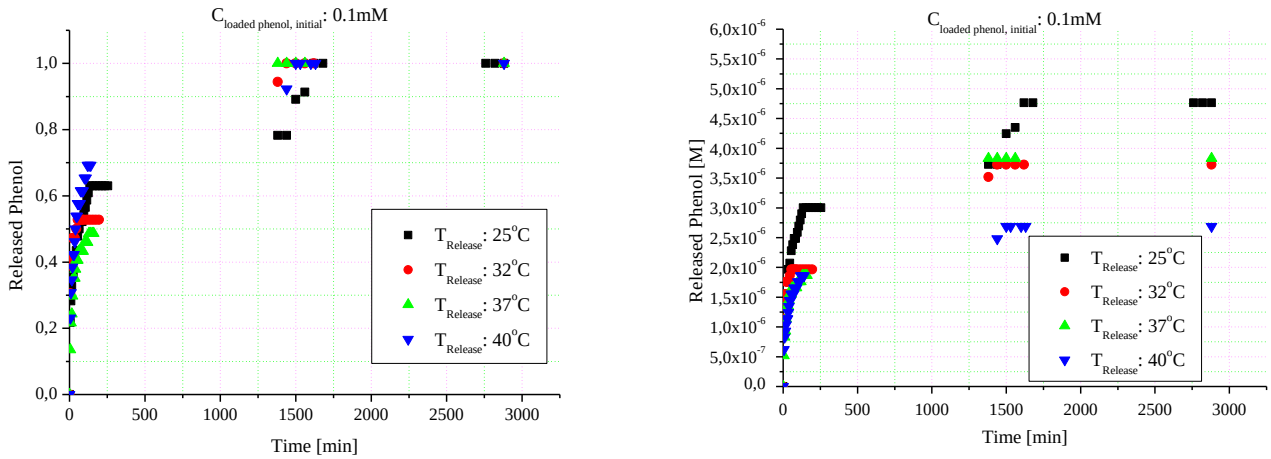

d

Fig. 3.8: Cumulative amount of released phenol from the hydrogel at different temperatures (the initial concentrations of phenol a) 0.01, b) 0.04, c) 0.08, and d) 0.10 mM) [Naddaf and Bart, 2011-b]

At all temperatures, the different phenol-loaded poly(NIPAAm) hydrogels follow the same release profiles. Nevertheless, and regardless of the concentration of loaded phenol, the amount of the cumulative release at 40°C is the lowest due to the network structure collapse, which entraps the phenol molecules inside the matrix and retards the release [Naddaf and Bart, 2011-b]. For the lower concentrations of phenol, the hydrogel that subjected to diffusion at 32°C exhibits the highest cumulative release. By increasing the initial concentration of phenol, the effect of the temperature (being around the LCST) is eliminated due to the contribution of the phenol ring, causing the matrix to collapse. The gel-water interaction modifies due to the reduction in the LCST associated with phenol concentration increase [Kosik et al. 2007].

3.7.2. Release of phenol at different initial concentrations

Fig. 3.9 represents the cumulative amount of released phenol from the poly(NIPAAm) at different concentrations of phenol (0.01mM, 0.04mM, 0.08mM, and 0.10mM) at different release temperatures of 25°C, 32°C, 37°C, and 40°C [Naddaf and Bart, 2011-b]. As indicated, the cumulative amount of released phenol slows down by decreasing the initial concentration of the loaded phenol. Elevating the temperature from 25°C to 40°C reduces the cumulative

amount of released phenol at about one-half. At the early stage of diffusion, the cumulative mass release curve increases linearly with time. This behaviour indicated that desorption of phenol was controlled by Fickian diffusion. At the long-term measurements, the cumulative mass release curves follow a non-smooth stepwise approach toward equilibrium, as can be seen clearly at 25°C and with a similar trend at 32°C in Fig. 3.9a and Fig. 3.9b. Due to the dramatic and fast dimensional changes during desorption, this behaviour, which is due to controlling the viscoelastic relaxation of the polymeric chains of the diffusion [Patton et al., 1984], was not observed above the LCST. This kind of two-stage diffusion kinetics was also observed for organic vapour sorption in glassy polymers, and it has been explained in detail by McDowell [McDowell et al., 1999]. In all these cases, the release of the loaded phenol is relatively low at 25°C and 32°C and continues to decrease to reach the lowest released amount at 40°C (Table 3.2) [Naddaf and Bart, 2011-b].

Table 3.2: Percentage of the cumulative amount of released phenol

	% released at T=25°C	**% released at T=32°C**	**% released at T=37°C**	**% released at T=40°C**
C_{phenol}=0.01mM	22.5%	29.0%	17.0%	12.0%
C_{phenol}=0.04mM	6.90%	8.12%	6.90%	5.60%
C_{phenol}=0.08mM	4.40%	4.40%	4.40%	3.12%
C_{phenol}=0.10mM	4.75%	3.75%	3.60%	2.75%

The big difference in the cumulative amount of released phenol between 25°C and 40°C is due to the hydrogel shrinking by exceeding the LCST. The shrunken hydrogel entrapped the phenol within the collapsed lattice of the poly(NIPAAm) and prevented the complete release. Because the hydrogels were loaded and allowed to swell to equilibrium at 25°C, they were expected to release the complete portion at a release temperature below the LCST [Tasdelen et al., 2005]. Nevertheless, the effect of the benzene ring, which modifies the order structure of the bulk water, cannot be ignored, as explained above.

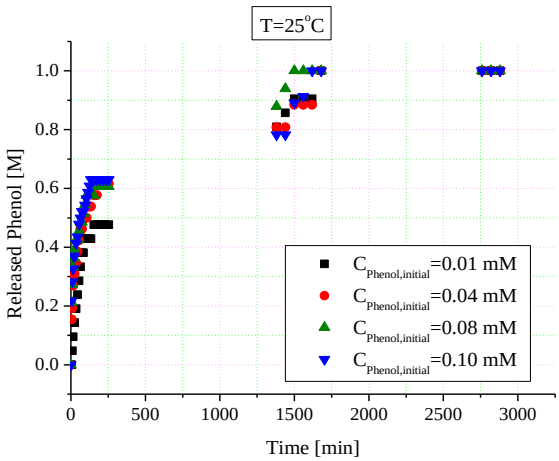
T=25°C
Released Phenol [M]
Time [min]
C Phenol,initial =0.01 mM
C Phenol,initial =0.04 mM
C Phenol,initial =0.08 mM
C Phenol,initial =0.10 mM

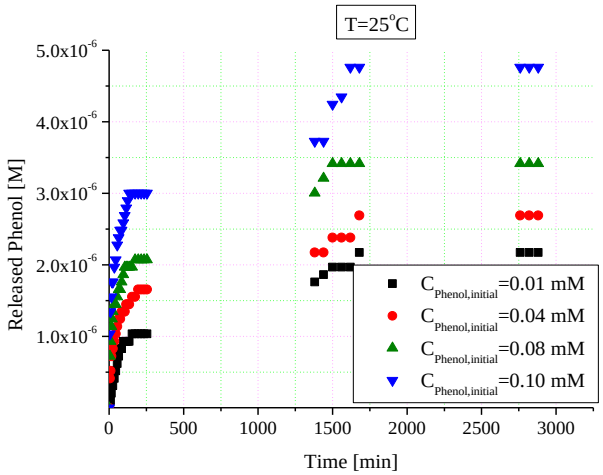
T=25°C
Released Phenol [M]
Time [min]
C Phenol,initial =0.01 mM
C Phenol,initial =0.04 mM
C Phenol,initial =0.08 mM
C Phenol,initial =0.10 mM

a)

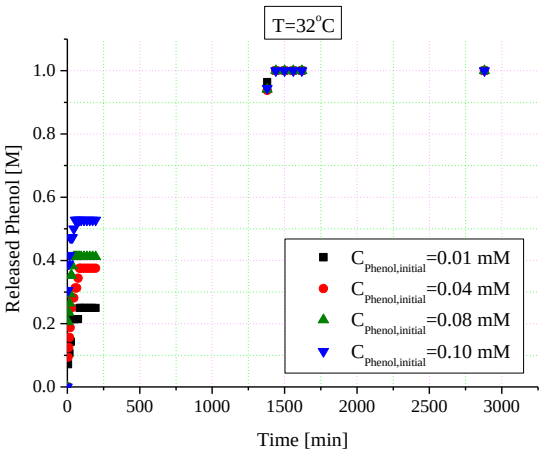
T=32°C
Released Phenol [M]
Time [min]
C Phenol,initial =0.01 mM
C Phenol,initial =0.04 mM
C Phenol,initial =0.08 mM
C Phenol,initial =0.10 mM

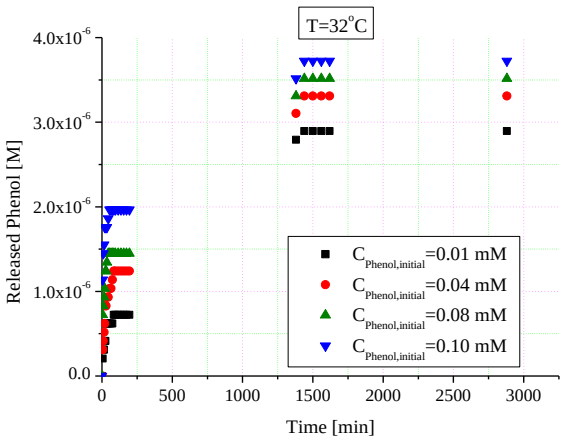
T=32°C
Released Phenol [M]
Time [min]
C Phenol,initial =0.01 mM
C Phenol,initial =0.04 mM
C Phenol,initial =0.08 mM
C Phenol,initial =0.10 mM

b)

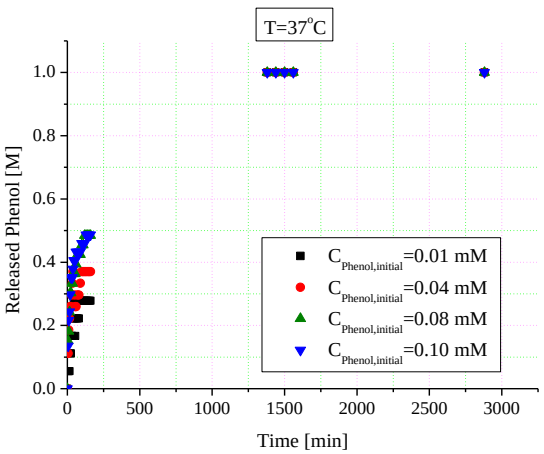
T=37°C
Released Phenol [M]
Time [min]
C Phenol,initial =0.01 mM
C Phenol,initial =0.04 mM
C Phenol,initial =0.08 mM
C Phenol,initial =0.10 mM

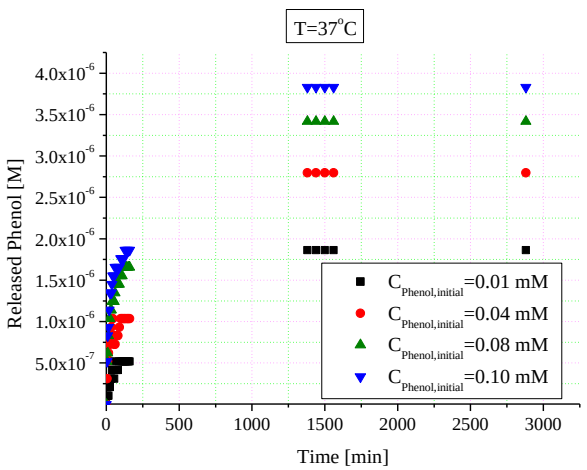
T=37°C
Released Phenol [M]
Time [min]
C Phenol,initial =0.01 mM
C Phenol,initial =0.04 mM
C Phenol,initial =0.08 mM
C Phenol,initial =0.10 mM

c)

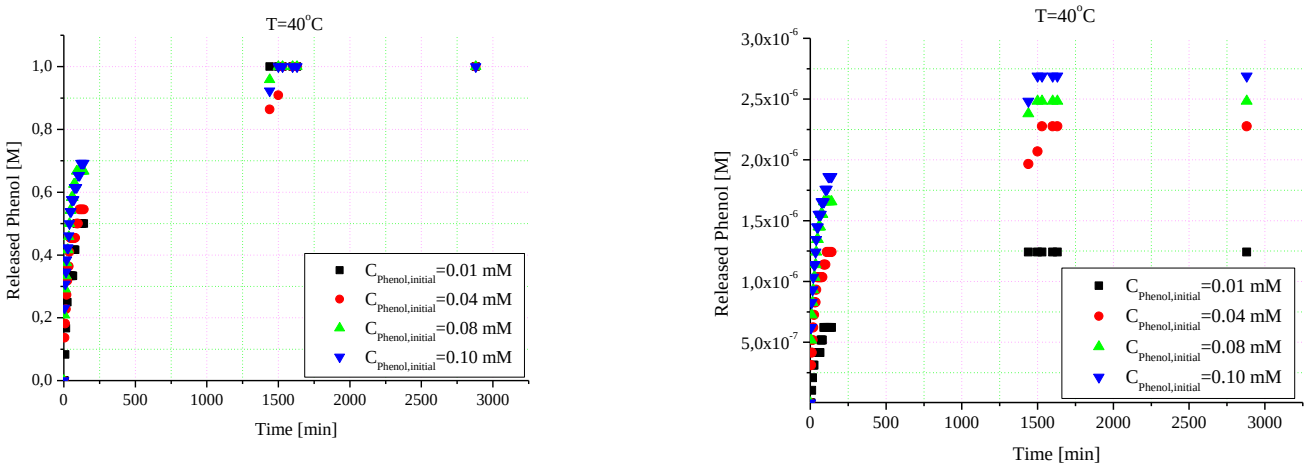

d)

Fig. 3.9: Cumulative amounts of released phenol from the hydrogel for different initial concentrations (the release temperatures a) 25°C, b) 32°C, c) 37°C, and d) 40°C) [Naddaf and Bart, 2011-b]

3.8. Summary

The present chapter, which based on our publication [Naddaf and Bart, 2011-b], investigates the dimensional changes accompanied with the volume phase transition of the thermosensitive poly(NIPAAm) hydrogel produced by free radical polymerization. Four different dried cylinders of the poly(NIPAAm) hydrogel were immersed in an excess phenol solution of known concentrations of 0.01, 0.04, 0.08, and 0.10 mM. Phenol was loaded into each hydrogel up to equilibrium by swelling in the phenolic solution. To investigate the effect of temperature-sensitive properties of the poly(NIPAAm) hydrogel on protein release profiles, the in vitro release experiments were carried out at different release temperatures of 25°C, 32°C, 37°C, and 40°C. In the case of swelling in pure deionized water, the hydrogels follow a continuous thermo-shrinking volume transition due to the effect of the entropy contribution; the reduction in the chemical potential of water molecules occurs by increasing the temperature. This continuous volume change is expected to eliminate by increasing the concentration of the loaded phenolic solution due to the presence of the benzene ring, which plays a significant role in modifying the order structure of the bulk water, modifying the hydrogel-water interaction and enhancing the formation of hydrogen-bonded structure. At 25°C, the phase transition was accompanied by reversible volume and mass changes for all tested phenol concentrations. This indicates that the high concentration of phenol could have a temporary effect on the lattice by

modifying the water-hydrogel interaction during the swelling. This effect, which is directly related to the hydrogen-bonded contribution, is supposed to disappear, by drying, without damaging the internal structure of the hydrogel or changing its swelling properties in the short term. This change in the local environment of the polymer progress at the same order was not expected at higher temperatures because the concentrated phenol solution lowers the LCST for the NIPAAm, which is accompanied by enthalpy reduction and was accurately proven based on Raman spectra. Around and above the LCST, the formation of the hard shrunken thick layer hinders the release of phenol from the hydrogel during the initial period of diffusion, resulting in the internal pressure increasing inside the hydrogels. Increasing the internal pressure is seen as a response to increasing the shrinking rate; the hydrogel shrinks at 40ºC faster than it does at 32ºC, and the interior solute is rapidly expelled causing the lowest cumulative release. As a result, the dense layer cracks and a hunch that contains a large amount of liquid inside will appear on the upper surface of the hydrogel. During the diffusion of water, dramatic changes of the upper half of the hydrogel cylinder will occur, but the lower half keeps almost its same dimensions at all tested temperatures. The swelling and release rate of gels are relatively slow at 25°C. Therefore, the hydrogel requires less time to reach its systematic cylindrical shape at higher release temperatures, e.g. 65 minutes at 40°C compared to 1,380 minutes at 25°C. At the end of the release time, the volume of the hydrogel subjected to diffusion at 40°C is about 16 times smaller than that at 25°C. Regardless of the concentration of loaded phenol, the amount of the cumulative release at 40°C was the lowest due to the collapsed network structure, which entraps the phenol molecules inside the matrix and retards the release. Moreover, elevating the temperature from 25°C to 40°C reduces the cumulative amount of released phenol about one-half. It was noticed that at the early stage of diffusion, the cumulative mass release curves increase linearly with time. This behaviour indicated that desorption of phenol was controlled by Fickian diffusion. At the long-term measurements, the cumulative mass release curves follow a non-smooth stepwise approach toward equilibrium due to controlling the viscoelastic relaxation of the polymeric chains of the diffusion. This was not observed above the LCST due to the dramatic and fast dimensional changes during desorption. Because the hydrogels were loaded and allowed to swell to equilibrium at 25°C, they were expected to release the complete portion at release temperature below the LCST. Nevertheless, the effect of the benzene ring, which modifies the order structure of the bulk water, cannot be ignored, as explained above.

4. Raman spectroscopy: hydrogel characterization and experimental set-up

4.1. Principle

Raman spectroscopy is a nonintrusive laser technique and a vibrational (e.g., bending and rotational vibrations) method to characterize a material. The vibrational stretching modes of this spectroscopy method are highly characteristic for special chemical bonds and often allow for compositional identification. Raman scattering is an inelastic scattering phenomenon of photons by phonons or electrons in materials.

Based on the analysis of scattered light, special spectral peak shifts, which are unique in their position and intensity, are formed to provide highly sensitive measurements of the material [Gouadec and Colomban, 2007, Nakashima and Harima, 1997]. Raman spectroscopy is performed with a laser as an excitation source; its effect occurs when the laser (photon source) impacts the material and interacts with the bonds of that molecule. The photon excites the molecule from the ground state to a virtual intermediate state, which forms Raman scattering. Later on, the molecule relaxes and returns to a rotational state above (or below) the ground state by emitting photons. In order to keep the total energy of the system balanced, the difference in energy between the original state and the new state leads to a shift in the emitted photon's frequency away from the excitation wavelength. Theoretically (Fig. 4.1), the incident photons can lose energy, i.e., the final vibrational state of the molecule is more energetic than the initial state, and then the emitted photon will be shifted to a lower frequency (Stokes shift). On the other hand, the incident photons can also gain energy by a vibrational quantum of the target molecule. In this case, the final vibrational state is less energetic than the initial state, and the emitted photon will be shifted to a higher frequency (Anti-Stokes shift). In the case of ordinary scattering (Rayleigh), the photon is absorbed to a higher virtual level and is instantly scattered elastically back to the initial level. Raman scattering is an example of inelastic scattering through which energy transfer occurs between the photons and the molecules during interaction. The Raman shift is represented in wave numbers with respect to the excitation. However, its spectra always show a peak, representing the Rayleigh scattering together with the

Raman shifted photons. The resulting Raman peaks give the Raman spectra chemical sensitivity [Bauer, 2010].

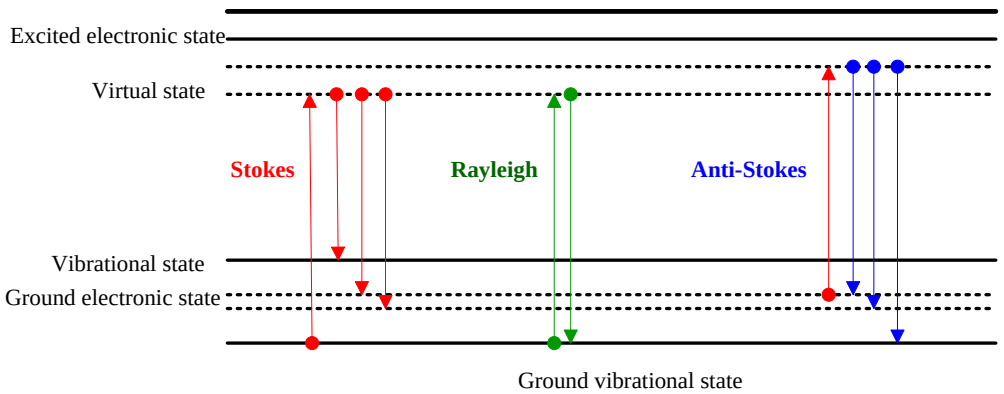

Fig. 4.1: The Jablonski diagram compares Raman and Rayleigh scattering

In general, the scattered light is very weak. Therefore, a special spectrometer designed to eliminate strong Rayleigh light is needed. Double or triple monochromators with gratings have been used widely to disperse the scattered light and reject stray light. With Raman confocal set-up, the scattering volume can be controlled and the spatial resolution and signal-to-noise ratio can be improved using an intense beam. By controlling these factors, compositional mapping with sub-micrometer resolution is possible using Raman spectroscopy [Bauer, 2010]. While spectrometers are generally used to separate the elastic scattering and Raman scattering signals, the large mismatch in scattering intensity can enable the elastically scattered light to dominate the Raman light via stray light. Therefore, the presence of notch filters is necessary to reject the elastically scattered light prior to entering the spectrometer. These mentioned factors improve the sensitivity of Raman spectroscopy and allow precise identification of the material composition [Hahn, 2007].

Being a powerful technique to determine the composition of a heterogeneous material, Raman spectroscopy was recently applied to study the structure of the hydrogel, the surface interfacial profiles of the gel under transition conditions and the concentration profile during the diffusion of solute through the gel lattice [Kwak and Lafleur, 2003]. In contrast to a swollen hydrogel, the well-defined structure of the shrunk hydrogel increases the resolution of Raman spectra and resulted in sharp peaks formation. Moreover, when using Raman laser spectroscopy, the

possibility to get non-invasive data from any point in a sample is possible. Unlike other techniques such as the infrared IR spectroscopy, Raman spectrumcan be obtained without any major interference from water bands, which have a weak Raman signal. Therefore, diffusion studies in hydrogels using Raman spectroscopy are of high advantage. Raman spectroscopy is described more in details elsewhere [Bauer, 2010].

4.2. Experimental setup

The experimental setup (Fig. 4.2) used in this research to characterize the hydrogel and to measure the mutual diffusion coefficient in hydrogel is a confocal spectrometer (Jobin-Yvon HR800) equipped with an internal exciting light source of He-Ne ion laser. It consists mainly of a camera, a collective system, a diffusion cell, and a Labview program®. Raman spectroscopy measurements for all the experiments were carried out under the same optical conditions.

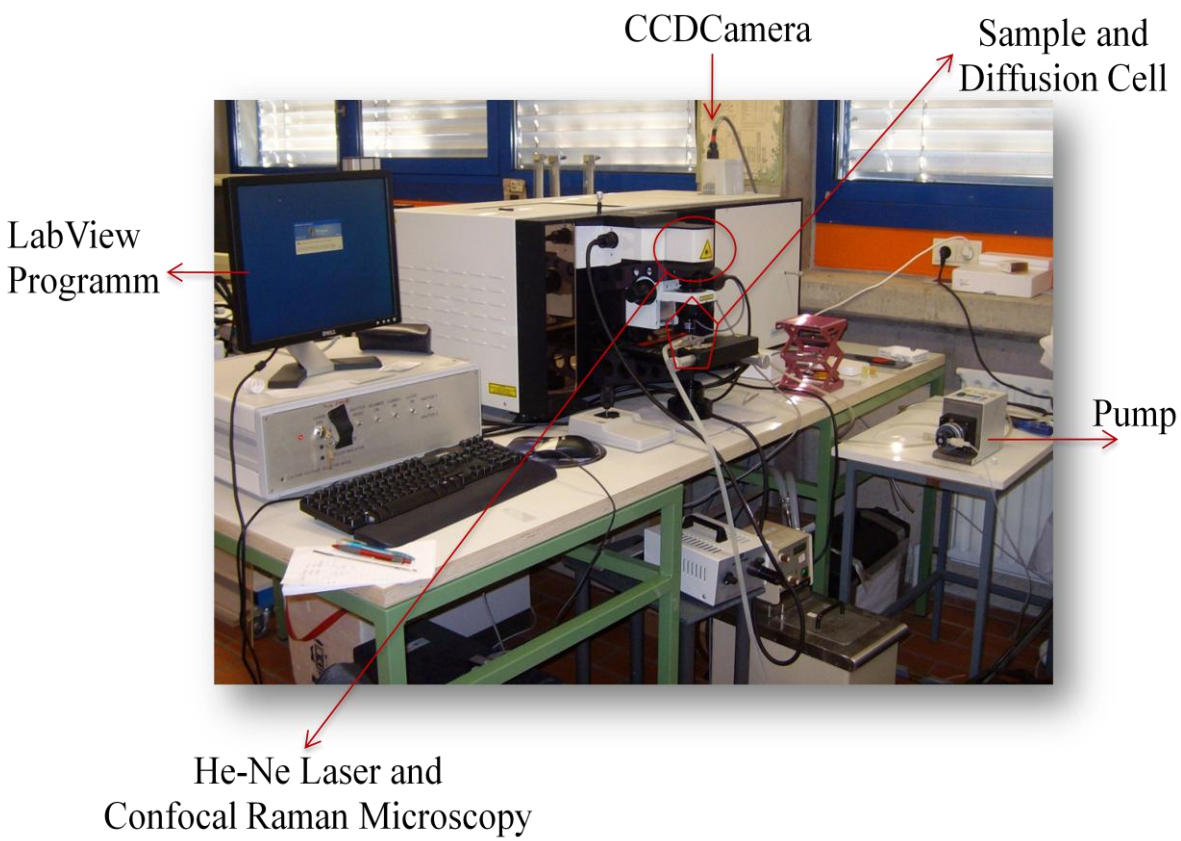

Fig. 4.2: Raman spectroscopy: the experimental setup

Fig. 4.3 shows a detailed description of the experimental setup used for measuring the mutual diffusion coefficient in hydrogel [Naddaf and Bart, 2011-a, c]. The designed system consists of two parts: Part 1contains the camera and the collective system, and Part 2 includes the autofocus system and the diffusion cell. As mentioned above, Raman spectra were recorded using a confocal spectrometer (Jobin-Yvon HR800) equipped with an internal exciting light source of He-Ne ion laser polarized vertically with a power of 20 mW at a wavelength of 632.817 nm. After filtering out the plasma lines of the laser, by using an appropriate interferential filter, the laser beam (H) is then completely reflected with an appropriate angle by the Laser Injection Rejection System (LIRS), which is composed of a mirror and the notch filter (I). The LIRS reflects the laser (H) towards the hydrogel sample through the diffusion cell (Part 2) under a microscope of high stability (BX 40) and focus graduation of 1μm. Raman scattering is then totally collected and transmitted through a lens (C5), which produces a beam at an angle of 90^{o} towards a confocal hole and the entrance slit of the spectrograph (K). The beam is coupled to a fibre optic and focused on the hydrogel sample using the 50xNA 0.7 microscope objective. A set of lenses (C1-C3) focuses the signal toward the entrance slit (D) and the confocal aperture (F) of the spectrograph. The Raman signal is collected by the microscope objective in back scattering configuration follows the same way back. The reflection of the sample on the laser line (Rayleigh) is reflected again by the notch filter (I). Meanwhile, the passed Raman beam through the notch forms its image on the entrance slit of the confocal hole (spectrograph) by the aid of lens 5 (C5). The spectrograph forms a spectrum on the photo detector (L) that has standard 1024×256 pixels of 26 microns. To detect the spectra, a computer with Labspec software was connected to the CCD video camera (A) and Rio card for TV image digitalization. Raman spectroscopy measurements for all the hydrogel samples were carried out under the same optical conditions. A rectangular PVC diffusion cell with inner dimensions of 4.8×1.3×0.7 mm was maintained at 25°C and connected with a peristaltic pump (Samtec® REGLO FMI V1.05) to provide the solute loaded hydrogel cylinder with a continuous flow rate (1 ml/min) of deionized water (Fig. 4.3, Part 2).

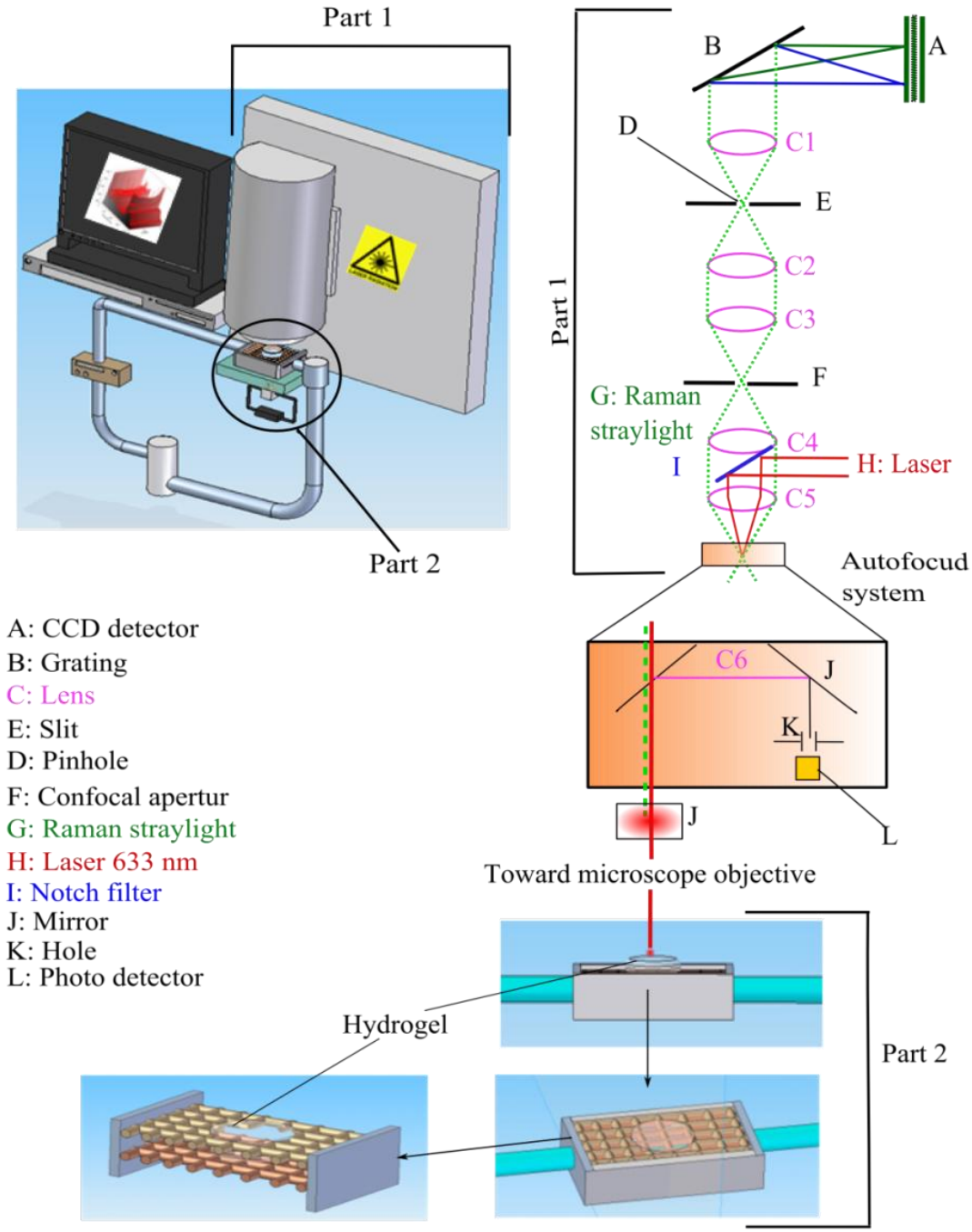

Fig. 4.3: Experimental setup to determine the mutual diffusion coefficient, using Raman spectroscopy [Naddaf and Bart, 2011-a, c]

The transparent hydrogel cylinder, which is located in the diffusion cell and immersed in the flowing solution, is assumed to absorb a negligible amount of energy. The diffusion cell was

designed in a way to keep the hydrogel samples fixed in position by being sealed with a metal grid to prevent sample movement caused by the flow of water. Moreover, to avoid the evaporation of the solution due to exposure to ambient air, the hydrogel diffusion cell was covered with a microscope slide that included a central tiny hole to allow the laser to transmit directly to the hydrogel at the required detecting point [Naddaf and Bart, 2011-a, b].

4.3. Swelling characterization experiments

The used confocal Raman spectroscopy has been considered an efficient device to investigate the volume phase transitions and the structural composition as well as to characterize thermosensitive poly(NIPAAm) hydrogels. Their properties were measured at different temperatures, different pH-values, and different concentrations of various solutes in terms of Raman spectra. Fig. 4.4 shows the Raman spectrum of the poly(NIPAAm) hydrogel and its main synthesis components (including the used monomer and cross linker, the two initiators).

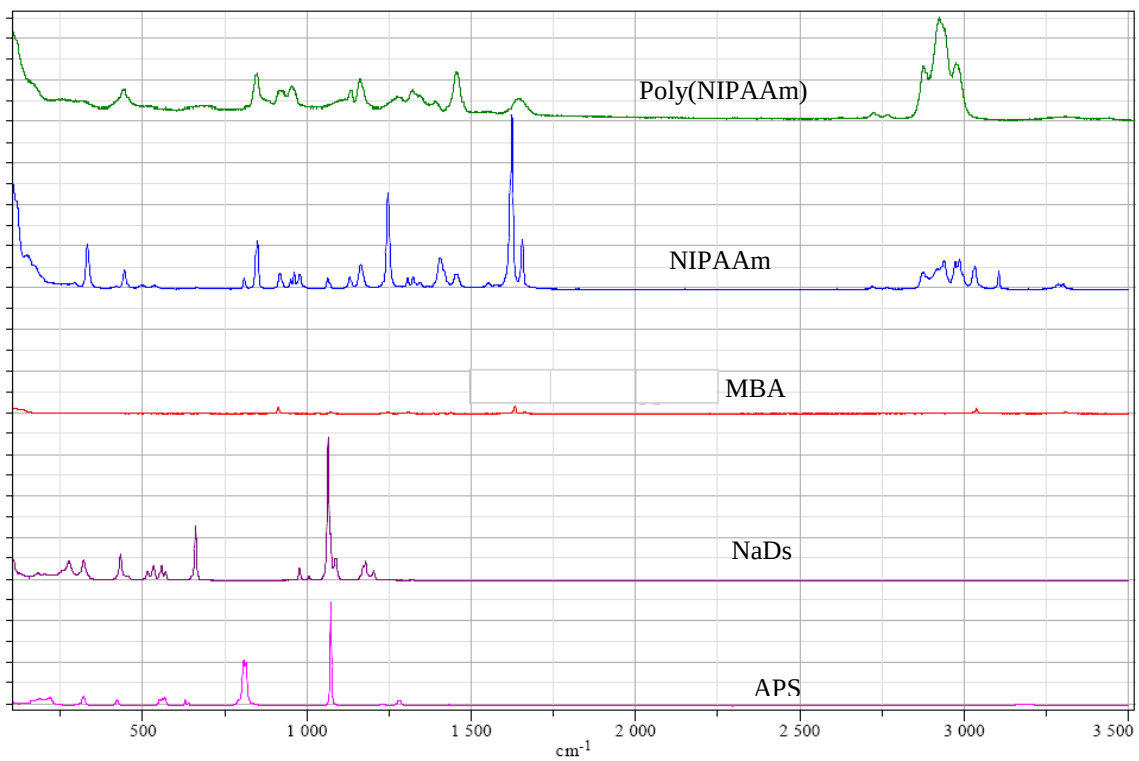

Fig. 4.4: Raman spectrum of the frame components of the poly(NIPAAm) hydrogel

All the chemical compounds and the hydrogel have significant Raman peaks between 300 and 1200 cm^{-1} except the monomer (NIPAAm) and the hydrogel itself, which have Raman spectra between 300 and 3000 cm^{-1} whilst the carbonyl group at 1680 cm^{-1}characterizesthe pure NIPAAm [Joachimiak et al., 2005]. Therefore, the significant spectrum along the range 300-3000 cm^{-1} has been used to investigate the hydrogel response to a variety of environmental stimuli. Fig. 4.5 shows the Raman spectrum of the dried poly(NIPAAm) hydrogel. The distinct peak for the isopropyl group [Ding et al., 2006 and Winnik et al., 1993] at 2925 cm^{-1} is a characteristic signal of poly(NIPAAm) and the band at 1640 cm^{-1} is attributed to the amide group. While the strong peak at 1450 cm^{-1} belongs to the CH_3 group, the Raman spectrum of water places between 3037 and 3735 cm^{-1}. More identified peaks are given elsewhere [Naddaf and Bart, 2008].

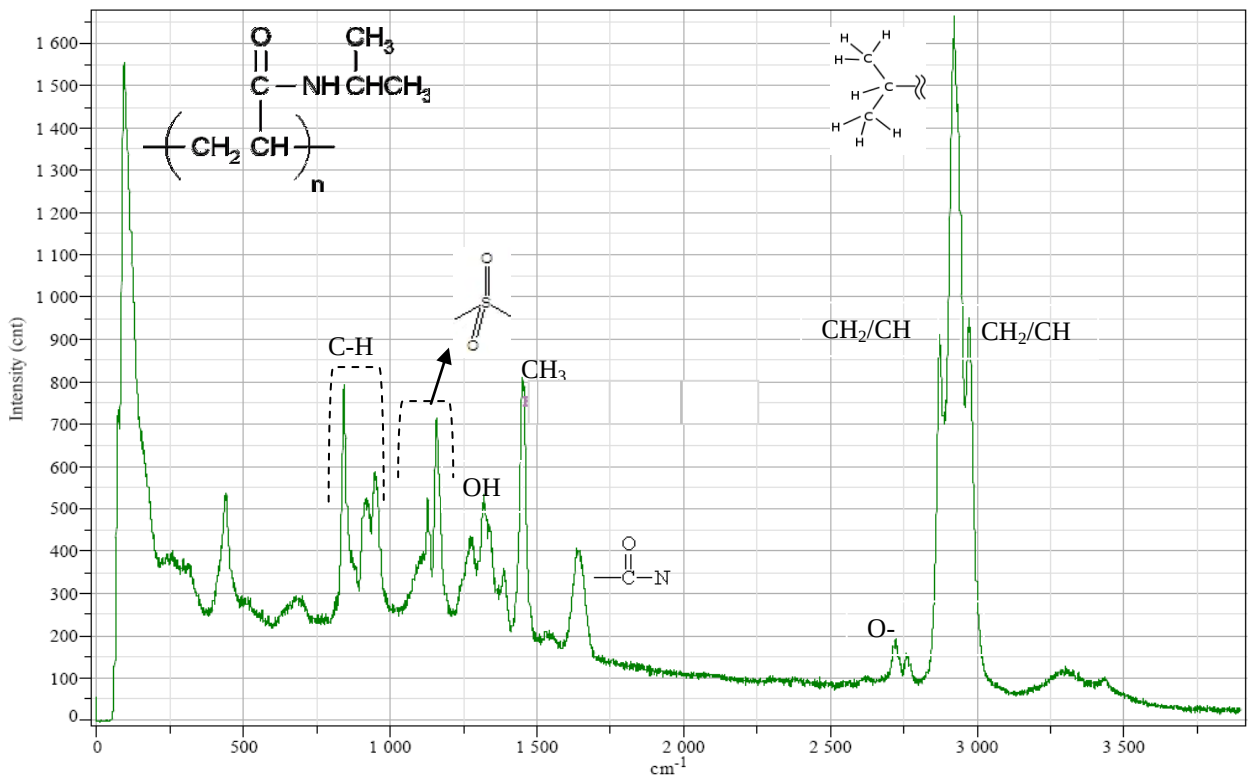

Fig. 4.5: Raman spectrum of the dried poly(NIPAAm) hydrogel, including the important groups

4.4. Thermal equilibrium swelling

The thermal related swelling/deswelling Raman spectrum of poly(NIPAAm) at different equilibrium temperatures is shown in Fig. 4.6.

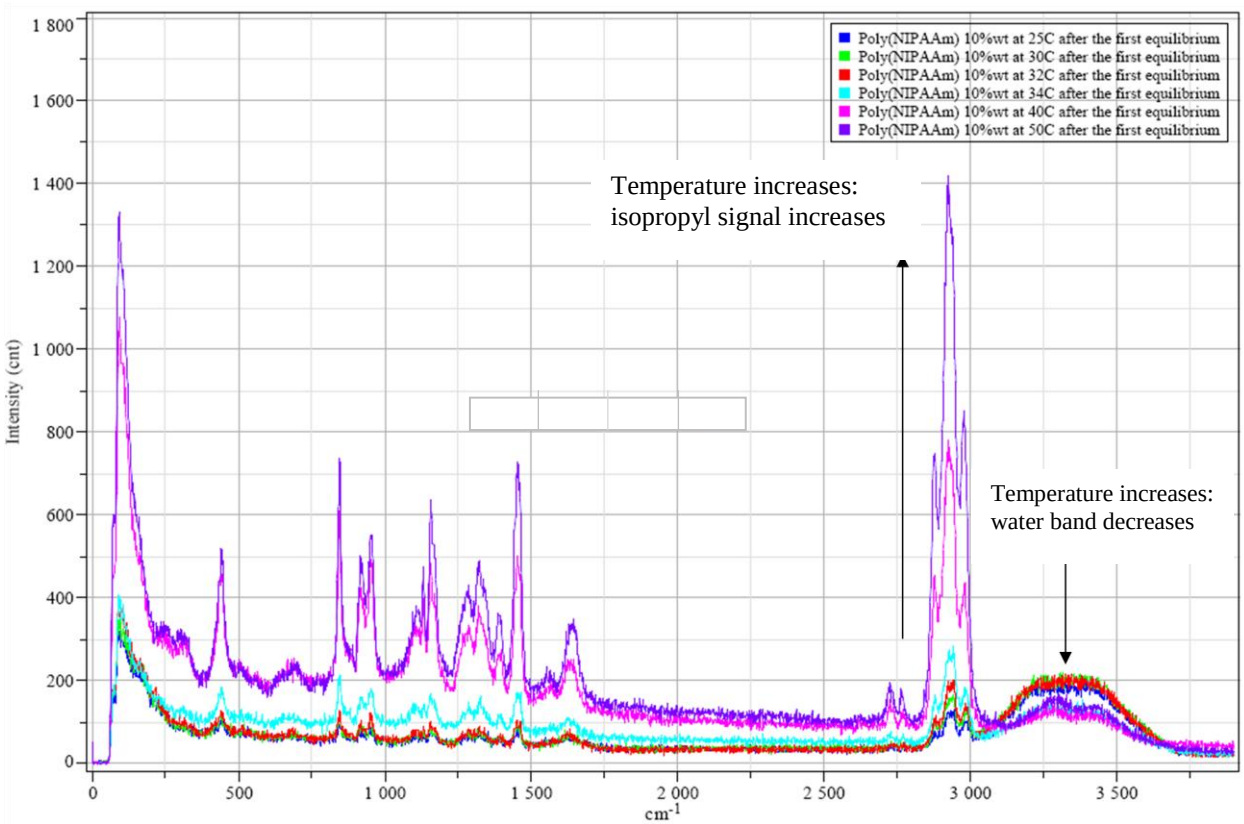

Fig. 4.6 : Raman spectrum for poly(NIPAAm) as a function of temperature after set to the first equilibrium at pH of seven

In addition, Raman spectroscopy has been used to investigate volume phase transition as a function of temperature [Naddaf and Bart, 2008]. It was found that the poly(NIPAAm) has a lower critical solution temperature (LCST) between 32°C and 34°C in agreement with other related investigations [Hirotsu et al., 1987, Brazel and Peppas, 1995, Sayil and Okay, 2000, Peppas, 2004, Ding et al., 2006]. Based on this experimental result, one can assume that by increasing the temperature, the water inside the hydrogel is released through the pores as presented by the decrease in Raman spectra of water between 3037-3735 cm^{-1} (Fig. 4.6). Meanwhile, the hydrogel chemical peaks rose between 300 and 1700 cm^{-1}, which indicate that the hydrogel is shrinking and the chemical density of the structural composition increased

[Ding et al., 2006]. The ratio of the band area due to the isopropyl group, $A_{isoprop.}$ to that of the water, A_{water} within the range 2823-3034 cm^{-1} and 3037-3735 cm^{-1}, respectively confirm that changes inside the hydrogel lattice occur much more slowly under the LCST between 32°C and 34°C (Fig. 4.7).

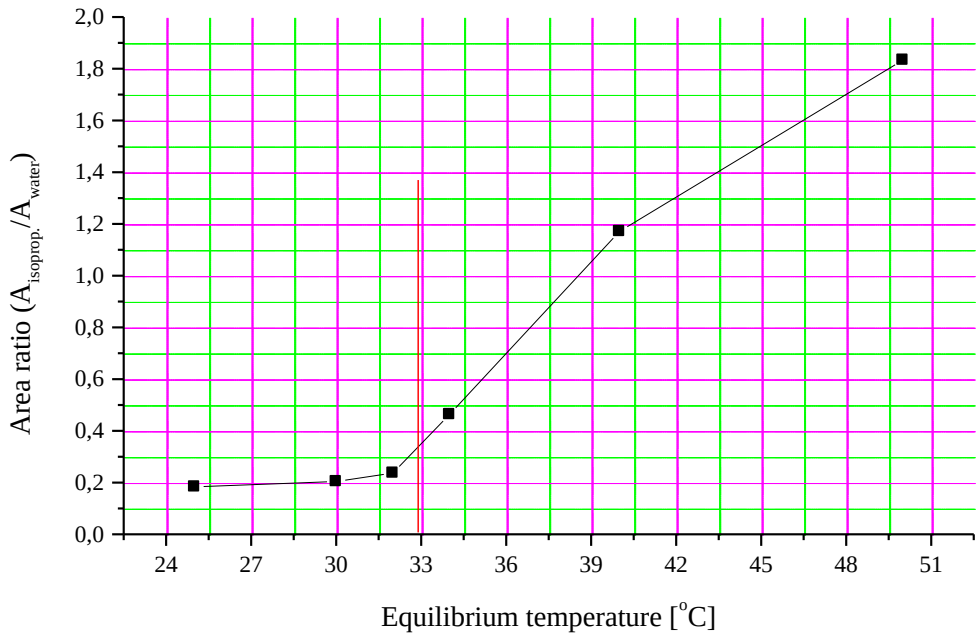

Fig. 4.7: The ratio of the areas under the bands obtained from Raman spectra of the isopropyl group and water at different equilibrium temperatures for poly(NIPAAm) hydrogel

By measuring the in-depth spectra of the poly(NIPAAm) at different temperatures, it was found that the content of water increases by increasing the depth meantime the area ratio, i.e., $A_{isoprop.}/A_{water}$ remains almost constant (Fig. 4.8). Moreover, the in-depth water content rising indicates that the collapse takes place at the outer surface of the hydrogel first and slows down uniformly in the central direction [Naddaf and Bart, 2008].

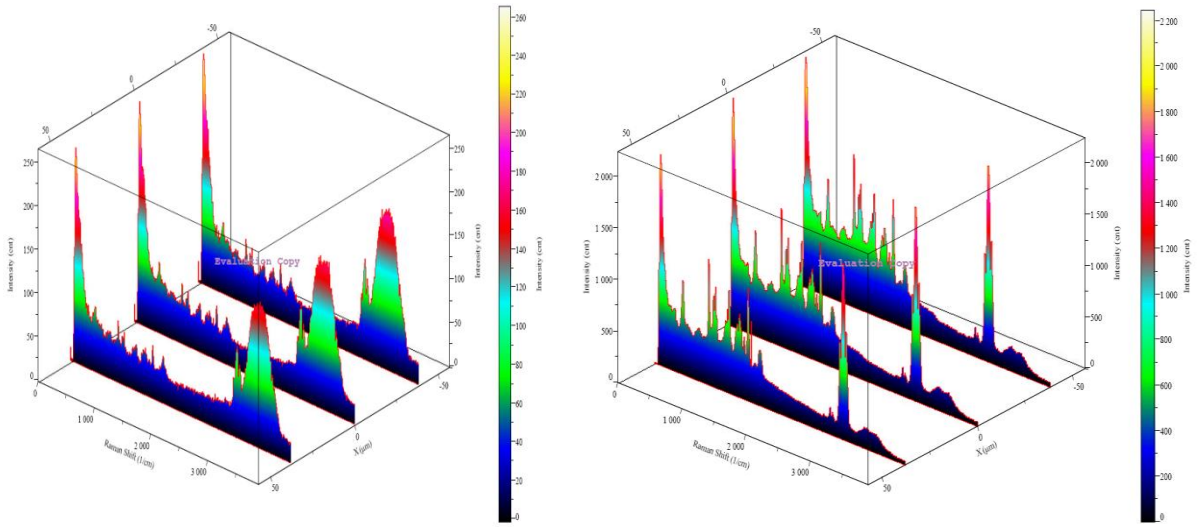

a. b.

Fig. 4.8: In-depth spectrum of the poly(NIPAAm) at (a) 25°C and (b) 50°C (pH=7)

4.5. Hydrogel thermo reversibility

To check the thermal reversibility of the poly(NIPAAm), the samples were set to the equilibrium conditions to a second time for seven days. At the second equilibrium and below the LCST, Raman spectra still show proportional increases between the equilibrium temperature and the isopropyl group intensity. This proportionality disappeared above 34°C, i.e., the hydrogel subjected to the second equilibrium at 40°C has a sharper Raman spectrum than the sample at 50°C. In other words, one can conclude that the self-synthesis poly(NIPAAm) exhibits relatively irreversible swelling/deswelling behaviour at temperatures above the LCST (Fig. 4.9) [Naddaf and Bart, 2008].

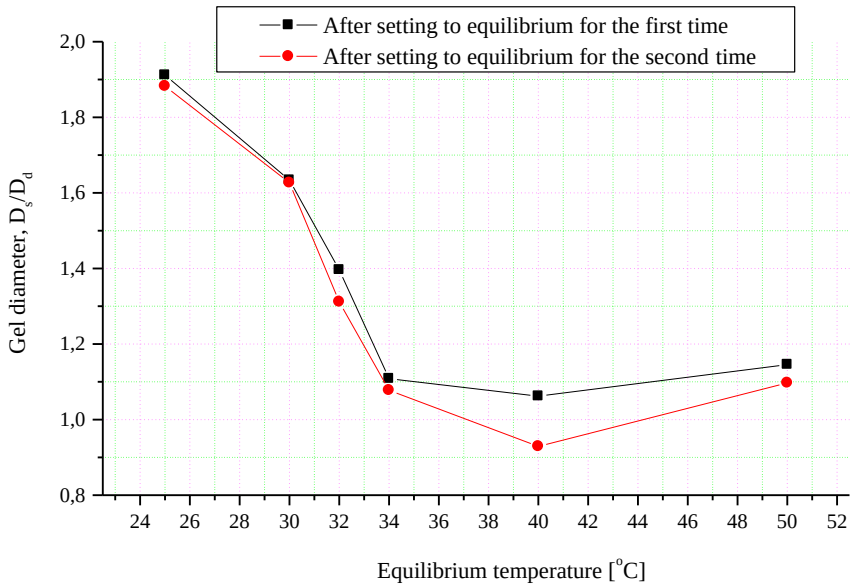

Fig. 4.9: Volume ratio of poly(NIPAAm) at the two equilibrium as a function of temperature at pH=7 [Naddaf and Bart, 2008]

4.6. Volume phase transition

According to our present work [Naddaf and Bart, 2008, Naddaf and Bart, 2001-b], at 25°C the phase transition is accompanied by reversible volume and mass changes for all tested phenol concentrations (Fig. 4.10). This indicates that the high concentration of the phenol could have a temporary effect on the lattice by modifying the water-hydrogel interaction during swelling. This effect, which is directly related to the hydrogen-bonded contribution, is supposed to disappear, by drying, without damaging the internal structure of the hydrogel or changing its swelling properties in the short term. This change in the local environment of the polymer progress at the same order is not expected at higher temperatures because the concentrated phenol solution lowers the LCST for the NIPAAm [Hirotsu et al., 1987, Watanabe and Iwata, 1996], which is accompanied by enthalpy reduction [Otake et al., 1990]. This assumption can be accurately proven based on Raman spectra. Fig. 4.11 represents the ratio of the area under the band due to the isopropyl group for hydrogel equilibrated in pure water at 25°C, $A_{isoprop.,H_2O}$ to that of the isopropyl group for hydrogel equilibrated in phenol, $A_{isoprop.,phenol}$ within the range 2851-3005 cm^{-1} and 3037-3735 cm^{-1}, respectively. The ratio was measured by setting the same

sample to the same conditions to equilibrium twice. The result obtained (Fig. 4.11) indicates the increase of the intensity by increasing the phenol concentrations and confirms that the changes inside the hydrogel lattice are happening by increasing the concentration of phenol [Naddaf and Bart, 2001-b].

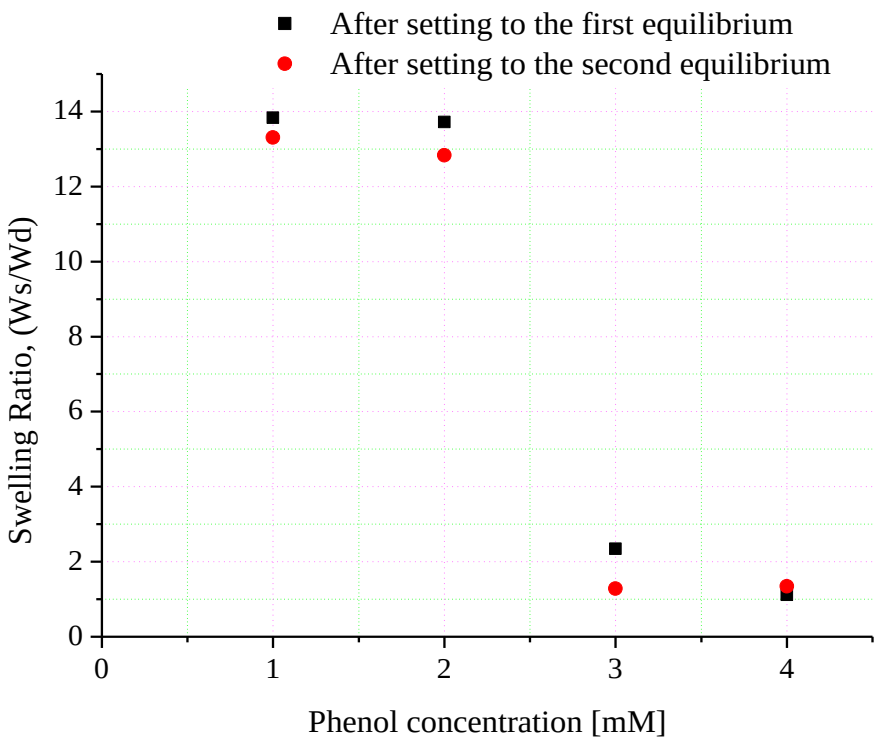

Fig. 4.10: The swelling ratio of poly(NIPAAm) hydrogel at 25^{o}C as a function of phenol concentration [Naddaf and Bart, 2001-b]

This non-reversible thermo performance is due to the non-uniform collapse in the gel net, which occurs first near the surface, creating a dense layer of hydrophobic gel [Ding et al., 2006]. This layer slows the diffusion of water through the hydrogel. In addition, this non-uniform collapse eliminates the expansion of the hydrogel to a certain dominant level.

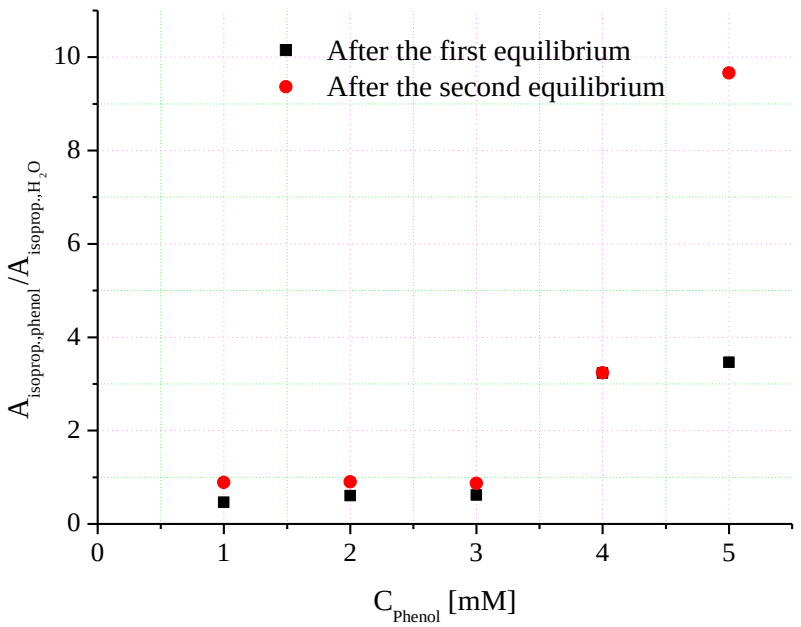

Fig. 4.11: The area under Raman peaks ratio of poly(NIPAAm) hydrogel 25^{o}C as a function of phenol concentration [Naddaf and Bart, 2001-b]

According to this work, the synthesized poly(NIPAAm) demonstrates a sharp swelling transition as a function of pH, i.e., the hydrogel lattice collapsed due to the high acidity (pH < 1.0) and high alkalinity (pH > 9.0) [Naddaf and Bart, 2008]. Moreover, it was found that high concentration of phenol could have a temporary effect on the lattice by modifying the water-hydrogel interaction during swelling. This effect, which is directly related to the hydrogen-bonded contribution, is supposed to disappear, by drying, without damaging the internal structure of the hydrogel or changing its swelling properties in the short term. This assumption was accurately proven based on Raman spectra (Fig. 4.11). The obtained result confirms that the changes inside the hydrogel lattice are happening by increasing the concentration of phenol. The high concentration of phenol could have a temporal effect on the lattice by modifying the water-hydrogel interaction during swelling and enhance the formation of hydrogen bonded structures [Naddaf and Bart, 2001-b].

4.7. Results and discussion

4.7.1. Characterization and image analysis

Fig. 4.12 shows Raman spectrum of poly(NIPAAm) hydrogel immersed to equilibrium in a phenol solution of 0.10mM. Raman spectrum of water is found due to the O-H stretching vibration to be an abroad band between 3200 cm^{-1} and 3735 cm^{-1}, and the distinct peak for the isopropyl group at 2925 cm^{-1} is a characteristic signal of poly(NIPAAm) [Winnik et al., 1993, Ding et al., 2006]. In addition, particularly at 3066 cm^{-1}, another small distinct peak was observed to refer to the presence of phenol [Naddaf and Bart, 2012]. Such a characteristic peak was not distinguishable for BSA because the Raman spectra of BSA resulted from the CH_3-stretching vibration, which integrates from 2910 cm^{-1} to 2965 cm^{-1} and also is caused from the poly(NIPAAm) signal [Peters et al., 1988].

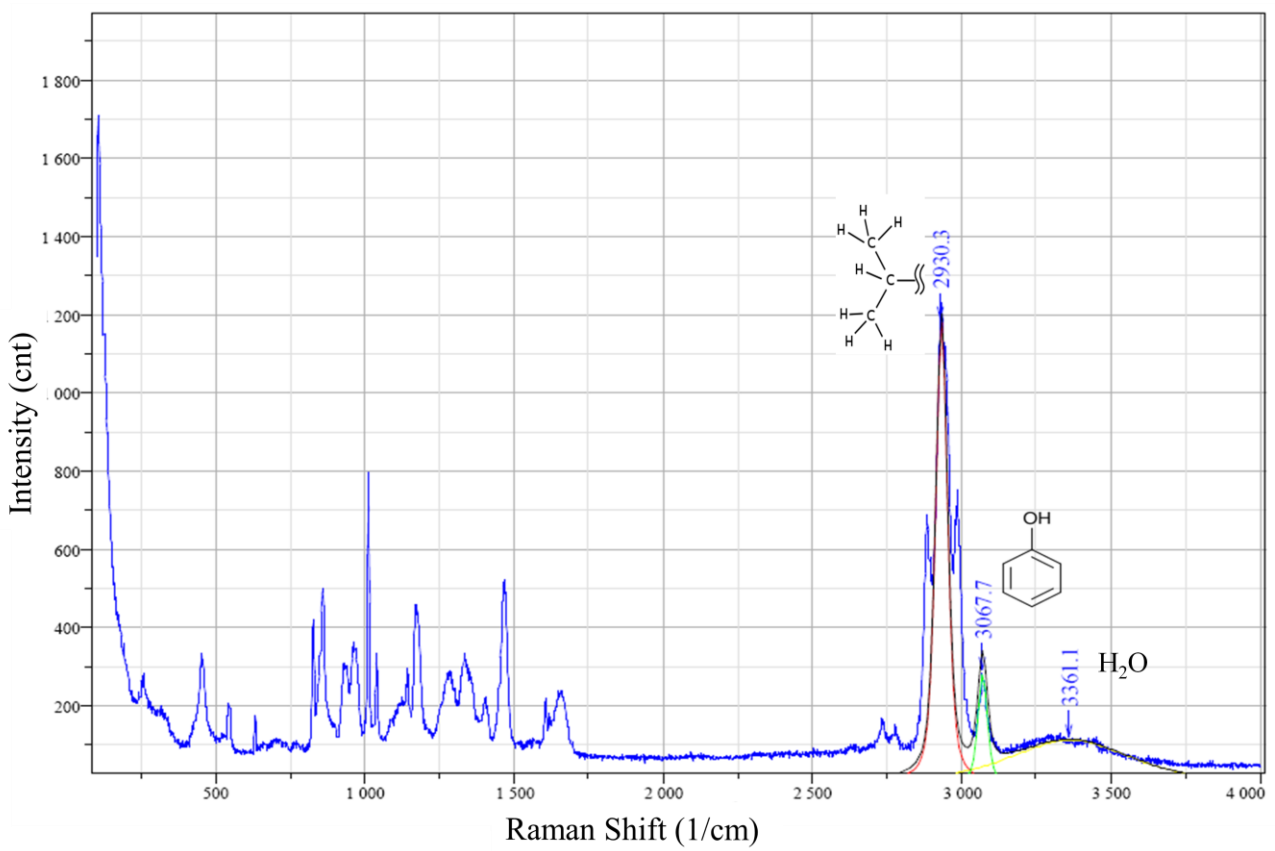

Fig. 4.12: Expanded Raman spectrum for poly(NIPAAm) in phenol [Naddaf and Bart, 2001-b]

4.7.2. Diffusion coefficient: experimental determination

Fig. 14.13 shows a description of the diffusion cell used for measuring the mutual diffusion coefficient in hydrogel [Naddaf et al., 2010]. As mentioned in Section 4.2, the diffusion cell was designed in a way to keep the hydrogel samples in fixed positions by being sealed with a metal grid to prevent sample movement caused by the flow of water. Moreover, to avoid the evaporation of the solution due to exposure to ambient air, the diffusion cell was covered with a microscope slide that included a central tiny hole that allowed the laser to transmit directly to the hydrogel at the required detecting point [Naddaf and Bart, 2011-a, c].

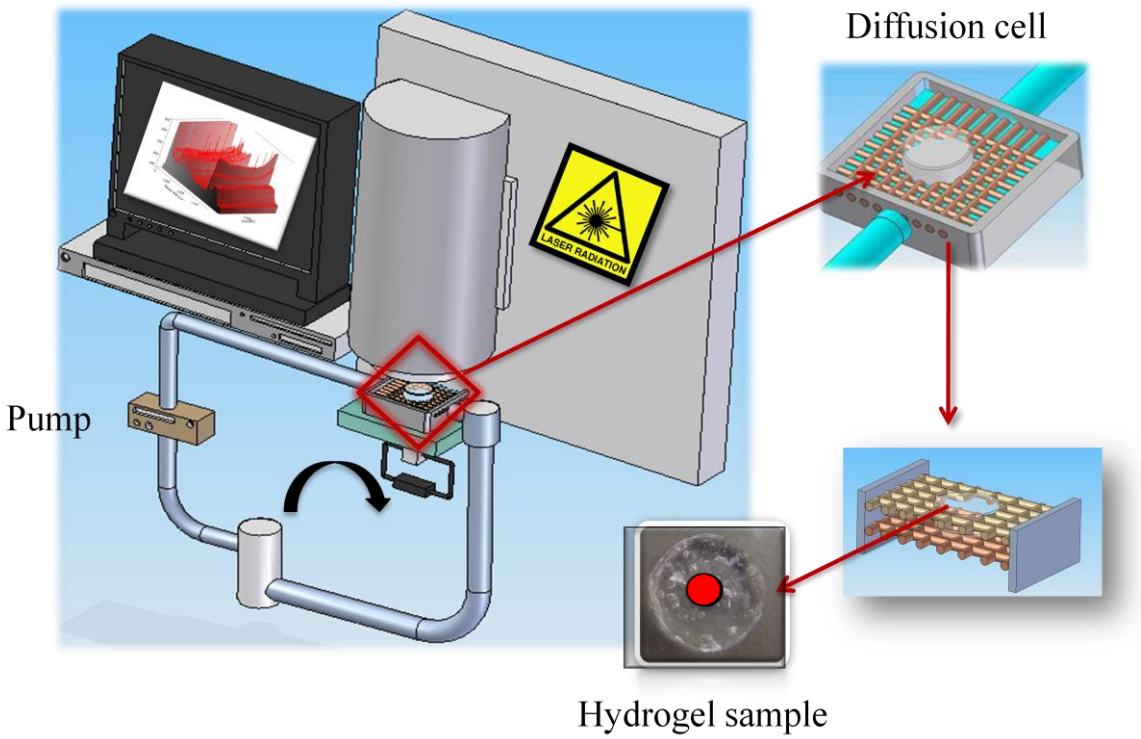

Fig. 4.13: The diffusion cell

The intensity map of the poly(NIPAAm)/phenol (and poly(NIPAAm)/BSA) system during the continuous diffusion was determined as explained by Naddaf and Bart, 2012. The Raman spectra were obtained at fixed spatial positions within the hydrogel near the outer surface. Fig. 4.14 gives a transient Raman intensity map for the poly(NIPAAm)/BSA system for a regulated

time interval between two spectrums of 10 seconds. The variation of the distinct peak intensity at 2925 cm^{-1} relates to the change in the concentration of the BSA inside the poly(NIPAAm) hydrogel during the diffusion. At the beginning of the diffusion, the spectra have a high peak signal and refer to the high concentration of BSA in hydrogel. With time, the height of the peaks (and the concentration of the BSA in the hydrogel) starts to decrease gradually, compared to the water band, until it becomes constant. Then, the mutual diffusion coefficient was calculated based on the concentration change of the drug sample in the hydrogel cylinder related to the variation of the distinct peaks of the poly(NIPAAm)/drug system [Naddaf and Bart, 2011].

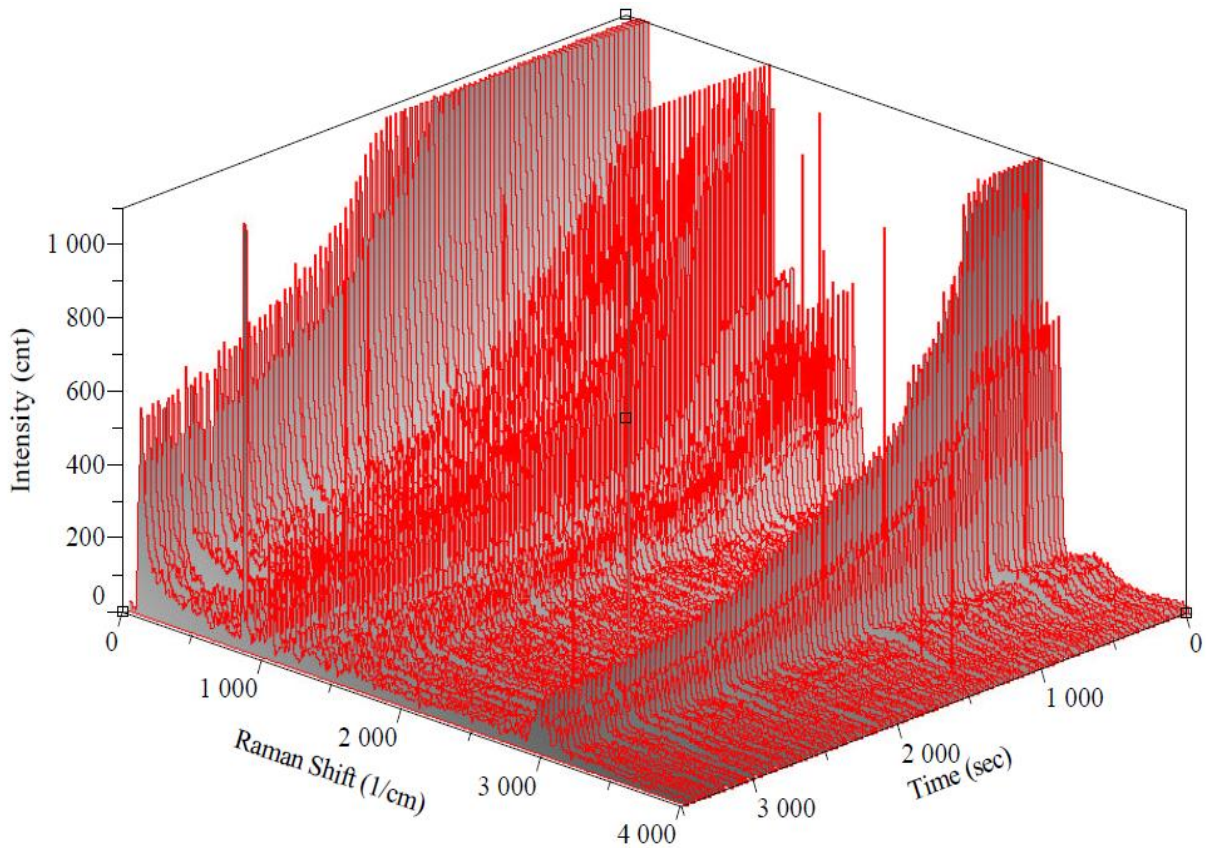

Fig. 4.14: Transient Raman map for the poly(NIPAAm)/BSA system at a fixed spatial position

The deionized water starts to diffuse into the gel initially at time *t=0* by remaining the concentration at the hydrogel/solution interface C_0 constant. The minimal amount of solute dissolving into the flowing cell reservoir during the experiment is negligible. The diffusion coefficient (*D*) was calculated as a function of concentration (*C*) at distance (*x*) from the interface at elapsed time interval by assuming a semi-infinite media [Crank, 1975, Kwak and Lafleur, 2003] according to the equation:

$$C = C_o \cdot erf\left[x \Big/ 2\left(\sqrt{D \cdot t}\right)\right] \tag{4.1}$$

By assuming the hydrogel as a semi-infinite media, the diffusion of the solute out of the hydrogel can be studied and analysed via Raman spectroscopy by replacing the concentration term in the developed expression of equation (4.1) with the intensity [Naddaf and Bart, 2011-a, c]. To determine the relation between the initial solute concentration and Raman intensity, different samples of poly(NIPAAm) cylinders were allowed to swell at 25^{o}C to equilibrium in BSA and phenol solutions at different concentrations. From this, two calibration curves (for BSA and phenol) resulted relating the Raman intensity ($I_{CH}(t,x)$) to the solute concentration as follows [Naddaf and Bart, 2011-a, c]:

$$I_{CH,H_2O}\, f\left(C_{solution\ (phenol,BSA)}(t,x)\right) = I_{CH}^{\text{int}} \cdot erf\left[x \Big/ 2\left(\sqrt{D_{mut} \cdot t}\right)\right] \tag{4.2}$$

I_{CH}^{Int} is the intensity at the hydrogel/water interface boundary and D_{mut}, is the mutual diffusion coefficient. In addition, although the hydrogels were taken from the same synthesized batch and have the same geometries, the effect of the local dynamic inhomogeneity appears. The dynamic inhomogeneity is found to be a result of the difference in the molecular environment, e.g., the difference in the local gel concentration and/or cross-linking density. It may also occur due to the distributions of the holes in the lattice and the swelling of hydrogel that happens during the diffusion. This inhomogeneity may affect the scattered intensity [Norisuye et al., 2004] and, as consequence, gives different local data in the long-term averaged measurement

based on Raman spectroscopy to calculate the mutual diffusion coefficient. Therefore, for each data point in Fig. 4.14, the mutual diffusion coefficient was calculated from equation (4.2) using Matlab® (Fig. 14.15), and then the average diffusion coefficient was determined. The relation between the solute concentration and Raman intensity of poly(NIPAAm), which is characterized by the distinct peak of the isopropyl group at 2925 cm^{-1}, was taken into account.

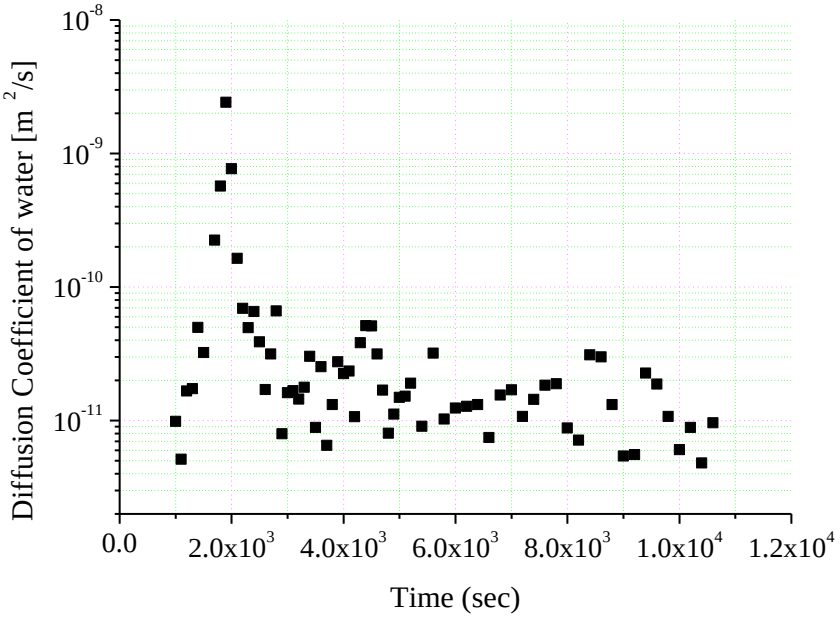

Fig. 14.15: The effect of the scattered intensity on the mutual diffusion coefficient as a function of time for phenol (0.01mM) at 25ºC [Naddaf and Bart, 2011-c]

To determine the mutual diffusion coefficient as a function of the solute concentration, several samples were loaded to equilibrium in phenol solutions as mentioned above. By using equation (4.2), the variation of the average calculated mutual diffusion coefficient at 25°C was determined (Fig. 4.16). It was found [Naddaf and Bart, 2011-b] that as the concentration of phenol increases, the mutual diffusion coefficient also increases. Similar results, indicating that the diffusion coefficient is concentration-dependent, have been reported [Koros et al., 1976, Dubreuil et al., 2003]. This dependency of diffusivity on concentration was found to be a result of the solute-hydrogel interaction [Lewus and Carta, 1999]. For the varied concentrations of

loaded phenol —0.01mM, 0.04mM, 0.08mM, and 0.1mM— the corresponding average diffusion coefficients were 5.6185×10^{-11}, 1.64338×10^{-10}, 2.87919×10^{-10}, and 3.34565×10^{-9} m^2/s respectively, as reported in previous work [Naddaf and Bart, 2011-b, c]. Although the change of the concentrations studied here is significant, the values obtained for the mutual diffusion coefficient of poly(NIPAAM)/BSA varied only slightly, from $5.67\cdot10^{-14}$ m^2/s to $6.07\cdot10^{-14}$ m^2/s for 1.51M to 0.1M, respectively. Nevertheless, these values are still close to the reported effective diffusion coefficient of acrylamide hydrogel/BSA system [Andersson et al., 1997], which indicates an increase in the resistance to diffusion inside the hydrogel due to the high swelling ratio. Another case study found that the mutual diffusion coefficient is strongly influenced by internal gel properties, such as the average free hole volume [Vrentas and Vrentas, 1992]. Hence, larger average free hole volume will lead to larger diffusivity at a given solute concentration. For a solute with a high molecular weight (such as BSA), the network has a considerable effect on diffusion, i.e., the diffusivity in a thermosensitive hydrogel is restricted by obstruction phenomenon for large molecules [Andersson et al., 1997]. However, this gives diffusion coefficients for BSA at about four magnitudes smaller than phenol [Naddaf and Bart, 2011-a, c].

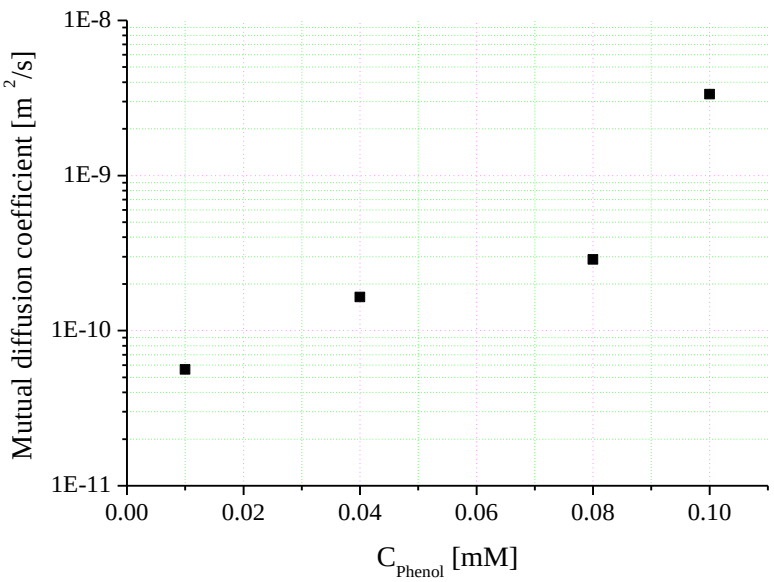

Fig. 4.16: Averaged mutual diffusion coefficients for different initial phenol concentrations [Naddaf and Bart, 2011-a, c]

4.8. Summary

The investigated self-synthesized poly(N-isopropylacrylamide) hydrogel showed both thermally-induced and pH-induced volume phase transitions. The used confocal Raman spectroscopy has been an efficient device in investigating the volume phase transitions and the structural composition of the produced hydrogels.

Both Raman spectra profiles and the swelling ratio calculations showed hydrogel lattice collapse as a response to temperature increase. The collapse was distinguished by the appearance of sharp Raman spectra and by a sharp reduction in the swelling ratio, especially above the lower critical solution temperature (LCST). Increasing the temperature above the LCST causes a non-reversible thermo effect deformation within the hydrogel lattice. The same result is obtained in the case of equilibrating the hydrogel in phenol, i.e., Raman intensity increases by increasing the phenol concentrations and confirming that the changes inside the hydrogel lattice are happening. The mentioned non-reversible thermo effect showed in terms of changes in Raman intensity for the isopropyl group. The hydrogel follows volume phase transition due to the high acidity and high alkalinity. The lattice collapse due to the pH-value of the equilibrium solution is more noticeable in terms of swelling ratio than Raman spectra.

Besides obtaining information about the chemical composition of the hydrogel/phenol system, Raman spectroscopy was used to study the change of intensity with the solute concentration during the diffusion, from which the mutual diffusion coefficient, D_{mut} in the thermosensitive poly(NIPAAm) hydrogel loaded with different initial concentrations of phenol (0.01mM, 0.04mM, 0.08mM and 0.1mM) at a selected temperature of 25°C was calculated. The mutual diffusion coefficient was calculated for a long period at a fixed spatial position within the hydrogel near the outer surface for both solutes (BSA and phenol) at 25°C. For the thermosensitive poly(NIPAAm), which were swelled to equilibrium in different concentrated phenol and BSA solutions, the mutual diffusion coefficient was calculated based on a relation between the solvent concentration and Raman intensity of the poly(NIPAAm)/solvent system. Poly(NIPAAm) hydrogels were loaded and allowed to swell to equilibrium with either aqueous

phenol or BSA solutions. The phenol solutions prepared were 0.01mM, 0.04mM, 0.08mM, and 0.1mM, and the BSA solutions were 0.01M, 0.05M, 0.10M, and 1.51M.

The diffusion coefficient increase by increasing the concentration of phenol. The mutual diffusion coefficient varied from 5.61845×10^{-11} to 3.34565×10^{-9} m^2/s for the hydrogel cylinder loaded with phenol concentrations of 0.01mM and 0.1mM, respectively. This dependency of diffusivity on concentration is due to the solute-hydrogel interaction. Although the change of the concentrations studied here is significant, the values obtained for the mutual diffusion coefficient of poly(NIPAAM)/BSA varied only slightly, from $5.67\cdot10^{-14}$ m^2/s to $6.07\cdot10^{-14}$ m^2/s for 1.51M to 0.1M, respectively. The results, compared to phenol, indicate an increase in resistance to diffusion inside the hydrogel due to a high swelling ratio and/or the average free hole volume, which strongly influences the mutual diffusion coefficient. The larger average free hole volume of a solute with a high molecular weight (such as BSA) leads to larger diffusivity at a given solute concentration.

5. Mechanical properties: hydrogel characterization and experimental setup

5.1. Introduction

Mechanical properties, which define the deformation, flow, and rupture of hydrogels under an external load, are among the most important and least understood physical properties of hydrogels. As mentioned previously, hydrogels have been investigated by many researchers for applications in biotechnological, medical, biological, and pharmaceutical fields (contact lenses, membranes for biosensors, sensors, actuators linings for artificial hearts, and materials for artificial skin) [Peppas and Langer, 1994, Walther et al., 1995, Peppas et al., 2000, Chung et al., 1999, Melekaslan et al., 2003]. Such load bearing applications require an optimal hydrogel that is relatively strong yet elastic. In addition, for these applications, hydrogel is in direct contact with body fluids, which requires ensuring both accurate and targeted adsorption/desorption of an aqueous solution and a certain level of mechanical strength to maintain shape and performance. Therefore, the mechanical properties are important for both basic studies of gels and for determining the utility of the polymer in an appropriate application [Liu et al., 2007, Hakiki and Her, 1994, Muniz and Geuskens, 2001, Alenichev et al., 2007]. Controlling the polymerization conditions, such as temperature, light intensity, ionic strength, and pH, plays the main role in achieving the desired mechanical properties of the hydrogel [Baker et al., 1994, Crump, 2001]. Other techniques, such as the addition of a compound [Philippova et al., 1994] and thermal recycle [Cha et al., 1993] or changing the cross-linking density, can also affect the hydrogel strength. The dependence of the mechanical desired properties of hydrogels on various parameters was summarized elsewhere [Peppas et al., 2000, Anseth et al., 1996]. Although the mechanical properties should be the prime consideration in determining the suitable application, little is known about the mechanical behaviour of hydrogels. In recent years, however, experiments were performed to study the mechanical behaviour of the hydrogels under different conditions.

In this work [Naddaf and Bart, 2008, Naddaf and Bart, 2001c], hydrogels are characterized by their stress-strain properties and their response to mechanical deformation, e.g., compression and elongation. Despite the applied load, they are still able to recover their initial shape.

Hydrogels can be synthesized as long cylinders, large disk spheres, or slabs because their geometry is an important factor that affects their mechanical strength. We worked with cylindrical gels that good contact surface and have a better ability for trap, transport, and drug release. According to our work, the collective diffusion coefficient, D_{col}, based on the mechanical properties of hydrogel, was examined. For this purpose, an experimental setup (uniaxial compression apparatus) was designed to measure the diffusion coefficient for aqueous phenol and BSA solutions through a cylindrical poly(NIPAAm) hydrogel based on its viscoelastic properties as a function of its equilibrium temperature. The collective diffusion coefficient was calculated using the correlation developed by Tanaka [Tanaka et al., 1973]. The mean measurements and the calculated elastic modulus of hydrogel cylinders were based on the designed experimental setup and the procedure followed is detailed in Appendix F.

5.2. Experimental setup

The compression test apparatus used in this research was designed to compress the hydrogel uni-axially at a constant rate. The instantaneous applied load was transferred continuously and simultaneously to the hydrogel cylinder, by which the load is conducted along the direction of the stress (Fig. 5.1)..

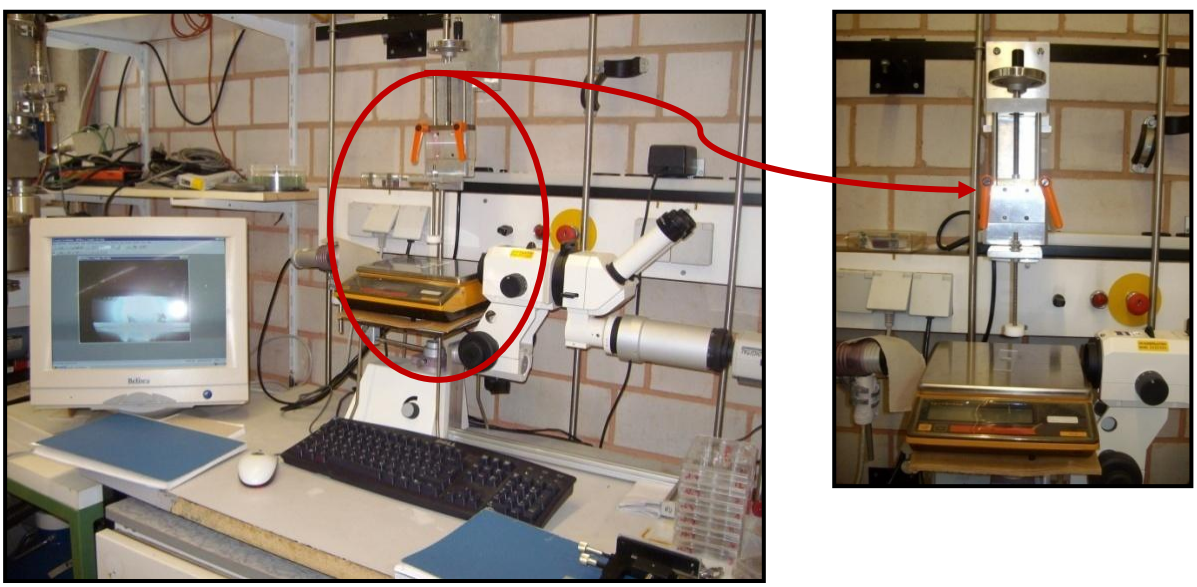

Fig. 5.1: System used for measuring the applied force and the hydrogel dimensional changes during compression

The mechanical properties examination in addition to the collective diffusion coefficient measurements were accomplished at a thermostated environment of 25°C using the uniaxial compression apparatus shown in Fig. 5.2 [Naddaf and Bart, 2011-c]. A vertical load was applied manually through the piston (E, G, and F) on the cylindrical hydrogel samples (H), which were placed directly above a digital scale (D) (L610-**D Sartorius GmbH). The transmitted compression force (and the applied stress) to the hydrogel cylinder was calculated from the reading of the balance. Meanwhile, the resulting deformations (associated strain) were detected using a microscope (C) (Stemi SV 11) connected to a colour video camera (A) (JVC.TK-C1381) and an objective (B) (Imtronic GmbH). The required measurements were carried out accurately using a PC (J) with a Grab&View® software and Image-C program®.

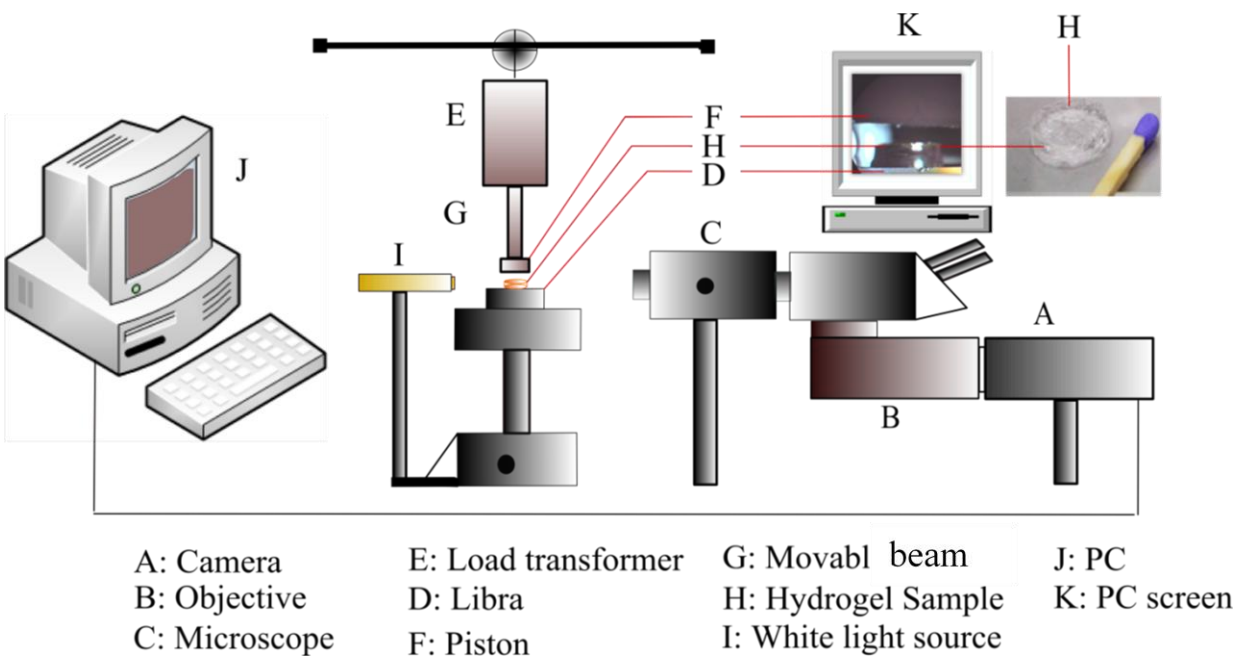

Fig. 5.2: The detailed description of the uniaxial compression system [Naddaf and Bart, 2011-c]

In the elastic stage, the applied stress increased proportionally with strain until reaching the yield point, at which point the hydrogel cylinder becomes less elastic and broken. The Young

modulus is affected at a certain swelling ratio degree with the temperature elevation [Muniz and Geuskens, 2001, Koros et al., 1976]. The hydrogel cylinders subjected to a load at high temperatures (i.e., 37ºC) have less elasticity

5.3. Viscoelastic characterization

The compression system described in Section 5.2 was designed to increase the force gradually until reaching the rupture state or maximal possible applied force, i.e., the behaviour of a hydrogel submitted to a continuous stress increase was monitored via the camera until the maximum deformation was reached. The mean recorded measurements are the mass of the hydrogel before and after compression, the changes in the diameter, ΔD, and the thickness, Δl, of the hydrogel as a response to the applied load.

5.3.1. Mechanical behaviour

With the designed compression test apparatus, the applied load was increased gradually on the individual poly(NIPAAm) cylinders in their swollen state by a force step of 0.2N. Depending on the equilibrium conditions, some poly(NIPAAm) cylinders were able to bear a force up to 4N without breaking down. The initial diameter of the hydrogel cylinder affects the final force the hydrogel can withstand. Figs. 5.3 and Fig. 5.4 show force versus diameter change of poly(NIPAAm) cylinders of different initial diameters, d_0, and different concentrations of phenol and BSA at 25ºC, respectively. The measuring time of the data points, which ranged according to the hydrogel cylinder conditions between 9 and 17 points, was kept as short as possible to avoid weight loss due to evaporation in the open system. The resulting relation between the applied load and the deformations seems to be non-linear, and poly(NIPAAm) cylinders with a high initial diameter can withstand higher load [Naddaf and Bart, 2011-c].
Meanwhile, a larger force is required to obtain a given degree of deformation for the thicker poly(NIPAAm) cylinders, as can be seen from Figs. 5.5 and Fig. 5.6, for phenol and BSA loaded hydrogels, respectively. The minus sign of the thickness change, Δl, refers to the reduction of thickness due to the uniaxial applied load.

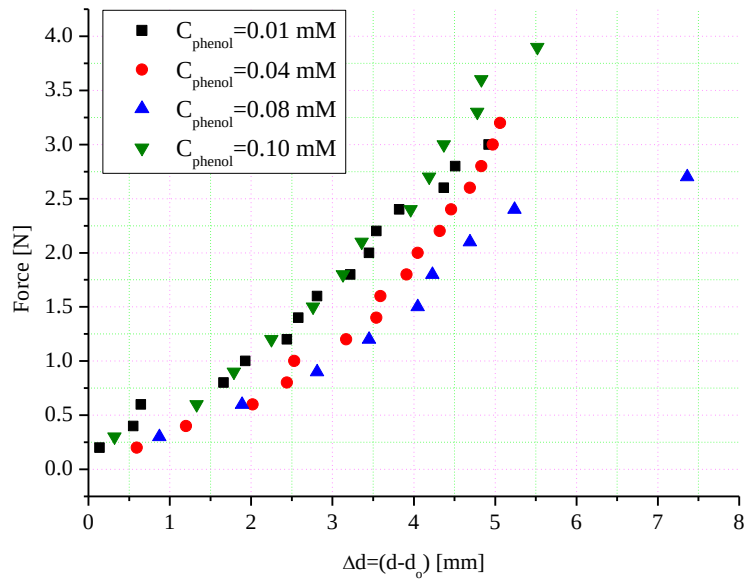

Fig. 5.3: Force versus diameter change of four poly(NIPAAm) cylinders of different initial diameters ($d_{0=}$ ■ 13.156mm; ●13.064 mm; ▲12.42 mm; ▼13.064 mm) and different concentrations of phenol at 25ºC [Naddaf and Bart, 2011-c]

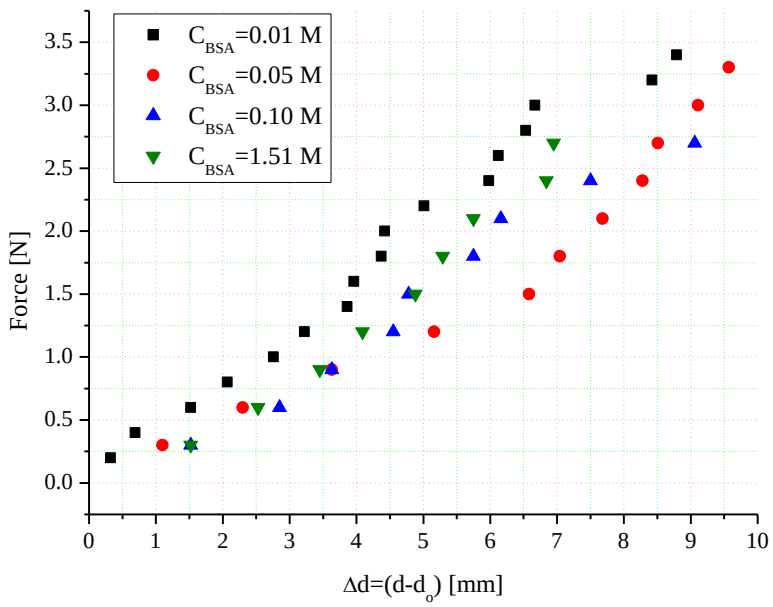

Fig. 5.4: Force versus diameter change of four poly(NIPAAm) cylinders of different initial diameters (d_0 =■ 12.742mm; ●13.478 mm; ▲11.914 mm; ▼12.006 mm) and different concentrations of BSA at 25ºC [Naddaf and Bart, 2011-c]

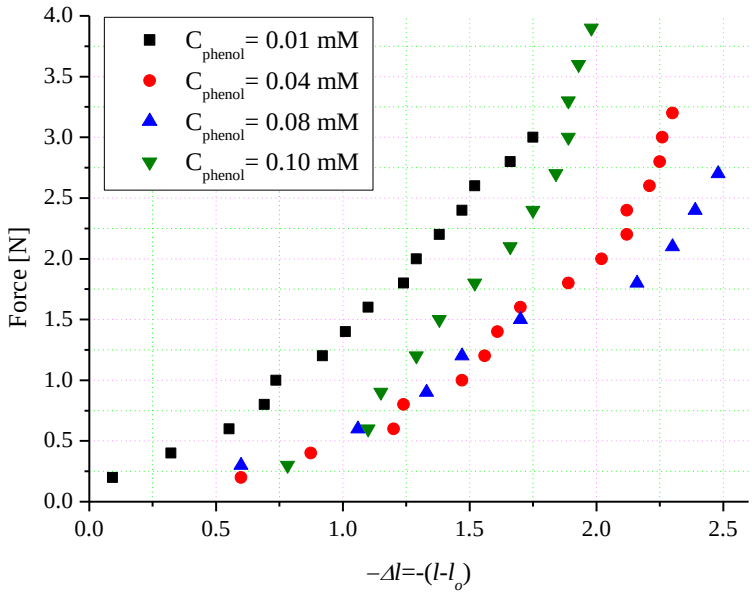

Fig. 5.5: Force versus thickness change of four poly(NIPAAm) cylinders of different initial thicknesses (l_o=■ 2.852mm; ●3.772mm; ▲3.588 mm; ▼ 2.944 mm) and different concentrations of phenol at 25ºC [Naddaf and Bart, 2011-c]

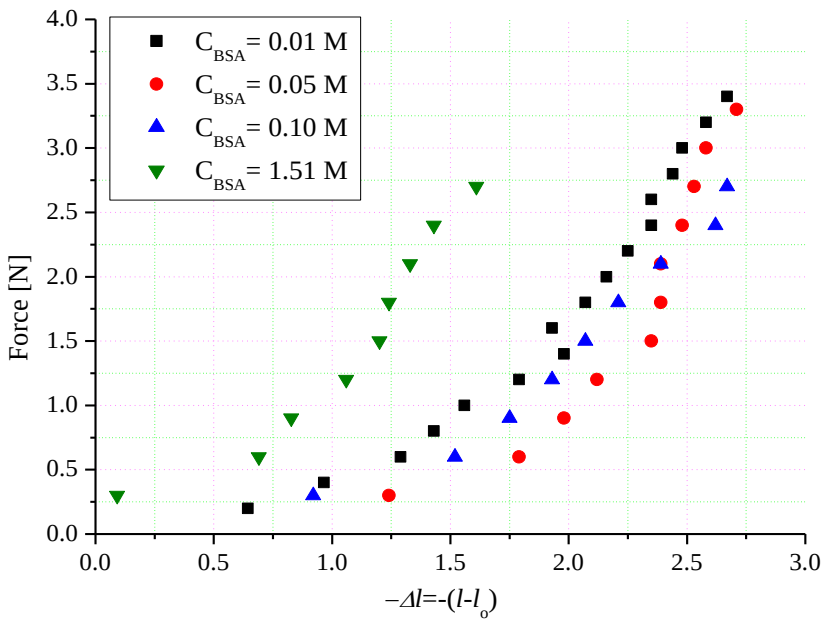

Figs. 5.6: Force versus thickness change of four poly(NIPAAm) cylinders of different initial thicknesses (l_o=■ 3.634 mm; ●3.358 mm; ▲ 3.818 mm; ▼3.22 mm) and different concentrations of BSA at 25ºC [Naddaf and Bart, 2011-c]

Typical obtained stress-strain data are shown in Fig. 5.7. The included insets show the images of the hydrogel cylinder at the corresponding deformation. The shown poly(NIPAAm) hydrogel cylinder consists of an MBA mole fraction of 0.0115 (Hydrogel_1) and exhibits a sigmoidal stress-strain relationship in the elastic region, which ended at 7 MPa. The stress continues rising until the hydrogel cylinder ruptures. This typical curve is affected by change in temperature and concentration [Naddaf and Bart, 2011-c].

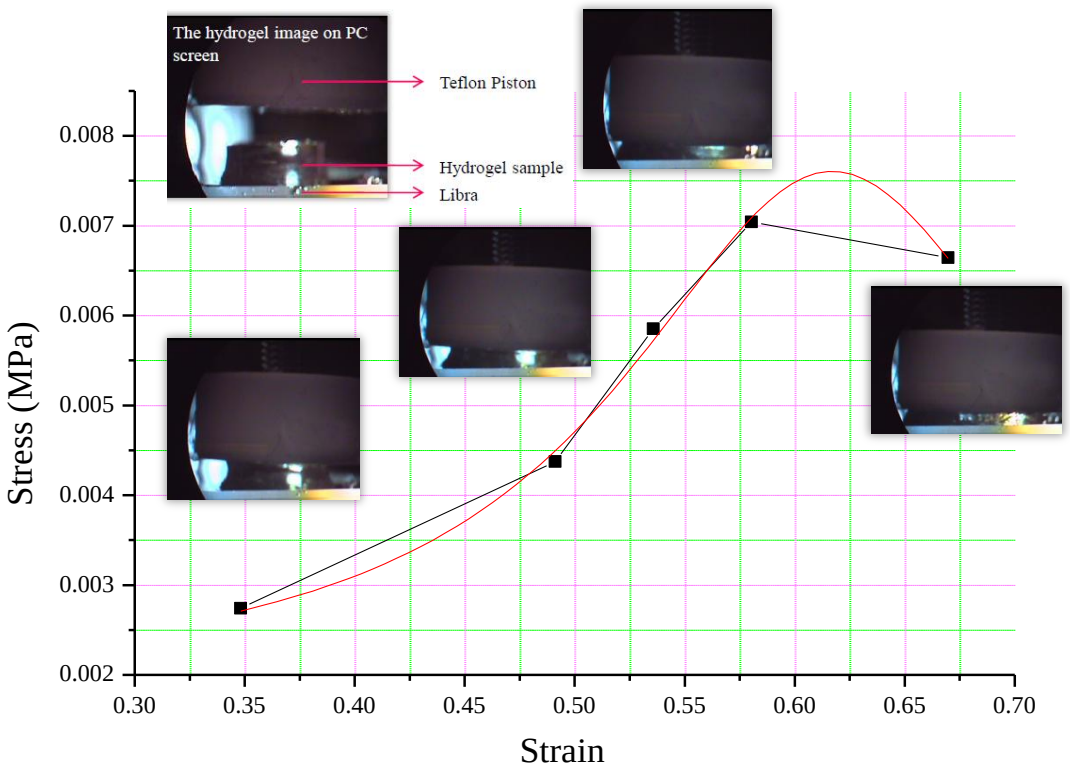

Fig. 5.7: Stress-strain data for poly(NIPAAm) of a matrix ration of 0.105 after swelled to an equilibrium at 25°C in deionized water [Naddaf and Bart, 2011-c]

As can be seen from Figs. 5.8 and Fig. 5.9 [Naddaf and Bart, 2011-c], both hydrogel/phenol and hydrogel/BSA loaded cylinders show a lower linear strain response below the LCST, which indicates demonstration of elastic behaviour. For example, at 25ºC the maximum strain was not exceeding 75% for phenol and BSA with a corresponding maximal compression stress of 0.0144 MPa and 0.009 MPa, respectively. Similarly, at 32ºC the maximum achieved strain was 83% for phenol and 79% for BSA. At higher temperatures, the linear strain response,

which is combined with dynamic viscoelastic behaviour, becomes more remarkable until reaching its maximum. The hydrogel/phenol cylinder was able to reach 90% deformation at 40ºC and to withstand a maximum stress of 0.195 MPa without rupture (Fig. 5.8). Less maximum deformation of 85% was achieved for the hydrogel/BSA cylinder. Here, the concentration of the solute plays a minor role in the hydrogel lattice deformation [Naddaf and Bart, 2011-c]. As can be seen from Figs. 5.8 and Fig. 5.9, each sample was subsequently deformed to a specific compressive strain level, by which the strain changes proportionally with the applied load. Moreover, the stress increases strongly from 25ºC to 40ºC.

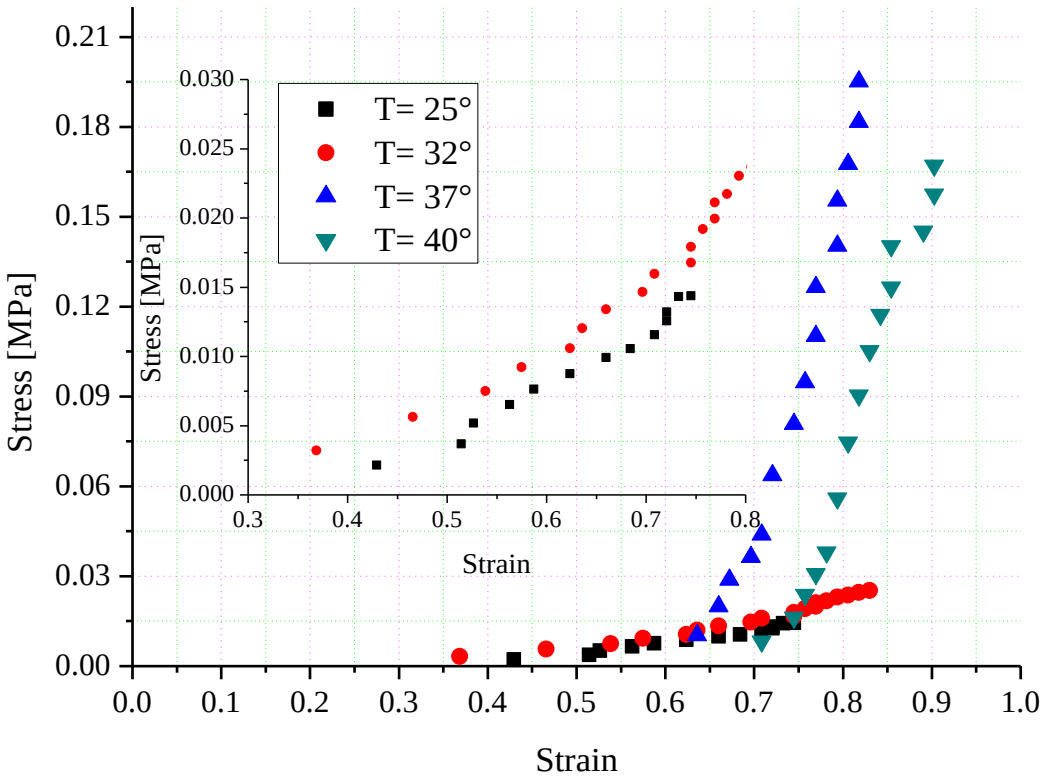

Fig.5.8: Stress-strain curves for hydrogels swelled in 0.10 mM phenol solution at different temperatures

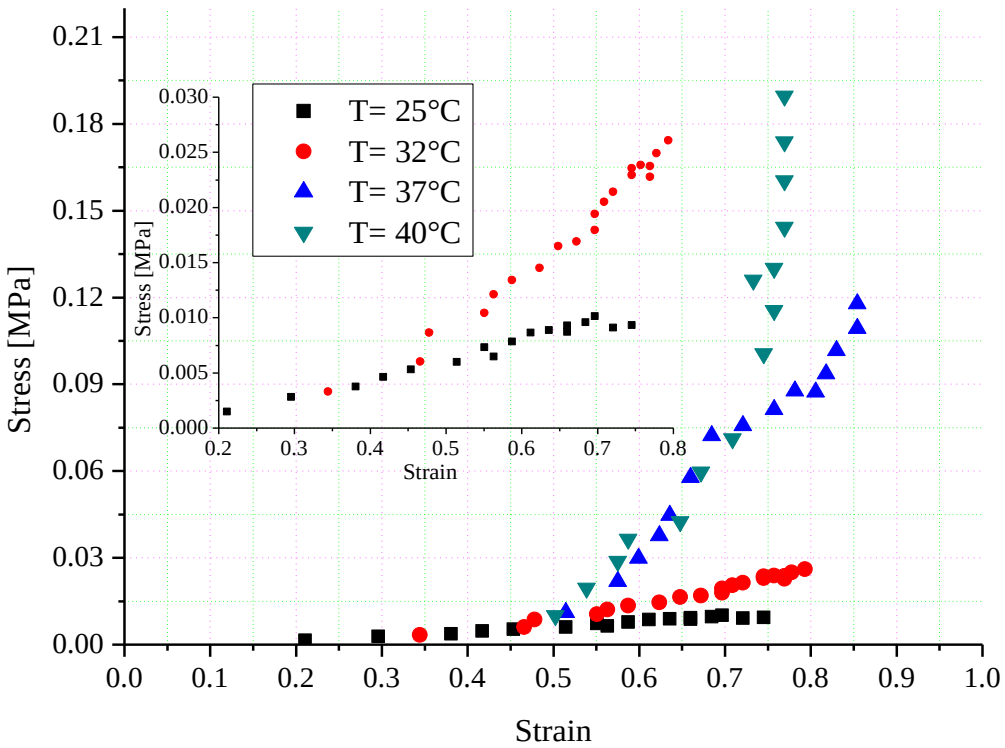

Fig. 5.9: Stress-strain curves for hydrogels swelled in 0.01M BSA solution at different temperatures

This behaviour can be understood better by relating it to the dependency of the swelling ratio on the temperature presented in Fig. 5.10. By increasing the temperature, the hydrogel shrinks and becomes harder due to the denser network. By temperature elevation from 25ºC to 37ºC for hydrogel/phenol system, the compressive stress increased from 0.015 MPa up to 0.20 MPa. For the same temperature elevation range, the compressive stress increased from about 0.008 MPa to 0.12 MPa for the hydrogel/BSA system [Naddaf and Bart, 2011]. The increase in the compressive stress of the hydrogel/phenol cylinder can be related to the contribution of phenol molecules, which participate in forming a dense layer of the hydrogel network [Watanabe and Iwata, 1996, Kosik et al., 2007]. In both cases, the increase of the compressive stress may suggest that temperature elevation influences the mechanical properties and leads to a stronger hydrogel.

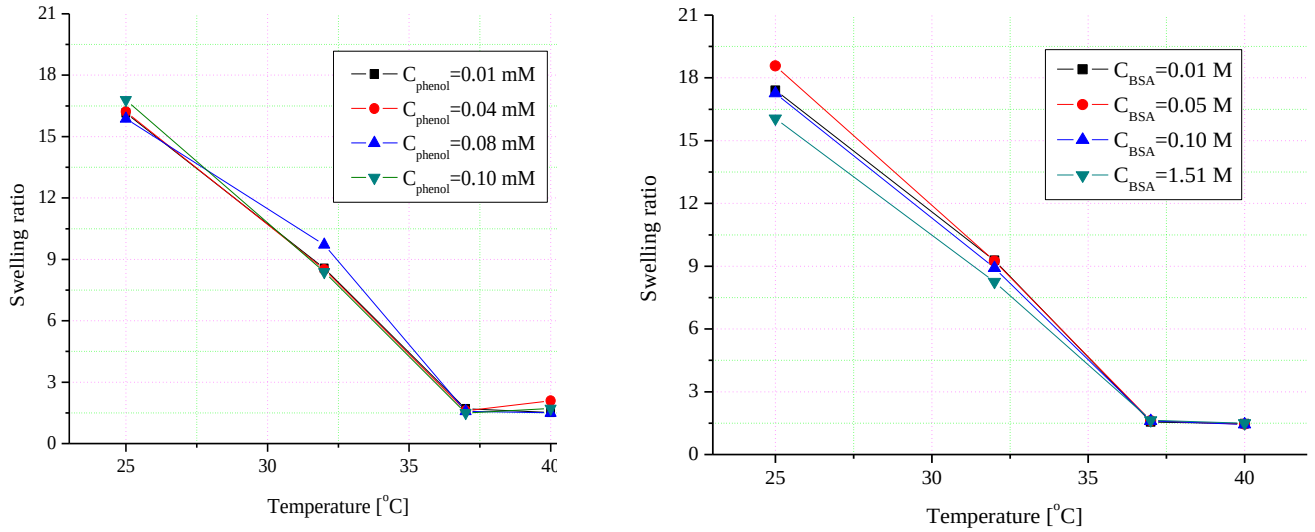

(a) (b)

Fig. 5.10: Swelling ratio as a function of temperature for poly(NIPAAm) immersed to equilibrium in (a) phenol and (b) BAS

5.3.2. Young's modulus

Young's modulus provides information to predict the behaviour of the hydrogel under compression. The Young's modulus (Y) of the hydrogels at different swelling ratios was determined from the initial portion of the stress-strain data obtained from the compression test using equation:

$$Y \equiv \frac{Stress}{Strain} = \frac{F/A_\circ}{\Delta l/l_\circ} = \frac{Fl_\circ}{A_\circ \Delta l} \qquad (5.1)$$

F is the uniaxial force acting per unit cross-sectional area (A_o); Δl is the deformation ratio, and l_o is the initial thickness. In this work, Young's modulus was determined from the initial portion of the stress-strain data in compression tests up to 30% strain. The behaviour of a hydrogel submitted to a continuous stress increase was monitored until the maximum deformation was reached.

Fig. 5.11 shows the increase of the Young's modulus, with elevating the temperature as an indication for the local stiffness increase, which occurs because of the network collapse

[Harmon et al., 2003]. Increasing the Young modulus was also the response of the hydrogels set to equilibrium in alkali and acidic solutions. As obtained from the experimental data, the hydrogel undergoes a major phase change for pH in between 5.0 and 7.0 in agreement with previous work [Sudipto et al., 2002, Naddaf and Bart, 2008].

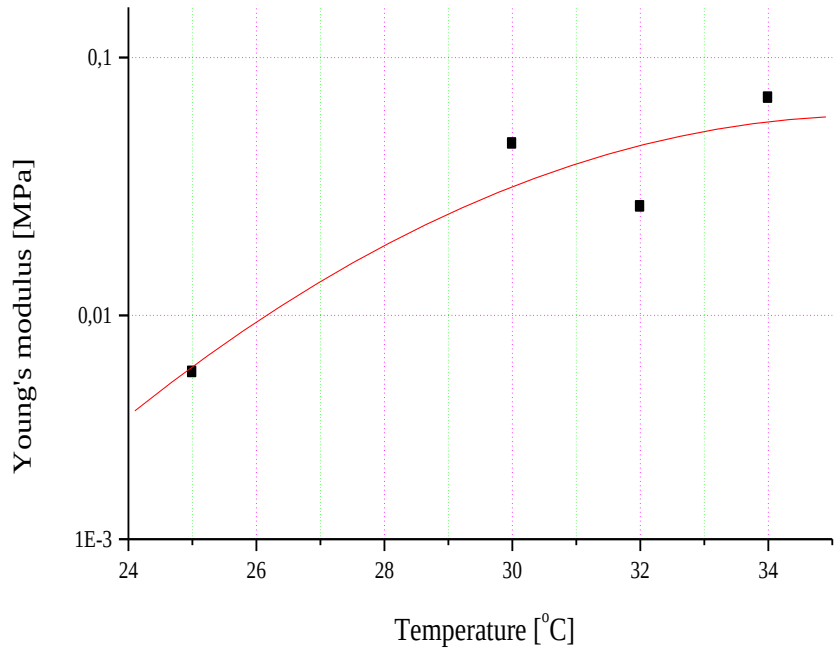

Fig. 5.11: The Young modulus as a function of the equilibrium temperatures (pH=7) [Naddaf and Bart, 2008]

The Young's modulus changes by varying the swelling ratio of hydrogel cylinders swelled to equilibrium in different concentrations of phenol solutions and BSA solutions are given in Fig. 5.12 and Fig. 5.13, respectively [Naddaf and Bart, 2011-c]. The rapid changes of the Young modulus at a certain swelling ratio degree are clearly contributed due to the temperature elevation and are less sensitive to concentration changes. Exceeding the LCST expels the liquid from the hydrogel lattice, causing a substantial increase in the Young modulus from about 0.14MPa for 0.1mM phenol solution and about 0.3MPa for 1.51M BSA, compared to 0.02MPa for 0.1mM phenol solution and about 0.035MPa for 1.51M BSA, at 25^{o}C [Naddaf and Bart, 2011-c]. At this range of temperatures, the poly(NIPAAm) forms a physical entanglement, which increases the apparent cross-linking density of the hydrogel and then the compressive

elastic modulus [Muniz and Geuskens, 2001, Muniz and Geuskens, 2001]. The effect of the concentration of solute (phenol or BSA) shows less effect on the Young's modulus compared to the effect of temperature. Nevertheless, the deviation in the Young's modulus with changing BSA concentration is more obvious than that of phenol.

The calculated Young's modulus variation with initial thickness is illustrated in Fig. 5.14 and Fig. 5.15 for phenol and BSA, respectively. The cross sectional areas combined with hydrogel cylinder deformation were measured with the aid of the optical microscope and the image analysis software described above. The obtained results indicate that the mechanical strength of the hydrogel cylinders decreases with increasing the thickness of the sample [Naddaf and Bart, 2011-c].

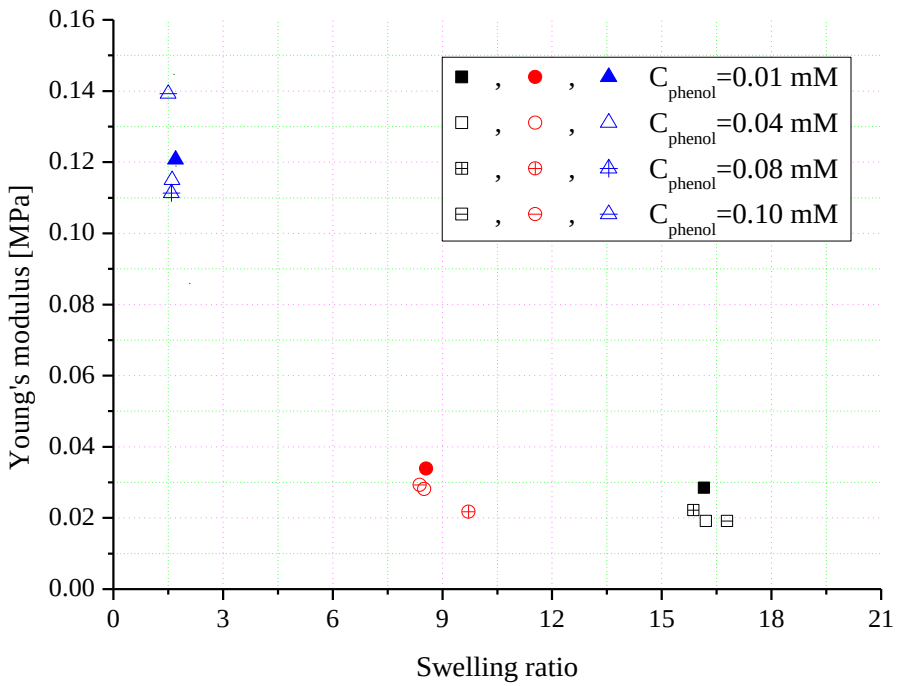

Fig. 5.12: Young's modulus variation for different phenol solutions at different temperatures: (■) 25°C; (●) 32°C; (▲) 37°C [Naddaf and Bart, 2011-c]

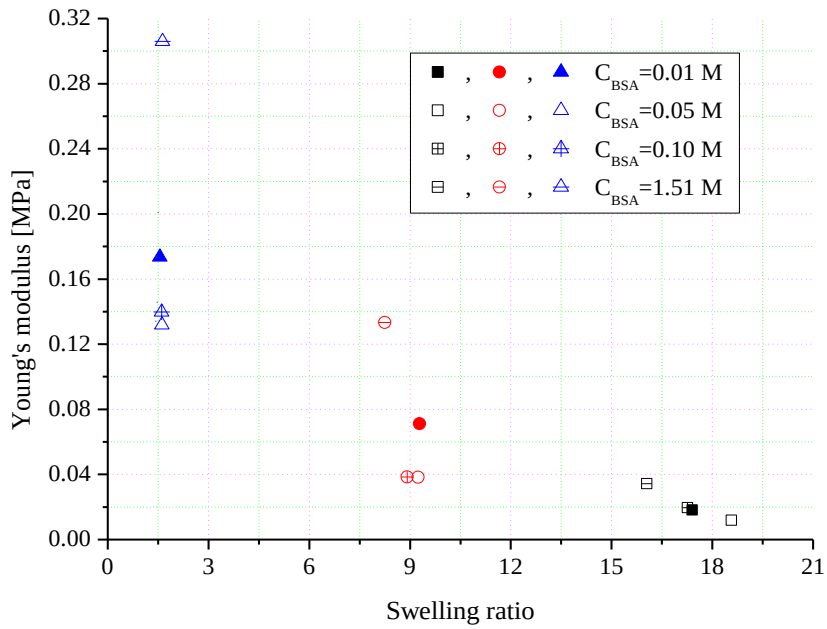

Fig. 5.13: Young's modulus variation for different BSA solutions at different temperatures: (■) 25°C; (●) 32°C; (▲) 37°C [Naddaf and Bart, 2011-c]

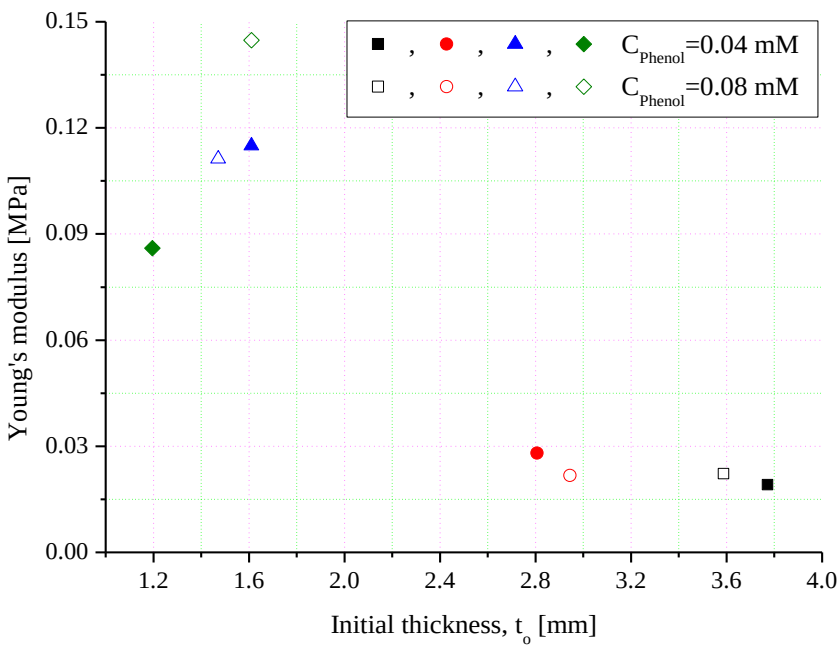

Fig. 5.14: Young's modulus for hydrogels swelled in 0.04mM and 0.04mM phenol solution at different temperatures: (■) 25°C; (●) 32°C; (▲) 37°C; (♦) 40°C [Naddaf and Bart, 2011-c]

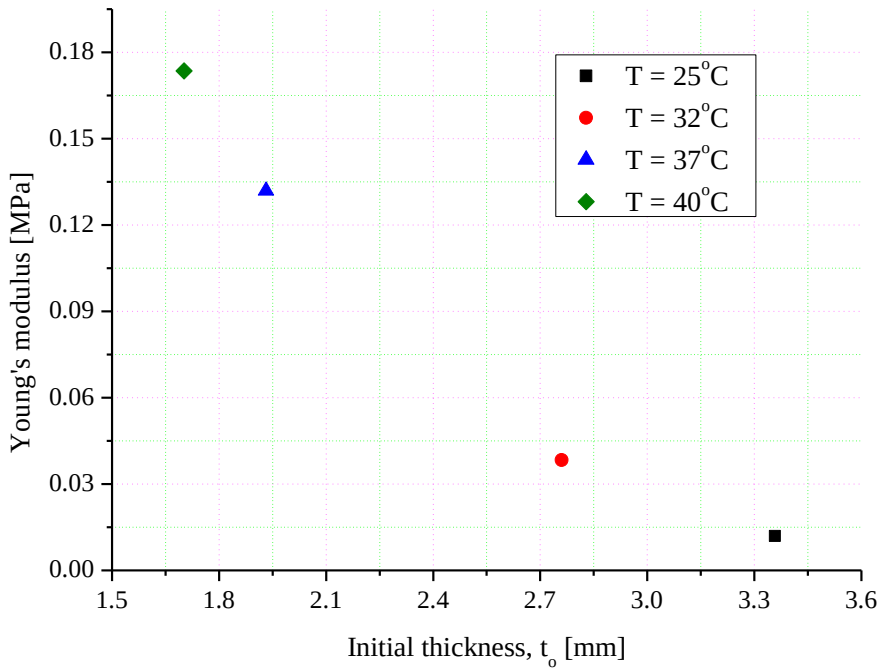

Fig. 5.15: Young's modulus for hydrogels swelled in 0.05M BSA solution at different temperatures [Naddaf and Bart, 2011-c]

5.4. Results and discussion

5.4.1. Collective diffusion coefficient

As mentioned above, from the compression test, the primary elastic modules, such as the Young's modulus, shear modulus, and the bulk modulus (Appendix F), were calculated using Matlab® (Appendix G). With those obtained modules, the collective diffusion coefficient, D_{col}, was determined using the Tanaka-Fillmore equation [Tanaka et al., 1973]:

$$D_{col} = \left(K + \frac{4\mu}{3} \right) \Big/ f \tag{5.2}$$

$$K = Y/3(1-2v) \tag{5.3}$$

$$\mu = Y/2(1+\nu) \tag{5.4}$$

Here, K is the bulk modulus [N\m2], μ is the shear modulus [N\m2], ν is the Poisson's ratio, and f is the friction coefficient, which describes the viscous interaction between the polymer and the solvent. As mentioned previously, the Young's modulus was determined from the initial part of the stress-strain data of the compression test using equation (5.1).

Based on the experimental values obtained from the compression measurements, the viscoelastic properties (bulk modulus, shear modulus, Poisson's ratio, and the friction coefficient) were calculated using Matlab® and used to calculate the collective diffusion coefficient.

Table 5.1: Experimental data obtained from the compression measurements and used to calculate the collective diffusion coefficient [Naddaf and Bart, 2011-c]

Material	Concentration (M)	T(ºC)	Diameter, d (m)		Thickness, l (m)		D_{col}, $(m^2/s) \times 10^{-9}$
			Initial	Final	Initial	Final	
Phenol	10^{-5} M	25	0.013156	0.015088	0.002852	0.002116	0.0074
Phenol	10^{-5} M	37	0.005336	0.005704	0.001242	0.000782	0.0855
Phenol	10^{-5} M	40	0.004622	0.004830	0.001932	0.001518	0.1939
Phenol	$4 \cdot 10^{-5}$ M	25	0.013064	0.015594	0.003772	0.002300	0.0056
Phenol	$4 \cdot 10^{-5}$ M	32	0.010120	0.012420	0.002806	0.001564	0.0070
Phenol	$4 \cdot 10^{-5}$ M	37	0.004922	0.005290	0.001610	0.000874	0.0840
Phenol	$4 \cdot 10^{-5}$ M	40	0.005244	0.005934	0.001196	0.000552	0.0518
Phenol	$8 \cdot 10^{-5}$ M	25	0.012420	0.015226	0.003588	0.002254	0.0035
Phenol	$8 \cdot 10^{-5}$ M	32	0.010212	0.012466	0.002944	0.001288	0.0082
Phenol	$8 \cdot 10^{-5}$ M	37	0.004784	0.005474	0.001472	0.000736	0.0607
Phenol	$8 \cdot 10^{-5}$ M	40	0.005290	0.005566	0.001610	0.001104	0.1074
Phenol	10^{-4} M	25	0.013064	0.014858	0.002944	0.001794	0.0092

Phenol	10^{-4} M	32	0.009752	0.012374	0.003220	0.001748	0.0041
Phenol	10^{-4} M	37	0.004876	0.005382	0.001794	0.001104	0.0826
Phenol	10^{-4} M	40	0.005474	0.005792	0.001288	0.000828	0.0883
BSA	10^{-2} M	25	0.012742	0.015502	0.003634	0.002070	0.0049
BSA	10^{-2} M	32	0.010166	0.011500	0.002392	0.001978	0.0070
BSA	10^{-2} M	37	0.004692	0.005336	0.002070	0.001380	0.0731
BSA	10^{-2} M	40	0.005060	0.005474	0.002024	0.001334	0.0934
BSA	$5\cdot10^{-2}$ M	25	0.013478	0.017112	0.003358	0.001380	0.0032
BSA	$5\cdot10^{-2}$ M	32	0.009982	0.012466	0.002760	0.001840	0.0002
BSA	$5\cdot10^{-2}$ M	37	0.005198	0.005888	0.001932	0.001242	0.0614
BSA	$5\cdot10^{-2}$ M	40	0.004968	0.005382	0.001702	0.001196	0.1033
BSA	0.1M	25	0.011914	0.015548	0.003818	0.002070	0.0006
BSA	10^{-1} M	32	0.010074	0.012190	0.002116	0.001426	0.0052
BSA	10^{-1} M	37	0.005060	0.005888	0.002070	0.001334	0.0494
BSA	10^{-1} M	40	0.005106	0.005382	0.002024	0.001288	0.1022
BSA	1.51 M	37	0.004876	0.005474	0.001840	0.001518	0.0479
BSA	1.51 M	40	0.004876	0.005336	0.002070	0.001518	0.1026

It was found [Naddaf and Bart, 2011-c] that the collective diffusion coefficient for the different hydrogel sample is measured to be identical at 25ºC and 32ºC (below and around the LCST), regardless of the BSA (or phenol) concentration used (Fig. 5.16). Meanwhile, above the LCST, it varied significantly, at which the temperature elevation, which plays a remarkable role in hydrogel shrinking, caused an increase in the diffusion coefficient in the hydrogel/phenol system. For example, at 25°C, the diffusion coefficient of the hydrogel cylinder immersed to equilibrium in the 0.01mM phenol equals 7.4×10^{-12} m/s^2 and this value increased about two orders of magnitude by increasing temperature to reach 1.939×10^{-10} m/s^2 at 40^{o}C (Fig. 5.16) [Naddaf and Bart, 2011-c]. The effect of temperature on the diffusion coefficient follows the

same trend for all phenol concentrations. Nevertheless, the highest concentration of phenol (0.10mM), which also affects the hydrogel shrinking at low temperatures, is responsible for decreasing the diffusion coefficient compared to the lowest concentration of phenol (0.01mM) in an order of magnitude from 9.2×10^{-12} m/s^2 to 8.83×10^{-11} m/s^2. From Fig. 5.16 and Fig. 5.17, the temperature elevation also causes an increase in the diffusion coefficient for the hydrogel/BSA system but with less divergence compared to the hydrogel/phenol system. Meanwhile, the diffusion coefficient of 0.01M BSA varied from 4.9×10^{-12} m/s^2 at 25^{o}C to reach 9.34×10^{-11} m/s^2 at 40^{o}C (Fig. 5.17) [Naddaf and Bart, 2011-c]. In contrast to phenol, the higher concentration of BSA has almost no remarkable effect on changing the diffusion coefficient, i.e., it increased from 1.92×10^{-11}m/s^2 for the 0.01M BSA to 1.026×10^{-10}m/s^2 for the 1.5M BSA. This means that the concentration of BSA has less effect on shrinking compared to the interactions caused by the ring-shaped phenol molecule, which can act as a proton donor or acceptor [Watanabe and Iwata, 1996]. More about the effect of phenol on the thermosensitive hydrogel is available elsewhere [Kosik, et al., 2007].

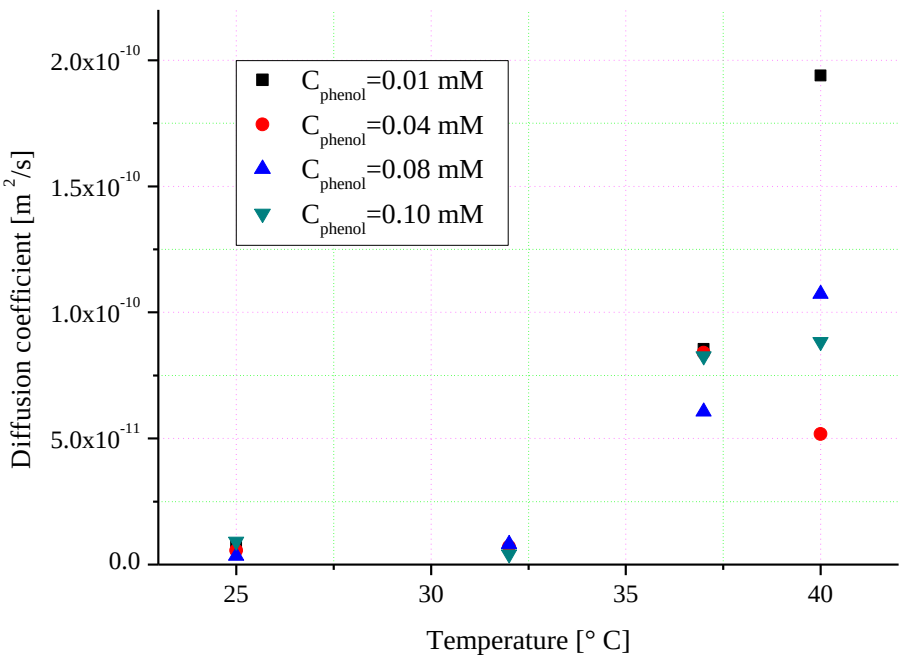

Fig. 5.16: D_{col} with temperature change for different concentrations of phenol [Naddaf and Bart, 2011-c]

The diffusion coefficient of 0.01M BSA varied from 4.9×10^{-12} m/s^2 at 25^{o}C to reach 9.34×10^{-11} m/s^2 at 40^{o}C (see Fig. 5.17) [Naddaf and Bart, 2011-c]. The effect of temperature on the diffusion coefficient follows the same trend for all BSA concentrations. In contrast to phenol, the higher concentration of BSA had almost no remarkable effect on changes of the diffusion coefficient, i.e., they increased for the 1.5M BSA from 1.29×10^{-11} m/s^2 to 1.026×10^{-10} m/s^2 [Naddaf and Bart, 2011-c]. This related to the mechanical strength measurements of the hydrogel swelled in BSA protein, which demonstrated that the Young's modulus does not vary with the presence of proteins [Khoury et al., 2003]. The direct effect of the Young's modulus on the collective diffusion coefficient appears in equations (5.3) and (5.4).

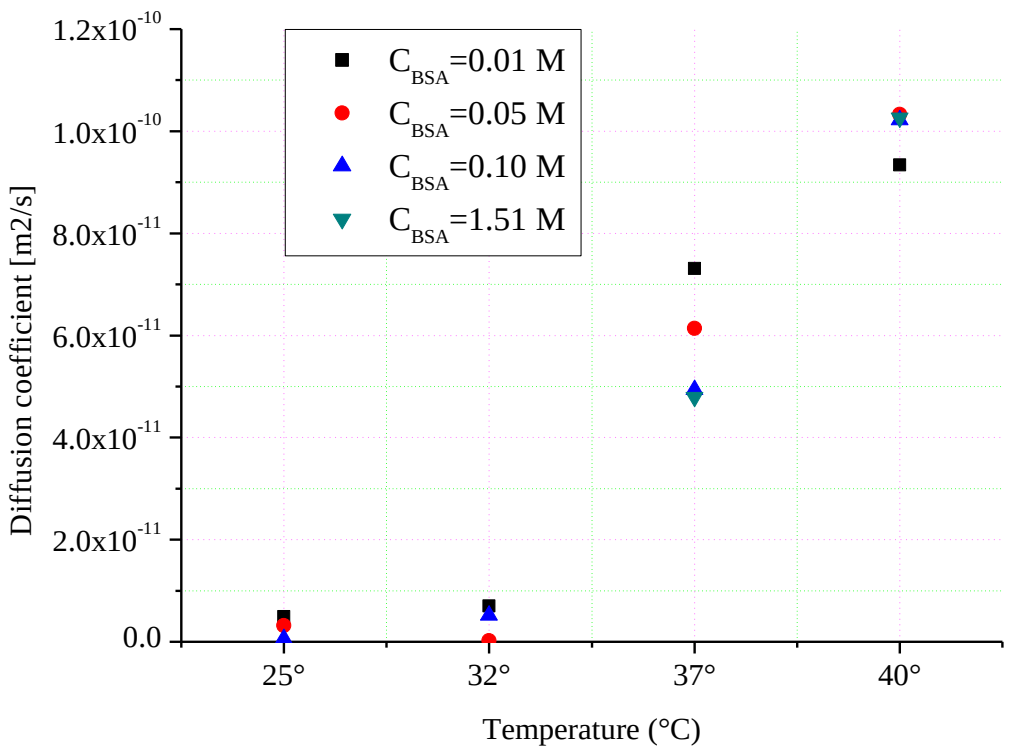

Fig. 5.17: D_{col} with temperature change for different concentrations of BSA [Naddaf and Bart, 2011-c]

5.5. Summary

According to this work [Naddaf and Bart, 2008, Naddaf and Bart 2011-a, c], for the thermosensitive poly(NIPAAm) hydrogels, which were swelled to equilibrium in different concentrated phenol and BSA solutions, the collective diffusion coefficients were calculated after a model [Tanaka et al., 1973] based on measurements of bulk modulus, shear modulus, and the frictional coefficient between the solvent and the hydrogel network.

Poly(NIPAAm) hydrogels were loaded and allowed to swell to equilibrium with either aqueous phenol or BSA solutions. The phenol solutions prepared were 0.01mM, 0.04mM, 0.08mM, and 0.1mM, and the BSA solutions were 0.01M, 0.05M, 0.10M, and 1.51M. A uniaxial compression apparatus was designed to examine the mechanical properties and to determine the collective diffusion coefficient in poly(NIPAAm) hydrogels equilibrated in different solute concentrations at 25ºC, 32ºC, 37ºC, and 40ºC. Depending on the equilibrium conditions, the poly(NIPAAm) cylinders were able to bear an axial load up to 4N without break down. The lower initial diameter is a main factor that affects the final force that a hydrogel can withstand, i.e., a poly(NIPAAm) cylinder with a lower initial diameter can withstand a higher load. However, larger force is required to obtain a given degree of deformation for the thicker poly(NIPAAm) cylinders. Poly(NIPAAm) hydrogel cylinders exhibit a sigmoidal stress-strain relationship in the elastic region. This typical curve is affected by temperature and the composition of the equilibrium solution in the linear stress domain until rupture. At higher temperature, the hydrogels need higher stress for a given deformation and remain in the elastic state even by reaching 90% of the maximal applied strain. Moreover, the stress increases strongly by increasing the temperature from 25°C to 40°C. This behaviour may be better understood relating it to the dependency of the swelling ratio on the temperature, which increases the hardness of the hydrogel due to shrinking. Therefore, temperature elevation is suggested to influence the mechanical properties and leads to a mechanically stronger hydrogel. Both hydrogel/phenol and hydrogel/BSA cylinders show a linear strain response combined with a dynamic viscoelastic behaviour below the LCST. At higher temperatures, this becomes more remarkable until reaching its maximal stress. The Young's modulus is affected at a certain swelling ratio degree with temperature elevation [Muniz and Geuskens, 2001, Koros et al., 1976]. The hydrogel cylinders subjected to a load at high temperatures (i.e., 37ºC) have less

elasticity. The concentration of phenol and BSA shows less effect on the Young's modulus compared to the effect of temperature. Nevertheless, less maximal deformation of 85% was achieved for the hydrogel/BSA cylinder in which the concentration of the diffusing solute plays a minor role in the deformation of the hydrogel lattice. Based on the compression test, the Young's modulus was determined from the initial portion of the stress-strain data. The obtained results indicate that the mechanical strength of the hydrogel cylinders decreases with an increasing of the thickness of the sample.

From the compression measurements and by using a Matlab® Program, the viscoelastic properties, such as the Young's modulus, the shear modulus, and the bulk modulus, were calculated and used to calculate the collective diffusion coefficients based on the Tanaka-Fillmore equation [Tanaka et al., 1973]. The diffusion coefficients below and around the LCST are almost identical. Meanwhile, above the LCST, the diffusion coefficients varied significantly. The temperature elevation from 25°C to 40°C caused an increase in the diffusion coefficient of the hydrogel/0.01mM phenol system within two orders of magnitude. The higher concentration of phenol affects the hydrogel shrinking, even at low temperatures, and increases the diffusion coefficient of the hydrogel/0.1mM phenol system with only one order of magnitude at temperature elevation from 25°C to 40°C. Similarly, the diffusion coefficient of the hydrogel/BSA system increases by increasing the temperature, but with less divergence, above the LCST compared to hydrogel/phenol system because the concentration of the BSA has less effect in shrinking compared to the ring-shaped phenol molecule.

6. Bi-dimensional moving boundary diffusion model: theory and implementation

6.1. Introduction

For modelling swelling kinetics, the diffusion of solvent in polymers can be classified into several types [Flory, 1953]: Fickian, relaxation-controlled, non-Fickian, case II behaviour, and super case II behaviour. In Fickian diffusion, the swelling rate is limited by diffusion from the surface of the swollen polymer to the solvent front. In this kind of diffusion, the sorption rate is proportional to the square root of time, if the diffusion coefficient and the surface concentration remain constant [Sainio, 2005]. In the relaxation-controlled behaviour, the relaxation process is very slow compared to the diffusion rate. This behaviour exists if the polymer is in contact with a good solvent. If the weight uptake in the polymer is linear, then the solute diffusion follows the so-called case II behaviour. The intermediate transport between Fickian and case II can also take place where the rate of mass transport exhibit is dependent on time. In this case, the diffusion is a function of t^n where n is a number between 0.5 and 1.0. The super case II behaviour refers to a sudden acceleration in the rate of mass uptake, wherein the mass transport is affected by the hydrogel thickness. A comprehensive review on hydrogels for controlled release applications and the mathematical description of the release mechanism is given elsewhere [Lin and Metters, 2006, Ganji and Vasheghani-Farahani, 2009]. Diffusion is found to be one of the most important mechanisms in drug release, which allows the use of the polymeric network as a drug delivery system [He, 2006, Richter et al., 2008, Piai et al., 2008, Liu and De Kee, 2005, Mellott et al., 2001, Wu and Zhou, 1997]. Many factors affect diffusion, such as temperature, concentration, and the polymeric network. In poly(NIPAAm) hydrogel, the temperature has the most profound influence on the diffusion coefficient. The protein release in the hydrogel proceeds both diffusion and degradation mechanisms [Zhang, 2005]. The rate of protein release in hydrogel mainly depends on the pore size of the hydrogel, the structure and composition of the matrix, the protein's size, and protein-network interactions [Lin and Metters, 2006, Zhang et al., 2005]. In fact, the drug release mechanism depends on the hydrogel network, as well as on the drug-loading method [Wu and Brazel, 2008]. When the uptake of the drug is performed after the formation of the hydrogel network (the so-called

'post-loading'), the mechanism of uptake and release is then mainly governed by diffusion and/or swelling/shrinking [Wu and Brazel, 2008, Lin and Metters, 2006]. For this reason, the most applied models are still based on Fick's second law of diffusion [Ganji and Vasheghani-Farahani, 2009, Siepman et al., 1998, Russell et al., 2003, Amsden and Turner, 1999] or variable diffusion coefficients *D* [Russell et al., 2003, Russell and Carta, 2005]:

$$\frac{\partial C}{\partial t} = \frac{1}{x^{\beta}}\left(Dx^{\beta}\frac{\partial C}{\partial x}\right) \tag{6.1}$$

where C is the solute concentration in the hydrogel, x is the horizontal coordinate, t is the time, and β is a form factor: 0 (slab); 1 (cylinder); 2 (sphere).

Bi-dimensional models are applied [Siepman et al., 1998, Amsden and Turner, 1999] using an analytical solution for cylindrical particles of constant size. They are proposed for the case of moving boundaries due to swelling/shrinking of the hydrogel [Siepman et al., 1999]. The rate of protein release is generally diffusion-controlled through the aqueous channels within the hydrogels [Russell et al., 2003, Amsden and Turner, 1999, Russell and Carta, 2005]. The drug diffusivities are determined either empirically from fitting the experimental release curves [Van Tomme, 2007, Mellott et al., 2001, Amsden and Turner, 1999, Russell and Carta, 2005] or theoretically estimated (i.e., free volume, hydrodynamic, or obstruction-based theories) [Li and Tanaka, 1990, Kosto and Deen, 2004]. Alternatively, time-dependent power laws function for the cumulative drug release fraction M_t/M_∞ [Lin and Metters, 2006, Wu and Brazel, 2008] describe the diffusion or swelling mechanism on an empirically basis:

$$\frac{M_t}{M_\infty} = kt^n + \alpha \tag{6.2}$$

where α is time-independent term, which is employed to describe the burst release in drug delivery profile in both diffusion-controlled and swelling-controlled release systems, M_t is the mass uptake at time t, and M_∞ is the equilibrium mass uptake. The values of the exponent *n* are 0.5 (slab), 0.45 (cylinder), and 0.43 (sphere) [Lin and Metters, 2006]. Theoretically, the kinetic constant (*k*) should increase with increasing temperature according to the Eyring-theory,

i.e., the diffusion coefficient should be higher. But other research indicates that shrinking (leading to higher volume part of the polymer) decreases the diffusion [Amsden, 2001].

$$k = 4\left[D/\pi l^2 \right]^{1/2} \tag{6.3}$$

Based on experimental observations (as shown in Section 6.4) [Naddaf et al., 2010], the resistance of the hydrogel structure to diffusion increases at higher temperatures due to shrinking, i.e., lowers the diffusion. From equation (6.3), the dimension of the kinetic constant is [$1/s^n$]. The meaning of this kinetic constant can be seen from the solution of Fick's second law for a slab-shaped gel where n=1/2 to be proportional to the square root of the diffusion coefficient of the solvent in the polymer (D) and the gel thickness (l).

Above a threshold value of the penetrant activity, which depends on the temperature, the diffusion becomes 'anomalous' with respect to Fickian diffusion, and a plot of the weight uptake versus the square root of time is no longer linear but sigmoidal in shape, and it is thickness dependent [Gostoli and Sarti, 1986]. The same phenomenological approach as above is used to describe anomalous diffusion, applying in equation (6.2) values of n > 0.5 [Ganji and Vasheghani-Farahani, 2009, Lin and Metters, 2006]. At temperatures near the low critical solution temperatures, where gel shrinking dominates, solvent-polymer and polymer-polymer interactions are of greater importance. According to the Tanaka equation [Li and Tanaka, 1990], shrinking kinetics around the LCST is usually interpreted as collective diffusion [He, 2006, Mellott et al., 2001, Richter et al., 2008]. In all applications, a homogeneous gel structure is supposed, which undergoes an isotropic deformation [Lévesque et al., 2005]. The Tanaka equation was derived for ideal geometries (sphere, long cylinder, and large disk) [Li and Tanaka, 1990], but mostly are used in the form of spherical geometry:

$$\frac{\Delta r}{\Delta r_0} = \frac{6}{\pi^2} \sum n^{-2} \exp\left(-n^2 \frac{t}{\tau} \right) \tag{6.4}$$

Equation (6.3) describes the swelling/shrinking of gels as similar to a diffusion process with relaxation time proportional to the square of the gel size. In the above summation, the first term $\exp(t/\tau)$ at n=1 is dominant over the higher order terms; r_0 denotes the final radius of the gel at equilibrium state, and Δr_0 is the total increase in the radius on the entire process of swelling. The change of particle radius Δr at a given time is a multi-exponential function of the largest

characteristic, time $\tau = r_0^2 / D_{col}$, defined by the radius of the swollen particles (i.e., the initial radius for the release experiments) and the collective diffusion coefficient (the unique fitted parameter in equation (6.4)). For particles with cylindrical and disk shapes, the apparent collective diffusion coefficient is smaller than the value obtained directly from kinetics with spherical gels [Wu and Zhou, 1997].

In this section [Naddaf et al., 2010a, b], poly(NIPAAm) hydrogel was used to study the release kinetics of BSA by thermal deswelling at different temperatures around the critical solution temperature, i.e., in conditions of rapid shrinking of the hydrogel. The solvent release through the hydrogel was modelled with a bi-dimensional diffusion model with moving boundary conditions, and the experimental data showed a good agreement with the calculated data.

6.2. Protein loading and protein release

The swelling equilibrium method was used in order to load BSA into poly(NIPAAm) as described in Section 3.4. Section 3.5 describes the release experiments carried out at temperatures of 25°C, 32°C, 37°C, and 40°C. The change in the weight and size of the hydrogel particles was measured at the same time intervals as in the release experiments. Diameter and height of the cylindrical poly(NIPAAm) hydrogel particles were measured using a microscope equipped with a CCD video camera. For each time interval, the weight of the hydrogel disk was measured using digital balance with an accuracy of ±0.5 mg as described in Section 3.3.

6.3. Kinetics of shrinking

The change in the weight and size of the hydrogel particles was measured at the same time intervals as in the release experiments, i.e., the shrinking process combined with volume changes was observed for 24 hours by measuring the changes in weight and size of the cylindrical gel particle. The main change in the volume of the particles occurs in the first 130-150 minutes, as shown in Fig. 6.1 [Naddaf et al., 2010-b].

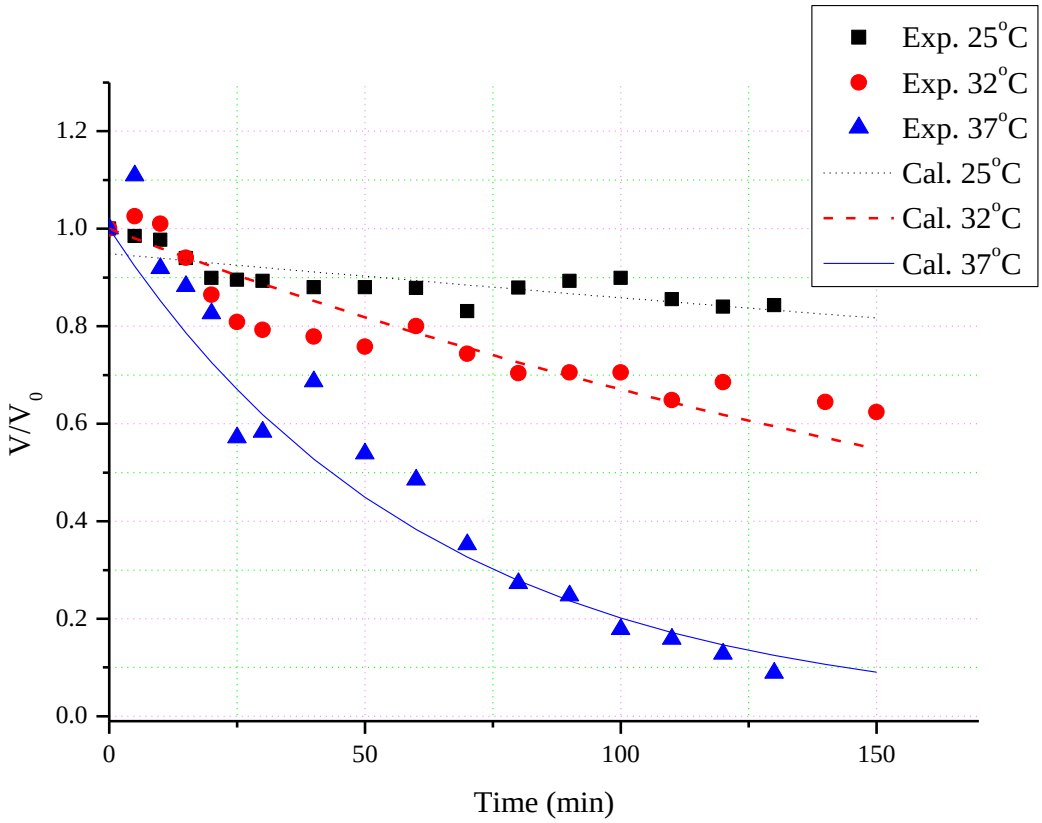

Fig. 6.1: Calculated and experimental volume changes for the gel particle at different temperatures during the release of BSA with initial concentration of 0.1M [Naddaf et al., 2010-b]

Near the LCST, the cylindrical particles with initial aspect ratio of 0.2 undergo a nearly isotropic deformation. This can be seen from the measured initial and final (t=1440min) H/D values for the different temperatures, shown in Fig. 6.2. In fact, a pulsatile behaviour of shrinking/swelling was observed during the experimental run, but the maximum final change in the aspect ratio tended to be about 15% [Naddaf et al., 2010-b].

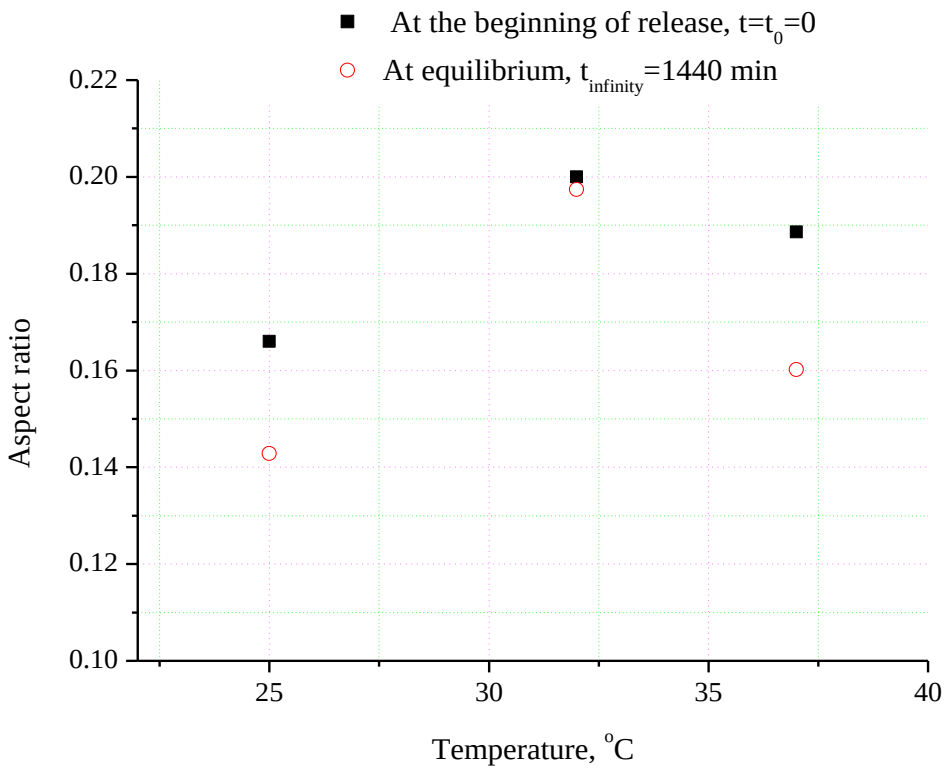

Fig. 6.2: Initial and final aspect ratio for the gel particles at different temperatures during BSA release [Naddaf et al., 2010-b]

The volume change of the gel particles around the LCST was successfully described as collective diffusion with the Tanaka-Fillmore equation (equation 6.4) [Tanaka et al., 1973]. The diffusion coefficient of the collapsing gel network was obtained from the experimental shrinking curves, calculated as the equivalent radius of the sphere. They were fitted to equation (6.4) to obtain D_{col}. The shrinking kinetics was satisfactorily predicted with $D_{col}=3\cdot10^{-10}m^2/s$, as can be seen from the comparison of calculated and experimental values in Fig. 6.3 [Naddaf et al., 2010-b].

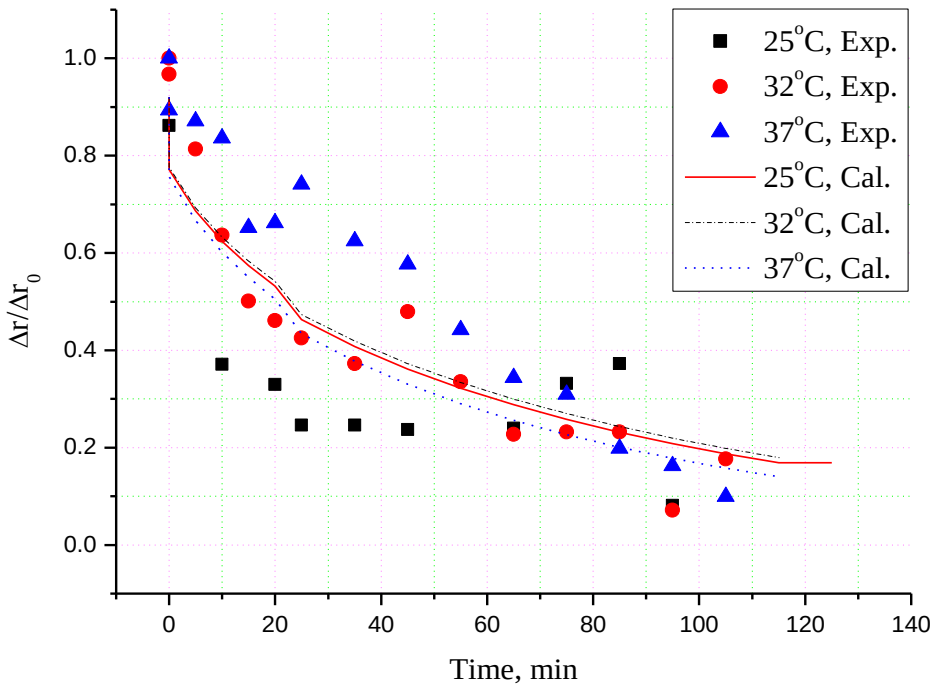

Fig. 6.3: Calculated and experimental change of the radius for poly(NIPAAm) hydrogel disc around and beyond the LCST [Naddaf et al., 2010-b]

As Fig. 6.1, Fig. 6.2 and Fig. 6.3 show, the release process is combined with dimensional changes in the hydrogel geometry before reaching equilibrium. The changes in both radius (r) and height (z) of the cylindrical hydrogel, which were obtained from the experimental investigation at different release temperatures, are reported in Table E.5 (Appendix E). Compared to the results obtained in Fig. 6.1, the dimensionless term $\Delta r/\Delta r_0$ shows less temperature dependence due to the influence of the temperature hidden in the maximum radius change of the particle.

6.4. Release kinetics

The cumulative release fractions of BSA from poly(NIPAAm) hydrogel were calculated as exponential functions of time, according to equation (6.2). The mass fraction of the released

liquid was calculated as given in equation (6.5) and the cumulative mass release curves for BSA shown in Fig. 6.4.

$$\frac{M(t)}{M_{\infty l}} = 1 - \frac{M(t)_{particle} - M_{final}}{M_{initial} - M_{final}} \tag{6.5}$$

where the mass of the gel particle at a given time t is defined as a sum of the contained mass of BSA solution and the constant mass of the dry gel particle as follows:

$$M(t)_{particle} = (V(t)_{particle} - V_{dry\ particle})\rho_{sol} + M_{dry\ particle} \tag{6.6}$$

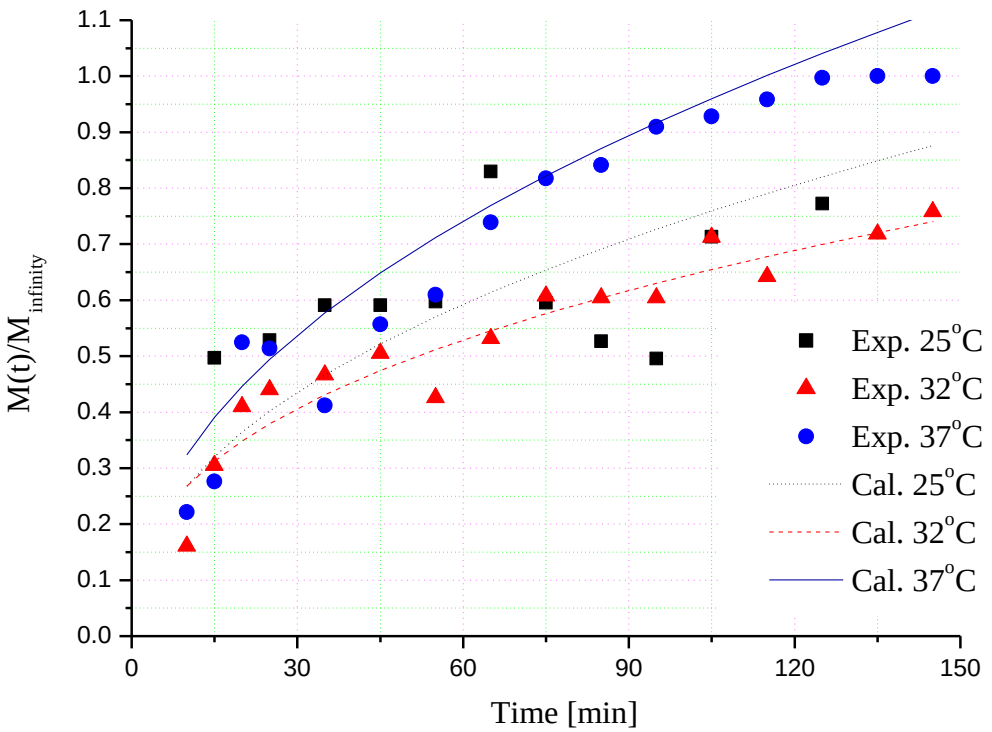

Fig. 6.4: The cumulative mass release curves for BSA with initial concentration of 0.1M [Naddaf et al., 2010-b]

The cumulative mass release curves for BSA were calculated as exponential functions of time according to equation (6.2), taking into consideration that the diffusion exponent n in equation

6.2 equals 0.45 for the cylinder (the values of the exponent are close to the theoretically expected for cylindrical geometry) and the burst time-independent term, α, is assumed to be equal to zero; a Fick's release kinetics is supposed. In addition to the obtained values for the constant *k* and the exponent *n* of equation (6.2), data for the measured mass and volume of the particles are given in Table 6.1 [Naddaf et al., 2010].

Table 6.1: Mass, volume and calculated *k, n, and* R^2 for hydrogel particles at different released temperatures [Naddaf et al., 2010-b]

Temperature	25°C	32°C	37°C
Mass of dry particle, $M_{dry\,particle}$ [g]	0.0162	0.0194	0.0167
Volume of dry particle [cm^3]	0.013572	0.018748	0.013944
Initial mass of the wet particle before release $M_{initial}$ [g]	0.3137	0.3566	0.2828
Final mass of the wet particle after release M_{final} [g]	0.249849	0.176764	0.023045
Density of the solution in the gel [g/cm^3]	1.04	1.14	1.28
K	0.097	0.087	0.112
N	0.442	0.440	0.462
R^2	0.661*	0.852	0.943

*At 25°C, due to the strong scatter of the experimental points, low correlation coefficient was obtained.

6.5. Modelling

A one-dimensional model for cylindrical particles is correct for a disc of aspect ratios > 10 [Wu, and Brazel, 2008]. In this work [Naddaf et al., 2008, Naddaf et al., 2010], particles have a cylindrical geometry with an aspect ratio of 0.2, a relation of the mass transfer areas (r- to z-direction) was in the range of 0.3-0.4; a bi-dimensional model with moving boundary conditions was used [Siepman et al., 1999] to predict the release kinetics of BSA through the

cylinders. Based on Fick's law of diffusion, the two isotropic and anisotropic diffusions can be handled in both r- and z-directions with constant or variable coefficients. The mass balance for the particle is given by the equation:

$$\frac{\partial C}{\partial t} = \frac{1}{r}\frac{\partial}{\partial r}(rD_r(r,z,t)\frac{\partial C}{\partial r}) + \frac{\partial}{\partial z}(D_z(r,z,t)\frac{\partial C}{\partial z}) \tag{6.7}$$

Based on this model, an isotropic diffusion ($D_r = D_z$) with concentration profile symmetry towards the axis of the cylinder (r=0) and the plane at 1/2 thickness of the particle (z=0):

$$\frac{\partial C}{\partial r} = \frac{\partial C}{\partial z} = 0 \qquad \text{z=0 and r=0} \tag{6.8}$$

Meanwhile, at the outer surface of the cylindrical particle, both concentration profile symmetry and equilibrium concentration are supposed:

$$C = C_{eq} \qquad 0 \le r \le R(t) \qquad z = Z(t) \tag{6.9}$$

and

$$0 \le z \le Z(t) \qquad r = R(t) \tag{6.10}$$

Here Z is the half thickness of the disc and R is its radius. The mass balance for the liquid phase in the vessel is given as:

$$\frac{\partial \overline{C}}{\partial t} = -\frac{V_{liq}}{V_{solid}}\frac{\partial C_l}{\partial t} \tag{6.11}$$

From the mass balance for the liquid phase in the vessel (equation 6.11), the volume averaged solid phase concentration was calculated using equation (6.12), by which the time dependent functions of the size change $Z(t)$ and $R(t)$ are given explicitly as obtained from the shrinking measurements [Naddaf et al., 2010-b]. As shrinking was found to proceed equally in both directions and was satisfactorily predicted by the Tanaka equation for temperatures near the LCST, it was used as a model function, describing the $Z(t)$ and $R(t)$ dependencies for temperatures near the LCST; it was solved numerically by a finite-difference method (radial step $= 0.01 \times R(t)$; axial step $= 0.01 \times Z(t)$ and time step of one minute) (Appendix H) [Naddaf

et al., 2010-b]. The calculated curves $C_l(t)$ were fitted to the experimental ones to estimate the effective diffusion coefficient inside the hydrogel.

$$\overline{C}(t) = \frac{2}{R^2 Z} \int_0^{Z(t)} \int_0^{R(t)} C(r,z,t)\ r\, dr\, \mathrm{dz} \tag{6.12}$$

At the liquid-solid interface (i.e., $z = Z$ and $r = R$), a partition coefficient of $K = 1$ was supposed between the concentration inside the pores and in the surrounding liquid. Reported values for the BSA partition coefficient for different hydrogels were found to be around unity [He, 2006, Shang et al., 1998]. Moreover, the initial liquid to solid ratios V_{liq}/V_{solid} were found in the order of 50-60. Experimentally, the BSA release was measured by UV-V spectrometry. Fig. 6.5 presents both calculated and experimental kinetic curves. For the four represented temperatures, the BSA release exhibits the same release profile. Regardless of the initial drug concentration, at high temperatures (i.e., 40°C), the system reaches the equilibrium release in shorter time than at below or around the LCST.

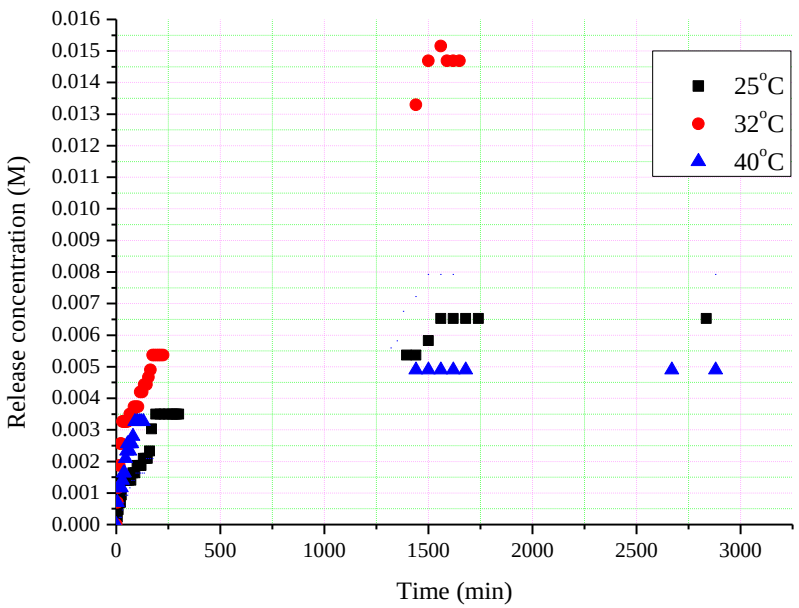

Fig. 6.5: The concentration of released BSA versus time at different temperatures for BSA initial concentration of 0.1M [Naddaf et al., 2010-b]

At the initial period of BSA diffusion, a burst release followed by a 'breakdown lane' was observed. This rapid desorption, causing the burst term, is related to the BSA molecules located at the surface of the hydrogel cylinder, which would transfer immediately to the surroundings due to the high BSA concentration gradient. Consuming the BSA molecules near the hydrogel surface causes the appearance of a breakdown [Naddaf et al., 2010-b]. At 40ºC, the release is eliminated due to the formation of a hard shrunken dense layer on the outer surface of the hydrogel (Fig. 6.5). This elimination of release from the hydrogel during the initial period of diffusion results in an increase in the hydrogels' internal pressure as a response to increasing shrinking rate. Due to the accumulation of internal pressure, the hydrogel shrinks at 40ºC faster than it does at 32ºC, and the interior solute is rapidly expelled, causing the lowest cumulative release among the other tested temperatures, as found in previous research [Kaneko et al., 1995, Naddaf et al., 2010]. This explains the achievement of the lowest cumulative release among other tested temperatures. The final equilibrium values of the experimentally observed release curve shown in Fig. 6.5 were used directly in the simulations [Naddaf et al., 2010-b].

6.5.1. Simulation with constant diffusion coefficient

Fig. 6.6 presents a comparison of the dimensionless experimental releases of BSA with the predicted kinetics as a function of time for BSA with an initial concentration of 0.1M. The presentation in dimensionless form better illustrates that the cited diffusion coefficient is able to describe the rate of the release for all three curves.

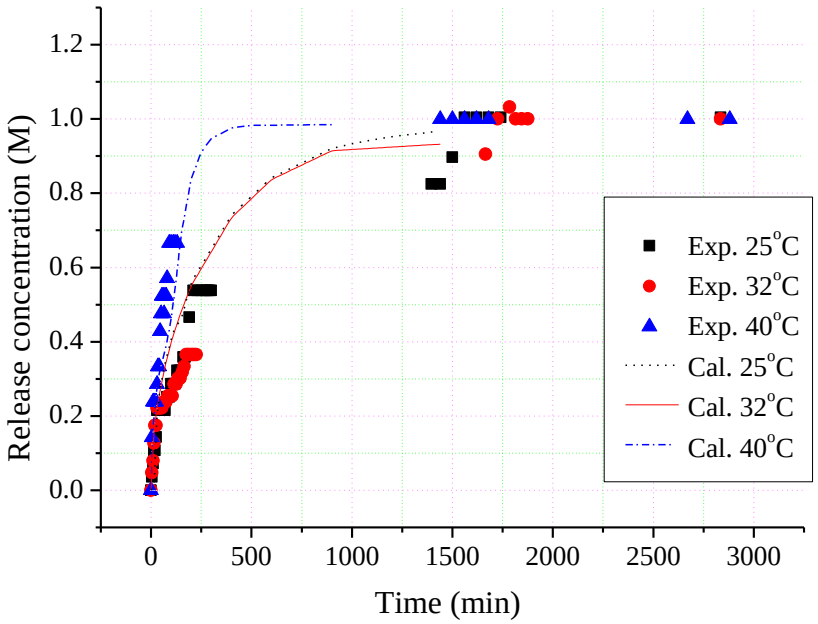

Fig. 6.6: Comparison of the dimensionless experimental release of BSA concentration with calculated kinetics versus time for BSA initial concentration of 0.1M [Naddaf et al., 2010-b]

It is found [Naddaf et al., 2008, Naddaf et al., 2010] that the experimental curves for 25°C, 32°C, and 40°C are satisfactorily described with a constant effective diffusion coefficient of $D_r=D_z=1.67\times10^{-11}m^2/s$ [Naddaf et al., 2010]. This corresponds to the reported values for BSA diffusion inside hydrogels: $2.0 – 2.4\times10^{-11}m^2/s$ [Amsden and Turner, 1999], $1\text{-}3.1\times10^{-11}$ m^2/s [Lévesque et al., 2005], $1.5\text{-}6.8\times10^{-11}m^2/s$ [Van Tomme, 2007], $1.5\text{-}8\times10^{-11}m^2/s$ [He, 2006]. For comparison, diffusion coefficients for BSA in free solutions are in the range of 5.8×10^{-11} and $6.4\times10^{-11}m^2/s$ [Van Tomme, 2007, Kosto and Deen, 2004, Coviello, et al., 2005]. Above LCST (at 40ºC), the difference in BSA released from the loaded hydrogels between the initial highest and the initial lowest concentrations, i.e., 1.51M and 0.01M, respectively, was 1.6%. Meanwhile, the release from the hydrogel loaded with BAS of initial concentration of 1.51M gave 5.9% more at 25°C [Naddaf et al., 2010]. Here, the constant diffusion coefficient predicts an earlier approach to equilibrium than observed in 300 minutes, in comparison with ≥1000min for the experiment. This can be explained with the decreasing diffusion time R^2/D_{eff}, due to

dramatic change in the radius $R(t)$ during shrinking. In the same time, the experimentally observed release is lower because of the lower diffusion coefficient in the more dense structure of the collapsing gel.

6.5.2. Simulation with variable diffusion coefficient

In a second set of simulations, a model with a variable diffusion coefficient was adapted to improve the description of the release kinetics when shrinking the gel was of utmost importance. As obtained from the experiments, the change in diffusion was related to the shrinking ratio as follows [Naddaf et al., 2010-b]:

$$\left(D_{eff}/D_{eff\,0}\right) \propto \left(V/V_0\right) \tag{6.13}$$

Calculations with two initial values of the diffusion coefficient are presented, D_{eff0} =1×10^{-5} cm^2/min (Dr =Dz = 1.67×10^{-11}m^2/s) and D_{eff0} = 0.5×10^{-5} cm^2/min (Dr =Dz = 0.83×10^{-11}m^2/s), to illustrate the sensitivity of the calculated curve toward D_{eff0} [Naddaf et al., 2010]. The effect of the variable diffusion coefficient is represented in Fig.6.7 and Fig. 6.8 [Naddaf et al., 2010] for temperatures below the LCST (at 25°C) and above it (at 37°C), respectively, where the initial parts of the kinetic curves are comparable with the calculated values. At 25°C where shrinking is less pronounced, the experimental results are satisfactorily described with the constant diffusion coefficient. In the second case (at 37°C), the decreasing (variable) diffusion coefficient describes the experimental curve better [Naddaf et al., 2010]. This is reasonable because the diffusion of BSA at temperatures near the LCST is strongly dependent on protein-network interactions. In such a case, the rate of diffusion is independent of the concentration of the drug in the hydrogel (there is no D_{eff}(C) relation), but depends on the polymer volume fraction [He, 2006, Khoury, 2003, Li et al., 2008]. For instance, a Fickian diffusion model was found to be consistent with the experimental observations [Tomme, 2007], where mass-transfer rates were strongly dependent on the gel polymer concentration and not on the solution concentration.

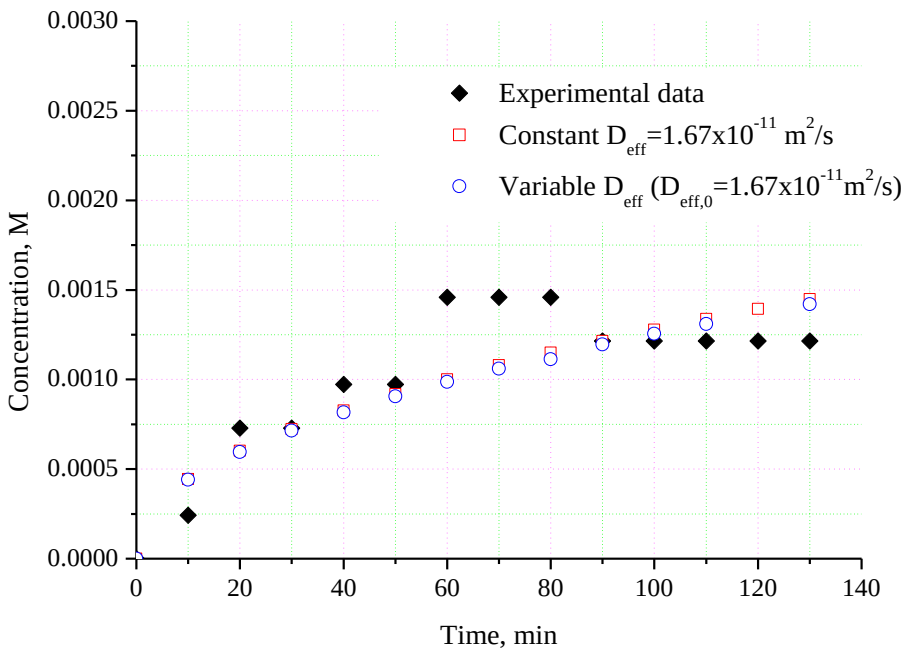

Fig. 6.7: The effect of the variable diffusion coefficient on the initial parts of the kinetic curves at 25°C [Naddaf et al., 2010-b]

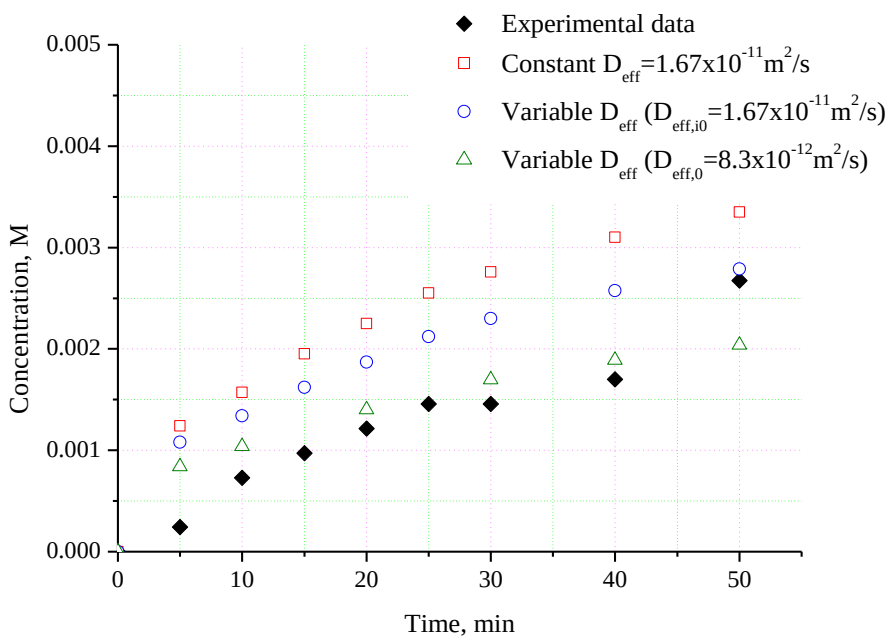

Fig. 6.8: The effect of the variable diffusion coefficient on the initial parts of the kinetic curves at 37°C [Naddaf et al., 2010-b]

As can be seen from Fig. 6.8, the influence of the variable diffusion coefficient is observed in the case of important deformation at 37°C and leads to better description of the kinetic curve [Naddaf et al., 2010-b]. Further investigations in this direction are required, supported by experimental observations of the structure and pore size of the polymer matrix and relations between the diffusion coefficient and the properties of the polymer network.

6.6. Summary

In this section [Naddaf et al., 2010-a, b], the volume changes and the release kinetics of BSA by thermal deswelling were measured. Lower release of BSA was observed for temperatures higher than the LCST, where diffusion is hindered by the more dense structure of the collapsing gel. The Tanaka equation was used to describe the shrinking kinetics of the hydrogel around the LCST using a two-dimensional model approach. The BSA release coupled with shrinking of the hydrogel particles was modelled with a bi-dimensional diffusion model [Siepman et al., 1999]. The model allows for radial and axial shrinking of the gel particles to be taken into account in the moving boundary conditions. A good correlation between experimental and calculated data was obtained for the effective diffusion coefficient of 1.67×10^{-11} m/s^2. The experimental curves for 25°C, where shrinking is less pronounced, are satisfactorily described with a constant effective diffusion coefficient of $D_r = D_z = 1.67\times10^{-11} m^2/s$. The effect of increasing temperature on the diffusion coefficient is compensated by the increased diffusional resistance inside the gel due to shrinking. Therefore, a variable diffusion coefficient was supposed in order to improve the description of the release kinetics when shrinking the gel is more pronounced. This is reasonable because the diffusion of BSA at temperatures near the LCST is strongly dependent on the protein-network interactions. At 40ºC (above LCST), the difference in BSA released from the loaded hydrogels between the initial highest and the initial lowest concentrations, i.e., 1.51M and 0.01M, respectively, was 1.6%. Meanwhile, the release from the hydrogel loaded with BAS, with an initial concentration of 1.51M, was more pronounced and gave 5.9% at 25°C.

7. Results in brief

7.1. Synthesis and equilibrium swelling

The polymerization of the non-ionic poly(NIPAAm) hydrogel was achieved and four kinds of hydrogels were produced based on the cross-linking ratio by the free radical polymerization under oxygen-free conditions at 25°C. In the case of swelling in pure deionized water, the hydrogel followed a continuous thermo-shrinking volume transition due to the effect of the entropy contribution, a reduction in the chemical potential of water molecules by increasing the temperature (Fig.7.1). These continuous volume changes are expected to vanish by increasing the concentration of phenol. The effect is due to the presence of the benzene ring, which plays a significant role in modifying the order structure of the bulk water, modifying the hydrogel-water interaction and enhancing the formation of hydrogen bonded structure.

At 25°C, the phase transition is accompanied by reversible volume and mass changes without damaging the internal structure of the hydrogel or changing its swelling properties in the short term. This change in the local environment of the polymer is not expected at higher temperatures due to the enthalpy reduction, which was accurately proven based on Raman spectra.

In general, the dimensional response of the poly(NIPAAm) cylinders to changes in temperatures is governed by the diffusion-limited transport of matter in and out of the polymeric networks [Chu et al., 2007]. Lower release of solute was observed for temperatures higher than the LCST, where the diffusion process is hindered by the dense structure of the collapsed gel. The formed hard shrunken thick layer on the outer surface of the hydrogel hinders the release of phenol from the hydrogel during the initial period of diffusion. This results in an increase of the internal pressure inside the hydrogels. Due to the increased internal pressure, the hydrogel shrinks at 40ºC faster than it does at 32ºC. Therefore, for temperatures higher than the LCST, the interior solute is rapidly expelled at a crack of the layer forming a hunch and the equilibrium is reached in shorter release. Elevating the temperature from 25^{o}C to 40^{o}C reduces the cumulative amount of released phenol at about one-half. At the early stage of diffusion, the cumulative mass release curves increase linearly with time, i.e., Fickian diffusion, and then follow a non-smooth stepwise approach toward equilibrium (Fig. 7.2).

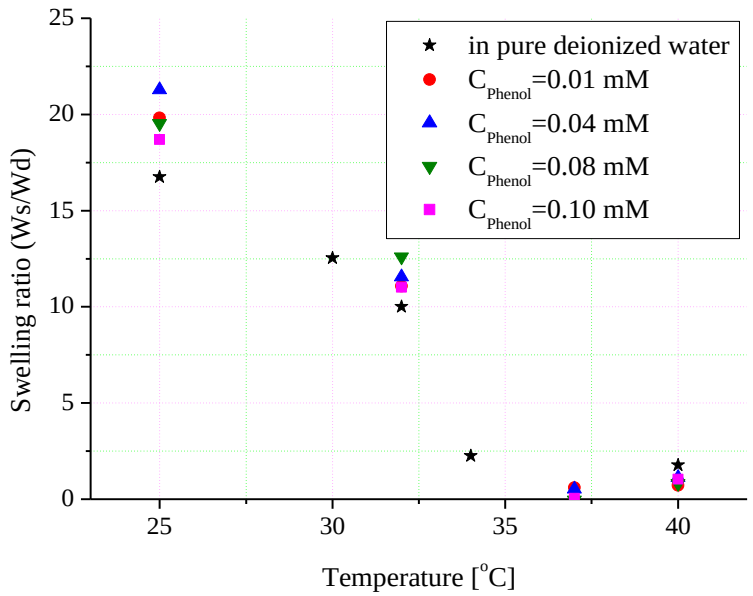

Fig. 7.1: The swelling ratio of poly(NIPAAm) equilibrated in phenol solutions of different initial concentrations and at varied temperatures [Naddaf and Bart, 2010-b]

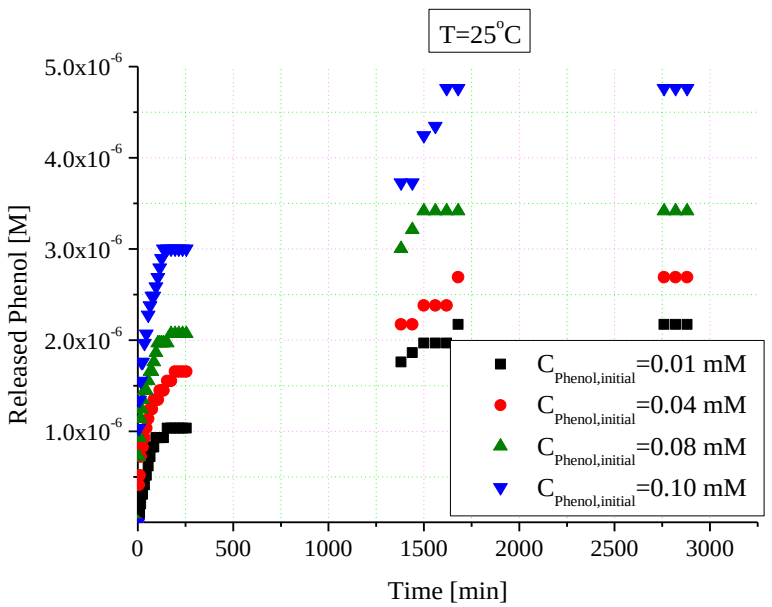

Fig. 7.2: Cumulative amounts of released phenol from the hydrogel for different initial concentrations (release temperatures 25°C)

7.2. Raman investigations

Raman spectroscopy was used to identify the spectra and to analyse the structure of the hydrogel. In addition, the mapping technique is a well-established and powerful tool for the chemical characterization of the materials, providing narrow spectral features, which constitute a sort of fingerprint for the investigated sample (Fig. 7.3) .Therefore, the presence of the bands, allows the use of Raman mapping to identify the structural homogeneity of the hydrogel. In addition, the diffusion of the solute in the hydrogel was determined using Raman spectroscopy. Raman spectra profiles showed that the hydrogel lattice collapse in response to temperature increase.

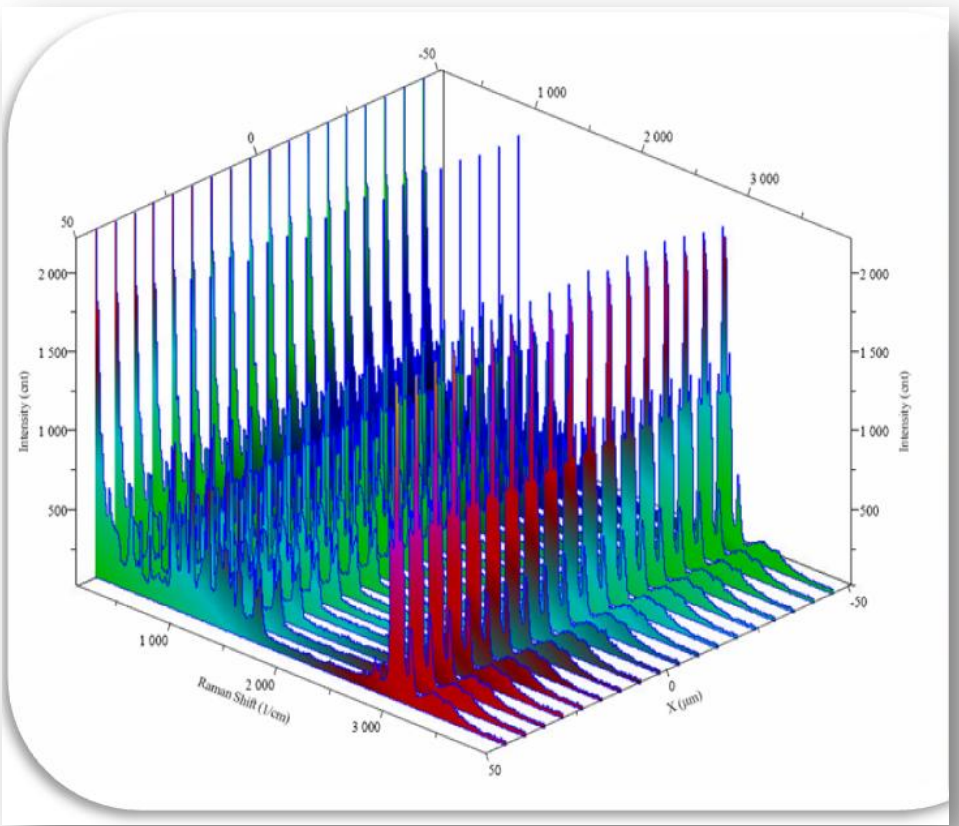

Fig. 7.3: Raman spectra at different depth of the poly(NIPAAm) hydrogel

7.2.1. Mutual diffusion coefficient

In addition to obtaining information about the chemical composition of the hydrogel/phenol system, Raman spectroscopy was used to study the change of intensity with the solute concentration during the diffusion, from which the mutual diffusion coefficient, D_{mut} in the thermosensitive poly(NIPAAm) hydrogel loaded with different initial concentrations of phenol and different initial concentrations of BSA at a selected temperature of 25°C. The Raman spectra were measured for a long period at a fixed spatial position in the hydrogel near the outer surface for both solutes (BSA and phenol). The mutual diffusion coefficient was then calculated using the equation (Section 4.7.2):

$$I_{CH,H_2O} f\left(C_{solution\ (phenol,BSA)}(t,x)\right) = I_{CH}^{\text{int}} \cdot erf\left[x \Big/ 2\left(\sqrt{D_{mut} \cdot t}\right)\right] \qquad (7.1)$$

The diffusion coefficient increases by increasing the concentration of phenol [Koros et al., 1976, Dubreuil et al., 2003]. The mutual diffusion coefficient was measured to vary from 5.61845×10^{-11}m^2/s to 3.34565×10^{-9}m^2/s for the hydrogel cylinder loaded with phenol concentration of 0.01mM and 0.1mM, respectively (Fig. 7.4). This dependency of diffusivity on concentration is due to the solute-hydrogel interaction [Lewus and Carta, 1999]. Meanwhile, D_{mut} of poly(NIPAAM)/BSA was found to vary slightly, from 5.67×10^{-14}m^2/s to 6.07×10^{-14}m^2/s for 1.51M to 0.1M, respectively. The results, compared to phenol, indicate an increasing resistance to diffusion inside the hydrogel due to a high swelling ratio and/or the average free hole volume, which strongly influences the mutual diffusion coefficient [Vrentas and Vrentas, 1992]. The larger average free hole volume of a solute with a high molecular weight (such as BSA) leads to larger diffusivity at a given solute concentration [Vrentas and Vrentas, 1992].

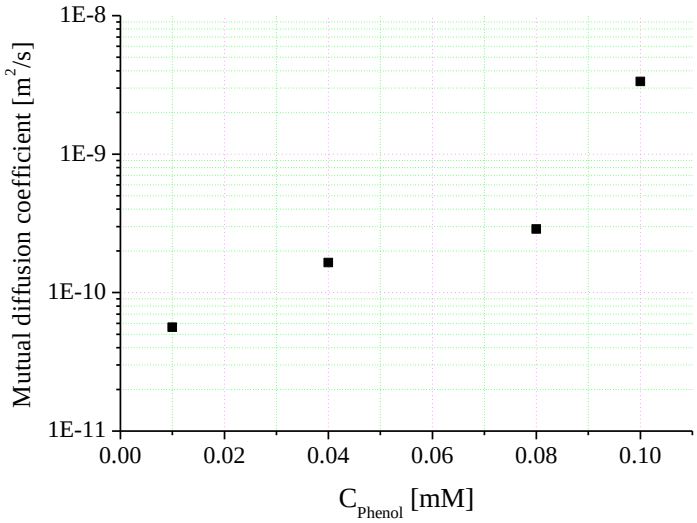

Fig.7.4: Averaged mutual diffusion coefficients for different initial phenol concentrations [Naddaf and Bart, 2010-b]

7.3. Mechanical properties

The mechanical experiments were conducted using a self-constructed uniaxial compression system. Briefly, a hydrogel disc was placed on a digital balance. Then, a load was transmitted vertically to the hydrogel through a piston fitted with a Teflon end plate. The force acting on the hydrogel was calculated from the reading of the balance *m* as $F=mg$, where *g* is the gravitational acceleration. The resulting deformation ΔD was measured using a microscope equipped with a CCD video camera and connected to a computer with *Image C*™. As indicated, an increase in the hydrogel disk thickness reduces the mechanical stress, which can be applied (Fig. 7.5). For example, a thickness difference of 1.722mm reduces the stress from 9.5×10^{-3}MPa to 7.0×10^{-3}MPa. In addition, the Young's modulus rises with temperature elevation' exceeding the LCST expels the liquid from the hydrogel lattice, causing a substantial increase in the Young's modulus from about 0.14MPa for 0.1mM phenol solution and about 0.3MPa for 1.51M BSA, compared to 0.02MPa for 0.1mM phenol solution and about 0.035MPa for 1.51M BSA at 25°C (Fig. 7.6.a and Fig. 7.6.b). Increasing the Young's modulus was also a response of the hydrogels set to equilibrium in alkali and acidic solutions; the hydrogel undergoes a major phase change for pH values between 5.0 and 7.0.

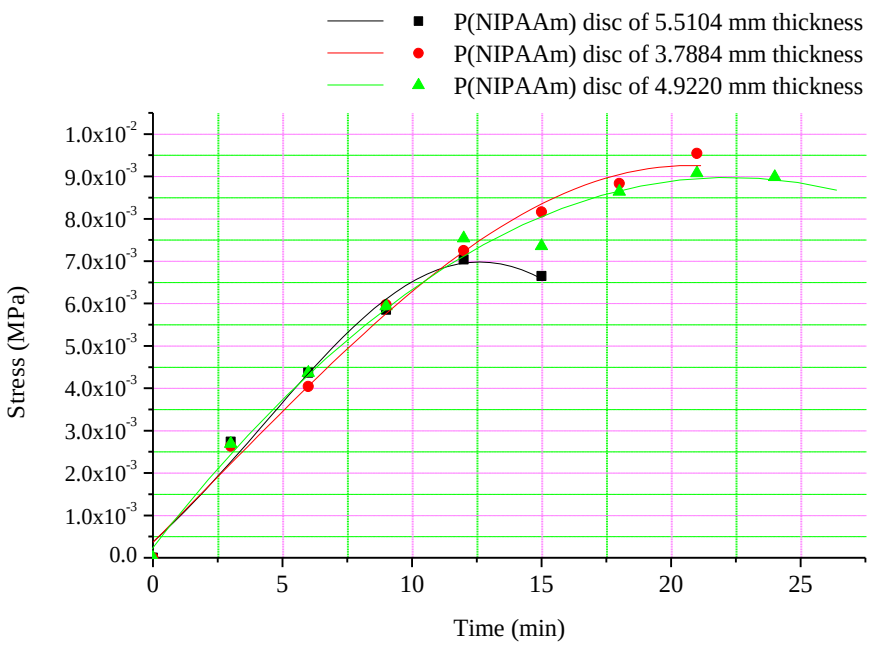

Fig 7.5: Mechanical stress for hydrogel disks with different initial thicknesses

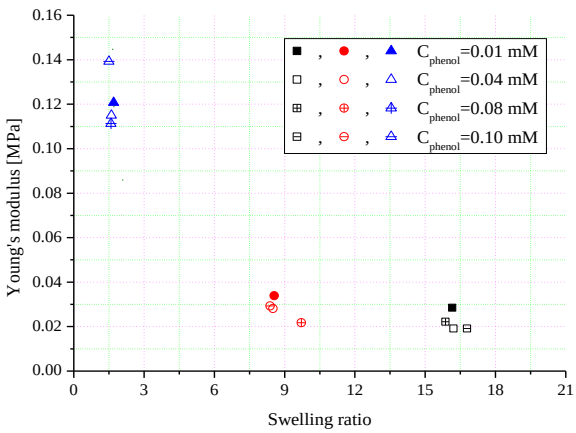

Fig 7.6.a: Young's modulus variation for different phenol solutions at different temperatures: (■) 25°C; (●) 32°C; (▲) 37°C

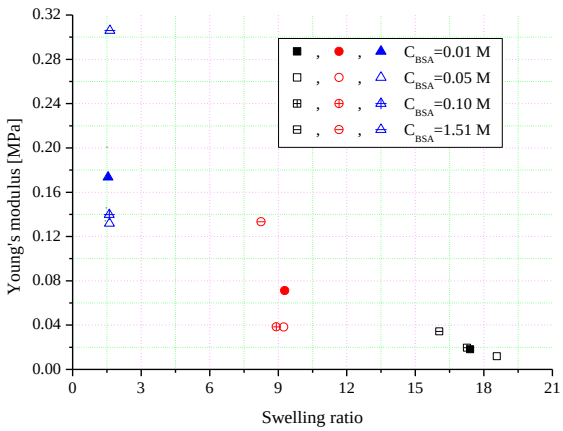

Fig 7.6.b: Young's modulus variation for different BSA solutions at different temperatures: (■) 25°C; (●) 32°C; (▲) 37°C

7.3.1. Collective diffusion coefficient

For the thermosensitive poly(NIPAAm) hydrogels, which were swelled to equilibrium in different concentrated phenol and BSA solutions, the collective diffusion coefficient was calculated after a model [Tanaka et al., 1973] based on measurements of the bulk modulus, the shear modulus, and the frictional coefficient between the solvent and the hydrogel network. The collective diffusion coefficient, D_{col}, which is based on the mechanical properties of the gel, was measured using the Tanaka-Fillmore equation given as:

$$D_{col}(r,t) = \frac{\left(K + \frac{4 \cdot \mu}{3}\right)}{f} \tag{7.2}$$

The collective diffusion coefficient for the different hydrogel sample was measured to be identical below and around the LCST, regardless of the solute concentration used. Meanwhile, above the LCST, it varied significantly, i.e., at 25^{o}C; the diffusion coefficient of the hydrogel cylinder immersed to equilibrium in the 0.01mM phenol equals 7.4×10^{-12}m/s^2, and this value increased about two orders of magnitude by increasing temperature to reach 1.939×10^{-10}m/s^2 at 40°C (Fig. 7.7.a and Fig. 7.7.b) [Naddaf and Bart, 2011-c]. The high concentration of phenol (0.10mM) is responsible for decreasing the diffusion coefficient compared to the lower tested concentration of phenol (0.01mM). Meanwhile, the diffusion coefficient of 0.01M BSA varied from 4.9×10^{-12}m/s^2 at 25^{o}C to reach 9.34×10^{-11}m/s^2 at 40^{o}C. But in contrast to phenol, the higher concentration of BSA had almost no remarkable effect on changing the diffusion coefficient, i.e., it increased from 1.92×10^{-11}m/s^2 for the 0.01M BSA to 1.026×10^{-10}m/s^2 for the 1.5M BSA [Naddaf and Bart, 2011-c].

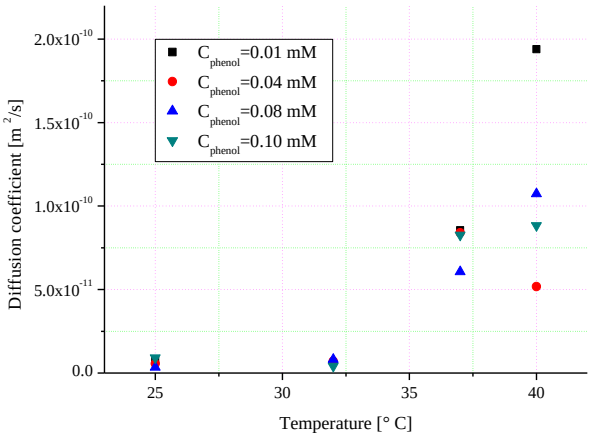

Fig. 7.7.a: D_{col} with temperature change for different concentrations of phenol

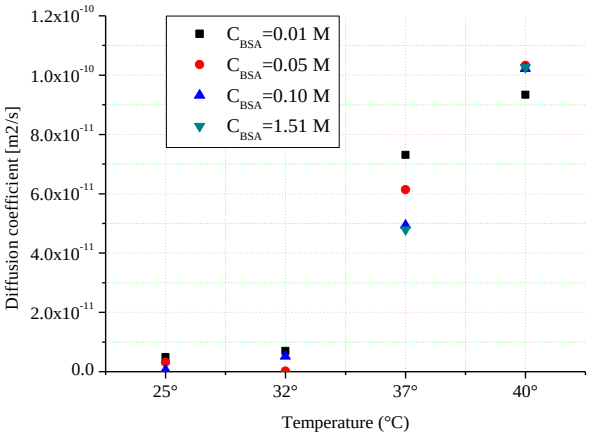

Fig. 7.7.b: D_{col} with temperature change for different concentrations of BSA

7.4. Collective versus mutual diffusion coefficient

Although the hydrogels were taken from the same synthesized batch, the comparison between the collective and mutual diffusion coefficients shows a higher measured mutual diffusion coefficient for different concentrations of phenol at 25°C (Fig. 7.8) [Naddaf and Bart, 2011-c]. This diversity in the values of diffusion coefficients between both methods is related to different effects. The dimensions of the hydrogel cylinder affect directly the collective diffusion coefficient [Tanaka et al., 1973, Tanaka and Fillmore, 1979], relate the swelling of the gel to the gradient of the stress, and describe small volume changes during swelling, i.e., the diffusion coefficient is dependent on the hydrogel geometry [Singh and Weber, 1996, Komori and Sakamot, 1989]. Moreover, due to the existence of the shear modules, the shear relaxation process occurs and causes a volume change that influences the value of the collective diffusion coefficients [Peters and Candau, 1988, Li and Tanaka, 1990]. In other words, for a cylinder, the diffusion occurs in two dimensions (radial and axial) and it is combined with volume change. Due to the existence of the shear modules, the shear relaxation process occurs and causes a volume change in the diffusion directions. This geometrical constraint results in a reduction of the speed of the diffusion in the diffusion directions [Peters and Candau, 1988, Li and Tanaka, 1990]. In contrast to this, the mutual diffusion coefficients of BSA and phenol were obtained

based on Raman spectra, which can be recorded without any major interference from geometrical changes or from the water band. Nevertheless, the local dynamic inhomogeneity may cause the scattered intensity and, as consequence, give different local data in the long term to calculate the mutual diffusion coefficient [Norisuye, et al., 2004]. In principle, Raman spectroscopy is a powerful technique for the investigation of the diffusion phenomena through poly(NIPAAm)/phenol as a function of time and distance from the hydrogel surface. Fig. 7.8 shows a comparison between the collective and the mutual diffusion coefficients for different concentrations of phenol at 25^{o}C.

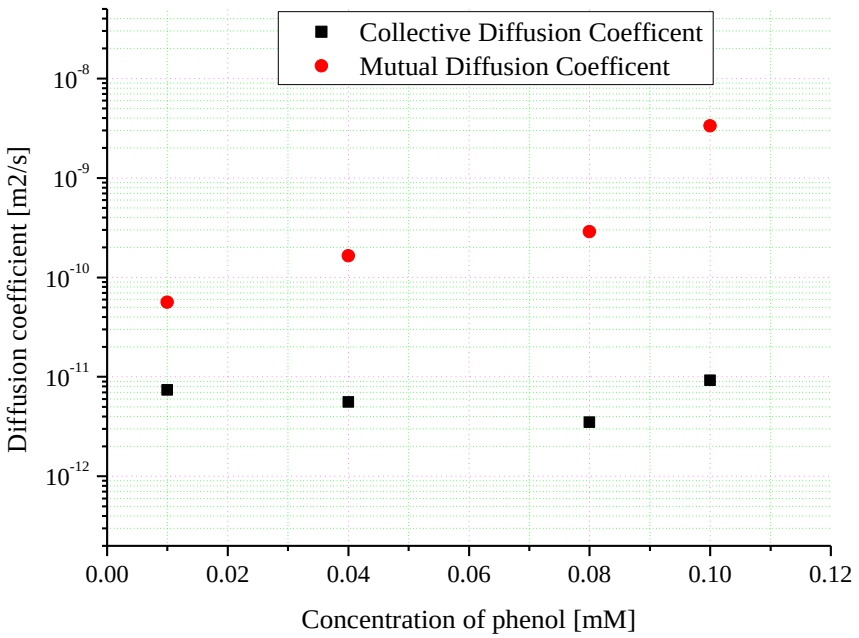

Fig. 7.8: Comparison between the D_{col} and D_{mut} for different concentrations of phenol at 25°C [Naddaf and Bart, 2011-c]

7.5. Transport properties and the mathematical modelling

The volume phase transition in the chemically cross-linked polymeric hydrogels is a major concern for developing a number of applications, ranging from food packaging to drug-delivery systems and micro electro mechanical systems (MEMS) [Carbonell and Sarti, 1990]. Therefore,

this work studied the diffusion of solvent through the temperature sensitive hydrogel. The diffusion of a solvent in the hydrogel lattice results into geometric alterations of the swollen hydrogel. These alterations are subjected to changes in both hydrogel volume and density. For the cylindrical shaped hydrogel, the solvent diffuses in both the axial and radial directions. To model the diffusion process into hydrogel, a bi-dimensional model with moving boundary conditions was used [Siepman et al., 1999] based on Fick's second law:

$$\frac{\partial C}{\partial t} = \frac{1}{r}\frac{\partial}{\partial r}(rD_r(r,z,t)\frac{\partial C}{\partial r}) + \frac{\partial}{\partial z}(D_z(r,z,t)\frac{\partial C}{\partial z}) \qquad (7.3)$$

In this model, an isotropic diffusion ($D_r = D_z$), concentration profile symmetry towards the axis of the cylinder ($r = 0$), and the plane at $1/2$ thickness of the particle (z=0) and equilibrium concentration at the particle surface were assumed. The final equilibrium values of the experimentally observed release curve shown in Fig. 7.9 were used directly in the simulations [Naddaf et al., 2010-b]. Fig. 7.10 presents the predicted rate of the process. The presentation in dimensionless form gives a better illustration of the fact that the cited diffusion coefficient is able to describe the rate of the release for all three curves.

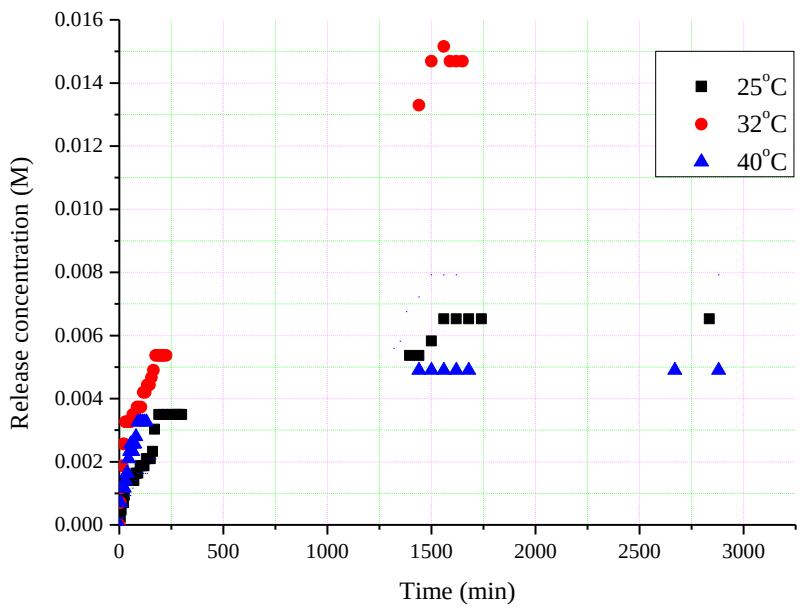

Fig. 7.9: The concentration of released BSA versus time at different temperatures for BSA initial concentration of 0.1M

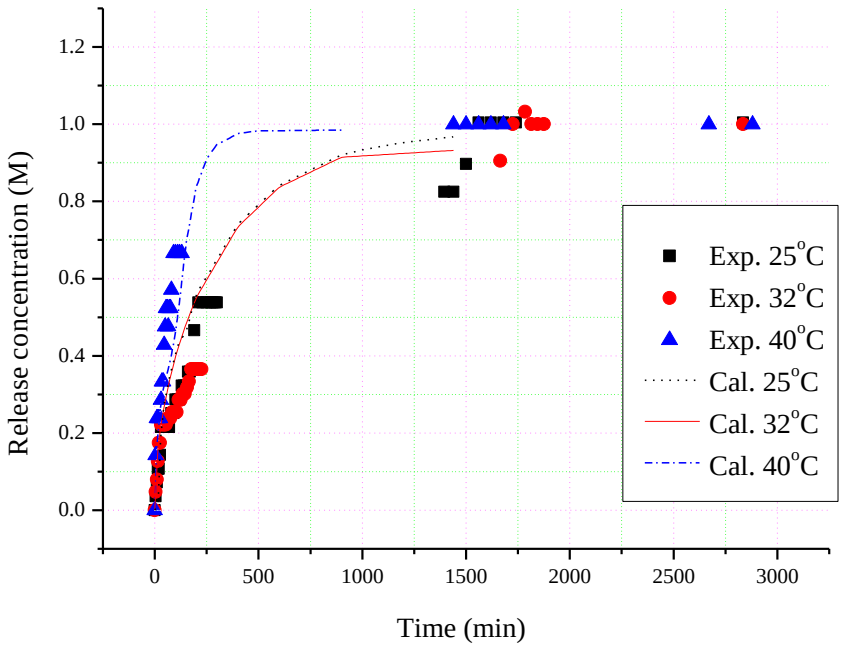

Fig. 7.10: Comparison of the dimensionless experimental released BSA concentration with calculated kinetics versus time for BSA initial concentration of 0.1M [Naddaf et al., 2010-b]

The experimental curves for 25°C and 32°C are satisfactorily described with a constant effective diffusion coefficient of $D_r = D_z = 1.67 \times 10^{-11} m^2 / s$. Above LCST, the difference in BSA released from the loaded hydrogels between the initial highest and the initial lowest concentrations, i.e., 1.51M and 0.01M, respectively, was 1.6%. Meanwhile, the release from the hydrogel loaded with BSA with an initial concentration of 1.51M gave, at 25°C, 5.9% more (Figs. 7.11 and 7.12) [Naddaf et al., 2010-b].

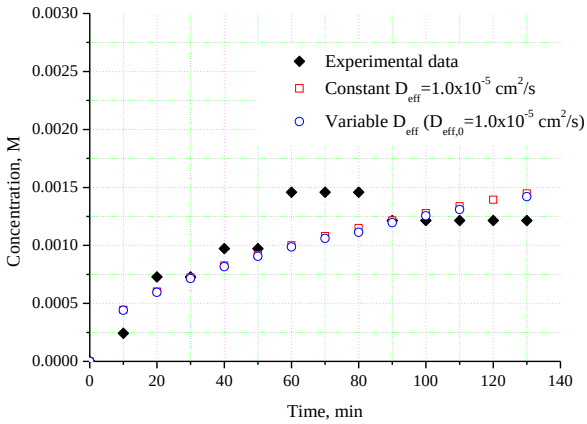

Fig.7.11: The effect of the variable diffusion coefficient on the initial parts of the kinetic curves at 25°C

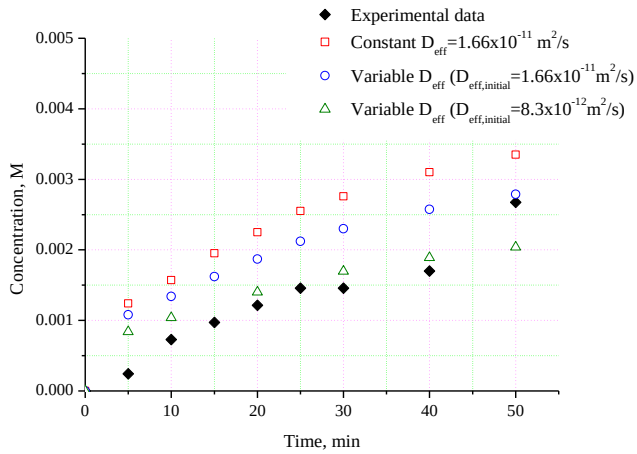

Fig.7.12: The effect of the variable diffusion coefficient on the initial parts of the kinetic curves at 37°C

8. Summary

- Poly(NIPAAm) is a thermo sensitive hydrogel, and below the LCST, its swelling/deswelling process is still thermally reversible.
- The LCST is dependent on cross-linker ratio and decreasing cross-linker increases the swelling ratio.
- Due to the solute-hydrogel interaction, increasing phenol concentration increases the release and changes the lattice configuration.
- Raman spectroscopy has been successfully applied to study the response of poly(NIPAAm) to different stimuli. Investigations show that hydrogel collapses, causing sharp Raman shift peaks, which help in identifying the hydrogel state. This method is effective in determining the mutual diffusion coefficient, which was found to be proportional to the phenol solute concentration.
- BSA diffusion into poly(NIPAAm) hydrogels has Fickian behaviour. At high *T*, the initial loaded concentration plays less of a role on BSA release because the molecular shape of BSA has less effect on shrinking compared to ring-shape phenol molecule.
- Characterization of the hydrogel mechanical properties is indispensable for the investigation of the adsorption/desorption process. Poly(NIPAAm) exhibits a sigmoidal stress-strain relationship in the elastic region. Moreover, the thicker disks withstand lower load, i.e., they have lower mechanical strength. It was found that hydrogels with less than 5mm thickness withstand loads of 4N. At higher temperatures, poly(NIPAAm) has better mechanical properties and larger collective diffusion coefficients, i.e., D_{col} increases about one order of magnitude by increasing the T from 25°C to 40°C. In general, shrinking results in a more dense polymer and decreases *D*.
- Above the LCST, the variable diffusion coefficient is proportional to the shrinking extent and describes the experimental kinetic curves better. Moreover, temperature elevation increases the diffusion, and the release equilibrium is reached more quickly, i.e., the hydrogel requires less time to form its systematic cylindrical shape at a higher temperature.

Zusammenfassung

- Polyp(NIPAAm) ist ein wärmeempfindliches Hydrogel und unterhalb der LCST noch thermisch reversibel schwillt und schrumpft.
- Die LCST ist abhängig von dem Vernetzerverhältnis; ein reduzierter Vernetzergehahlt erhöht das Quellverhältnis.
- Aufgrund der aromatischen Brückenwechselwirkungen des Phenols mit dem Hydrogel, bewirkt die Erhöhung der Phenolkonzentration eine Erhöhung seiner Freisetzung bewirkt durch eine Änderung (Aufweitung) der Gitterkonfiguration des Gels.
- Raman-Spektroskopie wurde erfolgreich angewandt, um die Reaktion von Poly(NIPAAm) auf unterschiedlichen Stimuli zu untersuchen. Der Zerfall der Hydrogelstrukturen verursacht eine starke Verschiebung der Raman-Peaks, die bei der Identifizierung der Hydrogele helfen. Dies ist eine wirksame Methode um die gegenseitigen Diffusionskoeffizienten, die proportional zur Konzentration des gelösten Stoffes (hier Phenol) sind, zu bestimmen.
- BSA-Diffusion in Poly(NIPAAm)-Hydrogelen ist vom Fick´schen Typ. Bei hohen Temperaturen hat die initiale Belastungskonzentration wenig Einfluss auf die BSA Freisetzung, da die Form des BSA-Moleküls im Vergleich zum ringförmigen Phenol-Molekülwenig Einfluss auf die Schrumpfung hat.
- Die Charakterisierung der mechanischen Eigenschaften des Hydrogels ist unverzichtbar für die Untersuchung der Adsorption/Desorption. Im elastischen Bereich besitzt Poly(NIPAAm) eine sigmoidale Spannungs-Dehnungs-Beziehung. Die dickeren Gelzylinder halten geringere Belastungen aus, d.h. sie besitzen eine geringere mechanische Festigkeit. Es wurde festgestellt, dass Hydrogele mit wenigem als 5mm Dicke einer Kraft von 4N standhalten können. Bei höheren Temperaturen hat Poly(NIPAAm) bessere mechanische Eigenschaften und einen größeren kollektiven Diffusionskoeffizient d.h. D_{col} steigt über eine Größenordnung durch die Erhöhung der Temperatur von 25°C bis 40°C. Im Allgemeinen führt eine Schrumpfung zu einem dichteren Polymer und bewirkt die Reduktionder Diffusion.

- Oberhalb der LCST ist der variable Diffusionskoeffizient proportional zum Schrumpfmaß und beschreibt die experimentelle Kinetik besser. Darüber hinaus beschleunigt die Erhöhung der Temperatur die Diffusion und das Abgabegleichgewicht wird in einer kürzeren Zeit erreicht. Beispielsweise benötigt das Hydrogel weniger Zeit zum Erreichen seiner systematischen zylindrischen Form bei höheren Temperaturen.

9. Symbols

Letters

A: area

C: solute concentration in the hydrogel [$mole\backslash l$]

d : gel diameter, [mm]

D: diffusion coefficients [$m^2\backslash s$]

E : yield modulus [$N\backslash m^2$]

f : friction coefficient between the network and fluid medium [N]

F : uni-axial force [N]

G : shear modulus [$N\backslash m^2$]

GM : hydrogel matrix ratio

h : gel height [mm]

H : hydration

I : intensity

k : constant incorporating characteristics of the macromolecular network/drug system and the release medium

K : bulk modulus [$N\backslash m^2$]

K: Kelvin

m : mass [g]

M_t / M_∞ : cumulative fraction of drug released at time t

n : value indicative the drug transport mechanism in the macromolecular network.

q: swelling ratio

r : radial coordinate [m]

r : radius[m]

R : radius of the hydrogel particle [m]

t : real time [s]

V : volume[cm^3]

W : mass of the hydrogel [g]

x : coordinate

x: hydrogel/solution interface

Y : Young's modulus

z : axial coordinate [m]

z : thickness [m]

Z : half thickness of the hydrogel particle[m]

Greek symbols

α : time-independent term

$ß$: form factor

ρ : density [g\cm^3]

μ: shear modulus [$N\backslash m^2$]

∞ : at equilibrium state (infinity)

ν : Poison's ratio

τ : relaxation time [s]

Subscripts

CH: isopropyl group

col : collective

d : initial dry state

eff : effective

eq : equilibrium

H_2O: water

Int.: interface

Isoprop.: isopropyl group

l : liquid

mut.: mutual diffusion coefficient

0: initial state

r : in r-direction

s : equilibrium swelling state

y_{MBA}: molarcross linking ratio

z : in z-direction

Abbreviations

APS: ammoniumperoxodisulfat

BSA: bovine serum albumin

GM: matrix ratio

IPNs: interpenetrating polymer network

MBA: *N*,*N*' - methylenbisacrylamide

NaDS: sodium metabissulfite

NIPAAm: n-isopropylacrylamide

LCST: low critical solution temperature

UCST: upper critical solution temperature

10.References

AlenichevI., Sedláková Z., Ilavský M., Swelling and mechanical behavior of charged poly(*N*-isopropylmethacrylamide) and poly(*N*-isopropylacrylamide) networks in water/ethanol mixtures. Cononsolvency effect. Polymer Bulletin, 58 (1) (2007) 191-199.

Ali M., Horikawa S., Venkatesh S., Saha J., Hong J. W., Byrne M.E., Zero-Order Therapeutic Release From Imprinted Hydrogels Contact Lenses Within in Vitro Physiological Ocular Tear Flow, Journal of Controlled Release124 (3) (2007) 154-162.

Amiya T., Hirokawa Y., Hirose Y., Li Y., Tanaka T., Reentrant Phase Transition of N-Isopropylacrylamide Gels in Mixed Solvent, Journal of Chemical Physics, 86 (1987) 2375-2379.

Amsden B., Diffusion in Polyelectrolyte Hydrogels: Application of an Obstruction-Scaling Model to Solute Diffusion in Calcium Alginate, Macromolecules 2001, 34, 1430-1435.

Amsden B., Turner N., Diffusion Characteristics of Calcium Alginate Gels, Biotechnology and Bioengineering, 65 (5) (1999) 605-610.

Andersson M., Axelsson A., Zacchi G.,Diffusion of glucose and insulin in a swelling N-isopropylacrylamide gel, International Journal of Pharmaceutics, 157 (2) (1997) 199-208.

Ansell R. J., Kritz D., Mosbach K., Molecularly imprinted polymers for bioanalysis: Chromatography, binding assays and biomimetic sensors, Current Opinion in Biotechnology 7 (1996) 89-94.

Anseth K.S., Bowman C.N., Brannon-Peppas L., Mechanical Properties of Hydrogels and Their Experimental Determination, Biomaterials, 17 (1996) 1647-57.

Baker J. P., H. Hong L., Blanch H. W., Prausnitz J. M., Effect of Initial Total Monomer Concentration on the Swelling Behavior of Cationic Acrylamide-Based Hydrogels, Macromolecular, 27 (6) (1994) 1446-1454.

Beek M. Van, Jones L., Sheardown H., Hyaluronic acid containing hydrogels for the reduction of protein adsorption, Biomaterials 29 (2008) 780-789.

Beltran, S.; Baker, J. P.; Hooper, H. H.; Blanch, H. W.; Prausnitz, J. M., Swelling Equilibria for weakly ionizable, temperature-sensitive hydrogels. Macromolecules, 24 (1991) 549-551.

Bhardwaj Y. K., Kumar V., Sabharwal S., Swelling Behavior of Radiation-Polymerized Polyampholytic Two-Component Gels: Dynamic and Equilibrium Swelling Kinetics, Journal of Applied Polymer Science, 88 (3) (2003) 730-742.

Bignotti F., Sartore L., Penco M., Ramorino G., Peroni I., Effect of Montmorillonite on the Properties of Thermosensitive Poly(N-isopropylacrylamide) Composite Hydrogels, Journal of Applied Polymer Science, 93 (2004) 1964-1971.

Brazel S., Peppas N., Synthesis and Characterization of Thermo- and Chemomechanically Responsive Poly(N-idopropylacrylamide-co-methacrylic acid) Hydrogels. Macromolecules, 28 (1995) 8016-8020.

Bauer, M., Raman spectroscopy of laser induced material alterations, Ludwig-Maximilians-Universität München Dissertation, 2010.

Carbonell R. G., Sarti G. C., Coupled deformation and mass-transport processes in solid polymers, Industrial & Engineering Chemistry Research, 29 (7) (1990) 1194-1204.

Caspers P. J., Lucassen G. W., Carter E. A., Bruining H. A., Puppels G. J., In Vivo Confocal Raman Microspectroscopy of the Skin: Noninvasive Determination of Molecular Concentration Profiles, Journal of Investigative Dermatology, 116 (3) (2001) 434-433.

Cha W., Hyon S., Graiver D., Ikasa Y., Sticky poly(vinyl alcohol) hydrogels, Journal of Applied Polymer Science 1993, 47, 339- 343.

Chen J., Park K., Superporous Hydrogel: Fast Responsive Hydrogel System, Journal of Macromolecular Science, Part A: Pure and Applied Chemistry36 (7-8) (1999) 917-930.

Chu L.-Y., Kim J.-W., Shah R. K.,Weitz D. A., Monodisperse Thermoresponsive Microgels with Tunable Volume-Phase Transition Kinetics. Advanced Functional Materials17 (2007) 3499–3504.

Chung J. E., Yokoyama M., Yamato M., Aoyagi T., Sakurai Y., Okano T., Thermo-responsive drug delivery from polymeric micelles constructed using block copolymers of poly(N-isopropylacrylamide) and poly(butylmethacrylate), Journal of Controlled Release, 62 (1999) 115–127.

Coviello T., Palleschi A., Grassi M., Matricardi P., Bocchinfuso G. and Alhaique F., Scleroglucan: A Versatile Polysaccharide for Modified Drug Delivery, Molecules, 10 (1) (2005) 6-33.

Crank J., The Mathematics of Diffusion, Clarendon Press, Oxford 1975, p.12.

Crump S., Composites Convention and Trade Show, Florida, 2001.

Dagani, R., Intelligent Gels, Chemical and Engineering News 75 (23) (1997) 26-37.

De S. K., Aluru N.R., Johnson B., Crone W.C., Beebe D.J., Moore J., Equilibrium Swelling and Kinetics of pH-responsive Hydrogels; Models, Experiments and Simulations, Journal Microelectromechanics Systems., 11 (5) (2002) 544-555.

Ding X., Fries D., Jun B., A study of hydrogel thermal-dynamics using Fourier transform infrared spectrometer. Polymer, 47 (2006) 4718-4725.

Doi M., Matsumoto M., Hirose Y., Deformation of ionic polymer gels by electric fields, Macromolecules 25 (1992), 5504-5511.

Dubreuil A.-C., Doumenc F., Guerrier B., Allain C., Mutual diffusion in PMMA/PnBMA copolymer films - Influence of the solvent induced glass transition, Macromolecules, 36 (14) (2003) 5157-5164.

El Sayed H., Kirkwood R.C., Graham N. B., The Effects of a Hydrogel Polymer on the Growth of Certain Horticultural Crops under Saline Conditions. Journal of Experimental Botany, 42 (240) (1991) 891-899.

Engish A., Mafé S., Manzanares J., Yu X., Grosberg A., Tanaka T., Equilibrium swelling properties of polyampholytic hydrogels. Journal of Chemical Physics, 104 (21) (1996) 8713-8720.

Feil H., Bae Y.H., Feijen J., Kim S.W., Effect of comonomer hydrophilicity and ionization on the lower critical solution temperature of N-isopropylacrylamide copolymers, Macromolecules, 26 (1993) 2496-2500.

Flory P. J., Principles of Polymer Chemistry**,** Cornell University Press Ltd. (1953) London.

Freitaz R., Cussler E., Temperature sensitive gels as extraction solvent. Chemical Engineering Science, 42 (1) (1987) 97-103.

Friedli G.-L., Interaction of deamidated soluble wheat protein (SWP) with other food proteins and metals. PhD Thesis, the University of Surrey (1996).

Galino F., Lima J. C., Luis S. V., Melo M. J., Parola A. J., Pina F., Water/humidity and ammonia sensor, based on a polymer hydrogel matrix containing a fluorescent flavylium compound. Journal of Material Chemistry, 15 (2005)2840-2847.

Ganji F., Vasheghani-Farahani E., Hydrogels in Controlled Drug Delivery Systems, Iran. Polym. J., 18 (1) (2009) 63-88.

Gayet JC., Fortier G., High water content BSA-PEG hydrogel for controlled release device: Evaluation of the drug release properties. Journal of Controlled Release, 38 (2-3) (1996) 177-184.

Gostoli C., Sarti G.C., Diffusion and Localized Swelling Resistances in Glassy Polymers, Polymer Engineering and Science, 22 (16) (1982) 1018-1026.

Gouadec G., Colomban P., Raman Spectroscopy of nanomaterials: How spectra relate to disorder, particle size and mechanical properties. Progress in Crystal Growth and Characterization of Materials, 53 (1) (2007) 156.

Gutkowska A., Bae Y.H., Feijen J., Kim S.W., Heparin Release from Thermosensitive Hydrogels, Journal of Controlled Release, 22 (1992) 95-104.

Hahn D., Raman Scattering Theory, Department of Mechanical and Aerospace Engineering, University of Florida, 2007.

Hakiki A., Herz J. E., A study of the kinetics of swelling in cylindrical polystyrene gels: Mechanical behavior and final properties after swelling, Journal of Chemical Physics, 101 (10) (1994) 9054-9060.

Harmon M., Kuckling D., Frank C., Photo-Cross-Linkable PNIPAAm Copolymer. 5. Mechanical Properties of Hydrogel Layers. Langmuir, 19 (2003) 10660-10665.

He H., Multifunctional Medical Devices Based on pH-Sensitive Hydrogels for Controlled Drug Delivery, Diss., The Ohio State University (2006).

Hiratani H., Alvarez-Lorenzo C., Timol uptake and release by imprinted soft contact lenses made of N,N-diethylacrylamide and methacrylic acid, Biomaterials 29 (2008) 780-789.

Hirotsu S., Hirokawa Y., Tanaka T., Volume-Phase Transition of Ionized N-isopropylacrylamide Gels. Journal of Chemical Physics, 87 (2) (1987) 1392-1395.

Ho ML., Fu YC., Wang GJ., Chen HT., Chang JK., Tsai TH., Wang CK., Controlled release carrier of BSA made by W/O/W emulsion method containing PLGA and hydroxyapatite. Journal Controlled Release,128 (2) (2008)142-148.

Hoffman S., Hydrogels for biomedical applications. Advanced Drug Delivery Reviews 54 (1) (2002) 3-12.

Hong Y. P., Bae Y. C., Phase Behaviors of Partially Ionized Hydrogels in Aqueous Salt Solutions: Applicability of the Modified Double-Lattice Model, Journal of Polymer Science: Part B: Polymer Physics, 40 (2002) 2333–2338.

HuangX., Brazel C.S., On the Importance and Mechanisms of Burst Release in Matrix-Controlled Drug Delivery Systems, Journal Controlled Release, 73 (2001) 121–136.

Hubbell JA. Hydrogel systems for barriers and local drug delivery in the control of wound healing. Journal Controlled Release. 39 (2-3) (1996) 305-313.

Hudson S., Zhang S., Intelligent Stimuli-Sensitive Material Fibers and Fabrics. M98-A16, Final Report, North Carolina State University, USA (2001).

Hüther A., Xu X., Maurer G., Swelling of N-isopropyl acrylamide hydrogels in aqueous solutions of sodium chloride, Fluid Phase Equilibria 240 (218) (2006) 186-196.

Iveković D., Milardović S., Grabarić B.S., Palladium hexacyanoferrate hydrogel as a novel and simple enzymeimmobilization matrix for amperometric biosensors, Biosensors & Bioelectronics, 20 (2004) 872-878.

Jen A. C., Wake M. C., Mikos A. G., Review: Hydrogels for cell immobilization, Biotechnology and Bioengineering, 50 (1996) 357-364.

Jiang H. J., Campbell G., Boughner D., Wan W.-K., Quantz M., Design and manufacture of a polyvinyl alcohol (PVA) cryogel tri-leaflet heart valve prosthesis, Medical Engineering & Physics , 26 (4) (2004) 269-277.

Joachimiak A., Halamus T., Wojciechowski T., PUlanski J., Structure of Hydrogels Based on Lyotropic Phases of Celulose Derivative as Studied by Raman Spectroscopy. Macromolecular Chemistry and Physics, 206 (1) (2005) 59-65.

Johnson B.D., Niedermaier D.J., Crone W.C., Moorthy J., Beebe D.J., Proceedings of the SEM Annual Conference on Experimental Mechanics, Milwaukee, WI 2002.

Kaneko Y., Yoshida R., Sakai K., Sakurai Y., Okano T., Temperature-responsive shrinking kinetics of poly (N-isopropylacrylamide) copolymer gels with hydrophilic and hydrophobic comonomers, Journal of Membrane Science, 101 (1-2) (1995) 13-22.

Kawasaki H., Sasaki S., Maeda H., Mihara S., Tokita M., Komai T., Saccharide-Induced Volume Phase Transition of Poly(N-isopropylacrylamide) Gels. Journal of Physical Chemistry, 100 (40) (1996) 16282–16284.

Khoury Chr., Adalsteinsson Th., Johnson B., Crone W.C., Beebe D.J., Tunable Microfabricated Hydrogels – A Study in Protein Interaction and Diffusion, Biomedical Microdevices, 5 (1) (2003) 35-45.

Kim D., Heo J-Y., Kim K., Choi I., Formation of Thermosensitive Poly(N-isopropylacrylamide)/Dextran Particles by Atom Transfer Radical Polymerization. Macromolecular Rapid Communications, 24 (2003) 517-521.

Kim S. J., Yoon S. G., Lee S. M., Lee S. H., Kim S. I., Electrical Sensitivity Behavior of a Hydrogel Composed of Polymethacrylic Acid/Poly(vinyl alcohol). Journal of Applied Polymer Science, 91 (2004) 3613–361.

Kishi R., Osada Y., Reversible volume change of microparticles in an electric field, Journal of the Chemical Society, Faraday Transactions, 1 (85) (1989) 655-662.

KomoriT.and Sakamoto R., On Tanaka-Fillmore's kinetics swelling of gels, Colloid and Polymer Science,267 (1989) 179-183.

Koros J. W., Paul D. R., Rocha R., Carbon dioxide sorption and transport in polycarbonate, Journal of Polymer Science, Part B: Polymer Physics, 14 (1976), 687-702.

Kosik K., Wilk E., Geissler E., László K., Distribution of Phenols in Thermoresponsive Hydrogels,Macromolecules, 40 (6) (2007) 2141–2147.

Kosto K.B., Deen W.M., Diffusivities of Macromolecules in Composite Hydrogels.American Institute of Chemical Engineers, 50 (11) (2004) 2648 -2658.

Kwak S, Lafleur M.,Raman Spectroscopy as a Tool for Measuring Mutual-Diffusion Coefficients in Hydrogels,Applied Spectroscopy, 57(7) (2003) 768-773.

Langer R., Peppas N. A., Advances in biomaterials, drug delivery and bionanotechnology, American Institute of Chemical Engineers, 49 (12) (2003) 2990–3006.

László K., Kosik K., Rochas C., Geissler E., Phase Transition in Poly(N-isopropylacrylamide) Hydrogels Induced by Phenol. Macromolecular, 36 (2003) 7771-7776.

Lévesque S.G., Lim R.M., Shoichet M.S., Macroporous Interconnected Dextran Scaffolds of Controlled Porosity for Tissue-Engineering Applications, Biomaterials, 26 (2005) 7436-7446.

Lewus R. K., Carta G., Protein diffusion in charged polyacrylamide gels - Visualization and analysis , Journal of Chromatography, A. 865 (1) (1999) 155-168.

Li B., Jiang Y., Liu Y., Wu Y., Yu H., Zhu. M., Novel Poly(N-isopropylacrylamide)/ Clay/ Poly(acrylamide) IPN Hydrogels with the Response Rate and Drug Release Controlled by Clay Content, Journal of Polymer Science, Part B: Polymer Physics, 47 (1) (2008) 96-106.

Li Y., Tanaka T., Kinetics of Swelling and Shrinking of Gels, Journal of Chemical Physics, 92 (2) (1990) 1365-1371.

Lin Ch-Ch., Metters AT., Hydrogels in controlled release formulations: Network design and mathematical modeling, Advanced Drug Delivery Reviews58(12-13) (2006) 1379–1408.

Linden H., Olthuis W., Bergveld P., An efficient method for the fabrication of temperature-sensitive hydrogel microactuators. The Royal Society of Chemistry, 4 (2004) 619-624.

Liu, K. Ovaert T. C., Mason J. J, Preparation and mechanical characterization of a PNIPA hydrogel composite. Journal of Materials Science: Materials in Medicine, 19 (4) (2008) 1815-1821.

Liu Q., De Kee D., Modeling of diffusion through polymeric membranes, Rheologica Acta, 44 (2005) 287-294.

M.T. Quinn, J.A. Grodzinsky, Longitudinal Modulus and Hydraulic Permeability of Poly(methacrylic acid) Gels: Effects of Charge-Density and Solvent Content. Macromolecules, 26 (1993) 4332-4338.

Malcolm B., Huglin, MBZ., Swelling properties of copolymeric hydrogels prepared by gamma irradiation. Journal of Applied Polymer Science, 31 (1986) 457-475.

Mamada A., Tanaka T., Kungwatchakun D., Irief M., Photoinduced Phase Transition of Gels. Macromolecules, 23 (1990) 1517-1519.

Mao L., Hu Y., Piao Y., Chen X., Xian W., Piao D., Structure and Character of Artificial Muscle Model Constructed from Fibrous Hydrogel, Current Applied Physics, 5 (2005) 426-428.

Matsumoto A., Kurata T., Shiino D., and Kataoka K., Swelling and Shrinking Kinetics of Totally Synthetic,Glucose-Responsive Polymer Gel Bearing Phenylborate Derivative as a Glucose-Sensing Moiety, Macromolecules37 (2004)1502-1510.

McDowellC. C., FreemanB. D., McNeely G. W., Interval kinetic gravimetric sorption of acetone in random copolymers of poly(ethylene terephthalate) and poly(ethylene 2,6-naphthalate).Journal of Polymer Science, Part B: Polymer Physics, 37 (21) (1999) 2973–2984.

Melekaslan D., Gundogan N., Okay O., Elasticity of poly(acrylamide) gel beads. Polymer Bulletin, (50) (2003) 287- 294.

Mellott M. B., Searcy K., Pishko M. V., Release of Protein From Highly Cross-Linked Hydrogels of Poly(ethylene glycol) Diacrylate Fabricated by UV Polymerization, Biomaterials., 22 (9) (2001) 929-941.

Muniz E C., Geuskens G., Compressive elastic modulus of polyacrylamide hydrogels and semi-IPNs with poly(N-isopropylacrylamide), Macromolecules, 34 (13) (2001) 4480-4484.

Muniz E. C., Geuskens G., Polyacrylamide hydrogels and semi-interpenetrating networks (IPNs) with poly(N-isopropylacrylamide): Mechanical properties by measure of compressive elastic modulus, Journal of Materials Science: Materials in Medicine, 12 (10-12) (2001) 879-881.

Naddaf A., Bart H.-J. Swelling Characteristics of Poly(NIPAAm) Using Confocal Raman Microscopy. Proceedings of the 18th International Congress of Chemical and Process Engineering, CHISA (2008) Prague (Czech Republic).

Naddaf A., Bart H.-J., Raman Spectroscopy: Mutual Diffusion Coefficient in Hydrogels. Defect Diffusion Forum, 312-315 (2011) 193-198.

Naddaf A., Tsibranska I., Bart H.-J. Kinetics of BSA Release from Poly(N-isopropylacrylamide) Hydrogels. Chemical Engineering and Processing: Process Intensification, 49 (2010) 581-588.

Naddaf A., Tsibranska I., Bart H.-J., Diffusion Kinetics of BSA Protein in Stimuli Responsive Hydrogels. Defect and Diffusion Forum, 297-301 (2010) 664-669.

Nakashima S., Harima H., Raman Investigation of SiC Polytypes.physica status solidi (a) 162 (1) (1997) 39-64.

Nge T.T., Yamaguchi M., Hori N., Takemura A., Ono H., Synthesis and characterization of chitosan/poly(acrylic acid) polyelectrolyte complex, Journal of Applied Polymer Science, 83 (2002) 1025-1035.

Osada Y., Hasebe M., Electrically activated mechanochemical devices using polyelectrolyte gels, Chemistry Letters (1985) 1285-1288.

Otake K., Inomata H., Konno M., Saito S., Thermal Analysis of the Volume Phase Transition with N-Isopropylacrylamide Gels. Macromolecular, 23 (I) (1990) 283-289.

Panayiotou M., Synthesis and Characterization of Thermoresponsive, Polymers, Hydrogels and Microgels, Based on Poly (N-Substituted Acrylamides).Ecole polytechnique fédérale de Lausanne EPFL Thesis No 3174, (2004).

Patton C. J., Felder R. M., and Koros W. J., Sorption and Transport of Benzene in Poly(ethylene Terephthalate).Journal of Applied Polymer Science, 29 (1984)1095-1110.

Pelton R.,Poly(N-isopropylacrylamide) (PNIPAM) is never hydrophobic.Journal of Colloid and Interface Science, 348 (2) (2010) 673-674.

Peppas N. A., "Hydrogels" in "Biomaterials Science: An Introduction to Materials in Medicine," B.D. Ratner, A.S. Hoffman, F.J. Schoen and J.E. Lemons, Academic Press, New York, NY, 2nd edn., 2004, 100-107.

Peppas N. A., Bures P. Leobandung W., Inchikawa H., Hydrogel in pharmaceutical formulations. European Journal of Pharmaceutical and Biopharmaceutics, 50 (2000) 27-46.

Peppas N. A., Huang Y. Torres-Lugo J. H., Zhang J., Physicochemical foundations and structural decision of design of hydrogels in medicine and biology. Annual Review of Biomedical Engineering, 2 (2000) 9-29.

Peppas N.A., Langer R.,New challenges in biomaterials. Science 263 (5154) (1994) 1715-1720.

Peters A., Candau S. J.,Kinetics of swelling of spherical and cylindrical gels. Macromolecules, 21 (7) (1988) 2278-2282.

Philippova O.E., Karibyants N.S., Stardubtzev S.G., Conformational changes of hydrogels of poly(methacrylic acid) induced by interactions with poly(ethylene glycol). Macromolecules (27) (1994) 2398–2401.

Piai J. F., de Moura M. R., Rubira A. F., Muniz E. C., Kinetic Study of Bovine Serum Albumin (BSA) Released from Alginate-Ca^{2+}/PNIPAAm Hydrogels. Macromolecules Symposia, 266 (1) (2008) 108–113.

Quarfoot A. J., Hyla P. H., Patience D., Hydrogel wound dressing. The KendallCompany US4909244 (1990).

Qiu, Y.; Park, K., Environment-sensitive hydrogels for drug delivery, Adv. Drug DeliveryRev. 53 (2001) 321-339.

Quinn M. T., Grodzinsky J. A., Longitudinal Modulus and Hydraulic Permeability of Poly(methacry1ic acid) Gels: Effects of Charge Density and Solvent Content. Macromolecules, 26 (1993) 4332-4338.

Richter A., Paschew G., Klatt St., Lienig J., Arndt K.-F.,P. Adler H.-J., Review on Hydrogel-Based pH Sensors and Microsensors. Sensors., 8 (2008), 561-581.

Roorda W. E., Boddé H. E., De Boer A. G., Junginger H. E., Synthetic Hydrogels as Drug Delivery Systems. Pharmaceutisch Weekblad Scientific Edition, 8 (1986) 165-189.

Russell S. M. Carta G., Multicomponent Protein Adsorption in Supported Cationic Polyacrylamide Hydrogels. American Institute of Chemical Engineers, 51 (9) (2005) 2469-2480.

Russell S. M., Belcher E.B., Carta G., Protein Partitioning and Transport in Supported Cationic Acrylamide-Based Hydrogels.American Institute of Chemical Engineers, 49 (5) (2003) 1168-1177.

Sayil Ç., Okay O., The effect of preparation temperature on the swelling behavior of poly (N-isopropylacrylamide) gels. Polymer Bulletin, 45 (2000) 175-182.

Shalaby A., Abdallah A.A., Park H., Park K., Loading of bovine serum albumin into hydrogels by an electrophoretic process and its potential applications to protein drugs. Pharmaceutical Research10 (1993) 457–460.

Shang L., Zhang S., Du H., Venkatraman S.S., A Novel Approach for the Control of Drug Release Rate Through Hydrogel Membrane: I. Effect of Drug Immobilization on Drug Release Rate by Copolymerization Method.European Journal of Pharmaceutics and Biopharmaceutics, 68 (3) (2008) 715-723.

Sainio T., Ion-exchange resins as stationary phase in reactive chromatography, PhD-thesis, (2005) Lappeenranta University of Technology, Finland

Siepman J., Ainaoui A., Vergnaud J.M., Bodmeier R., Calculation of the Dimensions of Drug-Polymer Devices Based on Diffusion Parameters. Journal of Pharmaceutical Sciences, 87 (7) (1998) 827-832.

Siepman J., Podual K., Sriwongjanya M., Peppas N. A., Bodmeier R., A New Model Describing the Swelling and Drug Release Kinetics from Hydroxypropyl Methylcellulose Tablets. Journal of Pharmaceutical Sciences, 88 (1) (1999) 65-72.

Singh J., Weber M. E., Kinetics of one-dimensional gel swelling and collapse for large volume change, Chemical Engineering Science, 51 (19) (1996) 4499-4508.

Son Y.-K., Jung Y. P., and Kim J.-H., Preparation and Properties of PEG-Modified PHEMA Hydrogel and the Morphological Effect. Macromolecules Research , 14, (3) (2006) 394-399.

Stile A. R., Healy E. K., Poly(N-isopropylacrylamide)-Based Semi-interpenetrating Polymer Networks for Tissue Engineering Applications. 1. Effects of Linear Poly(acrylic acid) Chains on Phase Behavior. Biomacromolecules, 3 (2002) 591-600.

Sudipto K. De, N. R. Aluru, B. Johnson, W. C. Crone, David J. Beebe and J. Moore., Equilibrium Swelling and Kinetics of pH-Responsive Hydrogels: Models. Experiments and Simulations. Journal of Microelectromechanical Systems, 11 (5) (2002) 544-555.

Suzuki, Y.; Tomonaga, K.; Kumazaki, M.; Nishio, I., Change in phase transition behavior of an NIPA gel induced by solvent composition: hydrophobic effect.Polymer GelsandNetworks, 4 (1996) 129–142.

Norisuye T., Tran-Cong-Miyata Q., Shibayama M., Dynamic Inhomogeneities in Polymer Gels Investigated by Dynamic Light Scattering.Macromolecules, 37 (2004)2944–2953.

Takahara J., Takayama K., Isowa K., Nagai T., Multi-objective simultaneousoptimization based on artificial neural network in a ketoprofen hydrogel formula containing O-ethylmenthol as a percutaneous absorption enhancer. International Journal of Pharmaceutics, 158 (2) (1997) 203-210.

Takahashi K., Takigawa T., Masuda T., Swelling and Deswelling Kinetics of Poly(N-isopropylacrylamide) Gels. Journal of Chemical Physics, 120 (6) (2004), 2972- 2979.

Tanaka T., Fillmore D., Kinetics of swelling of gels.Journal of Chemical Physics, 70 (1979) 1214-1218.

Tanaka T., Collapse of gels and the critical endpoint. Physical Review Letters, 40 (12) (1978) 820-823.

Tanaka T., Hocher L.O., Benedek G.B, Spectrum of light scattered from a viscoelastic gel. Journal of Chemical Physics,59 (9) (1973) 5151-5159.

Tasdelen B., Kayaman-Apohan N., Misirli Z., Güven O., Baysal B. M., Preparation, Characterization, and Drug-Release Properties of Poly(N-isopropylacrylamide) Microspheres Having Poly(Itaconic Acid) Graft Chains. Journal of Applied Polymer Science, 97 (2005) 1115–112.

Tokita M., Tanaka T., Friction Coefficient of Polymer Networks of Gels. Journal of Chemical Physics, 95 (6) (1991) 4613-4619.

Van Tomme S., Self-assembling Microsphere-Based Dextran Hydrogels for Pharmaceutical Applications, Thesis, Department of Pharmaceutics, Utrecht University, Netherlands (2007).

Vrentas J. S., Vrentas C. M., Fickian diffusion in glassy polymer-solvent systems.Journal of Polymer Science Part B: Polymer Physics, 30 (9) (1992) 1005-1011.

Walther D.H., Sin G.H., Blanch H.W., and Prausnitz J. M.,Pore-size distributions of cationic 2-hydroxyethyl methacrylate (HEMA) hydrogels.Polymer Gels Networks, 3 (1) (1995) 29-45.

Watanabe H., Iwata S., Theoretical studies of geometric structures of phenol-water clusters and their infrared absorption spectra in the O–H stretching region. Journal of Chemical Physics, 105 (2) (1996) 420- 431.

Weis D., Hand book of pharmaceutical controlled release technology. CRC Press, USA (2000).

Winnik F., Ottaviani M., Bossman S., Pan W., Garcia-Garibay M., Turro N., Phase Separation of Poly(N-isopropylacrylamide) in Water: A Spectroscopic Study of a Polymer Tagged with a Fluorescent Dye and a Spin Label. Journal of Chemical Physics, 97 (1993)12998-13005.

Whiting C. J., Voice A.M., Olmsted P.D., Mcleish T.C., Shear modulus of polyelectrolyte gels under electric field, Journal of Physics: Condensed Matter, 13 (2001) 1381-1393.

Wu C., Zhou S., Light Scattering Study of SphericalPoly(N-isopropylacrylamide) Microgels, Journal of Macromolecular Science, Part B: Physics, 836(3)(1997)345-355.

Wu L., Brazel Chr. S., Mathematical Model to Predict Drug Release, Including the Early-Time Burst Effect from Swellable Homogeneous Hydrogels.Industrial & Engineering Chemistry Research, 47 (5) (2008)1518-1526.

Yoshida M., Uezu K., Goto M., Furasaki S., Surface Imprinted Polymers Recognizing Amino Acid Chirality. Journal of Applied Polymer Science, 78 (2000) 695-703.

Yu, H., Grainger, D.W., Thermo-sensitive swelling behavior in crosslinked N-isopropylacrylamide networks: cationic, anionic, and ampholytic hydrogels. Journal of Applied Polymer Science,49 (1993) 1553-1563.

Zhang, J.; Peppas, N.A., Synthesis and characterization of pH- and temperature- sensitive poly(methacrylic acid)/poly(N-isopropylacrylamide) interpenetrating polymeric networks.Macromolecules, 33 (2000) 102-107.

Zhang X.-Z., Wu D.-Q., Chu C.-C., Synthesis, characterization and controlled drug release of thermosensitive IPN-PNIPAAm Hydrogels. Biomaterials, 25 (2004) 3793-3805.

Zhang Y., Zhu W., Wang B., Yu I., Ding J., Postfabrication Encapsulation of Model Protein Drug in a Negatively Thermosensitive Hydrogel. Journal of Pharmaceutical Sciences, 94 (8) (2005) 1676-1684.

APPENDIX A:
Materials and Chemicals

N-isopropylacrylamide	**NIPAAm**
Supplied by	Sigma- Aldrich Chemie GmbH
Type	White crystals
Molecular Formula	$H_2C=CHCONHCH(CH_3)_2$
Molecular Weight	113.16
Assay	>97%
Boiling Point	89-92 °C/2 mmHg
Melting point	60-63 °C

Chemical Structure

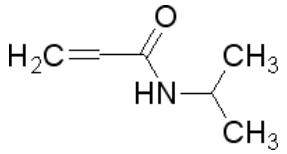

N,N-methylenbisacrylamide	**MBA**
Supplied by	Sigma- Aldrich
Type	White Powder
Molecular Formula	$(CH_2=CHCONH)_2CH_2$
Molecular Weight	154.17
Vapor Density	5.31 (vs air)
Assay	99%
Melting point	>300°C

Chemical Structure

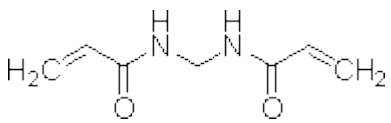

Sodium Metabissulfite	**NaDS**
Supplied by	Sigma- Aldrich
Type	White Powder
Molecular Formula	$Na_2S_2O_5$
	Na-O-(S=O)-O-(S=O)-O-Na
Molecular Weight	190.1
Specific Density	1,28 g/cm^3
Assay	>98%
Melting point	300 °C

Chemical Structure

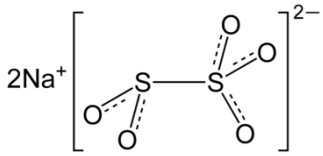

Ammoniumperoxodisulfat	**APS**
Supplied by	VWR
Type	White Powder
Molecular Formula	$(NH_4)_2S_2O_8$
Molecular Weight [g/mol]	228.2 at 20°C
Density [g/cm³]	1,98
Assay	>98%
Melting point	120 °C

Chemical Structure

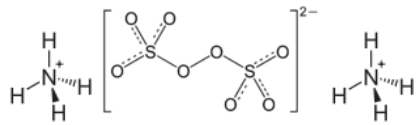

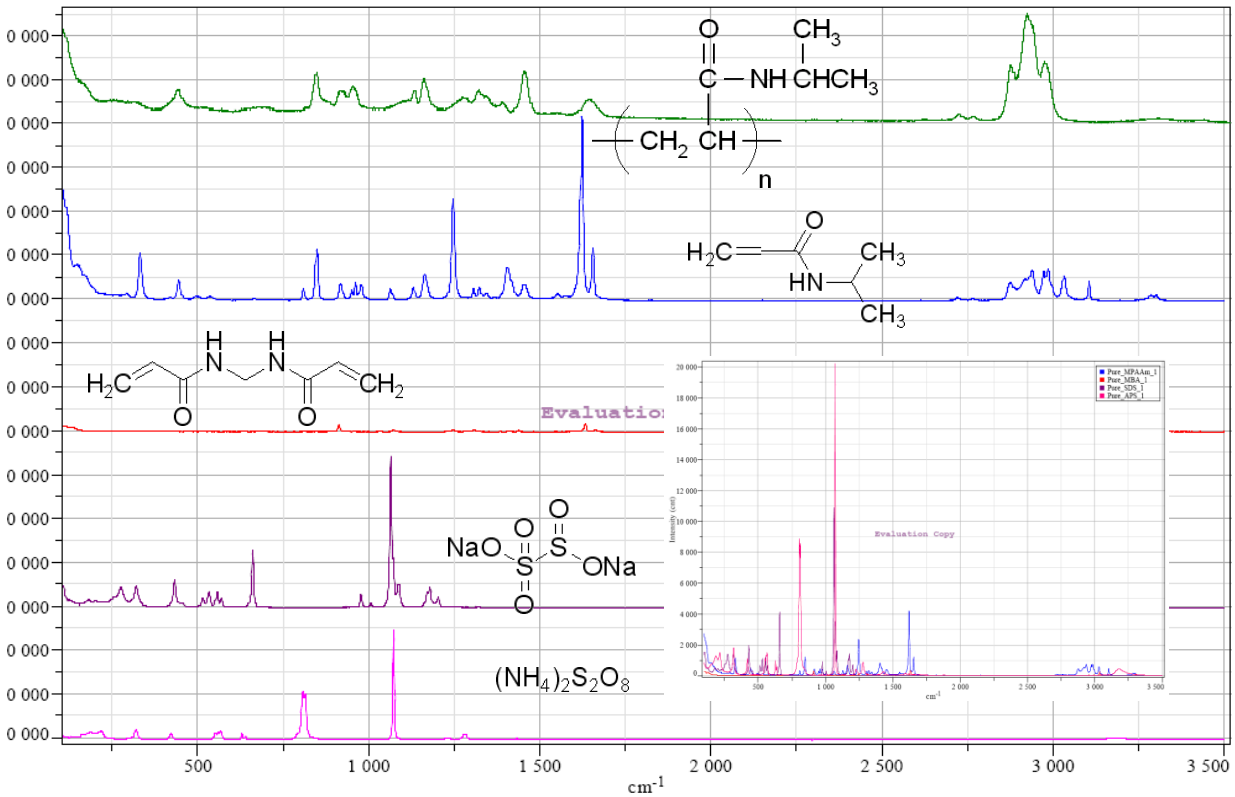

Fig. A.1: Raman Spectrum for the main pure component of the poly(NIPAAm)

APPENDIXB:
Hydrogel Synthesis

Tables B.1-B.4: The four kinds of hydrogels were produced based on the mole fraction of the cross linking ratio

Table B.1: Hydrogel_1

m_{NIPAAm}/m_{MBA}	**~63%**
NIPAAm [g]	9.30
MBA [g]	0.1476
H_2O [g]	80.064
$(NH_4)_2S_2O_8$ [g]	0.0180
$Na_2S_2O_5$ [g]	0.0180
Summ [g]	90.0
GM	0.105
y_{MBA} (mol%)	0.0115

Table B.2: Hydrogel_2

m_{NIPAAm}/m_{MBA}	**~53%**
NIPAAm [g]	9.3
MBA [g]	0.1743
H_2O [g]	80.1
$(NH_4)_2S_2O_8$ [g]	0.0181
$Na_2S_2O_5$ [g]	0.0180
Summ [g]	90.0
GM	0.11
y_{MBA} (mol%)	0.0136

Table B.3: Hydrogel_3

m_{NIPAAm}/m_{MBA}	**~43%**
NIPAAm [g]	9.675
MBA [g]	0.2256
H_2O [g]	80.443
$(NH_4)_2S_2O_8$ [g]	0.0184
$Na_2S_2O_5$ [g]	0.0181
Summ [g]	90.38
GM	0.11
y_{MBA} (mol%)	0.0168

Table B. 4: Hydrogel_4

m_{NIPAAm}/m_{MBA}	**~33%**
NIPAAm [g]	8.6962
MBA [g]	0.3038
H_2O [g]	80.9640
$(NH_4)_2S_2O_8$ [g]	0.0180
$Na_2S_2O_5$ [g]	0.0180
Summ [g]	90.0
GM	0.1
y_{MBA} (mol%)	0.025

APPENDIX C:
Experimental Data

Hydrogel was produced and the matrix ration was calculated (Appendix B). After 24 hours and complete polymerization, the hydrogel samples were taken out and sliced into slices. Then the edges of each cylinder were removed. After that diameter, d_0, thickness, t_0, mass, m_0, mass, m_1, pH, temperature, T_0, Raman intensity, I_0 and picture under Raman were measured for each cylinder and before being subjected to equilibrium. The hydrogel cylinders were then placed in a TC-Plate 6 well. The samples were washed daily to remove the unreacted materials. The samples were equilibrated at different **temperatures (**each sample of the 6 should have different pH value**), pH** (NaOH and H_2SO_4), **concentrations** of NaCl, phenol, BSA and propanol. After equilibrium, again diameter, d_1, thickness, t_1, mass, m_1, pH, temperature, T_1, Raman intensity, I_1, and picture under Raman were measured. Tables C.1-C.7 represent the equilibrium parameters (**temperatures (T), pH**, **concentrations (C)**) and the measured changes in mass and dimensions. The bold data refers to the measure data obtained after equilibrium. Tables C.1-C.7 are for the hydrogel contains 63% NIPAAm. For the data of the other hydrogels are available in the included CD.

Table C.1: Samples 2.1 – 2.6 subjected to temperature variation

Parameter	Before equilibrium 2.1	**T_1** 2.1	Before Equilibrium 2.2	**T_2** 2.2	Before Equilibrium 2.3	**T_3** 2.3
Equilibrium T		**25**		**30**		**32**
Diameter, d_0[mm]	10.5340	**12.9517**	11.1320	**11.6935**	11.1320	**10.5560**
Thickness, t_0[mm]	2.0321	**2.1052**	1.7879	**1.4560**	2.1130	**2.1385**
Mass, m_0[g]	0.2016	**-**	0.1710	**-**	0.1968	**-**
Mass, m_1 [g]		**0.3709**		**0.2469**		**0.2428**
Meas. Temperature, T_0, °C		**18.9**		**18.9**		**18.8**
Parameter	Before Equilibrium 2.4	**T_4** 2.4	Before Equilibrium 2.5	**T_5** 2.5	Before Equilibrium 2.6	**T_6** 2.6
Equilibrium T		**34**		**40**		**50**
Diameter, d_0[mm]	10.6720	**6.3245**	11.0400	**5.3236**	10.5340	**5.0050**
Thickness, t_0 [mm]	2.3568	**1.0010**	1.5847	**0.6370**	2.0723	**0.4550**
Mass, m_0 [g]	0.2238	**-**	0.1709	**-**	0.1997	**-**
Mass, m_1 [g]		**0.0743**		**0.0325**		**0.0347**
Meas. Temperature, T_0, °C		**18.8**		**19.1**		**18.9**

Table C.2: Samples 3.1 – 3.6 subjected to pH variation using NaOH

Parameter	Before Equilibrium 3.1	**pH$_1$** 3.1	Before Equilibrium 3.2	**pH$_2$** 3.2	Before Equilibrium 3.3	**pH$_3$** 3.3
Equilibrium pH		**7.04**		**8.20**		**9.19**
Diameter, d_0[mm]	10.6720	**12.8765**	10.4420	**12.7855**	10.9940	**12.7440**
Thickness, t_0 [mm]	2.1942	**2.1840**	2.3978	**2.6845**	2.0317	**2.5480**
Mass, m_0 [g]	0.1957	-	0.2202	-	0.2115	-
Mass, m_1 [g]		**0.3749**		**0.4058**		**0.3584**
pH		**6.68**		**6.9**		**7.39**
Meas. Temperature, T_0, °C		**20.8**		**20.7**		**21.4**
Parameter	Before Equilibrium 3.4	**pH$_4$** 3.4	Before Equilibrium 3.5	**pH$_5$** 3.5	Before Equilibrium 3.6	**pH$_6$** 3.6
Equilibrium pH		**10.11**		**11.13**		**12.20**
Diameter, d_0[mm]	10.6720	**13.1495**	10.7180	**12.7855**	10.2120	**11.9665**
Thickness, t_0 [mm]	2.1130	**2.2750**	2.5603	**2.6405**	2.1942	**2.5480**
Mass, m_0 [g]	0.2003	-	0.2320	-	0.2222	-
Mass, m_1 [g]		**0.3780**		**0.4228**		**0.3230**
pH		**9.07**		**11.26**		**12.48**
Meas. Temperature, T_0, °C		**20.4**		**21.2**		**21.4**

Table C.3: Samples 4.1 – 4.6 subjected to pH variation using H_2SO_4

Parameter	Before Equilibrium 4.1	**pH$_1$** 4.1	Before Equilibrium 4.2	**pH$_2$** 4.2	Before Equilibrium 4.3	**pH$_3$** 4.3
Equilibrium pH	-	**0.45**	-	**1.12**	-	**2.04**
Diameter, d_0[mm]	10.2580	**11.4636**	10.2120	**12.3000**	10.0280	**13.4316**
Thickness, t_0 [mm]	2.3161	**2.5584**	2.6412	**2.0664**	2.3569	**3.1488**
Mass, m_0 [g]	0.2371	-	0.2363	-	0.2356	-
Mass, m_1 [g]		**0.2696**		**0.3022**		**0.4106**
pH		**0.44**		**1.12**		**2.01**
Meas. Temperature, T_0, °C		**18.8**		**18.9**		**18.9**
Parameter	Before Equilibrium 4.4	**pH$_4$** 4.4	Before Equilibrium 4.5	**pH$_5$** 4.5	Before Equilibrium 4.6	**pH$_6$** 4.6
Equilibrium pH	-	**3.05**	-	**4.27**	-	**6.14**
Diameter, d_0[mm]	10.5340	**13.4808**	10.4420	**14.4156**	10.4880	**12.7855**
Thickness, t_0 [mm]	2.3161	**2.8536**	1.9504	**1.9680**	1.9521	**2.4119**
Mass, m_0 [g]	0.2266	-	0.2028	-	0.1931	-
Mass, m_1 [g]		**0.3863**		**0.3591**		**0.3905**
pH		**3.01**		**4.67**		**6.36**
Meas. Temperature, T_0,°C		**20.4**		**20.4**		**21.5**

Table C.4: Samples 5.1 – 5.6 subjected to solute concentration variation using NaCl

Parameter	Before Equilibrium 5.1	**C_1** 5.1	Before Equilibrium 5.2	**C_2** 5.2	Before Equilibrium 5.3	**C_3** 5.3
Conc.	-	**0.1M**	-	**10^{-2}**	-	**10^{-3}**
Diameter, d_0[mm]	11.3045	**12.0120**	11.2044	**12.5125**	11.2046	**12.4215**
Thickness, t_0 [mm]	2.7001	**2.6390**	2.6544	**2.7060**	2.3798	**2.4600**
Mass, m_0 [g]	0.2470	**-**	0.2331	**-**	0.2042	**-**
Mass, m_1 [g]		**0.4427**		**0.3920**		**0.3743**
pH		**-**		**-**		**-**
Temperature, T_0		**19.1**		**19.1**		**19.1**
Parameter	Before Equilibrium 5.4	**C_4** 5.4	Before Equilibrium 5.5	**C_5** 5.5	Before Equilibrium 5.6	**C_6** 5.6
Conc.	-	**10^{-4}**	-	**10^{-5}**	-	**10^{-6}**
Diameter, d_0[mm]	11.7046	**13.3315**	11.4545	**13.7410**	11.1544	**12.7400**
Thickness, t_0 [mm]	1.7848	**2.0020**	2.1509	**2.1840**	2.5171	**2.5480**
Mass, m_0 [g]	0.1797	**-**	0.2099	**-**	0.2198	**-**
Mass, m_1 [g]		**0.3673**		**0.4189**		**0.4623**
pH		**-**		**-**		**-**
Temperature, T_0		**19.1**		**19.2**		**19.3**

Table C.5: Samples 6.1 – 6.6 subjected to solute concentration variation using phenol

Parameter	Before Equilibrium 6.1	**C_1** 6.1	Before Equilibrium 6.2	**C_2** 6.2	Before Equilibrium 6.3	**C_3** 6.3
Conc.		**10^{-3}**		**$2*10^{-3}$**		**$3*10^{-3}$**
Diameter, d_0[mm]	11.6046	**12.5125**	11.4545	**12.6945**	11.3045	**12.6035**
Thickness, t_0 [mm]	2.3802	**2.6390**	2.1967	**2.3205**	2.7917	**2.9120**
Mass, m_0 [g]	0.2146	**-**	0.2047	**-**	0.2436	**-**
Mass, m_1 [g]		**0.4102**		**0.4052**		**0.4545**
Temperature, T_0		**19.3**		**19.3**		**19.5**
Parameter	Before Equilibrium 6.4	**C_4** 6.4	Before Equilibrium 6.5	**C_5** 6.5	Before Equilibrium 6.6	**C_6** 6.6
Conc.		**$4*10^{-3}$**		**-**		**$5*10^{-3}$**
Diameter, d_0[mm]	11.2044	**5.5510**	11.3045	**-**	10.3041	**6.3245**
Thickness, t_0 [mm]	2.7459	**1.4560**	2.7917	**-**	3.8443	**2.7300**
Mass, m_0 [g]	0.2364	**-**	0.2444	**-**	0.2858	**-**
Mass, m_1 [g]		**0.0733**		**-**		**0.1260**
Temperature, T_0		**19.5**		**-**		**19.5**

Table C.6: Samples 7.1 – 7.6 subjected to solute concentration variation using Ethanol

Parameter	Before Equilibrium 7.1	**C_1** 7.1	Before Equilibrium 7.2	**C_2** 7.2	Before Equilibrium 7.3	**C_3** 7.3
Conc.		**$2*10^{-2}$**		**$4*10^{-2}$**		**$6*10^{-2}$**
Diameter, d_0[mm]	11.7548	**13.5135**	10.9043	**12.3760**	11.1044	**13.1040**
Thickness, t_0 [mm]	1.7848	**1.6835**	2.7001	**2.9575**	2.0136	**2.7556**
Mass, m_0 [g]	0.1690	**-**	0.2470	**-**	0.1672	**-**
Mass, m_1 [g]		**0.3338**		**0.5269**		**0.3683**
Temperature, T_0		**19.6**		**19.6**		**19.7**
Parameter	Before Equilibrium 7.4	**C_4** 7.4	Before Equilibrium 7.5	**C_5** 7.5	Before Equilibrium 7.6	**C_6** 7.6
Conc.		**$8*10^{-2}$**		**$1*10^{-1}$**		**-**
Diameter, d_0[mm]	11.3045	**13.2405**	11.5046	**13.0130**	11.0544	**-**
Thickness, t_0 [mm]	2.2425	**2.4115**	2.0136	**1.9110**	2.4713	**-**
Mass, m_0 [g]	0.1945	**-**	0.1778	**-**	0.2124	**-**
Mass, m_1 [g]		**0.3806**		**0.3423**		**-**
Temperature, T_0		**19.7**		**19.7**		**-**

Table C.6: Samples 7.1 – 7.6 subjected to solute concentration variation using Propanol

Parameter	Before Equilibrium 8.1	**C_1** 8.1	Before Equilibrium 8.2	**C_2** 8.2	Before Equilibrium 8.3	**C_3** 8.3
Conc.		**$2*10^{-2}$**		**$4*10^{-2}$**		**$6*10^{-2}$**
Diameter, d_0[mm]	11.4550	**13.1495**	11.7547	**13.3770**	11.6047	**13.1495**
Thickness, t_0 [mm]	2.3798	**2.7300**	3.0205	**2.8665**	2.3798	**2.4115**
Mass, m_0 [g]	0.2111	-	0.2086	-	0.1895	-
Mass, m_1 [g]		**0.4270**		**0.4268**		**0.4087**
Temperature, T_0		**19.7**		**19.8**		**19.8**
Parameter	Before Equilibrium 8.4	**C_4** 8.4	Before Equilibrium 8.5	**C_5** 8.5	Before Equilibrium 8.6	**C_6** 8.6
Conc.		**$8*10^{-2}$**		**$1*10^{-1}$**		**-**
Diameter, d_0[mm]	11.5546	**12.2850**	11.7046	**12.6490**	11.1544	**-**
Thickness, t_0 [mm]	2.2425	**2.3660**	2.3798	**2.1385**	2.7001	**-**
Mass, m_0 [g]	0.1770	-	0.1982	-	0.2276	-
Mass, m_1 [g]		**0.3236**		**0.3500**		**-**
Temperature, T_0		**19.8**		**19.8**		**-**

APPENDIX D:
Hydrogel Characterization

Hydrogels were characterized in terms of the swelling ratio, water uptake and hydration. For the equilibrium swelling ratio and water uptake, poly(NIPAAm) hydrogels were weighed in dried state and after release at equilibrium a temperature, which ranged between 25ºC to 40ºC. Meanwhile, for the hydration study, dimensions of poly(NIPAAm) hydrogels were measured in dried state and after release at equilibrium.

Tables D.1-D.3 present the different samples belong to hydrogel_4, hydrohel_3, and hydrogel_2 and the parameter used to characterize it. For example, Table D.3 shows, for hydrogel_2 with 53% mNIPPAm/mMBA, the experimental parameters such as temperature (samples 2.1-2.6), pH value (samples 3.1-3.6 and 4.1-4.6), NaCl concentration (samples 5.1-5.6), phenol concentration (samples 6.1-6.5), ethanol concentration (samples 7.1-7.5), and propanol concentration (samples 8.1-8.5). In addition, the hydrogel was characterized according to the equations given in Tables D.1-D.3, where W_s is the weight of swollen hydrogel (at released equilibrium), W_d is the weight of dried hydrogel, t_s is the thickness of swollen hydrogel, t_d is the thickness of the dried hydrogel, d_s is the diameter of swollen hydrogel, and d_d is the diameter of the dried hydrogel.

Table D.1: Hydrogel_4: mNIPAAm/mMBA=33%

		Before equilibrium	**1st equilibrium**	Dried hydrogel	Swelling ratio	Water uptake,	Before equilibrium	**1st equilibrium**	Dried hydrogel	Diameter Ratio	Before equilibrium	**1st equilibrium**
Sample	T, C	Mass, Wt	**Mass,Ws**	Mass, Wd	q, Ws/Wd	[(Ws-Wd)/Wd]*100	Diameter, dt	**Diameter, ds**	Diameter, dd	ds/dd	Thickness, tt	**Thickness, ts**
2.1	**25**	0.309	**0.352**	0.023	15.107	1410.730	11.948	**11.899**	6.224	1.912	3.524	**3.524**
2.2	**30**	0.387	**0.271**	0.025	11.049	1004.898	12.036	**10.618**	6.499	1.634	3.753	**3.158**
2.3	**32**	0.467	**0.253**	0.029	8.738	773.793	12.082	**9.840**	7.048	1.396	4.485	**3.661**
2.4	**34**	0.330	**0.059**	0.021	2.822	182.212	11.853	**6.545**	5.904	1.109	3.524	**1.694**
2.5	**40**	0.282	**0.033**	0.018	1.776	77.596	12.128	**5.492**	5.172	1.062	3.021	**1.373**
2.6	**50**	0.293	**0.041**	0.019	2.180	117.989	12.357	**5.400**	4.714	1.146	3.112	**0.971**

		Before equilibrium	**1st equilibrium**	Dried hydrogel	Swelling ratio	Water uptake,	Before equilibrium	**1st equilibrium**	Dried hydrogel	Diameter Ratio	Before equilibrium	**1st equilibrium**
Sample	pH	Mass, Wt	**Mass,Ws**	Mass, Wd	q, Ws/Wd	[(Ws-Wd)/Wd]*100	Diameter, dt	**Diameter, ds**	Diameter, dd	ds/dd	Thickness, tt	**Thickness, ts**
3.1	**6.4**	0.432	**0.409**	0.028	14.880	1388.000	11.853	**11.945**	6.361	1.878	4.439	**4.805**
3.2	**6.5**	0.265	**0.248**	0.016	15.128	1412.805	12.265	**11.899**	6.133	1.940	2.746	**2.609**
3.3	**6.92**	0.330	**0.319**	0.021	15.425	1442.512	12.036	**12.036**	5.767	2.087	3.615	**3.388**
3.4	**9.72**	0.369	**0.368**	0.024	15.317	1431.667	11.808	**11.853**	5.400	2.195	3.936	**3.936**
3.5	**10.88**	0.495	**0.417**	0.032	13.069	1206.897	11.899	**11.625**	5.858	1.984	4.943	**4.531**
3.6	**12.1**	0.457	**0.352**	0.030	11.878	1087.838	12.311	**11.350**	6.911	1.642	4.302	**4.210**

		Before equilibrium	**1st equilibrium**	Dried hydrogel	Swelling ratio	Water uptake,	Before equilibrium	**1st equilibrium**	Dried hydrogel	Diameter Ratio	Before equilibrium	**1st equilibrium**
Sample	pH	Mass, Wt	**Mass,Ws**	Mass, Wd	q, Ws/Wd	[(Ws-Wd)/Wd]*100	Diameter, dt	**Diameter, ds**	Diameter, dd	ds/dd	Thickness, tt	**Thickness, ts**
4.1	**0.45**	0.441	**0.255**	0.044	5.743	474.324	12.311	**9.702**	6.178	1.570	4.439	**2.570**
4.2	**1.03**	0.465	**0.357**	0.031	11.544	1054.369	12.265	**11.075**	6.361	1.741	5.080	**4.485**
4.3	**1.94**	0.338	**0.279**	0.021	13.620	1261.951	12.403	**11.396**	7.185	1.586	3.295	**3.066**
4.4	**2.99**	0.376	**0.335**	0.024	13.880	1287.967	12.036	**11.487**	7.002	1.641	3.890	**3.478**
4.5	**4.27**	0.370	**0.339**	0.024	14.287	1328.692	12.586	**11.304**	6.041	1.871	3.799	**3.478**
4.6	**4.12**	0.358	**0.306**	0.021	14.874	1387.379	11.945	**11.762**	5.767	2.040	3.570	**3.249**

		Before equilibrium	**1st equilibrium**	Dried hydrogel	Swelling ratio	Water uptake,	Before equilibrium	**1st equilibrium**	Dried hydrogel	Diameter Ratio	Before equilibrium	**1st equilibrium**
Sample	CNaCl	Mass, Wt	**Mass,Ws**	Mass, Wd	q, Ws/Wd	[(Ws-Wd)/Wd]*100	Diameter, dt	**Diameter, ds**	Diameter, dd	ds/dd	Thickness, tt	**Thickness, ts**
6.1	0.1	0.316	**0.223**	0.020	11.273	1027.273	5.355	**10.846**	5.355	2.026	3.982	**3.341**
6.2	1.00E-02	0.300	**0.338**	0.027	12.363	1136.264	4.943	**11.167**	4.943	2.259	3.890	**3.753**
6.3	1.00E-03	0.409	**0.310**	0.028	10.961	996.113	6.407	**11.213**	6.407	1.750	3.799	**3.387**
6.4	1.00E-04	0.360	**0.385**	0.028	13.949	1294.928	5.400	**11.579**	5.400	2.144	4.027	**3.661**
6.5	1.00E-05	0.407	**0.283**	0.022	13.120	1212.037	5.904	**11.167**	5.904	1.891	3.982	**3.204**
6.6	1.00E-06	0.299	**0.293**	0.022	13.498	1249.770	6.224	**11.625**	6.224	1.868	3.387	**3.432**

Table D.2: Hydrogel_3: mNIPAAm/mMBA=43%

		Before equilibrium	**1st equilibrium**	Dried hydrogel	Swelling ratio	Water uptake,	Before equilibrium	**1st equilibrium**	Dried hydrogel	Diameter Ratio	Before equilibrium	**1st equilibrium**
Sample	T, C	Mass, Wt	**Mass,Ws**	Mass, Wd	q, Ws/Wd	[(Ws-Wd)/Wd]*100	Diameter, dt	**Diameter, ds**	Diameter, dd	ds/dd	Thickness, tt	**Thickness, ts**
2.1	25	0.186	0.269	0.020	13.167	1216.667	10.620	11.610	8.595	1.351	2.025	2.381
2.2	30	0.197	0.214	0.021	10.269	926.923	10.485	10.575	7.200	1.469	2.070	2.115
2.3	32	0.183	0.169	0.019	8.889	788.947	10.620	9.810	7.561	1.298	1.710	1.485
2.4	34	0.185	0.049	0.021	2.361	136.058	10.530	5.850	5.310	1.102	2.070	1.126
2.5	40	0.193	0.073	0.020	3.616	261.576	10.530	6.075	5.670	1.071	1.890	0.765
2.6	50	0.227	0.067	0.026	2.577	157.692	10.440	6.255	5.445	1.149	2.565	1.261

		Before equilibrium	**1st equilibrium**	Dried hydrogel	Swelling ratio	Water uptake,	Before equilibrium	**1st equilibrium**	Dried hydrogel	Diameter Ratio	Before equilibrium	**1st equilibrium**
Sample	pH	Mass, Wt	**Mass,Ws**	Mass, Wd	q, Ws/Wd	[(Ws-Wd)/Wd]*100	Diameter, dt	**Diameter, ds**	Diameter, dd	ds/dd	Thickness, tt	**Thickness, ts**
3.1	6.4	7.040	0.150	0.222	0.013	16.654	1565.414	10.755	11.700	9.585	1.221	1.260
3.2	6.5	8.200	0.219	0.329	0.025	13.096	1209.562	10.125	11.250	7.335	1.534	1.305
3.3	6.92	9.120	0.172	0.239	0.018	13.369	1236.872	10.530	11.565	8.685	1.332	2.070
3.4	9.72	10.190	0.215	0.300	0.023	12.821	1182.051	10.485	11.475	7.335	1.564	1.845
3.5	10.88	11.140	0.178	0.227	0.019	12.265	1126.486	10.755	11.340	-	-	1.530
3.6	12.1	12.010	0.216	0.276	0.025	11.129	1012.903	10.260	11.025	7.290	1.512	1.845

		Before equilibrium	**1st equilibrium**	Dried hydrogel	Swelling ratio	Water uptake,	Before equilibrium	**1st equilibrium**	Dried hydrogel	Diameter Ratio	Before equilibrium	**1st equilibrium**
Sample	pH	Mass, Wt	**Mass,Ws**	Mass, Wd	q, Ws/Wd	[(Ws-Wd)/Wd]*100	Diameter, dt	**Diameter, ds**	Diameter, dd	ds/dd	Thickness, tt	**Thickness, ts**
4.1	0.45	0.450	0.134	0.136	0.026	5.309	430.859	10.530	9.765	6.300	1.550	1.260
4.2	1.03	1.120	0.147	0.181	0.017	10.832	983.234	10.395	11.385	9.855	1.155	1.305
4.3	1.94	2.010	0.173	0.244	0.022	11.296	1029.630	10.260	11.115	7.740	1.436	2.070
4.4	2.99	3.040	0.171	0.239	0.019	12.443	1144.271	10.305	11.160	-	-	1.845
4.5	4.27	4.360	0.161	0.241	0.018	13.464	1246.369	10.351	11.385	6.480	1.757	1.530
4.6	4.12	6.220	0.166	0.247	0.018	13.810	1281.006	10.485	11.475	7.425	1.545	1.845

		Before equilibrium	**1st equilibrium**	Dried hydrogel	Swelling ratio	Water uptake,	Before equilibrium	**1st equilibrium**	Dried hydrogel	Diameter Ratio	Before equilibrium	**1st equilibrium**
Sample	CNaCl	Mass, Wt	**Mass,Ws**	Mass, Wd	q, Ws/Wd	[(Ws-Wd)/Wd]*100	Diameter, dt	**Diameter, ds**	Diameter, dd	ds/dd	Thickness, tt	**Thickness, ts**
5.1	0.1	0.174	0.214	0.022	9.745	874.545	10.755	11.340	9.315	1.217	1.801	1.935
5.2	1.00E-02	0.167	0.235	0.017	13.766	1276.608	10.755	11.520	7.785	1.480	1.800	1.890
5.3	1.00E-03	0.173	0.236	0.018	13.403	1240.341	10.440	11.475	5.895	1.947	1.845	1.980
5.4	1.00E-04	0.194	0.280	0.022	12.785	1178.539	10.395	11.385	6.435	1.769	2.070	2.205
5.5	1.00E-05	0.182	0.283	0.021	13.686	1268.599	10.305	11.475	-	-	1.845	2.385
5.6	1.00E-06	0.207	0.315	0.023	13.623	1262.338	10.260	11.520	6.975	1.652	2.115	2.430

		Before equilibrium	**1st equilibrium**	Dried hydrogel	Swelling ratio	Water uptake,	Before equilibrium	**1st equilibrium**	Dried hydrogel	Diameter Ratio	Before equilibrium	**1st equilibrium**
Sample	Cethanol [M]	Mass, Wt	**Mass,Ws**	Mass, Wd	q, Ws/Wd	[(Ws-Wd)/Wd]*100	Diameter, dt	**Diameter, ds**	Diameter, dd	ds/dd	Thickness, tt	**Thickness, ts**
6.1	2.00E-02	0.210	0.295	0.020	15.138	1413.846	10.170	12.015	-	#WERT!	2.070	2.295
6.2	4.00E-02	0.216	0.313	0.019	16.233	1523.316	10.395	11.565	6.975	1.658	2.385	2.475
6.3	6.00E-02	0.194	0.290	0.020	14.371	1337.129	10.170	11.970	6.885	1.739	1.980	2.520
6.4	8.00E-02	0.194	0.283	0.018	15.793	1479.330	10.215	11.880	-	-	2.205	2.295
6.5	1.00E-01	0.201	0.297	0.017	17.075	1607.471	10.350	11.745	-	-	2.115	2.565
6.6	-				-	-				-		

		Before equilibrium	**1st equilibrium**	Dried hydrogel	Swelling ratio	Water uptake,	Before equilibrium	**1st equilibrium**	Dried hydrogel	Diameter Ratio	Before equilibrium	**1st equilibrium**
Sample	Cpropanol [M]	Mass, Wt	**Mass,Ws**	Mass, Wd	q, Ws/Wd	[(Ws-Wd)/Wd]*100	Diameter, dt	**Diameter, ds**	Diameter, dd	ds/dd	Thickness, tt	**Thickness, ts**
10.1	2.00E-02	0.217	0.300	0.020	15.223	1422.335	10.485	11.475	-	-	2.520	2.700
10.2	4.00E-02	0.249	0.353	0.026	13.847	1284.706	10.305	11.475	9.045	1.269	2.700	2.925
10.3	6.00E-02	0.217	0.349	0.021	16.299	1529.907	10.485	12.195	8.955	1.362	2.430	2.655
10.4	8.00E-02	0.199	0.278	0.015	18.137	1713.725	10.170	10.980	-	-	2.160	2.205
10.5	1.00E-01	0.204	0.278	0.018	15.169	1416.940	10.575	11.790	0.585	20.154	2.295	2.385
10.6	-				-	-				-		

Table D.3: Hydrogel_2: mNIPAAm/mMBA=53%

Sample	T, C	Before equilibrium Mass, Wt	**1st equilibrium Mass,Ws**	Dried hydrogel Mass, Wd	Swelling ratio q, Ws/Wd	Water uptake, [(Ws-Wd)/Wd]*100	Before equilibrium Diameter, dt	**1st equilibrium Diameter, ds**	Dried hydrogel Diameter, dd	Diameter Ratio ds/dd	Before equilibrium Thickness, tt	**1st equilibrium Thickness, ts**
2.1	25	0.243	0.395	0.024	16.750	1575.000	9.990	12.285	8.235	1.492	3.060	2.880
2.2	30	0.186	0.226	0.018	12.539	1153.889	9.945	10.845	7.831	1.385	2.250	1.845
2.3	32	0.230	0.234	0.023	10.000	900.000	9.855	10.080	8.055	1.251	2.880	2.745
2.4	34	0.263	0.061	0.027	2.257	125.746	9.720	5.265	5.085	1.035	3.195	1.800
2.5	40	0.222	0.041	0.023	1.774	77.391	10.035	4.815	5.490	0.877	2.520	1.350
2.6	50	0.242	0.031	0.024	1.282	28.151	9.945	4.635	5.040	0.920	2.610	1.215

Sample	pH	Before equilibrium Mass, Wt	**1st equilibrium Mass,Ws**	Dried hydrogel Mass, Wd	Swelling ratio q, Ws/Wd	Water uptake, [(Ws-Wd)/Wd]*100	Before equilibrium Diameter, dt	**1st equilibrium Diameter, ds**	Dried hydrogel Diameter, dd	Diameter Ratio ds/dd	Before equilibrium Thickness, tt	**1st equilibrium Thickness, ts**
3.1	6.4	7.040	0.242	0.397	0.024	16.730	1572.996	9.990	12.375	6.480	1.910	2,8350
3.2	6.5	8.200	0.220	0.367	0.022	17.047	1604.651	10.080	12.845	6.480	1.982	2,6100
3.3	6.92	9.190	0.200	0.334	0.019	17.882	1688.235	10.035	12.420	6.255	1.986	2,1150
3.4	9.72	10.110	0.206	0.306	0.019	16.266	1526.596	9.990	12.150	6.750	1.800	2,1600
3.5	10.88	11.130	0.194	0.324	0.021	15.159	1415.888	10.305	11.655	6.661	1.750	2,1600
3.6	12.1	12.200	0.225	0.324	0.020	16.541	1554.082	10.260	12.285	5.850	2.100	2,3850

Sample	pH	Before equilibrium Mass, Wt	**1st equilibrium Mass,Ws**	Dried hydrogel Mass, Wd	Swelling ratio q, Ws/Wd	Water uptake, [(Ws-Wd)/Wd]*100	Before equilibrium Diameter, dt	**1st equilibrium Diameter, ds**	Dried hydrogel Diameter, dd	Diameter Ratio ds/dd	Before equilibrium Thickness, tt	**1st equilibrium Thickness, ts**
4.1	0.45	0.233	0.224	0.042	5.351	435.084	10.395	9.945	7.335	1.356	2.700	2.160
4.2	1.12	0.203	0.280	0.022	12.741	1174.091	10.260	11.835	8.280	1.429	2.160	2.430
4.3	2.04	0.217	0.347	0.021	16.310	1530.986	10.350	12.105	8.685	1.394	2.655	2.790
4.4	3.05	0.220	0.338	0.020	17.230	1622.959	10.620	12.555	8.590	1.462	2.385	2.835
4.5	4.27	0.202	0.329	0.019	17.418	1641.799	10.485	12.420	9.495	1.308	2.250	2.385
4.6	6.12	0.180	0.313	0.018	17.790	1678.977	10.395	12.690	6.840	1.855	2.385	2.615

Sample	CNaCl	Before equilibrium Mass, Wt	**1st equilibrium Mass,Ws**	Dried hydrogel Mass, Wd	Swelling ratio q, Ws/Wd	Water uptake, [(Ws-Wd)/Wd]*100	Before equilibrium Diameter, dt	**1st equilibrium Diameter, ds**	Dried hydrogel Diameter, dd	Diameter Ratio ds/dd	Before equilibrium Thickness, tt	**1st equilibrium Thickness, ts**
5.1	1.00E-01	0.209	0.314	0.021	14.737	1373.709	10.710	12.105	9.315	1.300	2.475	2.520
5.2	1.00E-02	0.150	0.239	0.015	16.272	1527.211	10.980	12.555	6.660	1.885	1.800	1.935
5.3	1.00E-03	0.196	0.313	0.019	16.897	1589.730	10.350	12.285	7.020	1.750	2.340	2.475
5.4	1.00E-04	0.185	0.320	0.018	18.263	1726.286	10.665	12.600	9.900	1.273	2.115	2.475
5.5	1.00E-05	0.162	0.262	0.016	16.871	1587.097	10.710	13.455	9.675	1.391	1.800	2.070
5.6	1.00E-06	0.205	0.347	0.020	17.535	1653.535	10.350	12.375	8.685	1.425	2.340	2.700

Sample	CPhenol [M]	Before equilibrium Mass, Wt	**1st equilibrium Mass,Ws**	Dried hydrogel Mass, Wd	Swelling ratio q, Ws/Wd	Water uptake, [(Ws-Wd)/Wd]*100	Before equilibrium Diameter, dt	**1st equilibrium Diameter, ds**	Dried hydrogel Diameter, dd	Diameter Ratio ds/dd	Before equilibrium Thickness, tt	**1st equilibrium Thickness, ts**
6.1	0.001	0.211	0.361	0.021	17.085	1608.531	10.170	12.060	5.940	2.030	2.520	3.015
6.2	0.002	0.186	0.305	0.019	15.984	1498.429	10.305	12.060	8.055	1.497	2.385	2.430
6.3	0.003	0.163	0.240	0.015	16.000	1500.000	10.485	11.880	7.155	1.660	2.160	2.115
6.4	0.004	0.206	0.047	0.021	2.225	122.488	10.530	5.670	5.625	1.008	2.385	1.575
6.5	0.005	0.224	0.030	0.025	1.233	23.293	9.990	10.575	6.795	1.556	2.745	2.790
6.6	-	0.229	-	-	-	-	10.215		-	-	2.790	-

Sample	Cethanol [M]	Before equilibrium Mass, Wt	**1st equilibrium Mass,Ws**	Dried hydrogel Mass, Wd	Swelling ratio q, Ws/Wd	Water uptake, [(Ws-Wd)/Wd]*100	Before equilibrium Diameter, dt	**1st equilibrium Diameter, ds**	Dried hydrogel Diameter, dd	Diameter Ratio ds/dd	Before equilibrium Thickness, tt	**1st equilibrium Thickness, ts**
7.1	0.02	0.197	0.354	0.019	18.427	1742.708	10.530	12.690	6.660	1.905	2.340	2.565
7.2	0.04	0.190	0.324	0.018	17.873	1687.293	9.765	12.331	6.615	1.864	2.235	2.745
7.3	0.06	0.222	0.363	0.022	16.553	1555.251	10.260	12.240	6.525	1.876	2.700	3.060
7.4	0.08	0.205	0.331	0.020	16.530	1553.000	9.945	12.330	6.345	1.943	2.340	2.745
7.5	0.1	0.213	0.344	0.021	16.519	1551.923	9.990	12.465	6.460	1.930	2.475	2.265
7.6	-	0.213	-	-	-	-	9.945	-	-	-	2.430	-

Sample	Cpropanol [M]	Before equilibrium Mass, Wt	**1st equilibrium Mass,Ws**	Dried hydrogel Mass, Wd	Swelling ratio q, Ws/Wd	Water uptake, [(Ws-Wd)/Wd]*100	Before equilibrium Diameter, dt	**1st equilibrium Diameter, ds**	Dried hydrogel Diameter, dd	Diameter Ratio ds/dd	Before equilibrium Thickness, tt	**1st equilibrium Thickness, ts**
8.1	0.02	0.204	0.353	0.020	17.294	1629.412	10.485	12.780	6.345	2.014	2.475	2.700
8.2	0.04	0.228	0.413	0.023	17.780	1678.017	9.945	12.380	5.670	2.183	2.610	3.105
8.3	0.06	0.196	0.327	0.019	17.492	1649.198	10.080	12.555	7.830	1.603	2.475	2.655
8.4	0.08	0.197	0.325	0.019	17.557	1655.676	10.215	12.150	5.580	2.177	2.205	2.610
8.5	0.1	0.196	0.291	0.020	14.598	1359.799	10.215	11.970	6.930	1.727	2.160	2.565
8.6	-	0.212			-	-	10.305		-	-	2.745	

APPENDIX E:
Drug Release Data

The BSA solutions 10^{-3} M, $5.0 \cdot 10^{-3}$ M, $7.5 \cdot 10^{-2}$ M, 10^{-2} M, $5.0 \cdot 10^{-2}$ M, $7.5 \cdot 10^{-2}$ M and 10^{-1} M were prepared from a BSA mother solution has the concentration 0.9998 mg BSA/100 ml H_2O (1.51M). A calibration curve was drawn by measuring the absorbance versus the concentration of BSA solution. This calibration curve was used in order to determine the BSA released into the bulk solution from hydrogels by measuring the absorbance using UV-Visible recording spectrophotometer at wavelength, λ of 278 nm. The dried poly(NIPAAm) hydrogels were immersed in 15 ml of the different BSA solutions at 25ºC and maintained in a thermal bath for 48 h. Thus, BSA was loaded into each hydrogel up to equilibrium by swelling in the BSA-containing solution. After reaching the equilibrium, the hydrogels were weighed and its dimensions measured. Thereafter, the samples were dried at room temperature for 1-2 days to ensure its complete dryness and the samples were weighed and the dimensions were measured again (Tables E.1.1- E.4.1).

The in vitro release experiments were carried out at 25ºC, 32ºC, 37ºC and 40ºC to investigate the effect of temperature-sensitive property of the poly(NIPAAm) hydrogel on solute release profiles. The release experiments were done by immersing the BSA-loaded hydrogel samples in glass beakers with 10 ml deionized water at 25ºC, 32ºC, and 37ºC. The thermostated glasses beakers were covered with PARAFILM® paper to eliminate solution exposing to the ambient air and avoid the evaporation of the solution. At certain time intervals, a 3 ml aliquot of the solution was taken out and the amount of BSA release at that time was determined using the UV-spectroscopy measurement at 278 nm. At the same time, the hydrogels were removed from the beaker in order to determine later its dimensions. This process was repeated for 48h until reach a constant release concentration of BSA and dimensions of hydrogels, i.e., equilibrium. The samples used were returned to the original medium solution in order to maintain a constant volume of surrounding release medium and to keep, as possible, the overall loaded BSA concentration constant. The same procedure was carried out in case of phenol release experiments. The results were presented in terms of release concentration, diameter and thickness hydrogel as a function of time for both BSA and phenol as given in Tables E.1.2-E4.2 and Tables E5-E8.

Table E.1.1: BSA and phenol mass and dimensional data at 25°C

	BSA	Phenol
Sample	10.3	10.5
Absorbance	0,454	0,930
V_1, ml	15	15
equilibrium Solution		
M_1, g	145,790	147,629
Mass of the solution		
V_2, ml	14,75	14,9
After removing the hydrogel		
M_2, g	143,237	145,951
Mass of the solution after equi.		
m_d, g	0,3526*	0,3528*
mass before equilibrium		
(dried hydrogel)		
D_d, mm	131,850	129,150
Diameter before equilibrium		
t_d, mm	23,850	27,450
Thickness before equilibrium		
m, g	0,3137	0,3108
Mass of hydrogel at equi.		
D, mm	126,450	125,550
Diameter at equilibrium		
T, mm	23,850	25,650
Thickness at equilibrium		
m_r,	0,0162	0,0148
Mass after release		
(dried hydrogel)		
D_r, Diameter after release	69,301	63,900
t_r, Thickness after release	0,3600	0,4950

Equilibrium temperature**: 25 °C**

Release temperature: 25**°C**

Concentration of BAS**: 10^{-1}**

Concentration of Phenol: **10^{-4}**

Volume of the release deionized water**: 10 mL**

*The samples were not dried.

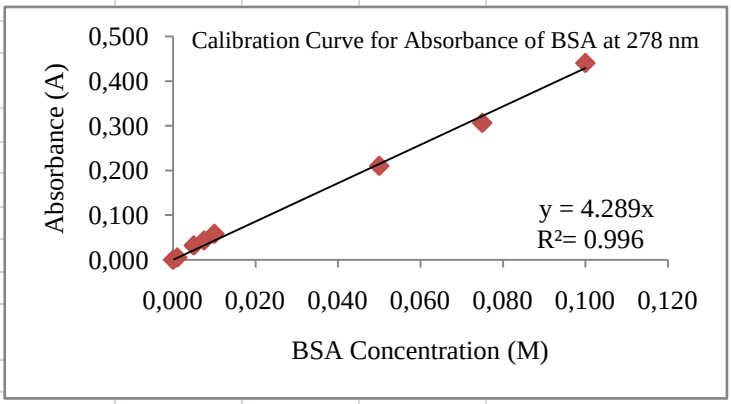

Fig. E.1: Calibration curve of BSA

Table E.1.2: BSA and phenol release data at 25°C

Time (min.)	BSA, UV	BSA, d (mm)	BSA, t (mm)	Phenol, UV	Phenol, d (mm)	Phenol, t (mm)
0	**0**	126,450	23,850	**0**	125,550	25,650
10	**0,001**	128,700	22,500	**0,021**	126,450	25,200
20	**0,003**	126,000	21,600	**0,027**	124,200	23,850
30	**0,003**	12,555o	21,600	**0,030**	123,300	23,150
40	**0,004**	124,650	21,600	**0,032**	125,550	22,950
50	**0,004**	124,650	21,600	**0,033**	124,650	22,950
60	**0,006**	124,550	21,600	**0,038**	124,650	22,050
70	**0,006**	123,750	20,700	**0,037**	123,750	21,150
80	**0,006**	123,300	22,050	**0,037**	123,300	20,700
90	**0,005**	126,900	21,150	**0,038**	123,300	20,700
100	**0,005**	127,350	21,150	**0,038**	126,000	20,250
110	**0,005**	126,900	20,250	**0,038**	126,900	20,250
130	**0,005**	126,000	20,250	**0,038**	123,300	22,050

Table E.2.1: BSA and phenol mass and dimensional data at 32°C

	BSA	Phenol
Sample	10.1	10.4
Abs.	0,433	0,923
V_1, ml equilibrium Solution	15	15
M_1, g Mass of the solution	147,388	147,515
V_2, ml After removing the hydrogel	14,95	14,8
M_2, g Mass of the solution after equi.	147,137	145,857
m_d, g mass before equilibrium (dried hydrogel)	0,3667*	0,3880*
D_d, mm Diameter before equilibrium	129,600	125,900
t_d, mm Thickness before	26,550	26,550
m, g Mass of hydrogel at equi.	0,3566	0,3549
D, mm Diameter at equilibrium	126,000	125,550
T, mm Thickness at equilibrium	25,200	25,550
m_r, Mass after release (dried hydrogel)	0,0194	0,0160
D_r, Diameter after release	81,450	79,661
t_r, Thickness after release	0,3600	0,4500

Equilibrium temperature**: 25 °C**
Release temperature: **32 °C**
Concentration of BAS**: 10^{-1}**
Concentration of Phenol: **10^{-4}**
Volume of the release deionized water**: 10 mL**

*****The samples were not dried.

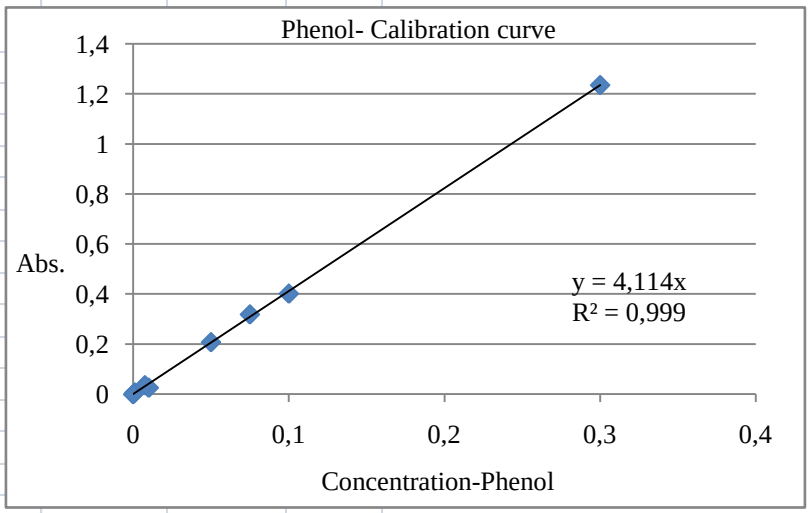

Fig. E.2: Calibration curve of phenol

Table E.2.2: BSA and phenol release data at 32°C

Time (min.)	BSA, UV	BSA, d (mm)	BSA, t (mm)	Phenol, UV	Phenol, d (mm)	Phenol, t (mm)
0	**0**	126,000	25,200	**0**	125,550	26,550
5	**0,005**	126,000	25,850	**0,016**	125,550	27,450
10	**0,005**	125,300	25,750	**0,024**	125,100	26,100
15	**0,005**	123,300	24,750	**0,030**	125,650	26,100
20	**0,005**	120,153	23,950	**0,032**	115,400	24,300
25	**0,006**	117,450	23,450	**0,035**	115,200	23,850
30	**0,006**	116,950	23,185	**0,036**	115,200	23,850
40	**0,008**	116,500	22,950	**0,045**	115,200	22,500
50	**0,009**	116,100	22,500	**0,048**	114,800	20,250
60	**0,006**	119,250	22,504	**0,038**	118,550	25,650
70	**0,007**	115,650	22,250	**0,038**	117,950	21,600
80	**0,007**	114,300	21,550	**0,039**	114,300	21,600
90	**0,007**	114,300	21,600	**0,039**	112,350	20,700
24 std	**0,018**	109,511	22,090	**0,039**	102,930	18,330

Table E.3.1: BSA and phenol mass and dimensional data at 37°C

	BSA	Phenol	
Abs.	0,432	0,922	
V_1, ml equilibrium Solution	15	15	Equilibrium temperature**: 25 °C** Release temperature: **37 °C**
M_1, g Mass of the solution	147,120	147,505	Concentration of BAS**: 10^{-1}** Concentration of Phenol: **10^{-4}**
V_2, ml After removing the hydrogel	14,5	14,5	Volume of the release deionized water**: 10 mL**
M_2, g Mass of the solution after equi.	141,596	144,023	
m_d, g mass before equilibrium (dried hydrogel)	0,3350*	0,3129*	
D_d, mm Diameter before equilibrium	126,450	127,800	
t_d, mm Thickness before equilibrium	21,600	22,050	
m, g Mass of hydrogel at equi.	0,2828	0,2749	
D, mm Diameter at equilibrium	119,250	123,300	
T, mm Thickness at equilibrium	19,800	21,150	
m_r, Mass after release (dried hydrogel)	0,0167	0,0146	
D_r, Diameter after release	53,100	46,800	
t_r, Thickness after release	0,6300	0,6300	

***The samples were not dried.

Table E.3.2: BSA and phenol release data at 37°C

Time (min.)	BSA, UV	BSA, d (mm)	BSA, t (mm)	Phenol, UV	Phenol, d (mm)	Phenol, t (mm)
0	**0**	119,250	19,800	**0**	123,300	21,150
5	**0,001**	121,500	21,150	**0,019**	120,650	19,800
10	**0,003**	117,000	18,900	**0,020**	117,450	18,450
15	**0,004**	117,500	18,000	**0,022**	107,100	15,300
20	**0,005**	116,650	17,100	**0,025**	106,400	15,300
25	**0,006**	102,600	15,300	**0,026**	97,200	16,650
30	**0,006**	96,751	17,550	**0,028**	87,750	18,000
40	**0,007**	86,850	25,650	**0,028**	87,301	27,000
50	**0,011**	75,600	26,550	**0,029**	76,050	27,900
60	**0,015**	68,850	28,814	**0,030**	69,300	28,800
70	**0,016**	63,900	24,300	**0,029**	65,250	24,750
80	**0,015**	59,600	21,600	**0,029**	56,700	22,550
90	**0,015**	58,050	20,700	**0,029**	54,000	22,050
100	**0,016**	54,900	16,650	**0,029**	54,000	16,650
110	**0,015**	54,900	14,850	**0,029**	53,550	14,400
120	**0,015**	54,500	12,150	**0,029**	53,350	12,150
130	**0,015**	52,650	0,9000	**0,029**	53,100	0,9450

Table E.4.1: BSA and phenol mass and dimensional data at 40°C

	BSA	Phenol	
Abs.	0,427	0,926	Equilibrium temperature**: 25 °C**
V_1, ml	15	15	Release temperature: **40 °C**
equilibrium Solution			Concentration of BAS**: 10^{-1}**
M_1, g	145,494	146,276	Concentration of Phenol: **10^{-4}**
Mass of the solution			Volume of the release deionized water**: 10 mL**
V_2, ml	14,5	14,75	
After removing the hydrogel			
M_2, g	144,093	144,976	
Mass of the solution after equi.			
m_d, g	0,2790*	0,2977*	
mass before equilibrium			
(dried hydrogel)			
D_d, mm	137,240	136,770	
Diameter before equilibrium			
t_d, mm	16,450	18,800	
Thickness before equilibrium			
m, g	0,2138	0,2381	
Mass of hydrogel at equi.			
D, mm	127,840	125,490	
Diameter at equilibrium			
T, mm	14,160	16,926	
Thickness at equilibrium			
m_r,	0,0128	0,0134	
Mass after release			
(dried hydrogel)			
D_r, Diameter after release	49,350	49,822	
t_r, Thickness after release	0,4256	0,3789	

***The samples were not dried.

Table E.4.2: BSA and phenol release data at 40°C

Time (min.)	BSA, UV	BSA, d (mm)	BSA, t (mm)	Phenol, UV	Phenol, d (mm)	Phenol, t (mm)
0	**0**	12,784	1,416	**0**	12,549	16,926
5	**0,004**	9,635	2,115	**0,011**	10,434	1,551
10	**0,005**	8,272	2,632	**0,019**	8,742	2,566
15	**0,006**	7,097	2,867	**0,022**	7,426	2,115
20	**0,007**	6,486	2,35	**0,023**	62,981	1,363
25	**0,007**	6,264	1,739	**0,024**	5,828	0,94
30	**0,008**	5,546	12,698	**0,026**	5,734	0,893
40	**0,008**	5,734	0,752	**0,024**	5,734	0,5659
50	**0,009**	5,781	0,658	**0,024**	5,734	0,564
60	**0,009**	5,687	0,64	**0,024**	5,734	0,564
70	**0,009**	5,546	0,705	**0,024**	56,401	0,564
80	**0,009**	5,405	0,7065	**0,024**	5,405	0,6128
90	**0,009**	5,409	0,564	**0,024**	5,734	0,6128

Table E.5: BSA and Phenol release data including the dimensional changes at 25°C

Time (min.)	BSA, UV	Concentration	BSA, d (mm)	Δd	Δr	BSA, t (mm)	Δt	Phenol, UV	Concentration	Phenol, d (mm)	Δd	Δr	Phenol, t (mm)	Δt
0	0	0.00E+00	12.65	0	0	2.385	0	0	0.00E+00	12.555	0	0	2.565	0
10	0.001	2.43E-04	12.87	-0.225	-0.1125	2.25	0.135	0.021	2.02E-06	12.645	-0.09	-0.045	2.52	0.045
20	0.003	7.29E-04	12.60	0.045	0.0225	2.16	0.225	0.027	2.59E-06	12.42	0.135	0.0675	2.385	0.18
30	0.003	7.29E-04	12.56	0.09	0.045	2.16	0.225	0.03	2.88E-06	12.33	0.225	0.1125	2.315	0.25
40	0.004	9.72E-04	12.47	0.18	0.09	2.16	0.225	0.032	3.08E-06	12.555	0	0	2.295	0.27
50	0.004	9.72E-04	12.47	0.18	0.09	2.16	0.225	0.033	3.17E-06	12.465	0.09	0.045	2.295	0.27
60	0.006	1.46E-03	12.46	0.19	0.095	2.16	0.225	0.038	3.65E-06	12.465	0.09	0.045	2.205	0.36
70	0.006	1.46E-03	12.38	0.27	0.135	2.07	0.315	0.037	3.56E-06	12.375	0.18	0.09	2.115	0.45
80	0.006	1.46E-03	12.33	0.315	0.1575	2.205	0.18	0.037	3.56E-06	12.33	0.225	0.1125	2.07	0.495
90	0.005	1.22E-03	12.69	-0.045	-0.0225	2.115	0.27	0.038	3.65E-06	12.33	0.225	0.1125	2.07	0.495
100	0.005	1.22E-03	12.74	-0.09	-0.045	2.115	0.27	0.038	3.65E-06	12.6	-0.045	-0.0225	2.025	0.54
110	0.005	1.22E-03	12.69	-0.045	-0.0225	2.025	0.36	0.038	3.65E-06	12.69	-0.135	-0.0675	2.025	0.54
130	0.005	1.22E-03	12.60	0.045	0.0225	2.025	0.36	0.038	3.65E-06	12.33	0.225	0.1125	2.205	0.36
24 std	0.013	3.16E-03	12.65	0	0	2.025	0.36	0.053	5.09E-06	12.1957	0.3593	0.17965	2.205	0.36

Table E.6: BSA and Phenol release data including the dimensional changes at 32°C

Time (min.)	BSA, UV	c	BSA, d (mm)	Δd	Δr	BSA, t (mm)	Δt	Phenol,UV	c	Phenol, d (mm)	Δd	Δr	Phenol, t (mm)	Δt
0	**0**	0.000E+00	12.60	0.000	0.000	2.520	0.000	**0.000**	0	12.56	0.000	0.000	2.655	0.000
5	**0.005**	1.215E-03	12.60	0.000	0.000	2.585	-0.065	**0.016**	1.538E-06	12.56	0.000	0.000	2.745	-0.090
10	**0.005**	1.215E-03	12.53	0.070	0.035	2.575	-0.055	**0.024**	2.307E-06	12.51	0.045	0.023	2.610	0.045
15	**0.005**	1.215E-03	12.33	0.270	0.135	2.475	0.045	**0.030**	2.883E-06	12.57	-0.010	-0.005	2.610	0.045
20	**0.005**	1.215E-03	12.02	0.585	0.292	2.395	0.125	**0.032**	3.075E-06	11.54	1.015	0.508	2.430	0.225
25	**0.006**	1.458E-03	11.75	0.855	0.428	2.345	0.175	**0.035**	3.364E-06	11.52	1.035	0.518	2.385	0.270
30	**0.006**	1.458E-03	11.70	0.905	0.453	2.319	0.202	**0.036**	3.460E-06	11.52	1.035	0.518	2.385	0.270
40	**0.008**	1.944E-03	11.65	0.950	0.475	2.295	0.225	**0.045**	4.325E-06	11.52	1.035	0.518	2.250	0.405
50	**0.009**	2.187E-03	11.61	0.990	0.495	2.250	0.270	**0.048**	4.613E-06	11.48	1.075	0.538	2.025	0.630
60	**0.006**	1.458E-03	11.93	0.675	0.337	2.250	0.270	**0.038**	3.652E-06	11.86	0.700	0.350	2.565	0.090
70	**0.007**	1.701E-03	11.57	1.035	0.518	2.225	0.295	**0.038**	3.652E-06	11.80	0.760	0.380	2.160	0.495
80	**0.007**	1.701E-03	11.43	1.170	0.585	2.155	0.365	**0.039**	3.748E-06	11.43	1.125	0.563	2.160	0.495
90	**0.007**	1.701E-03	11.43	1.170	0.585	2.160	0.360	**0.039**	3.748E-06	11.24	1.320	0.660	2.070	0.585
100	**0.007**	1.701E-03	11.43	1.170	0.585	2.160	0.360	**0.039**	3.748E-06	11.07	1.485	0.743	2.025	0.630
110	**0.007**	1.701E-03	11.43	1.170	0.585	1.985	0.535	**0.039**	3.748E-06	11.03	1.530	0.765	1.980	0.675
120	**0.007**	1.701E-03	11.39	1.215	0.608	2.115	0.405	**0.039**	3.748E-06	11.94	0.620	0.310	2.205	0.450
140	**0.007**	1.701E-03	11.17	1.435	0.718	2.070	0.450	**0.039**	3.748E-06	10.87	1.690	0.845	1.982	0.673
150	**0.007**	1.701E-03	10.98	1.620	0.810	2.070	0.450	**0.039**	3.748E-06	10.71	1.845	0.922	1.800	0.855
24 std	**0.018**	4.374E-03	10.95	1.649	0.824	2.209	0.311	**0.039**	3.748E-06	10.29	2.262	1.131	1.833	0.822

Table E.7: BSA and Phenol release data including the dimensional changes at 37°C

Time (min.)	BSA, UV	C	BSA, d (mm)	Δd	Δr	BSA, t (mm)	Δt	Phenol, UV	C	Phenol, d (mm)	Δd	Δr	Phenol, t (mm)	Δt
0	**0**	0.00E+00	11.93	0.000	0.000	1.980	0.000	**0.000**	0.00E+00	12.330	0.000	0.000	2.115	0.000
5	**0.001**	2.43E-04	12.15	-0.225	-0.113	2.115	-0.135	**0.019**	1.83E-06	12.065	0.265	0.133	1.980	0.135
10	**0.003**	7.29E-04	11.70	0.225	0.113	1.890	0.090	**0.020**	1.92E-06	11.745	0.585	0.293	1.845	0.270
15	**0.004**	9.72E-04	11.75	0.175	0.088	1.800	0.180	**0.022**	2.11E-06	10.710	1.620	0.810	1.530	0.585
20	**0.005**	1.22E-03	11.67	0.260	0.130	1.710	0.270	**0.025**	2.40E-06	10.640	1.690	0.845	1.530	0.585
25	**0.006**	1.46E-03	10.26	1.665	0.833	1.530	0.450	**0.026**	2.50E-06	9.720	2.610	1.305	1.665	0.450
30	**0.006**	1.46E-03	9.68	2.250	1.125	1.755	0.225	**0.028**	2.69E-06	8.775	3.555	1.778	1.800	0.315
40	**0.007**	1.70E-03	8.69	3.240	1.620	2.565	-0.585	**0.028**	2.69E-06	8.730	3.600	1.800	2.700	-0.585
50	**0.011**	2.67E-03	7.56	4.365	2.183	2.655	-0.675	**0.029**	2.79E-06	7.605	4.725	2.363	2.790	-0.675
60	**0.015**	3.65E-03	6.89	5.040	2.520	2.881	-0.901	**0.030**	2.88E-06	6.930	5.400	2.700	2.880	-0.765
70	**0.016**	3.89E-03	6.39	5.535	2.768	2.430	-0.450	**0.029**	2.79E-06	6.525	5.805	2.903	2.475	-0.360
80	**0.015**	3.65E-03	5.96	5.965	2.983	2.160	-0.180	**0.029**	2.79E-06	5.670	6.660	3.330	2.255	-0.140
90	**0.015**	3.65E-03	5.81	6.120	3.060	2.070	-0.090	**0.029**	2.79E-06	5.400	6.930	3.465	2.205	-0.090
100	**0.016**	3.89E-03	5.49	6.435	3.218	1.665	0.315	**0.029**	2.79E-06	5.400	6.930	3.465	1.665	0.450
110	**0.015**	3.65E-03	5.49	6.435	3.218	1.485	0.495	**0.029**	2.79E-06	5.355	6.975	3.488	1.440	0.675
120	**0.015**	3.65E-03	5.45	6.475	3.238	1.215	0.765	**0.029**	2.79E-06	5.335	6.995	3.498	1.215	0.900
130	**0.015**	3.65E-03	5.27	6.660	3.330	0.900	1.080	**0.029**	2.79E-06	5.310	7.020	3.510	0.945	1.170
24 std	**0.041**	9.96E-03	5.67	6.255	3.128	0.810	1.170	**0.058**	5.57E-06	5.625	6.705	3.353	0.765	1.350

Table E.8: BSA and Phenol release data including the dimensional changes at 40°C

Time (min.)	BSA, UV	C	BSA, d (mm)	Δr	Δd	BSA, t (mm)	Δt	Phenol, UV	C	Phenol, d (mm)	Δr	Δd	Phenol, t (mm)	Δt
0	**0**	0.00E+00	12.784	0.000	**0.000**	1.416	**0.000**	**0.000**	0.000E+00	12.549	0.000	**0.000**	1.693	**0.000**
5	**0.004**	9.72E-04	9.635	1.575	**3.149**	2.115	**-0.699**	**0.011**	1.057E-06	10.434	1.058	**2.115**	1.551	**0.142**
10	**0.005**	1.22E-03	8.272	2.256	**4.512**	2.632	**-1.216**	**0.019**	1.826E-06	8.742	1.904	**3.807**	2.566	**-0.873**
15	**0.006**	1.46E-03	7.097	2.844	**5.687**	2.867	**-1.451**	**0.022**	2.114E-06	7.426	2.562	**5.123**	2.115	**-0.422**
20	**0.007**	1.70E-03	6.486	3.149	**6.298**	2.350	**-0.934**	**0.023**	2.210E-06	6.298	3.125	**6.251**	1.363	**0.330**
25	**0.007**	1.70E-03	6.264	3.260	**6.520**	1.739	**-0.323**	**0.024**	2.307E-06	5.828	3.361	**6.721**	0.940	**0.753**
30	**0.008**	1.94E-03	5.546	3.619	**7.238**	1.270	**0.146**	**0.026**	2.499E-06	5.734	3.408	**6.815**	0.893	**0.800**
40	**0.008**	1.94E-03	5.734	3.525	**7.050**	0.752	**0.664**	**0.024**	2.307E-06	5.734	3.408	**6.815**	0.566	**1.127**
50	**0.009**	2.19E-03	5.781	3.502	**7.003**	0.658	**0.758**	**0.024**	2.307E-06	5.734	3.408	**6.815**	0.564	**1.129**
60	**0.009**	2.19E-03	5.687	3.549	**7.097**	0.640	**0.776**	**0.024**	2.307E-06	5.734	3.408	**6.815**	0.564	**1.129**
70	**0.009**	2.19E-03	5.546	3.619	**7.238**	0.705	**0.711**	**0.024**	2.307E-06	5.640	3.454	**6.909**	0.564	**1.129**
80	**0.009**	2.19E-03	5.405	3.690	**7.379**	0.707	**0.710**	**0.024**	2.307E-06	5.405	3.572	**7.144**	0.613	**1.080**
90	**0.009**	2.19E-03	5.409	3.688	**7.375**	0.564	**0.852**	**0.024**	2.307E-06	5.734	3.408	**6.815**	0.613	**1.080**
3600	**0.028**	6.80E-03	5.593	3.596	**7.191**	0.658	**0.758**	**0.038**	3.652E-06	5.358	3.596	**7.191**	0.517	**1.176**
7200	**0.048**	1.17E-02	5.405	3.690	**7.379**	0.564	**0.852**	**0.051**	4.901E-06	5.452	3.549	**7.097**	0.658	**1.035**

APPENDIX F:
Mechanical Properties Data

In order to characterize the mechanical properties of the hydrogel, the cylindrical hydrogel_4 samples we allowed to equilibrate at different solutions with varied concentration range. At different temperatures, the hydrogels were allowed to swell in different concentrations of NaOH, H_2SO_4, NaCl, phenol, ethanol, propanol, and BSA. The different concentrations were given with the corresponding temperatures in Tables F.1-F.21. During the first part of the experiment, the axial load was applied till reaching 1.0N. Thereafter, the stress, strain, Poisson's ratio, shear modulus, bulk modules, and the Young's modules were calculated from the mass change and the deformation of hydrogel cylinder under compression. According to Tables F.1-F.21, Δl is the thickness variation and l_0 is the initial thickness, d_0 is the initial diameter, A_0 is initial area and F is the applied force. The subscribes *bc* and *ac* are referring to the terms before compression and after compression respectively. The right side column for each sample refers to the initial diameter and initial thickness of the sample. Meanwhile, the left side column refers to the diameter and thickness after compression. Regarding to the modules, the right side column refers to the calculate modules in Pascal and the left side column refers to the modules in calculated in Mega-Pascal. During the second part of the experiments, the hydrogel samples were subjected to the applied load, which was increased gradually with a step of 0.2N and for some samples of 0.3N. Depending on the concentration and the temperature of the samples, some samples were able to bear a maximum force without breaking down. Tables F.16-F.21 shows the effect of the applied load increase on the mass and area of the hydrogel cylinder equilibrated in different solutions of BSA and at different temperatures. In addition, they include the corresponding calculated modules are also included.

Table F.1.1: The mechanical properties of cylindrical samples of hydrogel_4 equilibrated at different ph-values.

Parameter, pH-Value	**Sample 4.1**		**Sample 4.2**		**Sample 4.3**		**Sample 4.4**		**Sample 4.5**	
pH	**0.45**		**1.12**		**2.04**		**3.05**		**4.27**	
Diameter, d0, m	**1.183E-02**	**1.465E-02**	**1.288E-02**	**1.579E-02**	**1.338E-02**	**1.734E-02**	**1.333E-02**	**1.738E-02**	**1.383E-02**	**1.743E-02**
Thickness, *l* =t0, m	**3.395E-03**	**2.066E-03**	**2.066E-03**	**1.771E-03**	**2.460E-03**	**1.624E-03**	**2.952E-03**	**1.870E-03**	**2.263E-03**	**1.624E-03**
Mass, m_{bc}	**0.348**	-	**0.296**	-	**0.45**	-	**0.503**	-	**0.34**	-
Mass, m_{ac}	**100.219**	**100.219**	-	**100.044**	-	**100.98**	-	**100.219**	-	**100.105**
Force, N	**1**	**1**	**1**	**1**	**1**	**1**	**1**	**1**	**1**	**1**
Area, m2	1.099E-04		1.302E-04		1.405E-04		1.396E-04		1.503E-04	
del(*l*), m	1.328E-03		2.952E-04		8.364E-04		1.082E-03		6.396E-04	
Meas.Young's Modulus, Pa/Mpa	**2.325E+04**	**2.325E-02**	**5.375E+04**	**5.375E-02**	**2.093E+04**	**2.093E-02**	**1.954E+04**	**1.954E-02**	**2.355E+04**	**2.355E-02**
Calc. Stress, Pa/Mpa	9.098E+03	9.098E-03	7.679E+03	7.679E-03	7.115E+03	7.115E-03	7.164E+03	7.164E-03	6.655E+03	6.655E-03
Calc. Strain	3.913E-01		1.429E-01		3.400E-01		3.667E-01		2.826E-01	
Poisson's ratio, *v*	8.249E-01		1.920E+00		1.199E+00		1.159E+00		1.209E+00	
Bulk Modulus, Pa/Mpa	**-1.193E+04**	-1.193E-02	**-6.309E+03**	-6.309E-03	**-4.991E+03**	-4.991E-03	**-4.941E+03**	-4.941E-03	**-5.535E+03**	-5.535E-03
Shear Modulus, Pa/Mpa	6.370E+03	6.370E-03	9.205E+03	9.205E-03	4.759E+03	4.759E-03	4.525E+03	4.525E-03	5.330E+03	5.330E-03

Table F.1.2: The mechanical properties of cylindrical samples of hydrogel_4 equilibrated at different ph-values.

Parameter, pH-Value	**Sample 4.6**		**Sample 3.3**		**Sample 3.5**		**Sample 3.6**	
pH	**6.14**		**9.19**		**11.13**		**12.2**	
Diameter, d0, m	**1.370E-02**	**1.797E-02**	**1.392E-02**	**1.784E-02**	**1.338E-02**	**1.674E-02**	**1.279E-02**	**1.797E-02**
Thickness, *l* =t0, m	**2.116E-03**	**1.673E-03**	**2.706E-03**	**1.574E-03**	**2.854E-03**	**1.967E-03**	**2.755E-03**	**1.574E-03**
Mass, m_{bc}	**0.46**	-	**0.442**	-	**0.449**	-	**0.422**	-
Mass, m_{ac}	-	**100.53**	-	**100.096**	-	**100.542**	-	**100.956**
Force, N	**1**	**1**	**1**	**1**	**1**	**1**	**1**	**1**
Area, m2	1.473E-04		1.522E-04		1.405E-04		1.284E-04	
del(*l*), m	4.428E-04		1.132E-03		8.868E-04		1.181E-03	
Meas.Young's Modulus, Pa/Mpa	**3.243E+04**	**3.243E-02**	**1.571E+04**	**1.571E-02**	**2.290E+04**	**2.290E-02**	**1.817E+04**	**1.817E-02**
Calc. Stress, Pa/Mpa	6.788E+03	6.788E-03	6.568E+03	6.568E-03	7.115E+03	7.115E-03	7.789E+03	7.789E-03
Calc. Strain	2.093E-01		4.182E-01		3.108E-01		4.286E-01	
Poisson's ratio, *v*	1.970E+00		9.444E-01		1.071E+00		1.459E+00	
Bulk Modulus, Pa/Mpa	**-3.677E+03**	-3.677E-03	**-5.890E+03**	-5.890E-03	**-6.677E+03**	-6.677E-03	**-3.159E+03**	-3.159E-03
Shear Modulus, Pa/Mpa	5.460E+03	5.460E-03	4.039E+03	4.039E-03	5.526E+03	5.526E-03	3.696E+03	3.696E-03

Table F.2: The mechanical properties of cylindrical samples of hydrogel_4 equilibrated at different NaCl.

Parameter, C_{NaCl}, (M)	**Sample 5.1**		**Sample 5.3**		**Sample 5.4**		**Sample 5.5**	
NaCL	**1.0E-01**		**1.0E-03**		**1.0E-04**		**1.0E-05**	
Diameter, d0, m	**1.324E-02**	**1.688E-02**	**1.342E-02**	**1.720E-02**	**1.370E-02**	**1.720E-02**	**1.397E-02**	**1.615E-02**
Thickness, *l* =t0, m	**3.838E-03**	**2.755E-03**	**2.558E-03**	**1.919E-03**	**2.116E-03**	**1.771E-03**	**2.116E-03**	**1.820E-03**
Mass, m_{bc}	**0.504**	-	**0.426**	-	**0.348**	-	**0.443**	-
Mass, m_{ac}	-	**100.594**	-	**100.236**	-	**100.283**	-	**100.614**
Force, N	**1**	**1**	**1**	**1**	**1**	**1**	**1**	**1**
Area, m2	1.377E-04		1.415E-04		1.473E-04		1.532E-04	
del(*l*), m	1.082E-03		6.396E-04		3.444E-04		2.952E-04	
Meas.Young's Modulus, Pa/Mpa	**2.575E+04**	**2.575E-02**	**2.827E+04**	**2.827E-02**	**4.170E+04**	**4.170E-02**	**4.677E+04**	**4.677E-02**
Calc. Stress, Pa/Mpa	7.263E+03	7.263E-03	7.067E+03	7.067E-03	6.788E+03	6.788E-03	6.525E+03	6.525E-03
Calc. Strain	2.821E-01		2.500E-01		1.628E-01		1.395E-01	
Poisson's ratio, *v*	1.294E+00		1.481E+00		1.959E+00		1.302E+00	
Bulk Modulus, Pa/Mpa	**-5.406E+03**	-5.406E-03	**-4.805E+03**	-4.805E-03	**-4.763E+03**	-4.763E-03	**-9.723E+03**	-9.723E-03
Shear Modulus, Pa/Mpa	5.613E+03	5.613E-03	5.698E+03	5.698E-03	7.046E+03	7.046E-03	1.016E+04	1.016E-02

Table F.3: The mechanical properties of cylindrical samples of hydrogel_4 equilibrated at different phenol.

Parameter, C_{Phenol}, (M)	**Sample 6.1**		**Sample 6.2**		**Sample 6.3**		**Sample 6.6**	
C, Phenol	**1.0E-03**		**2.0E-03**		**4.0E-03**		**1.0E-02**	
Diameter, d0, m	**1.370E-02**	**1.711E-02**	**1.351E-02**	**1.720E-02**	**1.288E-02**	**1.761E-02**	**1.356E-02**	**1.638E-02**
Thickness, *l* =t0, m	**2.755E-03**	**1.870E-03**	**2.263E-03**	**1.722E-03**	**3.231E-03**	**2.312E-03**	**3.444E-03**	**2.460E-03**
Mass, m_{bc}	**0.472**	-	**0.43**	-	**0.52**	-	**0.552**	-
Mass, m_{ac}	-	**100.527**	-	**100.152**	-	**100.13**	-	**100.174**
Force, N	**1**	**1**	**1**	**1**	**1**	**1**	**1**	**1**
Area, m2	1.473E-04		1.434E-04		1.302E-04		1.444E-04	
del(*l*), m	8.856E-04		5.412E-04		9.181E-04		9.840E-04	
Meas.Young's Modulus, Pa/Mpa	**2.112E+04**	**2.112E-02**	**2.916E+04**	**2.916E-02**	**2.702E+04**	**2.702E-02**	**2.424E+04**	**2.424E-02**
Calc. Stress, Pa/Mpa	6.788E+03	6.788E-03	6.972E+03	6.972E-03	7.679E+03	7.679E-03	6.926E+03	6.926E-03
Calc. Strain	3.214E-01		2.391E-01		2.842E-01		2.857E-01	
Poisson's ratio, *v*	1.028E+00		1.485E+00		1.831E+00		9.282E-01	
Bulk Modulus, Pa/Mpa	**-6.664E+03**	-6.664E-03	**-4.932E+03**	-4.932E-03	**-3.383E+03**	-3.383E-03	**-9.435E+03**	-9.435E-03
Shear Modulus, Pa/Mpa	5.206E+03	5.206E-03	5.866E+03	5.866E-03	4.772E+03	4.772E-03	6.286E+03	6.286E-03

Table F.4: The mechanical properties of cylindrical samples of hydrogel_4 equilibrated at different ethanol.

Parameter, $C_{Ethanol}$, (M)	**Sample 7.1**		**Sample 7.2**		**Sample 7.3**		**Sample 7.4**	
C, Ethanol	**2.0E-02**		**4.0E-02**		**6.0E-02**		**8.0E-02**	
Diameter, d0, m	**1.420E-02**	**1.756E-02**	**1.347E-02**	**1.784E-02**	**1.388E-02**	**1.765E-02**	**1.392E-02**	**1.770E-02**
Thickness, *l* =t0, m	**1.771E-03**	**1.427E-03**	**3.739E-03**	**2.411E-03**	**2.608E-03**	**1.328E-03**	**2.214E-03**	**1.624E-03**
Mass, m_{bc}	**0.335**	**-**	**0.545**	**-**	**0.358**	**-**	**0.444**	**-**
Mass, m_{ac}	**-**	**100.525**	**-**	**100.923**	**-**	**100.062**	**-**	**100.514**
Force, N	**1**	**1**	**1**	**1**	**1**	**1**	**1**	**1**
Area, m2	1.583E-04		1.425E-04		1.513E-04		1.522E-04	
del(*l*), m	3.444E-04		1.328E-03		1.279E-03		5.904E-04	
Meas.Young's Modulus, Pa/Mpa	**3.249E+04**	**3.249E-02**	**1.976E+04**	**1.976E-02**	**1.348E+04**	**1.348E-02**	**2.463E+04**	**2.463E-02**
Calc. Stress, Pa/Mpa	6.318E+03	6.318E-03	7.019E+03	7.019E-03	6.611E+03	6.611E-03	6.568E+03	6.568E-03
Calc. Strain	1.944E-01		3.553E-01		4.906E-01		2.667E-01	
Poisson's ratio, *v*	1.524E+00		1.290E+00		7.958E-01		1.339E+00	
Bulk Modulus, Pa/Mpa	**-5.290E+03**	-5.290E-03	**-4.170E+03**	-4.170E-03	**-7.594E+03**	-7.594E-03	**-4.896E+03**	-4.896E-03
Shear Modulus, Pa/Mpa	6.437E+03	6.437E-03	4.315E+03	4.315E-03	3.752E+03	3.752E-03	5.266E+03	5.266E-03

Table F.5: The mechanical properties of cylindrical samples of hydrogel_4 equilibrated at different propanol.

Parameter, $C_{Propanol}$, (M)	**Sample 8.1**		**Sample 8.2**		**Sample 8.3**		**Sample 8.4**	
C, Propanol	**2.00E-02**		**0.04**		**0.06**		**0.08**	
Diameter, d0, m	**1.365E-02**	**1.761E-02**	**1.365E-02**	**1.752E-02**	**1.306E-02**	**1.747E-02**	**1.374E-02**	**1.743E-02**
Thickness, *l* =t0, m	**2.903E-03**	**1.870E-03**	**3.100E-03**	**1.919E-03**	**2.510E-03**	**1.722E-03**	**2.460E-03**	**1.427E-03**
Mass, m_{bc}	**0.451**	**-**	**0.463**	**-**	**0.425**	**-**	**0.4**	**-**
Mass, m_{ac}	**-**	**100.048**	**-**	**100.12**	**-**	**100.466**	**-**	**100.54**
Force, N	**1**	**1**	**1**	**1**	**1**	**1**	**1**	**1**
Area, m2	1.463E-04		1.463E-04		1.339E-04		1.483E-04	
del(*l*), m	1.033E-03		1.181E-03		7.876E-04		1.033E-03	
Meas.Young's Modulus, Pa/Mpa	**1.920E+04**	**1.920E-02**	**1.794E+04**	**1.794E-02**	**2.379E+04**	**2.379E-02**	**1.606E+04**	**1.606E-02**
Calc. Stress, Pa/Mpa	6.834E+03	6.834E-03	6.834E+03	6.834E-03	7.467E+03	7.467E-03	6.743E+03	6.743E-03
Calc. Strain	3.559E-01		3.810E-01		3.138E-01		4.200E-01	
Poisson's ratio, *v*	1.125E+00		1.032E+00		1.511E+00		8.905E-01	
Bulk Modulus, Pa/Mpa	**-5.121E+03**	-5.121E-03	**-5.618E+03**	-5.618E-03	**-3.922E+03**	-3.922E-03	**-6.852E+03**	-6.852E-03
Shear Modulus, Pa/Mpa	4.518E+03	4.518E-03	4.414E+03	4.414E-03	4.737E+03	4.737E-03	4.246E+03	4.246E-03

Table F.6: The mechanical properties at different applied load on hydrogel_2 cylinder equilibrated in BSA solution (0.01) at T=25°C.

T = 25°, 10^{-2} M BSA	**Sample 9.3**					
Diameter, d_0, m	1.274E-02		**Area$_0$, m^2**			
Thickness, $l = t_0$, m	3.634E-03		1.275E-04			
Force, N	**Diameter, d,m**	**Thickness, l =t,**	**Area, m^2**	**Calc. Stress, Pa/Mpa**	**Calc. Strain**	**Young's Modulus, Mpa**
0.2	1.306E-02	2.990E-03	1.340E-04	1.492E-03	2.107E-01	7.080E-03
0.4	1.343E-02	2.668E-03	1.417E-04	2.823E-03	2.957E-01	9.545E-03
0.6	1.426E-02	2.346E-03	1.597E-04	3.757E-03	3.807E-01	9.867E-03
0.8	1.481E-02	2.208E-03	1.723E-04	4.643E-03	4.172E-01	1.113E-02
1	1.550E-02	2.070E-03	1.887E-04	5.298E-03	4.536E-01	1.168E-02
1.2	1.596E-02	1.840E-03	2.001E-04	5.997E-03	5.143E-01	1.166E-02
1.4	1.661E-02	1.656E-03	2.166E-04	6.464E-03	5.629E-01	1.148E-02
1.6	1.670E-02	1.702E-03	2.190E-04	7.306E-03	5.507E-01	1.327E-02
1.8	1.711E-02	1.564E-03	2.300E-04	7.827E-03	5.872E-01	1.333E-02
2	1.716E-02	1.472E-03	2.312E-04	8.650E-03	6.114E-01	1.415E-02
2.2	1.776E-02	1.380E-03	2.476E-04	8.885E-03	6.357E-01	1.398E-02
2.4	1.872E-02	1.288E-03	2.753E-04	8.718E-03	6.600E-01	1.321E-02
2.6	1.887E-02	1.288E-03	2.795E-04	9.301E-03	6.600E-01	1.409E-02
2.8	1.927E-02	1.196E-03	2.918E-04	9.597E-03	6.843E-01	1.402E-02
3	1.941E-02	1.150E-03	2.960E-04	1.014E-02	6.964E-01	1.455E-02
3.2	2.116E-02	1.058E-03	3.517E-04	9.100E-03	7.207E-01	1.263E-02
3.4	2.153E-02	9.660E-04	3.640E-04	9.341E-03	7.450E-01	1.254E-02

Table F.7: The mechanical properties at different applied load on hydrogel_2 cylinder equilibrated in BSA solution (0.05) at T=25°C.

T = 25°, $5{\cdot}10^{-2}$ M BSA	**Sample 9.4**					
Diameter, d_0, m	1.348E-02		**Area$_0$, m^2**			
Thickness, $l = t_0$, m	3.358E-03		1.427E-04			
Force, N	**Diameter, d,m**	**Thickness, l =t,**	**Area, m^2**	**Calc. Stress, Pa/Mpa**	**Calc. Strain**	**Young's Modulus, Mpa**
0.3	1.458E-02	2.116E-03	1.670E-04	1.796E-03	4.415E-01	4.069E-03
0.6	1.578E-02	1.564E-03	1.955E-04	3.069E-03	5.872E-01	5.226E-03
0.9	1.711E-02	1.380E-03	2.300E-04	3.913E-03	6.357E-01	6.156E-03
1.2	1.864E-02	1.242E-03	2.728E-04	4.399E-03	6.722E-01	6.545E-03
1.5	2.006E-02	1.012E-03	3.159E-04	4.748E-03	7.329E-01	6.479E-03
1.8	2.052E-02	9.660E-04	3.306E-04	5.445E-03	7.450E-01	7.309E-03
2.1	2.116E-02	9.660E-04	3.517E-04	5.972E-03	7.450E-01	8.016E-03
2.4	2.176E-02	8.780E-04	3.718E-04	6.455E-03	7.682E-01	8.402E-03
2.7	2.199E-02	8.280E-04	3.797E-04	7.111E-03	7.814E-01	9.099E-03
3	2.259E-02	7.820E-04	4.007E-04	7.488E-03	7.936E-01	9.435E-03
3.3	2.305E-02	6.440E-04	4.171E-04	7.911E-03	8.300E-01	9.531E-03

Table F.8: The mechanical properties at different applied load on hydrogel_2 cylinder equilibrated in BSA solution (0.1) at T=25°C.

T = 25°, 10^{-1} M BSA	**Sample 9.5**					
Diameter, d_0, m	1.191E-02		**Area$_0$, m^2**			
Thickness, $l = t_0$, m	3.818E-03		1.115E-04			
Force, N	**Diameter, d,m**	**Thickness, l =t,**	**Area, m^2**	**Calc. Stress, Pa/Mpa**	**Calc. Strain**	**Young's Modulus, Mpa**
0.3	1.343E-02	2.898E-03	1.417E-04	2.117E-03	2.350E-01	9.008E-03
0.6	1.477E-02	2.300E-03	1.712E-04	3.504E-03	3.929E-01	8.918E-03
0.9	1.555E-02	2.070E-03	1.899E-04	4.740E-03	4.536E-01	1.045E-02
1.2	1.647E-02	1.886E-03	2.130E-04	5.634E-03	5.022E-01	1.122E-02
1.5	1.670E-02	1.748E-03	2.190E-04	6.850E-03	5.386E-01	1.272E-02
1.8	1.766E-02	1.610E-03	2.451E-04	7.345E-03	5.750E-01	1.277E-02
2.1	1.808E-02	1.426E-03	2.567E-04	8.181E-03	6.236E-01	1.312E-02
2.4	1.941E-02	1.196E-03	2.960E-04	8.109E-03	6.843E-01	1.185E-02
2.7	2.098E-02	1.150E-03	3.456E-04	7.813E-03	6.964E-01	1.122E-02

Table F.9: The mechanical properties at different applied load on hydrogel_2 cylinder equilibrated in BSA solution (1.51) at T=25°C.

T = 25°, 1,51 M BSA	**Sample 9.6**					
Diameter, d_0, m	1.201E-02		**Area$_0$, m^2**			
Thickness, $l = t_0$, m	3.220E-03		1.132E-04			
Force, N	**Diameter, d,m**	**Thickness, l =t,**	**Area, m^2**	**Calc. Stress, Pa/Mpa**	**Calc. Strain**	**Young's Modulus, Mpa**
0.3	1.352E-02	3.128E-03	1.436E-04	2.088E-03	1.743E-01	1.198E-02
0.6	1.454E-02	2.530E-03	1.660E-04	3.616E-03	3.322E-01	1.088E-02
0.9	1.546E-02	2.392E-03	1.876E-04	4.797E-03	3.686E-01	1.301E-02
1.2	1.610E-02	2.162E-03	2.036E-04	5.894E-03	4.293E-01	1.373E-02
1.5	1.688E-02	2.024E-03	2.238E-04	6.701E-03	4.657E-01	1.439E-02
1.8	1.730E-02	1.978E-03	2.350E-04	7.661E-03	4.779E-01	1.603E-02
2.1	1.776E-02	1.886E-03	2.476E-04	8.481E-03	5.022E-01	1.689E-02
2.4	1.884E-02	1.794E-03	2.789E-04	8.605E-03	5.264E-01	1.635E-02
2.7	1.895E-02	1.610E-03	2.821E-04	9.571E-03	5.750E-01	1.664E-02

Table F.10: The mechanical properties at different applied load on hydrogel_2 cylinder equilibrated in BSA solution (0.01) at T=32°C.

T = 32°, 10^{-2} M BSA	**Sample 10.1**					
Diameter, d_0, m	1.017E-02		**Area$_0$, m^2**			
Thickness, $l = t_0$, m	2.392E-03		8.117E-05			
Force, N	**Diameter, d,m**	**Thickness, l =t,**	**Area, m^2**	**Calc. Stress, Pa/Mpa**	**Calc. Strain**	**Young's Modulus, Mpa**
0.3	1.076E-02	2.484E-03	9.100E-05	3.297E-03	3.443E-01	9.575E-03
0.6	1.127E-02	2.024E-03	9.976E-05	6.015E-03	4.657E-01	1.291E-02
0.9	1.150E-02	1.978E-03	1.039E-04	8.665E-03	4.779E-01	1.813E-02
1.2	1.210E-02	1.702E-03	1.150E-04	1.044E-02	5.507E-01	1.895E-02
1.5	1.256E-02	1.656E-03	1.239E-04	1.211E-02	5.629E-01	2.152E-02
1.8	1.306E-02	1.564E-03	1.340E-04	1.343E-02	5.872E-01	2.287E-02
2.1	1.357E-02	1.426E-03	1.446E-04	1.452E-02	6.236E-01	2.328E-02
2.4	1.362E-02	1.334E-03	1.456E-04	1.648E-02	6.479E-01	2.544E-02
2.7	1.426E-02	1.242E-03	1.597E-04	1.691E-02	6.722E-01	2.515E-02
3	1.458E-02	1.150E-03	1.670E-04	1.796E-02	6.964E-01	2.579E-02
3.3	1.472E-02	1.150E-03	1.702E-04	1.939E-02	6.964E-01	2.784E-02
3.6	1.495E-02	1.104E-03	1.755E-04	2.051E-02	7.086E-01	2.894E-02
3.9	1.523E-02	1.058E-03	1.821E-04	2.142E-02	7.207E-01	2.972E-02
4.2	1.527E-02	9.660E-04	1.832E-04	2.293E-02	7.450E-01	3.078E-02
4.5	1.559E-02	9.660E-04	1.910E-04	2.356E-02	7.450E-01	3.163E-02
4.8	1.601E-02	9.200E-04	2.013E-04	2.385E-02	7.572E-01	3.150E-02
5.1	1.688E-02	8.740E-04	2.239E-04	2.278E-02	7.693E-01	2.962E-02
5.4	1.702E-02	8.740E-04	2.275E-04	2.373E-02	7.693E-01	3.085E-02
5.7	1.707E-02	8.420E-04	2.288E-04	2.492E-02	7.777E-01	3.204E-02
6	1.711E-02	7.830E-04	2.300E-04	2.609E-02	7.933E-01	3.289E-02

Table F.11: The mechanical properties at different applied load on hydrogel_2 cylinder equilibrated in BSA solution (0.05) at T=32°C.

T = 32°, $5{\cdot}10^{-2}$ M BSA	**Sample 10.2**					
Diameter, d_0, m	9.982E-03		**Area$_0$, m^2**			
Thickness, $l = t_0$, m	2.760E-03		7.826E-05			
Force, N	**Diameter, d,m**	**Thickness, l =t,**	**Area, m^2**	**Calc. Stress, Pa/Mpa**	**Calc. Strain**	**Young's Modulus, Mpa**
0.3	1.086E-02	2.438E-03	9.256E-05	3.241E-03	3.565E-01	9.093E-03
0.6	1.168E-02	2.070E-03	1.072E-04	5.596E-03	4.536E-01	1.234E-02
0.9	1.247E-02	1.840E-03	1.221E-04	7.374E-03	5.143E-01	1.434E-02
1.2	1.329E-02	1.610E-03	1.388E-04	8.645E-03	5.750E-01	1.503E-02
1.5	1.348E-02	1.518E-03	1.427E-04	1.051E-02	5.993E-01	1.754E-02
1.8	1.389E-02	1.338E-03	1.516E-04	1.188E-02	6.468E-01	1.836E-02
2.1	1.449E-02	1.288E-03	1.649E-04	1.273E-02	6.600E-01	1.929E-02
2.4	1.481E-02	1.242E-03	1.723E-04	1.393E-02	6.722E-01	2.072E-02
2.7	1.523E-02	1.150E-03	1.821E-04	1.483E-02	6.964E-01	2.129E-02
3	1.555E-02	1.104E-03	1.899E-04	1.580E-02	7.086E-01	2.230E-02
3.3	1.601E-02	1.012E-03	2.013E-04	1.640E-02	7.329E-01	2.237E-02
3.6	1.615E-02	9.660E-04	2.047E-04	1.758E-02	7.450E-01	2.360E-02
3.9	1.624E-02	9.200E-04	2.071E-04	1.883E-02	7.572E-01	2.487E-02
4.2	1.670E-02	9.200E-04	2.190E-04	1.918E-02	7.572E-01	2.533E-02
4.5	1.679E-02	8.740E-04	2.214E-04	2.032E-02	7.693E-01	2.642E-02
4.8	1.697E-02	8.280E-04	2.263E-04	2.121E-02	7.814E-01	2.714E-02
5.1	1.730E-02	7.820E-04	2.350E-04	2.171E-02	7.936E-01	2.735E-02
5.4	1.757E-02	7.810E-04	2.425E-04	2.227E-02	7.938E-01	2.805E-02
5.7	1.789E-02	7.360E-04	2.515E-04	2.267E-02	8.057E-01	2.813E-02
6	1.817E-02	6.900E-04	2.593E-04	2.314E-02	8.179E-01	2.829E-02

Table F.12: The mechanical properties at different applied load on hydrogel_2 cylinder equilibrated in BSA solution (0.1) at T=32°C.

T = 32°, 10^{-1} M BSA	**Sample 10.3**					
Diameter, d_0, m	1.007E-02		**Area$_0$, m^2**			
Thickness, $l = t_0$, m	2.116E-03		7.971E-05			
Force, N	**Diameter, d,m**	**Thickness, l =t,**	**Area, m^2**	**Calc. Stress, Pa/Mpa**	**Calc. Strain**	**Young's Modulus, Mpa**
0.3	1.095E-02	1.840E-03	9.414E-05	3.187E-03	5.143E-01	6.196E-03
0.6	1.155E-02	1.702E-03	1.047E-04	5.731E-03	5.507E-01	1.041E-02
0.9	1.219E-02	1.426E-03	1.167E-04	7.712E-03	6.236E-01	1.237E-02
1.2	1.265E-02	1.242E-03	1.257E-04	9.548E-03	6.722E-01	1.420E-02
1.5	1.334E-02	1.196E-03	1.398E-04	1.073E-02	6.843E-01	1.568E-02
1.8	1.366E-02	1.104E-03	1.466E-04	1.228E-02	7.086E-01	1.733E-02
2.1	1.403E-02	1.058E-03	1.546E-04	1.358E-02	7.207E-01	1.885E-02
2.4	1.458E-02	9.303E-04	1.670E-04	1.437E-02	7.544E-01	1.905E-02
2.7	1.500E-02	8.740E-04	1.766E-04	1.529E-02	7.693E-01	1.987E-02
3	1.513E-02	8.740E-04	1.799E-04	1.668E-02	7.693E-01	2.168E-02
3.3	1.532E-02	8.280E-04	1.843E-04	1.791E-02	7.814E-01	2.291E-02
3.6	1.615E-02	8.280E-04	2.047E-04	1.758E-02	7.814E-01	2.250E-02
3.9	1.661E-02	7.820E-04	2.166E-04	1.801E-02	7.936E-01	2.269E-02
4.2	1.674E-02	7.820E-04	2.202E-04	1.907E-02	7.936E-01	2.404E-02
4.5	1.697E-02	7.360E-04	2.263E-04	1.989E-02	8.057E-01	2.468E-02
4.8	1.700E-02	6.900E-04	2.270E-04	2.115E-02	8.179E-01	2.586E-02
5.1	1.701E-02	6.440E-04	2.272E-04	2.245E-02	8.300E-01	2.705E-02
5.4	1.702E-02	6.440E-04	2.275E-04	2.373E-02	8.300E-01	2.859E-02
5.7	1.734E-02	5.980E-04	2.362E-04	2.413E-02	8.421E-01	2.865E-02
6	1.757E-02	5.520E-04	2.425E-04	2.474E-02	8.543E-01	2.896E-02

Table F.13: The mechanical properties at different applied load on hydrogel_2 cylinder equilibrated in BSA solution (1.51) at T=32°C.

T = 32°, 1,51 M BSA	**Sample 10.4**					
Diameter, d_0, m	9.936E-03		**Area$_0$, m^2**			
Thickness, $l = t_0$, m	1.426E-03		7.754E-05			
Force, N	**Diameter, d,m**	**Thickness, l =t,**	**Area, m^2**	**Calc. Stress, Pa/Mpa**	**Calc. Strain**	**Young's Modulus, Mpa**
0.3	1.081E-02	1.702E-03	9.178E-05	3.269E-03	5.507E-01	5.935E-03
0.6	1.145E-02	1.518E-03	1.030E-04	5.823E-03	5.993E-01	9.716E-03
0.9	1.228E-02	1.288E-03	1.184E-04	7.599E-03	6.600E-01	1.151E-02
1.2	1.274E-02	1.242E-03	1.275E-04	9.411E-03	6.722E-01	1.400E-02
1.5	1.334E-02	1.104E-03	1.398E-04	1.073E-02	7.086E-01	1.515E-02
1.8	1.362E-02	1.012E-03	1.456E-04	1.236E-02	7.329E-01	1.687E-02
2.1	1.394E-02	9.660E-04	1.526E-04	1.376E-02	7.450E-01	1.847E-02
2.4	1.412E-02	9.200E-04	1.567E-04	1.532E-02	7.572E-01	2.023E-02
2.7	1.431E-02	8.740E-04	1.608E-04	1.679E-02	7.693E-01	2.183E-02
3	1.454E-02	8.280E-04	1.660E-04	1.808E-02	7.814E-01	2.313E-02
3.3	1.472E-02	7.820E-04	1.702E-04	1.939E-02	7.936E-01	2.444E-02
3.6	1.495E-02	7.820E-04	1.755E-04	2.051E-02	7.936E-01	2.584E-02
3.9	1.509E-02	7.360E-04	1.788E-04	2.181E-02	8.057E-01	2.707E-02
4.2	1.555E-02	6.900E-04	1.899E-04	2.212E-02	8.179E-01	2.705E-02
4.5	1.578E-02	6.900E-04	1.955E-04	2.302E-02	8.179E-01	2.814E-02
4.8	1.628E-02	6.440E-04	2.083E-04	2.305E-02	8.300E-01	2.777E-02
5.1	1.656E-02	5.980E-04	2.154E-04	2.368E-02	8.421E-01	2.812E-02
5.4	1.716E-02	5.060E-04	2.312E-04	2.335E-02	8.664E-01	2.695E-02

Table F.14: The mechanical properties at different applied load on hydrogel_2 cylinder equilibrated in BSA solution (0.01) at T=37°C.

T = 37°, 10^{-2} M BSA	**Sample 4.2**					
Diameter, d_0, m	4.692E-03		**Area$_0$, m^2**			
Thickness, $l = t_0$, m	2.070E-03		1.729E-05			
Force, N	**Diameter, d,m**	**Thickness, l =t,**	**Area, m^2**	**Calc. Stress, Pa/Mpa**	**Calc. Strain**	**Young's Modulus, Mpa**
0.2	4.784E-03	1.840E-03	1.798E-05	1.113E-02	5.143E-01	2.163E-02
0.4	4.830E-03	1.610E-03	1.832E-05	2.183E-02	5.750E-01	3.797E-02
0.6	5.060E-03	1.518E-03	2.011E-05	2.984E-02	5.993E-01	4.979E-02
0.8	5.198E-03	1.426E-03	2.122E-05	3.770E-02	6.236E-01	6.045E-02
1	5.336E-03	1.380E-03	2.236E-05	4.472E-02	6.357E-01	7.034E-02
1.5	5.750E-03	1.288E-03	2.597E-05	5.776E-02	6.600E-01	8.752E-02
2	5.934E-03	1.196E-03	2.766E-05	7.232E-02	6.843E-01	1.057E-01
2.5	6.486E-03	1.058E-03	3.304E-05	7.567E-02	7.207E-01	1.050E-01
3	6.854E-03	9.200E-04	3.690E-05	8.131E-02	7.572E-01	1.074E-01
3.5	7.130E-03	8.280E-04	3.993E-05	8.766E-02	7.814E-01	1.122E-01
4	7.636E-03	7.360E-04	4.580E-05	8.734E-02	8.057E-01	1.084E-01
4.5	7.820E-03	6.900E-04	4.803E-05	9.369E-02	8.179E-01	1.146E-01
5	7.912E-03	6.440E-04	4.917E-05	1.017E-01	8.300E-01	1.225E-01
5.5	8.004E-03	5.520E-04	5.032E-05	1.093E-01	8.543E-01	1.280E-01
6	8.050E-03	5.520E-04	5.090E-05	1.179E-01	8.543E-01	1.380E-01

Table F.15: The mechanical properties at different applied load on hydrogel_2 cylinder equilibrated in BSA solution (0.05) at T=37°C.

T = 37°, $5{\cdot}10^{-2}$ M BSA	**Sample 4.1**					
Diameter, d_0, m	5.198E-03		**Area$_0$, m^2**			
Thickness, $l = t_0$, m	1.932E-03		2.122E-05			
Force, N	**Diameter, d,m**	**Thickness, l =t,**	**Area, m^2**	**Calc. Stress, Pa/Mpa**	**Calc. Strain**	**Young's Modulus, Mpa**
0.2	5.290E-03	1.564E-03	2.198E-05	9.100E-03	5.872E-01	1.550E-02
0.4	5.382E-03	1.472E-03	2.275E-05	1.758E-02	6.114E-01	2.876E-02
0.6	5.566E-03	1.380E-03	2.433E-05	2.466E-02	6.357E-01	3.879E-02
0.8	5.658E-03	1.288E-03	2.514E-05	3.182E-02	6.600E-01	4.821E-02
1	5.888E-03	1.242E-03	2.723E-05	3.673E-02	6.722E-01	5.464E-02
1.5	6.164E-03	1.104E-03	2.984E-05	5.027E-02	7.086E-01	7.094E-02
2	6.394E-03	1.058E-03	3.211E-05	6.229E-02	7.207E-01	8.642E-02
2.5	6.670E-03	1.012E-03	3.494E-05	7.155E-02	7.329E-01	9.763E-02
3	6.716E-03	9.660E-04	3.543E-05	8.469E-02	7.450E-01	1.137E-01
3.5	6.946E-03	8.740E-04	3.789E-05	9.237E-02	7.693E-01	1.201E-01
4	7.130E-03	8.280E-04	3.993E-05	1.002E-01	7.814E-01	1.282E-01
4.5	7.406E-03	7.360E-04	4.308E-05	1.045E-01	8.057E-01	1.296E-01
5	7.406E-03	7.360E-04	4.308E-05	1.161E-01	8.057E-01	1.441E-01
5.5	7.544E-03	7.360E-04	4.470E-05	1.230E-01	8.057E-01	1.527E-01
6	7.636E-03	7.360E-04	4.580E-05	1.310E-01	8.057E-01	1.626E-01

Table F.16: The mechanical properties at different applied load on hydrogel_2 cylinder equilibrated in BSA solution (0.1) at T=37°C.

T = 37°, 10^{-1} M BSA	**Sample 3.6**					
Diameter, d_0, m	5.060E-03		**Area$_0$, m^2**			
Thickness, $l = t_0$, m	2.070E-03		2.011E-05			
Force, N	**Diameter, d,m**	**Thickness, l =t,**	**Area, m^2**	**Calc. Stress, Pa/Mpa**	**Calc. Strain**	**Young's Modulus, Mpa**
0.2	5.198E-03	1.702E-03	2.122E-05	9.425E-03	5.507E-01	1.711E-02
0.4	5.382E-03	1.564E-03	2.275E-05	1.758E-02	5.872E-01	2.995E-02
0.6	5.566E-03	1.472E-03	2.433E-05	2.466E-02	6.114E-01	4.033E-02
0.8	5.704E-03	1.380E-03	2.555E-05	3.131E-02	6.357E-01	4.925E-02
1	5.888E-03	1.334E-03	2.723E-05	3.673E-02	6.479E-01	5.669E-02
1.5	6.210E-03	1.242E-03	3.029E-05	4.952E-02	6.722E-01	7.368E-02
2	6.486E-03	1.150E-03	3.304E-05	6.053E-02	6.964E-01	8.692E-02
2.5	6.808E-03	1.058E-03	3.640E-05	6.868E-02	7.207E-01	9.529E-02
3	6.946E-03	9.660E-04	3.789E-05	7.917E-02	7.450E-01	1.063E-01
3.5	7.314E-03	8.740E-04	4.201E-05	8.330E-02	7.693E-01	1.083E-01
4	7.406E-03	7.860E-04	4.308E-05	9.285E-02	7.925E-01	1.172E-01
4.5	7.636E-03	7.820E-04	4.580E-05	9.826E-02	7.936E-01	1.238E-01
5	7.774E-03	7.820E-04	4.747E-05	1.053E-01	7.936E-01	1.327E-01
5.5	7.912E-03	7.360E-04	4.917E-05	1.119E-01	8.057E-01	1.388E-01
6	8.004E-03	6.900E-04	5.032E-05	1.192E-01	8.179E-01	1.458E-01

Table F.17: The mechanical properties at different applied load on hydrogel_2 cylinder equilibrated in BSA solution (1.51) at T=37°C.

T = 37°, 1,51 M BSA	**Sample 3.5**					
Diameter, d_0, m	4.876E-03		**Area$_0$, m^2**			
Thickness, $l = t_0$, m	1.840E-03		1.867E-05			
Force, N	**Diameter, d,m**	**Thickness, l =t,**	**Area, m^2**	**Calc. Stress, Pa/Mpa**	**Calc. Strain**	**Young's Modulus, Mpa**
0.2	5.336E-03	1.656E-03	2.236E-05	8.943E-03	5.629E-01	1.589E-02
0.4	5.382E-03	1.610E-03	2.275E-05	1.758E-02	5.750E-01	3.058E-02
0.6	5.382E-03	1.564E-03	2.275E-05	2.637E-02	5.872E-01	4.492E-02
0.8	5.428E-03	1.518E-03	2.314E-05	3.457E-02	5.993E-01	5.769E-02
1	5.474E-03	1.518E-03	2.353E-05	4.249E-02	5.993E-01	7.090E-02
1.5	5.474E-03	1.518E-03	2.353E-05	6.374E-02	5.993E-01	1.064E-01
2	5.520E-03	1.472E-03	2.393E-05	8.357E-02	6.114E-01	1.367E-01
2.5	5.520E-03	1.472E-03	2.393E-05	1.045E-01	6.114E-01	1.708E-01
3	5.612E-03	1.426E-03	2.474E-05	1.213E-01	6.236E-01	1.945E-01
3.5	5.612E-03	1.426E-03	2.474E-05	1.415E-01	6.236E-01	2.269E-01
4	5.704E-03	1.380E-03	2.555E-05	1.565E-01	6.357E-01	2.462E-01
4.5	5.750E-03	1.380E-03	2.597E-05	1.733E-01	6.357E-01	2.726E-01
5	5.750E-03	1.380E-03	2.597E-05	1.925E-01	6.357E-01	3.029E-01
5.5	5.750E-03	1.380E-03	2.597E-05	2.118E-01	6.357E-01	3.332E-01
6	5.842E-03	1.334E-03	2.680E-05	2.238E-01	6.479E-01	3.455E-01

Table F.18: The mechanical properties at different applied load on hydrogel_2 cylinder equilibrated in BSA solution (0.01) at T=40°C.

T = 40°, 10^{-2} M BSA	**Sample 12.5**					
Diameter, d_0, m	5.060E-03		**Area$_0$, m^2**			
Thickness, $l = t_0$, m	2.024E-03		2.011E-05			
Force, N	**Diameter, d,m**	**Thickness, l =t,**	**Area, m^2**	**Calc. Stress, Pa/Mpa**	**Calc. Strain**	**Young's Modulus, Mpa**
0.2	5.060E-03	1.886E-03	2.011E-05	9.946E-03	5.022E-01	1.981E-02
0.4	5.106E-03	1.748E-03	2.048E-05	1.953E-02	5.386E-01	3.627E-02
0.6	5.152E-03	1.610E-03	2.085E-05	2.878E-02	5.750E-01	5.005E-02
0.8	5.290E-03	1.564E-03	2.198E-05	3.640E-02	5.872E-01	6.199E-02
1	5.474E-03	1.334E-03	2.353E-05	4.249E-02	6.479E-01	6.559E-02
1.5	5.658E-03	1.242E-03	2.514E-05	5.966E-02	6.722E-01	8.876E-02
2	5.980E-03	1.104E-03	2.809E-05	7.121E-02	7.086E-01	1.005E-01
2.5	5.026E-03	1.012E-03	1.984E-05	1.260E-01	7.329E-01	1.719E-01
3	6.164E-03	9.660E-04	2.984E-05	1.005E-01	7.450E-01	1.349E-01
3.5	6.210E-03	9.200E-04	3.029E-05	1.156E-01	7.572E-01	1.526E-01
4	6.256E-03	9.200E-04	3.074E-05	1.301E-01	7.572E-01	1.719E-01
4.5	6.302E-03	8.740E-04	3.119E-05	1.443E-01	7.693E-01	1.875E-01
5	6.302E-03	8.740E-04	3.119E-05	1.603E-01	7.693E-01	2.084E-01
5.5	6.348E-03	8.740E-04	3.165E-05	1.738E-01	7.693E-01	2.259E-01
6	6.348E-03	8.740E-04	3.165E-05	1.896E-01	7.693E-01	2.464E-01

Table F.19: The mechanical properties at different applied load on hydrogel_2 cylinder equilibrated in BSA solution (0.05) at T=40°C.

T = 40°, 5·10^{-2} M BSA	**Sample 12.4**					
Diameter, d_0, m	4.968E-03		**Area$_0$, m^2**			
Thickness, $l = t_0$, m	1.702E-03		1.938E-05			
Force, N	**Diameter, d,m**	**Thickness, $l = t$,**	**Area, m^2**	**Calc. Stress, Pa/Mpa**	**Calc. Strain**	**Young's Modulus, Mpa**
0.2	5.106E-03	1.564E-03	2.048E-05	9.767E-03	5.872E-01	1.663E-02
0.4	5.152E-03	1.426E-03	2.085E-05	1.919E-02	6.236E-01	3.077E-02
0.6	5.198E-03	1.334E-03	2.122E-05	2.827E-02	6.479E-01	4.364E-02
0.8	5.244E-03	1.288E-03	2.160E-05	3.704E-02	6.600E-01	5.612E-02
1	5.382E-03	1.196E-03	2.275E-05	4.396E-02	6.843E-01	6.424E-02
1.5	5.428E-03	1.150E-03	2.314E-05	6.482E-02	6.964E-01	9.308E-02
2	5.566E-03	1.104E-03	2.433E-05	8.220E-02	7.086E-01	1.160E-01
2.5	5.612E-03	1.058E-03	2.474E-05	1.011E-01	7.207E-01	1.402E-01
3	5.704E-03	1.012E-03	2.555E-05	1.174E-01	7.329E-01	1.602E-01
3.5	5.796E-03	9.703E-04	2.638E-05	1.327E-01	7.439E-01	1.783E-01
4	5.934E-03	9.200E-04	2.766E-05	1.446E-01	7.572E-01	1.910E-01
4.5	6.256E-03	8.880E-04	3.074E-05	1.464E-01	7.656E-01	1.912E-01
5	6.302E-03	8.740E-04	3.119E-05	1.603E-01	7.693E-01	2.084E-01
5.5	6.394E-03	7.830E-04	3.211E-05	1.713E-01	7.933E-01	2.159E-01
6	6.486E-03	7.820E-04	3.304E-05	1.816E-01	7.936E-01	2.288E-01

Table F.20: The mechanical properties at different applied load on hydrogel_2 cylinder equilibrated in BSA solution (0.1) at T=40°C.

T = 40°, 10^{-1} M BSA	**Sample 12.2**					
Diameter, d_0, m	5.106E-03		**Area$_0$, m^2**			
Thickness, $l = t_0$, m	2.024E-03		2.048E-05			
Force, N	**Diameter, d,m**	**Thickness, $l = t$,**	**Area, m^2**	**Calc. Stress, Pa/Mpa**	**Calc. Strain**	**Young's Modulus, Mpa**
0.2	5.106E-03	1.610E-03	2.048E-05	9.767E-03	5.750E-01	1.699E-02
0.4	5.152E-03	1.564E-03	2.085E-05	1.919E-02	5.872E-01	3.268E-02
0.6	5.244E-03	1.472E-03	2.160E-05	2.778E-02	6.114E-01	4.543E-02
0.8	5.336E-03	1.380E-03	2.236E-05	3.577E-02	6.357E-01	5.627E-02
1	5.382E-03	1.288E-03	2.275E-05	4.396E-02	6.600E-01	6.660E-02
1.5	5.566E-03	1.196E-03	2.433E-05	6.165E-02	6.843E-01	9.009E-02
2	5.612E-03	1.196E-03	2.474E-05	8.085E-02	6.843E-01	1.182E-01
2.5	5.842E-03	1.104E-03	2.680E-05	9.327E-02	7.086E-01	1.316E-01
3	5.980E-03	1.012E-03	2.809E-05	1.068E-01	7.329E-01	1.457E-01
3.5	6.072E-03	1.012E-03	2.896E-05	1.209E-01	7.329E-01	1.649E-01
4	6.118E-03	9.800E-04	2.940E-05	1.361E-01	7.413E-01	1.835E-01
4.5	6.256E-03	9.660E-04	3.074E-05	1.464E-01	7.450E-01	1.965E-01
5	6.348E-03	9.200E-04	3.165E-05	1.580E-01	7.572E-01	2.087E-01
5.5	6.762E-03	8.820E-04	3.591E-05	1.532E-01	7.672E-01	1.996E-01
6	6.946E-03	8.280E-04	3.789E-05	1.583E-01	7.814E-01	2.026E-01

Table F.21: The mechanical properties at different applied load on hydrogel_2 cylinder equilibrated in BSA solution (1.51) at T=40°C.

T = 40°, 1,51 M BSA	**Sample 12.1**					
Diameter, d_0, m	4.876E-03		**Area$_0$, m^2**			
Thickness, $l = t_0$, m	2.070E-03		1.867E-05			
Force, N	**Diameter, d,m**	**Thickness, $l = t$,**	**Area, m^2**	**Calc. Stress, Pa/Mpa**	**Calc. Strain**	**Young's Modulus, Mpa**
0.2	4.876E-03	1.978E-03	1.867E-05	1.071E-02	4.779E-01	2.241E-02
0.4	4.922E-03	1.840E-03	1.903E-05	2.102E-02	5.143E-01	4.088E-02
0.6	5.106E-03	1.702E-03	2.048E-05	2.930E-02	5.507E-01	5.321E-02
0.8	5.244E-03	1.564E-03	2.160E-05	3.704E-02	5.872E-01	6.308E-02
1	5.336E-03	1.518E-03	2.236E-05	4.472E-02	5.993E-01	7.462E-02
1.5	5.520E-03	1.472E-03	2.393E-05	6.268E-02	6.114E-01	1.025E-01
2	5.888E-03	1.196E-03	2.723E-05	7.345E-02	6.843E-01	1.073E-01
2.5	6.302E-03	1.104E-03	3.119E-05	8.015E-02	7.086E-01	1.131E-01
3	6.578E-03	1.101E-03	3.398E-05	8.828E-02	7.093E-01	1.245E-01
3.5	6.900E-03	9.200E-04	3.739E-05	9.360E-02	7.572E-01	1.236E-01
4	7.084E-03	8.740E-04	3.941E-05	1.015E-01	7.693E-01	1.319E-01
4.5	7.268E-03	8.280E-04	4.149E-05	1.085E-01	7.814E-01	1.388E-01
5	7.452E-03	7.820E-04	4.362E-05	1.146E-01	7.936E-01	1.445E-01
5.5	7.774E-03	7.360E-04	4.747E-05	1.159E-01	8.057E-01	1.438E-01
6	7.820E-03	6.900E-04	4.803E-05	1.249E-01	8.179E-01	1.527E-01

APPENDIX G:
Collective Diffusion Coefficient Program

```
%Initial input given by the paper%
do=1.183; %Input diameter
d=1.4651; %final diameter
%r=0.5915;%inital radius
%A=1.0985989; %Area
lo=0.33948; %initial height
l=0.20664;%final height
F=1;%forec
g=9.82; %gravitional force
Ra=0.33;%
ra=0.025;%
da=0.19;%parameter to calculate(fdyn)
%************************************************************************%
%calcute radius intial
r=do/2; %.................(1)
% calculate area
A=3.14*r*r; %.................(2)

% Calculate Stress and strain. that is
stress=F/A; % .................(3)
strain=(lo-l)/lo; %.................(4)
% Calculate E
E=(stress/strain);% Youngmodulus.....(5)
%Calculate poission's ratio
v=-log(1+(do-d)/do)/(log(1+(lo-l)/lo)); %..............(6)
% calculate (fdyn)
fdyn=((8.95*10^10)/da)*(Ra/ra)^2; %farction coeff..(7)
%
%calculate fraction coefficient [N]
fn=fdyn*0.00001;% fn[N].........(8)
%calculate diffusion coefficient
def_coef=((E/3*(1-2*v))+4*E/(6*(1+v)))/fn; %deff_coffi....(9)
%calculating converting unit
def_coef_m=def_coef*0.0001;%converting unit(10)
% Calculate K
K=E/(3*(1-2*v));% value of K w.r.t E....(11)
% calcu1late G
G=(3*(1-2*v)*K)/(2*(1+v));%value of G w.r.t K......(12)
%calculate K w.r.t G
K2=(2*(1+v)*G)/(3*(1-2*v)); %value of K2 using G ....(13)
%value of G2 again w.r.t E
G2= E/(2*(1+v)); % value of G2 using E.....(14)
%calculate E2 using K
E2=3*(1-2*v)*K;%using K .................(15)
% calculate E3 using G
E3=2*G*(1+v);%using G.................(16)
```

APPENDIX H:
Bi-Dimensional Diffusion Model

Initial equation [Siepman et. al., 1999]:

$$\frac{\partial C}{\partial t} = \frac{1}{r}\frac{\partial}{\partial r}(rD_r(r,z,t)\frac{\partial C}{\partial r}) + \frac{\partial}{\partial z}(D_z(r,z,t)\frac{\partial C}{\partial z}) =$$

$$\underline{\qquad\qquad}\ \Lambda_r\ \underline{\qquad\qquad} \qquad \underline{\qquad\qquad}\ \Lambda_z\ \underline{\qquad\qquad}$$

Finite difference approximation:

$$\Lambda_r = \frac{1}{i\Delta r^2}\left[a_{i+1,k}(i+\frac{1}{2})(C_{i+1,k} - C_{i,k}) - a_{i,k}(i-\frac{1}{2})(C_{i,k} - C_{i-1,k})\right]$$

$$\Lambda_z = \frac{1}{\Delta z}\left[b_{i,k+1}\frac{C_{i,k+1} - C_{i,k}}{\Delta z} - b_{i,k}\frac{C_{i,k} - C_{i,k-1}}{\Delta z}\right]$$

where:

$$a_{i,k} = 0.5\left[D_r(r_i, z_k, \overline{t}) + D_r(r_{i-1}, z_k, \overline{t})\right]$$

$$b_{i,k} = 0.5\left[D_z(r_i, z_k, \overline{t}) + D_z(r_i, z_{k-1}, \overline{t})\right]$$

$$\overline{t} = t^j + 0.5\Delta\tau$$

$\Delta\tau$ – time step; j – time index.

Fixed number of grid points (I, K=101) were used and a variable spatial step, defined as:

$\Delta r = \frac{R(t)}{I}$ - radial; $\Delta z = \frac{Z(t)}{K}$ - axial.

The solution is made in two steps for every time (j):

$$\overline{C}_{i,k} = C^j_{i,k} + 0.5\Delta\tau\left(\Lambda_r(\overline{C}) + \Lambda_z(C^j)\right)$$

$$C^{j+1}_{i,k} = \overline{C}_{i,k} + 0.5\Delta\tau\left(\Lambda_r(\overline{C}) + \Lambda_z(C^{j+1})\right)$$

which means:

$$\overline{C}_{i,k} = C_{i,k}^{j} + 0.5\Delta\tau \left(\begin{array}{l} \dfrac{1}{i\Delta r^2}\left[a_{i+1,k}\left(i+\dfrac{1}{2}\right)\left(\overline{C}_{i+1,k}-\overline{C}_{i,k}\right) - a_{i,k}\left(i-\dfrac{1}{2}\right)\left(\overline{C}_{i,k}-\overline{C}_{i-1,k}\right)\right] \\ + \dfrac{1}{\Delta z}\left[b_{i,k+1}\dfrac{C_{i,k+1}^{j}-C_{i,k}^{j}}{\Delta z} - b_{i,k}\dfrac{C_{i,k}^{j}-C_{i,k-1}^{j}}{\Delta z}\right] \end{array} \right) \tag{H.1}$$

$$C_{i,k}^{j+1} = \overline{C}_{i,k} + 0.5\Delta\tau \left(\begin{array}{l} \dfrac{1}{i\Delta r^2}\left[a_{i+1,k}\left(i+\dfrac{1}{2}\right)\left(\overline{C}_{i+1,k}-\overline{C}_{i,k}\right) - a_{i,k}\left(i-\dfrac{1}{2}\right)\left(\overline{C}_{i,k}-\overline{C}_{i-1,k}\right)\right] \\ + \dfrac{1}{\Delta z}\left[b_{i,k+1}\dfrac{C_{i,k+1}^{j+1}-C_{i,k}^{j+1}}{\Delta z} - b_{i,k}\dfrac{C_{i,k}^{j}-C_{i,k-1}^{j}}{\Delta z}\right] \end{array} \right) \tag{H.2}$$

Equations (H.1) and (H.2) with the respective boundary conditions in r- and z-direction are then solved by the three-diagonal Thomas method to obtain the concentration field at a given time $j\Delta\tau$. Starting with the initial conditions the solution is repeated for each new time point $j+1$.

List of own Publications

This Dissertation consists of the following publications (1-9), which are appended as chapters and are referred to in the text by their numerals. The order is chronological. The complete list of publications can be found in the references section.

1. **Naddaf A. A.,** Bart H.-J., Diffusion Kinetics in Thermosensitive Hydrogel. Macromolecules Symposia 306-307(2011-c) 150–165.

2. **Naddaf A. A.,** Bart H.-J., Swelling Kinetics Associated with Diffusion of Poly (N-isopropylacrylamide) Hydrogel. J. of Mater. Sci. and Eng. B1 (2011-b), 247-258.

3. **Naddaf A. A.,** Bart H.-J., Raman Spectroscopy: Mutual Diffusion Coefficient in Hydrogels. Defect Diffusion Forum, 312-315 (2011-a) 193-198.

4. **Naddaf A.A.** und Bart H.-J., Transportvorgänge in Hydrogelen Chem. Eng. Tech. 82 (9) (2010-c) 1377.

5. **A. A. Naddaf**, I. Tsibranska and H.-J. Bart, Kinetics of BSA Release from Poly(N-isopropylacrylamide) Hydrogels. Chem. Eng. and Process. Process Intensification 49 (2010-b) 581-588.

6. **A. A. Naddaf**, I. Tsibranska, H.-J. Bart, Diffusion Kinetics of BSA Protein in Stimuli Responsive Hydrogels. Defect and Diffusion Forum, 297-301 (2010-a) 664-669.

7. **Naddaf A.** und Bart H.-J., Konfokale Raman Spektroskopie: Adsorptionskinetik in thermosensitiven Hydrogelen. Chem. Eng. Tech. 81 (8) (2009) 1080.

8. **Naddaf A.** und Bart H.-J., Raman Spectroscopy: Stimuli Responsive Hydrogels for Biomedical Applications. Chem. Eng. Tech. 80 (9) (2008) 1312.

9. **Naddaf A.,** H.-J. Bart., Swelling Characteristics of Poly(NIPAAm) Using Confocal Raman Microscopy. Proceedings of the 18TH International Congress of Chemical and Process Engineering, CHISA. Prague (Czech Republic) (2008) 24th -28th August.

Publications not related to this work:

10. **Naddaf A. A.**, El-Sinawi A. H., Haimour N., Kinetics of Superfix Scarlet X-2G oxidation from aqueous solutions using NaOCl. Proceedings of the 2th International chemical Engineering Conference (2010) Amman; Jordan.
11. **Naddaf A.**, Bart H.-J., Detemple P., Schmitt S., Bart H.-J., Hessel V., Faqir N., Microfabricated Hydrogen Sensitive Membranes. Chem. Eng. Tech. 32 (1) (2009) 103-113.
12. **Naddaf A.**, Detemple P., Schmitt S., Bart H.-J., Hessel V. and Krätz L., Herstellung und Charakterisierung von H2-selektiven Pd, Pd/Cu- und Pd/Ag Membranen. Chem. Eng. Tech. 79(9) (2007) 1348.

International Contributions

Oral Presentations

Presenting author is underlined

A. Naddaf and H.-J. Bart (2010). Transport Kinetics in Thermosensitive Hydrogels. 20th Polymer Networks Group Meeting (PNG-2010) Aug. 29th – Sep. 2nd, Goslar (Germany).

A. Naddaf and H.-J. Bart (2010). Raman Spectroscopy: Mutual Diffusion Coefficient in Hydrogels. The 6th International Conference on Diffusion in Solids and Liquid (DSL 2010), Paris (France).

A. Naddaf and H.-J. Bart (2009). Adsorption/Desorption Kinetics in Thermosensitive Hydrogels. Proceedings of the 10th International Thermodynamics Conference, Imperial College London (UK).

A. Naddaf and H.-J. Bart (2009). Raman Spectroscopy: Diffusion Kinetics of BSA Protein in Poly(NIPAAm). Hydrogele-Tagung 2009, Dortmund (Germany).

A. Naddaf, I. Tsibranska and H.-J. Bart (2009). Diffusion Kinetics of BSA Protein in Stimuli Responsive Hydrogels. Proceedings of the 5th International Conference on Diffusion in Solids and Liquid (DSL 2009), Rome (Italy).

A. Naddaf and H.-J. Bart (2008). Volume Phase Transition Characteristics of Poly(NIPAAm) Using Confocal Raman Microscopy. Material Science and Engineering Congress MSE. Nürnberg (Germany).

A. Naddaf and H.-J. Bart (2008). Swelling Characteristics of Poly(NIPAAm) Using Confocal Raman Microscopy. 18TH International Congress of Chemical and Process Engineering, CHISA, Prague (Czech Republic).

A. Naddaf and H.-J. Bart (2008). Raman Microscopy: Stimuli Responsive Hydrogels Characterization. Verfahren technisches Seminar 2008, Johanniskreuz (Germany).

Posters

A. Naddaf and H.-J. Bart (2010). Mechanical Properties: Collective Diffusion Coefficient in Thermosensitive Hydrogels. DECHEMA/GVC-Jahrestagungen 2010, Aachen (Germany).

A. Naddaf and H.-J. Bart (2010). Transport Processes in Hydrogels. Materials Science and Engineering (MSE 2010) 24-26 August 2010, Darmstadt (Germany).

A. Naddaf and H.-J. Bart (2010). Confocal Raman Spectroscopy: Adsorption/Desorption Kinetics in Thermosensitive Hydrogels. Verfahrenstechnisches Doktoranden-Seminar WS-2009, TU Kaiserslautern (Deutschland).

A. Naddaf and H.-J. Bart (2009). Adsorption/Desorption Kinetics in Thermosensitive Hydrogels. The 10th International Thermodynamics Conference 2009, Imperial College London (UK).

A. Naddaf and H.-J. Bart (2009). Confocal Raman Spectroscopy: Adsorption Kinetics in Stimuli Responsive Hydrogels. ProcessNet-Jahrestagung 2009, Mannheim (Germany).

A. Naddaf and H.-J. Bart (2008). Raman Spectroscopy: Stimuli Responsive Hydrogels for Biomedical Applications. ProcessNet-Jahrestagung 2008, Karlsruhe (Germany).

A. Naddaf, P. Detemple, S. Schmitt, H.-J. Bart, V. Hessel, L. Krätz and N. Faqir. Production and Characterization of Hydrogen-Selective Thin Layer Pd, Pd/Cu and Pd/Ag membranes. DECHEMA/GVC-Jahrestagungen 2007, Aachen (Germany).

Supervised Undergraduate Projects

María Carpe Marhuenda: Diffusion Coefficient: Experimental Determination for Thermosensitive Hydrogel using innovative techniques. Undergraduate Project for the Chemical Engineering Department, The University of Murcia, Spain, October 2009.

Marisa Medina Alcázar: Diffusion Coefficient: Experimental Determination base on the Mechanical Properties of Thermosensitive Hydrogel. Undergraduate Project for the Chemical Engineering Department, The University of Murcia, Spain, October 2009.

Vivo Fernandez, Rubén: Experimental Investigation of BSA Release From Poly(NIPAAm) Hydrogel. Undergraduate Project for the Chemical Engineering Department, The University of Murcia, Spain, October 2008.

Jad Rachid, Mohammad: Experimental and Theoretical Investigation of Phenol Diffusion Through Poly(NIPAAm) Hydrogel, Undergraduate Project for the Chemical Engineering Department, The University Kaiserslautern, October 2008.

Curriculum Vita

Personal Data

MSc. Eng. Aisha Ahmad Naddaf

- Place of Birth Kuwait, Kuwait
- Nationality Jordanian to Palestinian parents

Education

- 1985-1992, Primarily and Secondary Education, Kuwait-Kuwait.
- 1997, National High School Certificates, Amman-Jordan.
- 2002, Bachelor Degree in Chemical Engineering, Mu'tah University, Karak-Jordan.
- 2005, Master of Science Degree in Chemical Engineering, Jordan University, Joint Master Thesis: Kaiserslautern University & Institute of Microtechnology Mainz, IMM, with Jordan University, Amman-Jordan,

Employment

- 2003-2004, Teaching Assistant; Chemical Engineering Department, The University of Jordan, Amman-Jordan.
- 2004, Research Assistance; Chemical Engineering Department, The University of Jordan, Amman-Jordan, University & Institute of Microtechnology Mainz, IMM,
- 2006-2010, Scientific Co-worker, Thermische Verfahrenstechnik (Chair of Separation Science and Technology), TU Kaiserslautern, Germany.
- Since 2010, Engineer, BASF SE, Ludwigshafen-Germany.

Language

Arabic, English, and German.

Extracurricular Activities

- Member of Jordan Engineers Association; Amman-Jordan.
- Member of the Students Association (Hochschulgruppen), TU Kaiserslautern.
- Member of the German Engineers Association (Verein Deutscher Ingenieure, VDI); Germany.
- Member of the Cancer Association Rhineland-Palatinate e.V.

Award and Honors

- **Exchange Student Scholarship**; Undergraduate practical training. Arab Countries League, 2001, Mu'tah University (Jordan), Hilwan University (Egypt) and The National Cement Company (Hilwan- Egypt).

- **Award of Excellence for Alumni the Academic Year 2001/2002**. Mu'tah University, Karak (Jordan).

- **University Scholarship**; Master Degree Research 2004-2005. University of Jordan, University of Kaiserslautern and IMM Institute of Microtechnology Mainz GmbH, Amman (Jordan), Kaiserslautern and Mainz (Germany).

- **University Scholarship**; PhD Degree, 2006-2010. University of Kaiserslautern, Kaiserslautern (Germany).

- **Outstanding Young Scientist Award**. The 5^{th} International Conference on Diffusion in Solids and Liquid (DSL-2009), Rome (Italy).